CRANFIELD UNIVERSITY

Adair G. W. Williams

Aerodynamic Forces on High-Speed Multihulled Marine Vehicles

School of Engineering

Offshore Engineering & Naval Architecture Group

PhD Thesis

CRANFIELD UNIVERSITY
School of Engineering, Department of Structures, Impact & Machine Dynamics
Offshore Engineering & Naval Architecture Group

PhD Thesis
Academic Year 2008 - 2009

Adair G. W. Williams

Aerodynamic Forces on High-Speed Multihulled Marine Vehicles

Supervisor
Professor M. H. Patel

December 2008

This thesis is submitted in partial fulfilment
of the requiremetns for the degree
of Doctor of Philosophy

To my father;
a constant source of
enthusiasm and inspiration.

Abstract

The need for high-speed high-payload craft has led to a considerable interest in vehicles capable of bridging the gap between conventional ships and aircraft. One such concept uses the forward motion of the craft to create aerodynamic forces on a wing-like structure, and hence, alleviate the overall drag by reducing the wetted area.

This research focuses on the use of suitably shaped multihull geometries to achieve efficient aerodynamic lift for high-speed sea vessels. The problem is first studied in two dimensions using a simplified analytical approach and CFD modeling. The work is then extended into three dimensions and a final aerodynamic model is produced for a complete hull form, including the effects of hydrodynamic surfaces above the water. The aerodynamic analysis demonstrates that significant efficiency can be achieved through careful shaping of the side hull and cross deck, with lift-to-drag ratios of nearly 50 for a complete aerodynamic hull configuration.

Further analysis is carried out using a hybrid vehicle stability model to determine the effect of such aerodynamic alleviation on a theoretical planing hull vessel. Comparisons are made using the Savitsky planing model, and from this it is found that the resistance can be almost halved for a fifty metre, three hundred tonne vehicle with aerodynamic alleviation traveling at 70 knots.

A comparative study is made for the hybrid vehicle with regards to size, speed and weight, whilst attempting to match the proportion of aerodynamic lift with speed to a theoretical optimum. From this the likely configurations for future development are identified.

Acknowledgements

I would like to thank my supervisor, Professor Minoo H. Patel, for his support and encouragement throughout this project. I would also like to thank my colleagues in the OENA group for their help, in particular, Maurizio Collu, whose PhD study was undertaken in parallel to mine, and with whom I have spent much enjoyable time over the past three years. Thanks are also due to BAE Systems and the EPSRC, for their part in making this project possible.

I am especially grateful to my parents, Raymond and Pollyann, for their support and enthusiasm toward the project; my girlfriend Louise for exemplary displays of patience; and her family, for looking after me on such a regular basis.

I am indebted to you all.

Contents

List of Figures

List of Tables

Notation

a = Speed of sound

A = Cross-sectional area

B = Beam

C_D = Coefficient of drag

C_L = Coefficient of lift

C_M = Coefficient of moment

d = Draft

D_D = Diffuser drag

$D_{induced_a}$ = Induced drag from wing, air

$D_{induced_w}$ = Induced drag from hull, water

D_T = Total drag

D_{Va} = Viscous friction drag, air

D_{Vw} = Viscous friction drag, water

D_{Wac} = Air cushion wash drag

D_{Wh} = Hull wash drag

F_n = Froude number $U/\sqrt{gl}$

g = Gravity: 9.81 m/s^2

H_0 = Height of leading edge above ground plain

L = Length

$\dot{m}$ = Mass flow rate

M = Mach number

P = Static pressure

R = Specific gas constant ($R = 287\ J/kgK$ for air at standard conditions)

R_e = Reynolds number Ul/v

S = Planform area

SLR = Speed Length Ratio

S_w = Wetted surface area, water

T = Temperature

U = Velocity in the x direction

v = Kinematic viscosity of water: 1.188 x 10^{-6} m^2/s

W_G = Gross weight

α = Angle of attack

γ = Ratio of specific heat capacities for constant pressure and volume ($\gamma = 1.4$)

Γ = Vortex strength

λ = Source strength

ρ_w = Density of water: $1025kg/m^3$

ρ_a = Density of air: $1.23kg/m^3$

ϕ = Velocity potential

ψ = Stream function

σ = Doublet strength

ACV = Air Cushion Vehicle

PAR = Power Augmented Ram

SES = Surface Effect Ship

SWATH = Small Waterplane Area Twin Hull

WIGE = Wing In Ground Effect

WISE = Wing In Surface Effect

Subscripts

$_m$ = Characteristic Mach flow condition

$_n$ = Normal component

$_x$ = Conditions at point x down stream of inlet

$_0$ = Total condition (Total pressure P_0)

$_\nabla$ = Displaced volume

$_\infty$ = Free stream conditions

Chapter 1

INTRODUCTION

1.1 Background to the Research Project

1.1.1 Motivations

The modern transport market may be thought of as existing in two distinct sections: that of high-speed, low-payload vehicles, such as aircraft, and that of low-speed, high-payload vehicles, such as cargo ships. Constant pressure to carry more load and at greater speed, combined with environmental concerns over fuel efficiency has led companies and researchers to look for hybrid technologies capable of closing in on this gap in the market.

Shorter transit time for commercial produce is obviously a valuable asset. As indeed is the case for passenger ferries, where speed comes at a premium. More critical pressure for high-speed high-payload comes from the military and humanitarian aid organizations, where speed often means the difference between life and death. One poignant example comes from the 2004 tsunami in Southeast Asia. After news of the event reached the rest of the world, hundreds of thousands of people began giving money to aid the rescue operation. Over the next few days

however, very little could be done. People, and of course television crews, arrived almost immediately, unfortunately, the food, shelter and medical supplies were still at sea, along with most of the aid workers, who had not yet found room on a flight. The money was given, the supplies were bought and the people volunteered to help; but many people still died waiting for them to arrive.

Another example comes from the 2003 invasion of Iraq. During the first few days of the invasion soldiers poured into the country. Their tanks, armoured vehicles, ammunition, food supplies, desert equipment (most notably goggles) and toilet rolls, however, did not. This resulted in weeks of waiting whilst the essential supplies caught up with the soldiers and allowed them to move further into the country.

The benefits of a vehicle capable of sustaining high-speeds over vast stretches of open ocean whilst carrying significant weight in cargo are extremely tangible. Financial, tactical and humanitarian needs warrant a considerable amount of research into the field, and of course that research has already begun. Significant work has been done, largely by the Russians, on the field of 'wing in surface effect' or 'W.I.S.E' craft, being aircraft capable of utilizing the benefits of ground effect whilst flying close to the sea. Other work has focused on air cushion vehicles or hydrofoils. Whilst progress has been made, none has been able to remove a significant slice of the trade from standard cargo ships and aircraft. Most importantly, there is still much which is not yet understood about the design and capability of these hybrid vehicles.

1.1.2 Research Objectives and Limitations

This work is undertaken as part of a wider project supported by BAE Systems and the EPSRC into High-speed Sea Skimming Vehicles (HSSV) and is aimed at identifying and developing future technologies and areas of investment for the marine transport market.

The concept vehicle, being a hybrid HSSV, is proposed to have both hydrodynamic and aerodynamic properties, from which it may derive both lifting and control surfaces of an unspecified proportion.

The primary objective of this study is to identify and analyse novel configurations of existing technologies and to develop methods for analysing them. Thus a thorough review of the literature must first be conducted in order to gain an understanding of the state of the technologies available. Equally this will provide background on the combinations which have been tried and the various degrees of success achieved, as well as any experimental data or analytical methods which could be used for comparing the technologies.

Since this study is performed as part of a group project, the papers collected will form part of a central knowledge base. From this the most promising technologies can be identified and a rough configuration can be chosen for study.

The objectives for this project are as follows:

- To gather knowledge within the group about existing designs and technologies.
- Identify areas in which advancements can be made, either through improved design or hybridization of existing designs.

- Choose a suitable configuration.
- Analyse the configuration and identify any improvements which have been made or which could be made.
- Consolidate group material and provide information on the perceived advantages achieved so far and what further work could be done.
- Propose the most suitable configuration for scale model testing in the next stage of the project.

The limitations of this project stem from its sheer size. There may be many configurations which show promise for the future and for every configuration there may be many variations in design and operating conditions which will affect the performance. It will not be possible to analyse all such vehicles and configurations, and even a single chosen design can only be analysed within the time constraints available. Ideally, the chosen configuration would be tested numerically and then built as a prototype for comparative testing, however, this is a time consuming and expensive process. This becomes even more impractical if continuous alterations must be made to the model in order to find the optimum configuration.

It has been suggested that a scale model will form the next step in the project if the initial research provides a promising configuration. As such, the work will be focused on more general configurations and numerical testing methods which allow a greater number of configurations to be analysed as expeditiously and economically as possible.

Chapter 2

LITERATURE REVIEW

2.1 Current Technologies

The current range of transport technologies is quite extensive, and the hybridisation of many of these has made classification difficult. Figure 2.1 shows an interpretation of the various means of achieving lift for sea vehicles. The right hand side shows the gradient between hydrostatic and hydrodynamic lift, which are the most common types of sea-lift vessel. The left hand side shows powered lift, which is used for air cushion vehicles such as hovercraft.

A more complete design space may consider the additional dynamic contribution from air. Thus the triangle becomes that of static, dynamic and powered lift. Static lift will now include buoyancy from displaced air as well as water, that is, air ships or 'zeppelins' as well as boat hulls. Dynamic lift can now include planing hulls and hydrofoils as well as airfoils. Powered lift is generally limited to air cushions, however they are theoretically extended to helicopter blades, or, if one felt so inclined, rotational hydrofoil blades. This discussion was outlined during the High Speed Sealift Technology Workshop [11] where it was proposed that the sustention triangle be modified into a cube, or rather a set of four mutually

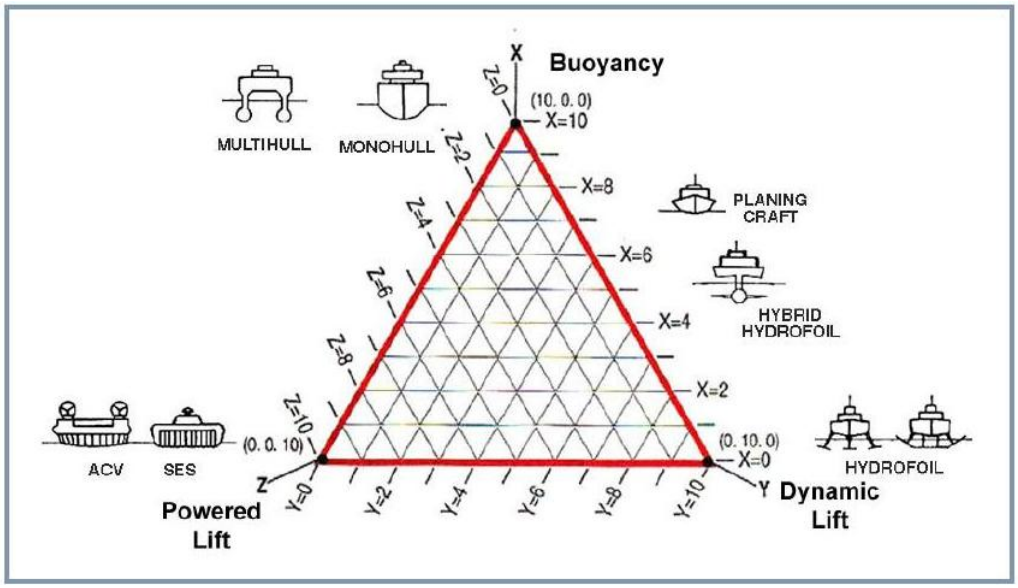

Figure 2.1: The sustention triangle[1]

orthogonal axes. The axes representing passive, active; static, dynamic; hydro, aero. This does however, lead to some interesting design spaces, for instance the concept of 'active hydrodynamics'. To quote the author:

'Continuing the excursion into the unknown, an attempt has been made to conceive a craft using active hydrodynamics. Consider what that means: It requires ahead speed to make lift, it uses moving parts, and it does this in water. The only concept this author can imagine is a sort of hydrofoil using Fletner rotors. Like a hydrofoil it requires ahead speed, but it also requires the rotation of the rotors to generate Magnus-effect circulation.'

Unsurprisingly, the idea is not taken further, however, the concept of using axes to map design space, and the example of how it forces one to consider unlikely combinations, is a useful reminder that there is often more to the design space than first meets the eye.

Any combination of the above technologies can be used, and the percentage of the total vehicle weight accounted for by each can vary from 0 to 100%. As a result the design space is extremely large and there exists a great deal of potential for realising novel configurations capable of out performing current designs.

2.2 Classification of Vehicles

A brief description of the current vehicle types and technologies in use is given below, along with some hybrid designs and technologies which are being considered for future service.

2.2.1 Displacement

A displacement ship uses the hydrostatic force of displaced water to support its load during transit, which allows it to carry heavy payloads. Such a ship will be characterised by smooth lines from bow to stern and in general, a long thin shape. The long thin shape and convex hull lines are necessary to prevent flow separation which would produce a significant drag on this type of vessel. Due to the shape, they are highly sensitive to increased speed and can only operate at Speed-to-Length Ratio of less than 1, where the SLR is defined by Savitski[12] as

$$SLR = \frac{V_k}{\sqrt{LWL}} \tag{2.1}$$

where V_k is the speed in knots and LWL is the loaded water line length (from bow to stern) in feet. This equation was originally developed by Froude, but his name was eventually given to the dimensionless version of the equation shown below:

$$F_n = U/\sqrt{gl} \tag{2.2}$$

This is the length based version of the equation, where U is the ship speed in ms^{-1}, g is gravity and l is the waterline length. A beam based version is often used for planing vessels as the ships' waterline length changes with trim angle. For lower speeds and for ease of classification, the SLR ratio is more convenient.

For an SLR greater than 1, the convex shape of the hull will result in hydrodynamic suction and increased friction. Furthermore, the vessel will start to climb the bow wave which will increase the trim angle and running resistance. This means that displacement ships are restricted to slow speeds unless they are extremely long. Savitski[12] points out that the speed limit is dependent upon the length, hence a long enough boat will be able to reach a desirable speed without planing. Unfortunately, the boat suggested is 1480 ft long (450 metres!) and achieves a theoretical speed of 50 knots. Although this is useful, it is not a significant departure from standard tanker design, and attempting to increase the speed through further elongation of the hull may be considered prohibitive, at least if one wishes to enter most ports. Such designs are unlikely to go beyond the 50 knot speed suggested by Savitsky. However, displacement ships are very efficient within their design speed range.

2.2.2 Semi-Displacement

In order to allow a hydrostatically supported vessel to operate at an SLR of 1.3 or greater the hull shape must be modified to reduce the large squat and trim angles experienced by standard displacement hullforms. Semi-displacement hulls are noticeably straighter along and below the waterline to avoid adverse pressure

and have a partially submerged transom stern. This is essentially a compromise, allowing a boat to operate efficiently at low speeds by retaining softer curves, whilst incorporating a transom and chine, which will encourage flow separation once adverse pressure gradients begin to form.

2.2.3 Planing

A planing hull is designed to run at SLRs of significantly greater than 3, which is the limit for a semi-displacement vessel. To achieve this, the hull must be hard chined, meaning that it has a flat hull with sharp edges to release the water from the sides and prevent suction. The bow is usually a sharp 'V' shape (whose angle is defined as the dead rise) which reduces toward the stern where the hull bottom is usually almost flat. This allows the bow to cut through waves, whilst the rear portion attains greater lift from its flatter, wider shape. The hull will then terminate in a dry transom to prevent suction. A planing hull uses the positive pressure created by the flat hull to lift out of the water and reduce drag, hence also reducing the hydrostatic component of lift. As a result planing hulls can be very fast and manoeuvrable but are inefficient at carrying loads. They are also adversely effected by rough seas and give a very uncomfortable ride in only a mild swell. Planing hulls however, play a dominant role in high speed sea transport. In 1992 the Italian vessel *Destriero*, designed by Donald Blount, won the Blue Riband Award for crossing the Atlantic in record time without refueling. The average speed was 53.1 knots, but a speed of 63 knots was achieved once the fuel tank got lighter. A description of the vessel is given in [11]. One of the most important points is the length of *Destriero* which is 67.7 m. Most planing hulls are considerably less than 30 m. This large planing hull represents a significant step towards high-speed high-payload transport. Equally, SES, discussed below,

use planing hulls to run at speed and sea planes have always used planing hulls to take-off from the water.

Much research has been done on planing craft, but due to the complexity of the problem, particularly the free surface and wave making, there is still much that is not well understood. The best method for testing planing hulls is in a towing tank, where the full hull geometry can be modeled; but this is expensive and time consuming. For more generalized analysis the hull form can be analyzed numerically or empirically via a number of models. Unfortunately, due to the complexity of the problem, small changes in trim angle, weight distribution or geometry can result in large changes to the pressure distribution on the hull. As a result, empirical models are usually restricted to set hull geometries and confined within the range tested. An example of experimental data in comparison with semi-empirical calculations are given by Savitsky [13]. Savitsky's method assumes a simplified prismatic hull geometry, the dimensions of which, are used to drive a set of empirical equations based on extensive experimental testing. Savitsky's equations offer a relatively simple analysis with reasonable results within the specified constraints of speed, trim angle and loading.

Added mass and water impact theory, also referred to as 2d + t theory, considers a boat planing on water to be analogous to a hull impacting on the water from above. When a hull shape is dropped on to the water, the decelerating force acting on the hull is directly proportional to the added mass of the hull form. In other words, by considering a vertical slice of water, the passage of a planing hull though the plane and the impact of a wedge in the shape of the hull being dropped from above, will appear the same. From this, the deceleration force on the wedge is equated to the lift force on the planing hull. This approach, pioneered by Von Karman [14] and Wagner [15], and later by Payne [16], allows more complicated hull shapes to be analysed, but without such extensive experimental data.

Wagner [15] suggested that the flow under the hull was the same as that on the high pressure side of a wing. He proposed that the jet (or stagnation point) was parallel to the planing surface. This was later rectified by Green [17] who observed that the jet was directed upward toward the hull in the fashion of a wing. This theory was used for simple flat plates, however, it has led to the use of aerodynamic tools such as vortex lattice methods being used to study the flow around planing hulls. Vortex lattice codes have a distinct advantage in that they can account for complex hull geometries and the effect of the free surface, however they are computationally expensive and difficult to implement. Pemberton *et al* [18], give a comparison of the methods outlined above and conclude that due to the complexities of planing craft, no single method is yet adequate. Although all make reasonable predictions within their limitations, they vary considerably at higher trim angles. In particular, the Savitsky method consistently over predicts the lift coefficient for hulls with larger dead rise angles.

2.2.4 Multihulls

The term multihull refers to a vessel with more than one hull. The number and type of hulls is not limited but ships with more than three hulls are rare. The most common configuration is the catamaran (from the Tamil word *kattu maram* meaning "tied trees" [19]) which consists of two hulls. Trimaran, quadrimaran and pentamaran are often used to refer to vessels of three, four and five hulls, respectively. The advantage of having multiple hulls is largely from stability. Where a monohull has good longitudinal stability, it will suffer from lateral instability or roll. A catamaran or similar multihull however, will have greater roll stability in proportion to the distance between the hulls. This seakeeping ability can be a great asset for preserving passengers and cargo in rough seas. The choice of number of hulls may be more complicated and is effected by many factors, some

of which are discussed by Doctors[20]. Tuck and Lazauskas [21] & [22] discuss the effect of varying the number and spacing of hulls and conclude that the optimum (long) monohulls are always better than the optimum catamarans or trimarans of the same total displacement, in terms of total calm water drag alone, unless there are restrictions on the ships' geometry. Such restrictions however, are likely to occur. In particular, optimum monohulls are often very long and thin and are consequently highly unstable, difficult to manoeuvre, structurally weak and unsuitable for most ports. Equally, there is the question of speed and the relative importance of frictional components affected by it. The total friction is comprised of many components, including skin friction and wave resistance, the proportion of which, is dependent on the speed and geometry of the vessel. Detailed analysis of the wave resistance of high-speed catamaran hulls is given by Molland *et al* in [23]. For displacement multihulls the wave drag can be the most significant factor and careful design is needed to avoid excessive drag. In addition the the shape and spacing of the hulls, the depth of water can greatly affect the wave pattern and resistance. Gourlay *et al* [24] investigated the bore phenomenon produced between the hulls of a catamaran and found a significant variation in drag over the range of experimental data. Such factors must be considered in the design of a multihull when choosing the number, size and location of a ships hulls. Tuck and Lazuskas [21] & [22] note that the optimum length of a vessel changes dramatically with speed as well as the separation of the hulls. Although monohulls can have lower resistance when optimized mathematically, when more realistic constraints are applied to maximum length to beam ratio, a catamaran can often become superior to a monohull and certain multihulls such as pentamarans[25] in diamond configurations can exhibit wave cancelation features allowing for much reduced drag at particular speeds in calm water. As a general rule, less hulls are better, and in the case of complex multihulls, the central hull is usually significantly larger than any satellite hulls, which are primarily for stability and wave

cancellation rather than load bearing.

2.2.5 SWATH

Small Waterplane Area Twin Hull vessels, or SWATH [26], use submerged bodies which taper to a narrow support along the waterline. This reduces wave drag and some rough sea effects. The design is not necessarily limited to twin hulls and both single and multiple hull designs can work. However, they require control surfaces as they are naturally unstable at higher speeds and can suffer in high seas due to wave slamming on the under side of the deck. Since this is effectively a hydrostatic support it is also most efficient at low speeds. The required control surfaces however, need dynamic forces to work; but are limited in speed due to the effects of cavitation, which is discussed in the hydrofoil section.

2.2.6 Hydrofoil

Hydrofoils are submerged wings which can be used to lift a vessel at speed. They offer huge advantages in rough seas as the ship can run above the waves while the wings are submerged below them. This also greatly reduces the wetted surface area.

Hydrofoils, however, encounter problems at high speeds if the pressure on the upper surface becomes less than or equal to the vapourisation pressure of water. This results in cavitation, or the formation of pockets of water vapour over the suction surface of the foil. This is potentially very damaging to the foil and causes a significant reduction in lift and stability. The main cause of damage during cavitation is the collapse of the vapour bubbles which cause shock waves. When this happens on the surface of the foil it can chip away at the surface,

destroying the foil. In order to prevent this, some high-speed foils are designed to supercavitate. Such a foil has a sharp profile which induces cavitation at the very tip of the foil from where the pressure is kept low enough to prevent the collapse of the cavitation sheet until it has left the trailing edge of the foil. In this way the foil is not damaged. However, the turbulent nature and transition from cavitating to supercavitating conditions make them unstable and unpredictable as well as having reduced performance during cavitation, largely as a result of the dramatic change in the density of the surrounding water.

Further problems are encountered if the wave height is too great and the waves slam against the hull. This is a problem in particularly stormy or shallower water where the wave slope becomes steeper. In large rolling swells the foil can follow the wave contours like hills.

Hydrofoil craft are generally limited to about 40 knots and due to the problems of cavitation, cannot be expected to carry heavy loads at speeds in excess of 50 knots given the present technologies. A good overview of hydrofoil theory and application is presented in chapter 6 of 'hydrodynamics of high-speed marine vehicles' by Faltinsen [27].

Hydrofoils can be analysed in much the same way as airfoils, except for the problem of interaction with a free surface and the associated wave making drag which complicates the matter. This has been extensively researched in two dimensions by Piperni [28] and later by Lia and Troesch [29] who use a vortex lattice method with an altered method of images to solve the free surface elevation. Although this work was two dimensional, it is stated that an extension into three dimensions would be perfectly possible.

Many high-speed vessels make use of hydrofoils, even if only for control effectors and as such it is likely that they will play a role in the design of a high-speed

sea-skimming vehicle. However, due to the problems of cavitation it is unlikely that they will provide the primary source of lift at higher speeds.

2.2.7 ACV

Hovercraft, or Air Cushion Vehicles, use air trapped in a flexible skirt to float over the surface of the water. The skirt pressure is maintained by lifting fans and continually escapes from under the base of the skirt. As a result the hovercraft does not touch the surface (providing the surface is relatively smooth) giving it amphibious capabilities. Due to the lack of water contact ACVs have very low frictional resistance and can travel at high speed. However, they require power to inflate the skirt which is analogous to drag and limits the load capacity. They are also known to have a relatively large induced wave drag at low speeds. Furthermore they are directionally unstable and cannot easily be manoeuvred accurately at high speed.

At lower speeds ACV suffer from the effective drag, or energy used in maintaining the cushion pressure. The cushion pressure can also result in a large wave drag, Barratt[30] describes the wave resistance of a hovercraft, clearly showing the high levels of drag at lower speeds. A further consideration to the drag of a hovercraft is the momentum drag caused by the air taken in to inflate the cushion. Since air is constantly leaking from the skirt, it must be brought in by the fans at the same rate to counterbalance the effect. This results in a change of momentum as the air from outside of the vehicle is accelerated up to the speed of the air inside the cushion, which is travelling at the vehicle speed. This is perhaps easier to imagine in the case of a wind tunnel experiment, where the moving air must be decelerated to join the stationary cushion, resulting in a drag force. The two cases are of course analogous.

Air cushion vehicles are severely limited in rough seas. If the skirt cannot maintain the required gap it will allow the air to escape too quickly and sink. Equally, if the gap closes the skirt will come into contact with the water and significantly increase the drag. Unlike a planing hull, which will gradually impact a wave as the sharp bow cuts into the water, a hovercraft can be struck from underneath with the full force of a wave. This means that in rough seas they can be forced to stop and drift until the storm passes. Usually however, the operation of air cushion vehicles is limited to only the calmest of seas.

2.2.8 SES

A Surface Effect Ship is a catamaran in combination with an air cushion created by seals at the bow and stern. With the lift fans off, the ship will act as a pure displacement catamaran, whilst at design conditions it will be planing on the hulls with typically around 80% cushion support; but this can be increased until the side walls are lifted out of the water, at which point it may be considered an ACV. The main advantages of an SES are the stronger side walls, which allow a higher cushion pressure, improved sea-keeping due to the ability of the side hulls to pierce smaller waves without releasing cushion pressure, and better directional stability. However, there is increased frictional resistance and structural weight. The resistance of an SES is the combination of many components, including the viscous drag from air and water, pressure drag, wave drag from the hulls and air cushion as well as aerodynamic profile drag and momentum drag from the cushion fan. As a result, the most significant drag component can vary enormously with speed and design as well as the sea state. A description of the resistance components of a surface effect ship is given by Doctors [31].

SES craft have taken on a dominant role in marine transport, Lavis [32] records

the extensive use to which these craft have been successfully put over the years. Indeed as far back as 1969 projects were started to build a 100 tonne 100 knot SES. According to Clark *et al*[1] the vessel SES100-B established a sustained speed record of 91.9 knots in calm water and was able to operate at 35 knots in 6 to 8 foot waves. This is quite an achievement, however, the effect of waves on the craft is extremely significant and makes this top speed an unrealistic goal for normal sea conditions (the test being run on lake Ponchartrain) and the efficiency of the craft at such high speeds was greatly reduced, although far better than any equivalent vehicle at the time.

Another approach to SES technology comes from the PACSCAT, or Partial Air Cushion Supported Catamaran concept [33]. This vehicle uses only a partial air cushion support at lower speeds, of around 20 knots, but with high cargo capacity and good efficiency predicted. However, the vehicle is only designed for operation on rivers and its performance in waves would be limited in the same fashion as other SES.

2.2.9 WIGE

Aeroplanes flying in close proximity to the ground encounter an increase in efficiency caused by the interaction of the wing tip vortices with the ground. The flow over a three dimensional wing is of greater intricacy than for a two dimensional foil section due to the 'end effects'. This is the result of the high pressure on the underside of the wing following the pressure contour around the wing tip to the lower pressure on the upper side, causing the wing tip spiral vortices which can occasionally be seen behind airplanes in cloud. Figure 2.2 shows the vortices formed behind a rectangular wing in a smoke tunnel. These tip vortices create a down wash as the spiral rotates onto the top surface of the wing causing the

upper surface pressure to increase and also changing the local apparent angle of incidence. This has a detrimental affect on the wing's performance and is why many planes (and birds) have winglets which can derive lift from the rotational component of flow. Since these effects occur at the end of the wings, it is beneficial to have a long, or high aspect ratio wing, so that the end affected region accounts for a smaller percent of the total wing. This is of course limited by the structural integrity of the wing.

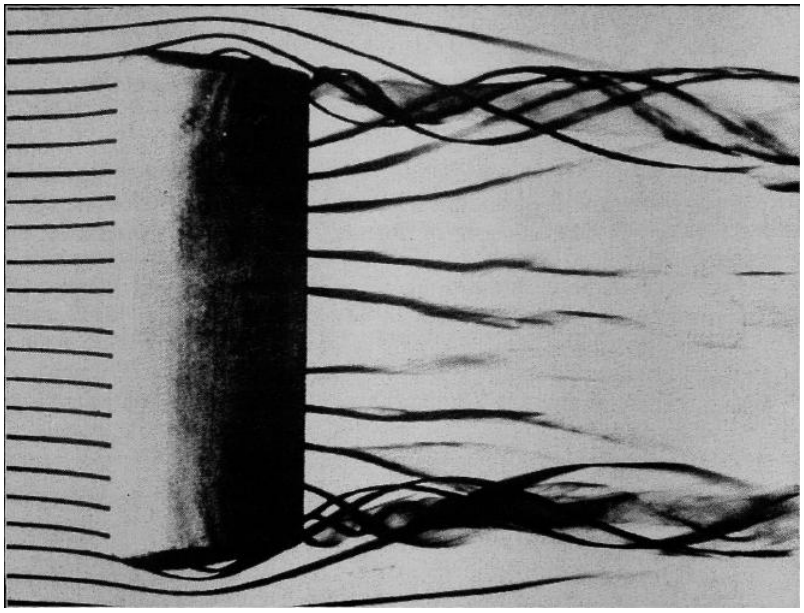

Figure 2.2: Wing tip vortices behind a rectangular wing in a smoke tunnel. Reproduced from Anderson [2]

When a wing becomes close to the ground the wing tip vortices may be interfered with, and their flow pattern changed. If the ground is close enough, the flow will be significantly modified and the downwash will have dramatically less effect on the wing. This is due to the wing tip vortices becoming 'squashed' by the ground and forming further out and above the wing tips than usual. This is shown in Figure 2.3. The result is that less of the high pressure under the wing escapes

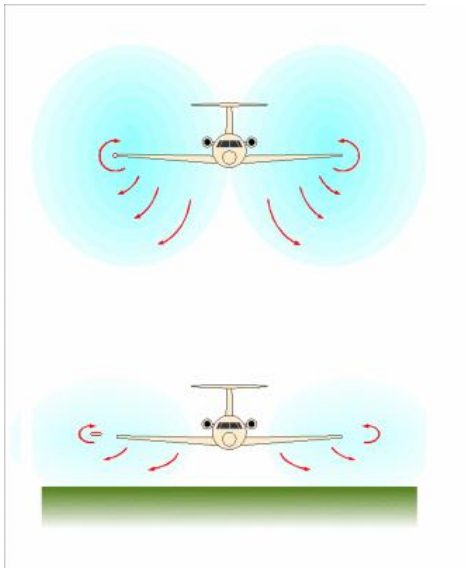

Figure 2.3: Ground influence on an aeroplane flying at height and close to the ground. Reproduced from The WIG Page [3]

onto the upper surface and the wing experiences greater lift, or by decreasing the angle of attack, less drag for the same lift. This increase in performance due to the ground is called ground effect and craft which use this are known as WIGEs (Wing In Ground Effect) or *ekranoplan* from the French for ground-plane. If the wing flies over a deformable surface such as water, then it is considered to be in surface effect. Surface effect has much the same results, but an associated wave drag is caused by the free surface deformation, however this is usually quite small at high Froude numbers. The Froude number being the ratio of the speed of the vehicle to the wave speed and is analogous to the Reynolds number. Ground effect is encountered when a wing is at a height of around one wing span or less but is not usually significant until a height of less than half of the wing span, [34]. If a wing flies at a height equal to or less than its chord, it may encounter ram effects. This is especially true of wings at high angles of attack and results from

air stagnating under the wing and creating high pressure in a similar manner to a parachute. This can produce very high lift as shown by [35] & [36], but also very high drag, and is prone to excessive flow separation, particularly at high angles of attack and this can result in the instability often witnessed in small high speed racing craft such as those discussed in [37]. As the ground is approached the effect of airfoil thickness becomes more significant and the effects of camber can be greater. If the trailing edge of the wing is too close to the ground it can create a venturi effect as the air rushes out at high speed causing a low pressure which sucks the wing down. This is a viscous effect which is highly sensitive to scale and speed as described by Kim *et al* in [38]. It is therefore important to consider the Reynolds number of a flow when dealing with objects in close proximity, as the depth of boundary layer can effect the distance at which the forces reverse. That is to say, there may be two contributing factors, the channelling effect of the bodies causing a venturi effect which increases speed and reduces the pressure, and the boundary layers interacting which causes the flow to slow down and increase in pressure. The Reynolds number will deturmine the size of the boundary layer and thus dictate the relative importance of these effects. Although it is unlikely that wings of the size and speed used on ekranoplans will have boundaries large enough to interact with the ground, the effects must be considered, especially for scale tests in wind tunnels.

A great deal of research has been done on the performance characteristics and stability of wings in ground effect. Extensive wind tunnel tests such as [39] have studied wings in ground effect in wind tunnels with rolling roads. The rolling road allows the floor to move at the same speed as the air and helps to counteract boundary layer problems which can develop on a stationary floor in a wind tunnel. A further method of dealing with this problem is to use a reflected image as in [40] and [7]. This method uses a line of symmetry between two foils to simulate a ground plane. Although this method is not as real as a rolling road, it does

entirely eliminate the boundary layer problem which can result from scale models, as discussed above. In addition, this work is of particular interest because it was conducted at Reynolds numbers of over 10^6, which is difficult to achieve in wind tunnels and which corresponds more readily with large scale, high-speed wings. Hayashi *et al* [41] have considered flow around an airfoil at higher angles of attack where separation occurs and have shown that flow separation can occur more easily, or at lower angles of attack, whilst in ground effect. This may be affected to some extent by boundary layers in the wind tunnel, but the results have been confirmed by further tests and and computations as well as other work such as that by Paulson [42].

The advances in Computational Fluid Dynamics (CFD) has increasingly led researchers to study wing in ground effect is this way. Comparative studies such as that by Zerihan and Zhang [43] have shown that CFD can provide a very good comparison with wind tunnel tests. This particular work was on inverted airfoils near ground, for motor sport applications. Indeed, CFD is now an industry standard for aerodynamic design of racing cars and Cranfield's Library is teaming with work on the subject, which is especially popular with masters students. Much can be learnt about the effect of end plates and body geometry wakes on downstream foil performance, however, the essential characteristics of wings in ground effect are not studied beyond that of the work outlined above.

More recent wind tunnel experiments by Chun *et al*[44] and Ahmed *et al*[45] have considered wings in very close proximity to the ground with rolling road conditions. They have begun to identify the complex nature of two dimensional wing geometry in such close proximity to the ground and note that although high lift and efficiency can be achieved, there can also be reductions in performance when suction occurs from the venturi effect at low heights and zero angle of attack. As discussed above, this is the interaction of the body geometry causing a funneling

of the air which reduces the pressure. This experiment was not conducted at low enough heights to encounter boundary layer interaction and there was consequently no further change in force as described in [38], however it is clear that the lift generated by wings at extremely low height wings with zero angle of attack can vary considerably for only small changes in separation, from positive to negative as the ground is approached. Furthermore, if the ground is approached sufficiently for the boundary layers to interact, the force can change again to that of positive lift. This latter effect is reduced as the size of the wing is increased, but it does illustrate the complex nature of wings in very close proximity to the ground.

Since the vehicle is designed to fly over water, it will be in surface effect and will therefore have an associated free surface deformation caused be the pressure around the wing. The problem of a wing flying in close proximity to the water was studied by Tuck [46] in one dimension and later by Grundy [47]. This approach considered the pressure distribution on the free surface whilst the free surface was travelling at the same speed as the wing, effectively ignoring wave making effects. In reality the water is moving past the wing and the pressure deformation will therefore result in a wave train. The effect of trailing edge vortices from a wing in free flight over a water surface has been studied by Barber [48]. The work shows that minimal deformation is caused by the pressure directly below the wing, but that the vortices behind the wing result in significant deformation. This has been confirmed with observations from WIGE vehicles where the spiral vortices are the most apparent feature in the wake.

Much of the work on wing in ground effect was done in Russia, and many Russian built WIGEs have been successfully demonstrated. Craft such as Orlyonok (Figure 2.4) and the KM "Caspian sea monster" typify the early designs. They have a single hull body with short, stocky wings and a large, high tail plane. This design

Figure 2.4: The Russian built Orlyonok WIGE craft flying in ground effect. Reproduced from The WIG Page [3]

works but is very inefficient and considered quite dangerous to use, even in calm seas. More recent designs proposed by Balow *et al* [34] discusses an attempt to produce a WIGE vehicle with a load capacity of 22 tonnes. After considerable parametric analysis, the vehicle arrives at a similar design to the Russians, with the addition of PAR technology. PAR or Power Augmented Ram, uses the engines to channel air under the wing and create lift at lower speeds [49]. This should allow the vehicle to take-off faster and reduce the hydrodynamic drag during take-off, which reduces the engine size. Unfortunately, the engine size required for successful PAR take-off was not much different from the original design, and only modest improvements where made for the entire vessel.

Although much has been learned about the physics of wings in close proximity to the ground, no real advances in WIGE design appear to have have been made

from them since the Orlyonok. The problem with WIGE vehicles appears to be more fundamentally rooted in their concept. That is, they are effectively airplanes, subject to the same structural limitations as other aircraft, who attempt to increase their efficiency by flying in ground effect. The cost of which is a hydrodynamic hull, which is less aerodynamic and must be made stronger and heavier, as well as a shorter wing span in order to allow manoeuvring close to the surface, and these must also be strengthened to insure against water loading and corrosion. The result of which is that the disadvantages often outweigh the advantages quite considerably. Not to mention the need to fly out of ground effect in rough seas and the inherent danger of flying in ground effect in unsettled seas. The proximity of the wing tip to the sea surface during even the slightest of banked turns can be seen on the Orlyonok in Figure 2.4. This manoeuvre would clearly be impossible in rough conditions. The result has been that only the smallest WIGEs have proved viable as 'hobby craft' and even these only operate in calm waters such as small lakes and estuaries, although some have been used more recently on ice sheets.

2.3 Hybrid Vehicles

Hybrid vehicles can make use of any combination of the technologies described above, and as mentioned before, this results in a very large design space. The following is a summary of the main types of hybrid vehicle which have been analysed or built. Evidently there are many technologies, such as hydrofoils, which require some hybridisation, in this case static support while the hydrofoils are inactive. Thus hybrid in this context will refer to a vehicle which makes use of multiple technologies or mediums during cruise.

Perhaps the most common hybrid is a combination of hull and hydrofoil. As

opposed to fully foil borne craft, the hybrid versions usually support the majority of their weight on the hulls and use the foils for a combination of lift and trim angle adjustment. Many modern multihull ferries use this to achieve lower drag and smoother running.

2.3.1 WIGE and Hydrofoil

The SEABUS project [50] & [51] developed a WIGE craft concept using hydrofoils as additional lift and control surface effectors. The concept was supposed to achieve a cruise speed of 120 knots with a take-off weight of 500 tonnes and payload of 266.5 tonnes. The vehicle used hulls for static and low speed, with foils for the transition and wings for the cruise phase. The hydrofoil control effectors being left in the water in order to allow safe manoeuvring near the water surface rather than for load bearing. An initial iteration was done without the hydrodynamic control surfaces, but it was thought that the risk of impact with the water was too high and the greater forces provided by the water would be required to maintain control. The hydrodynamic control surfaces where found to provide sufficiently safe manoeuvring, however, they also increased the drag to an unacceptable level. The vehicle was hindered by the low aspect ratio wing and dramatically increased drag due to hydrodynamic friction.

2.3.2 Airlifted Catamaran

Allenstrom *et al* [52] discusses an airlifted catamaran design by Howard Harley. The design uses air blown into a hollow cavity in the rear of each catamaran hull as an air cushion. This reduces the skin friction of this part of the craft dramatically, but at the cost of extra installed thrust for the fans. Allenstrom claims that the

air lifted catamaran requires only 20% of the power of a conventional catamaran, which is considerable achievement. In essence this design can be thought of as a pair of long thin SES ships in catamaran formation, but without any skirting. Replacing the front skirt with a wave piecing hull is certainly an advantage in rough seas but the extra surface area will result in greater skin friction. This design has the stability and rough sea advantages of a catamaran but with lower resistance. An SES ship would suffer more in head swells but has greater efficiency and speed.

2.3.3 Dynamic PAR

A Russian design of vehicle discussed in [53], called Transport Amphibious Platforms (TAP) uses a catamaran formation with a tail flap on the upper deck. Air from the thruster engines is channeled into the cavity in the manner of the PAR technology discussed above. The air trapped acts as an air cushion and this allows the vehicle to operate like an SES with the side hulls in contact with the water and the flap forming the semi seal at the back. The craft is said to have amphibious qualities, however, this requires full thrust from the engines, and since the hulls and flap are rigid the ground must necessarily be very smooth to avoid causing damage to both the hull and ground surface. Sandy beach landings should be perfectly possible though. Again, the rigid rear flap could cause problems in waves if they impact and this may result in the need to rase the flap and lose much of the pressure. One of the big advantages is the lack of front skirt. This not only eliminates the impact on waves (accepting the potential rear flap problems) but also allows one of the larger components of SES drag to be put to good use. That is, the air pressure that builds up on the front of the skirt of an SES and causes drag (due to the typically square fronted design of an SES to accommodate the skirt) can instead cause stagnation or ram pressure between the hulls and aid the lift

force. This does not reduce this component of drag as such, since the momentum of the air is still changed, however, it does make better use of the pressure since some lift is generated along with the drag.

This concept is also discussed by Liang *et al* in [54] where the author refers to vehicles using a combination of a small wing-like wetted deck (being the underside of any suitably shaped multihull) with rigid side hulls as 'Dynamic Air Cushion Wing In Ground effect craft', or DACWIG. The vessel championed in the paper is a trimaran and has amphibious qualities in the same manner as the TAP craft. Again the author notes the difficulty of achieving static hover with such large air gaps and the resulting increase in installed power that is required. However, the author pays more attention to the WIG effects of the craft at speed. Since the air cushion is trapped by a highly deflected trailing edge flap, it is likely that this is ram air pressure more than actual wing effects, especially in the case of the TAP where the upper profile is far from aerodynamically optimised for lift.

2.3.4 Aerodynamic Alleviation of Planing Craft

Ekranocats, from the French word 'Ekranoplan' and catamaran, refer to the use of a wing-like structure to join the hulls of a catamaran. The name was proposed by Doctors [55], but the concept has been suggested elsewhere, as in [56]. These vehicles do not use any engine thrust to trap or channel air, only the forward motion of the vessel is used to generate lift. Doctors proposed a catamaran, whilst Walker *et al* [56] and later Matveev *et al* [57] suggest using a trimaran. The theory is quite simple. As the boat speed increases the wing generates lift which alleviates the hulls and reduces hydrodynamic drag at the expense of the far smaller aerodynamic drag. This theory is perfectly sound, however, it has been difficult to propose a vehicle to provide sufficient aerodynamic lift at realistic

speeds, especially since the wings are very low aspect ratio. As McKesson points out in [11], if stagnation pressure could be achieved for a vehicle of comparable size and footprint to a 6000 tonne SES it would have to be travelling at around 200 knots to achieve total air support. A lively speed indeed for a 6000 tonne ship, but even SES ships do not usually run on full air support and can achieve significant drag reduction at much lower cushion pressure ratios, although around eighty percent air lift seems to be the best for most air cushion type vehicles [5] & [27]. The ekranocat design has some distinct advantages. Particularly in that it does not require any front or rear skirt, which eliminate a lot of drag and wave impact problems as well as not needing any extra engines to provide PAR style thrust. This means that any aerodynamic lift created by fairing the deck area into a wing shape is effectively free, since the profile drag should be much the same, and indeed may even be reduced. Tunnel hull racing boats have effectively been using this principle on a smaller scale for some time [37] & [58]. It is to be noted that they can achieve very high speeds, the world record being over 275 knots, but even at much lower speeds the aerodynamics can be significant and boats can become fully airborne at speeds closer to 100 knots.

On a slightly larger scale the KUDU II [8] is an 11 m long 4 m wide twin hull ram wing planing craft capable of speeds as high as 85 knots, with open ocean cruise speeds of around 69 knots. This speed is only achievable through considerable amounts of aerodynamic alleviation from the ram wing joining the hulls.

An interesting report is given by Hockberger [4] who describes the performance of a quadrimaran ship with aerodynamic lift capabilities. The vessel's four hulls shown in Figures 2.5 and 2.6 are almost identical and form three channels along the wetted deck. Conventional wisdom would most likely lead to a dismissal of such a design as it appears to have an unnecessarily large surface area. Indeed both Doctors [20] and Tuck [21] argue that fewer hulls are almost always preferable.

The quadrimaran, however, produced some interesting results. Along with its natural stability provided by the relative width of the vessel it has additional stability from the time averaged effects of the hulls. This being caused by the hulls sitting atop a variety of wave peaks at any one time without descending into the troughs. Furthermore, the hulls are designed to create dynamic lift and as such, much of the hull area is lifted from the water, significantly reducing the wetted area drag. The most remarkable aspect however, was unanticipated and is due to aerodynamic effects of the hulls.

It was found during trial runs of the 17.5 metre test model "Alexander" that at full throttle the ship would go noticeably faster into a strong head wind. From this it was realised that the air flow between the hulls was actually creating a ram wing effect and lifting the hulls. Reports from riders who lay down near the bow suggest that a visible depression caused by the air pressure could be seen, and that this actually helped not only to reduce frictional resistance by lifting the vessel out of the water, but also helped to dampen the motion in rough seas. It is also claimed to have reduced the wash height and thus, the wave drag.

Unfortunately, the test model Alexander was used as a demonstrator and not as a proper test model, meaning that although reports are generally consistent they must be read with caution. For example, some speeds were calculated by riders who measured approximate distances and timed them on their wrist watches.

Further testing was done of a scale model at the Bassin d'Essais des Carenes and the Institute Aerotechnique de Saint-Cyr in Paris which provided promising results for both the tow tank and wind tunnel tests. There may, however, have been problems with scaling effects as the report suggests that the model sat much lower in the tow tank than Alexander had at sea.

The results from the tests are shown in Figure 2.7 as calculated for a 56 metre

Quadrimaran with a full load displacement of 270 tonnes. It is interesting to note the dramatic increase in aerodynamic lift at higher speeds. It can easily be seen how such an effect would be overlooked for ships of less than thirty knots; but Alexander was able to reach 60 knots and at this speed, the contribution is considerable. It is also worth noting that although the wetted deck was raised slightly to allow more air into the ducts (and there is no mention of whether this had a beneficial effect) no modifications were made to the hull shapes. As they where originally designed purely for hydrodynamic purposes, it is perhaps fair to assume that improvements from a purely aerodynamic aspect can still be made.

The problem of scaling effects has been the subject of much controversy for the Quadrimaran team and until better model tests are conducted the results are given tentatively. They are currently estimating that the aerodynamic effects will decrease with size while increasing with speed. Thus a larger ship would need to travel faster to derive the same benefits.

Figure 2.5: View of hulls and wetted deck [4]

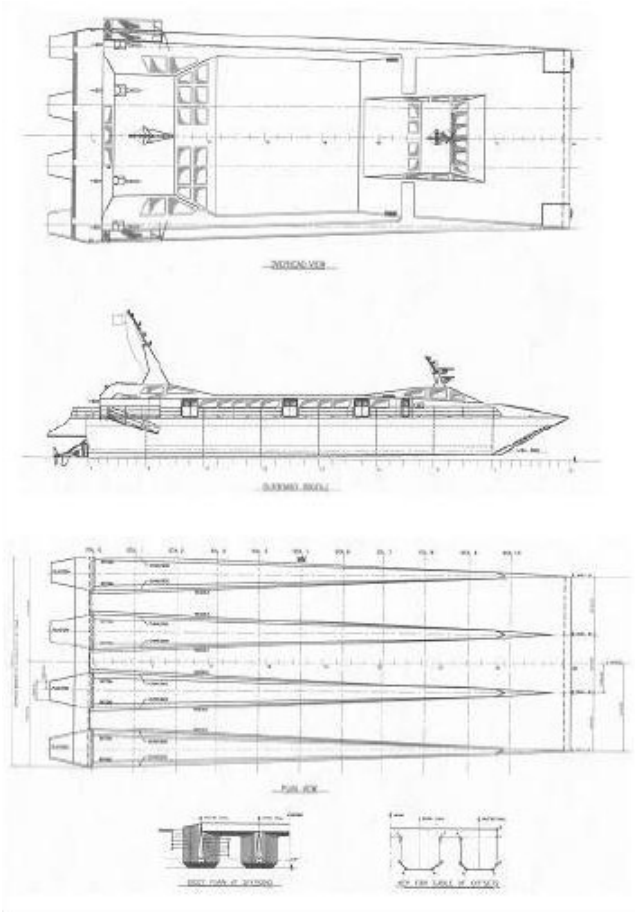

Figure 2.6: 56 metre Quadrimaran ferry [4]

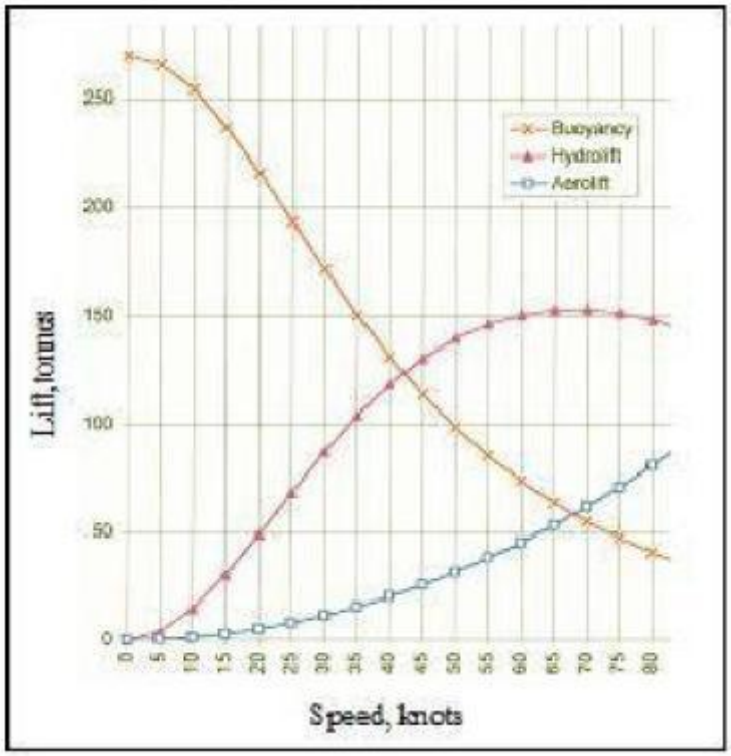

Figure 2.7: Lift curve for 56 metre Quadrimaran [4]

2.4 Proposed Configuration

The most significant problem for high-speed sea-lift vehicles is the dramatic increase in hydrodynamic drag at speed. The aim of all of the technologies discussed above is to reduce the wetted area of the craft for a given loading and it is for this reason that the WIGE craft, having no contact with water during cruise, look so good in theory. In practice it is very difficult to realise this potential. As discussed earlier, the problems of flying close to the water, combined with danger from waves as well as structural and power requirements during take-off often result in an unsatisfactory design. On a more practical front, ACVs have demon-

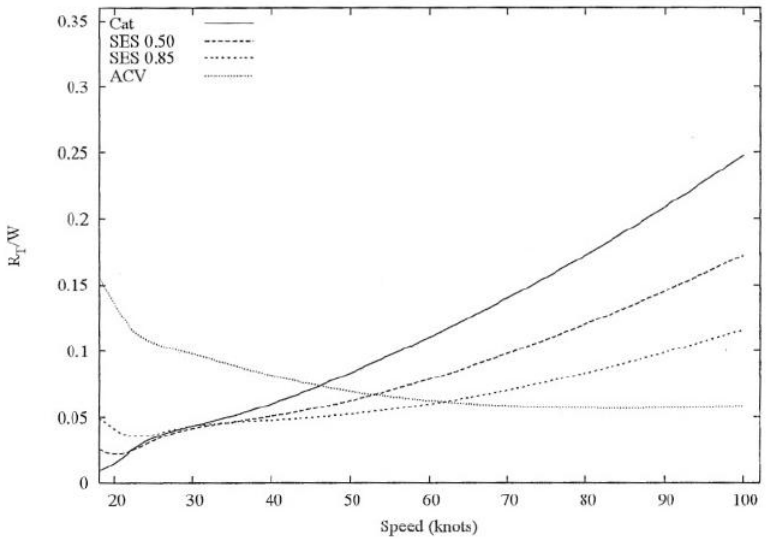

Figure 2.8: Resistance-to-weight ratio as a factor of speed for theoretically optimal vehicles. From Lazauskas [5]

strated some excellent progress using aerostatic alleviation, particularly the SES whose planing hulls allow for better stability and rough sea performance.

Lazauskas [5], devoted an entire thesis to the comparison and optimization of a selection of standard marine vehicles and concluded that the optimization was entirely dependent on the use, that is, the speed, size, range and payload of the vehicle. He states that for a seventy five knot design the only feasible answer is the air cushion vehicle or SES, with both catamaran and trimaran designs unable to carry enough fuel (let alone cargo) to complete the required 1000 km voyage. However, at lower speeds the catamaran and trimaran are significantly better. Figure 2.8 shows the resistance-to-weight ratio as a function of speed for the various optimised vessels. It should be noted that the SES 0.50 and SES 0.85 have a cushion support, as a fraction of their total weight, of 0.50

and 0.85 respectively. Equally, the catamaran and ACV are effectively at zero and 100 percent cushion pressure, being equivalent to an SES 0.00 and SES 1.00 respectively. The graph clearly shows the cross over point at forty to fifty knots where air cushion, or other hybrid vehicles, become advantageous in comparison to standard sea-lift vessels. More importantly however, it shows the clear potential for a hybrid vehicle capable of changing its lift fraction with speed. Consider the line of least resistance through the graph. This would begin as a catamaran up to around thirty knots, at which point all of the planing hull vehicles have a similar resistance. Up to 50 knots there is a need for some cushion pressure, with 0.85 being best, but 0.50 still better than a complete ACV. Beyond seventy knots the ACV is the best vehicle and the resistance decreases in proportion to the amount of cushion support. Evidently, a vehicle capable of increasing its cushion support with forward speed, in proportion to the values described above, would have a significant advantage. Such a vessel being able to compete at all speed ranges with all current vehicles, whilst out performing most vehicles, most of the time.

The ideal situation would seem to be a compromise between the SES and WIGE as described by Doctors [55] among others and discussed above. Potentially, an ekranocat can perform at cruise with the same characteristics as an SES, having around eighty percent of its weight supported aerodynamically and twenty percent hydrodynamically. In this configuration however, there would be no need for extra lifting fans, no skirt drag or wave slamming and a significantly improved aerodynamic profile. Such a design could potentially prove both more efficient and better in rough seas. The problem so far has been the poor ratio of aerodynamic to hydrodynamic forces. As McKesson points out in [11], when compared to an SES footprint a wing has to travel prohibitively fast in order to achieve the same lift forces. This finding has been confirmed by others where simple tests of standard low aspect ratio wings have been used to alleviate a theoretical hull, such as in [57] where a trimaran hull is joined by a triangular wing. However, it is suggested

that the dismissal of aerodynamically alleviated designs on such grounds is flawed on at least two counts. Firstly, the aerodynamics are poorly understood, and secondly the vehicle size and weight are assumed to be comparable to a full size displacement ship or SES.

The aerodynamics are usually based on a standard wing-in-ground effect, which for a very low aspect ratio wing is quite inefficient. In the case of Doctors [55], the wing is assumed to be two dimensional due to the 'end plate' effect of the hulls which can dramatically improve the performance of the wing. However, merely describing the hulls as end plates is a serious simplification of reality. Since the area formed by the wing and hulls is now much closer to a duct than a wing with end plates. The full shape of a wing, hulls and free surface is a considerably different problem from that of a two dimensional wing. It is worth noting that the quadrimaran [4] gained significant aerodynamic lift without any wing-like superstructure at all. Looking from this perspective it is clear that the hulls and free surface could play just as significant a role in some cases as the wing its self, and it is for this reason that the aerodynamics must be studied in greater detail. It is proposed that in the same fashion as a diffuser creates pressure, a divergent/convergent duct shaped into the space between the hulls of an ekranocat could significantly increase the lift generated.

On the second point, it is stated that although it may not be possible to create a vehicle directly comparable to an SES it may be possible to achieve similar areo/hydro load ratios at a reduced payload, or increased size. This is a problem if the larger vehicle is then less efficient, however, if the size is only necessary to aid the aerodynamic aspects, and through careful structural design, results in little extra weight, the vehicle may still perform better for the same payload despite an increased 'foot print'. It is much the same as considering the extra 'size and weight' of adding wings to an aeroplane fuselage. Indeed it is not necessary for

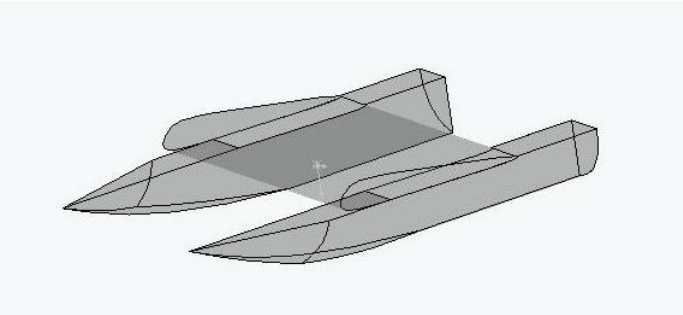

Figure 2.9: An aerodynamically alleviated catamaran configuration

the aerodynamics to achieve the full eighty percent of the total vehicle weight for the vehicle to experience improved performance. Furthermore, unlike an SES the aerodynamics improve with speed, meaning that it may be possible that there is a knock on effect, in that although a vehicle may only be expected to reach a speed of fifty knots, at which point the aerodynamic loading may only be a few percent. This few percent may allow the vehicle to travel faster and thus attain further aerodynamic loading.

As ship speeds increase and many high-speed multihulls reach speeds beyond forty knots, an understanding of the effects of aerodynamics on such vessels, and indeed the potential benefits that can be derived from lift generation are becoming increasingly important. It is the purpose of this thesis to concentrate on the aerodynamics of ducted hulls for high-speed marine vehicles and the advancement of future hull design. Figure 2.9 shows an aerodynamically alleviated catamaran concept, such as the one proposed by Doctors [55]. It is the aim of this work to study the reality of such aerodynamic designs, being a ducted hull shape, as opposed to a simple wing-in-ground effect as it has been portrayed in the past. In particular, the effect of the side hulls needs be accounted for and the potential for beneficial 'diffuser' effects should be studied.

2.5 Methodology

The aerodynamically alleviated catamaran configuration will be studied using a simplified method at first. Initial analysis will focus on considering the bound area between the hulls and cross deck as a duct, so that an estimate of the available lift can be made. The drag of the craft will then be analysed to estimate the potential benefits of aerodynamic alleviation and the case for continuing the research. The research will then develop to study the effect of varying hull geometry in two dimensions, observing the effect of the side hulls on the pressure within the duct. The approach will start with simplified analysis so that a wider field of knowledge can be used to estimate the appropriate design for more complex three dimensional analysis of the complete aerodynamic hull performance. This data will then be used to determine the affect of aerodynamic loading on the total drag of a theoretical vehicle.

Chapter 3

FLOW MODELING IN DUCTED HULLS

It is proposed that the vessel be analysed by forming a simplified lift and drag model from which the various components can be studied and expanded to greater accuracy as required. Thus, a characteristic Mach flow analysis will be used in combination with a skin friction estimation using a drag coefficient and the ITTC line for the air and water respectively. This analysis is intended to highlight the potential performance of ducted-hull ship geometry as an alternative to simple wing shapes.

3.1 Characteristic Mach Calculations

Due to the lack of research in this area it is perhaps wise to begin with a simplified analysis of the problem in order to ascertain the potential of such a scheme and hence, whether it is likely to warrant further investigation.

As a first effort, the author proposes to calculate the lift force through the duct of a multihull vessel due to the changing area of the captured stream tube using

the thermodynamic equations for a calorifically perfect gas.

The flow field is evaluated with reference to the free stream conditions and the conditions at the characteristic Mach flow for a given stream tube. It should be noted that although the equation is referenced to conditions at Mach 1, the equations are not limited to high speeds and remain valid for all values below this.

The characteristic flow conditions at $M_m = 1$ and hence $U_m = a_m = \sqrt{\gamma R T_m}$ define the conditions in the rest of the stream tube.
The total pressure for the stream tube is calculated as:

$$P_0 = P_\infty \left(1 + \frac{\gamma - 1}{2} {M_\infty}^2\right)^{\frac{\gamma}{\gamma - 1}} \tag{3.1}$$

And hence the static pressure at Mach conditions is calculated as:

$$P_m = \frac{P_0}{\left(1 + \frac{\gamma - 1}{2}\right)^{\frac{\gamma}{\gamma - 1}}} \tag{3.2}$$

Thus, using the pressure ratios, the characteristic density and temperature can be calculated.

$$\rho_m = \rho_\infty \left(\frac{P_m}{P_\infty}\right)^{\frac{1}{\gamma}} \tag{3.3}$$

$$T_m = T_\infty \left(\frac{P_m}{P_\infty}\right)^{\frac{\gamma - 1}{\gamma}} \tag{3.4}$$

Therefore, from the continuity equation, the Mach area can be calculated as:

$$A_m = \frac{A_\infty U_\infty \rho_\infty}{U_m \rho_m} \tag{3.5}$$

The Mach number of the stream tube at point x can be evaluated from the ratio

of the area at point x to the characteristic Mach area from the following equation:

$$\left(\frac{A_x}{A_m}\right)^2 = \frac{1}{{M_x}^2}\left[\frac{2}{\gamma+1}\left(1+\frac{\gamma-1}{2}{M_x}^2\right)\right]^{\frac{(\gamma+1)}{(\gamma-1)}} \tag{3.6}$$

This equation is not easily turned inside out. However, it can be solved for M_x from the known values of A_x and A_m using a Newton-Raphson iterative approximation method, which yields results accurate to a few decimal places in three or four iterations.

The values of M_x can then be used to evaluate the static pressure along the duct:

$$P_x = \frac{P_0}{\left(1+\frac{\gamma-1}{2}{M_x}^2\right)^{\frac{\gamma}{\gamma-1}}} \tag{3.7}$$

Thus, if the variation in tunnel area is known as a function of x, then via equations (3.6) and (3.7) $P_x = f(x)$
Taking the variation in tunnel area as a function of x only, the duct can be modelled as a roof of height h_x with a constant unitary width bound by walls of zero thickness.

A suitable duct may be described by:

$$h_x = -0.04(x-5)^2 + 2 \tag{3.8}$$

This is illustrated in Figure 3.1. The pressure may now be evaluated at any point in the duct. However, due to the need to perform a set of Newton-Raphson approximations for each calculation, the process can become laborious. For the present work the pressure has been evaluated at ten evenly spaced stations from the inlet to exit which have been used to find a trend curve and hence approximate equation. From manipulation of equation (3.6), it can be seen that a sixth order

polynomial should give an accurate description of the results and this has been applied to the graphical results of $P_x = f(x)$.

Thus, the total pressure along the duct can be calculated from the trend line function as:

$$\sum P_x = \int_0^{10} f(x)dx \tag{3.9}$$

A scaling factor can be added to equation (3.9) to expand it from unit length to the desired length L.

Hence, the resultant force per unit area can be calculated for a 2D section by subtracting the atmospheric pressure above the duct from the internal duct pressure. This in turn can be multiplied by the width B to give the resultant force F for the full duct, hence:

$$F = \frac{LB}{10}\left[\left(\int_0^{10} f(x)dx\right) - P_\infty\right] \tag{3.10}$$

3.1.1 Model Geometry

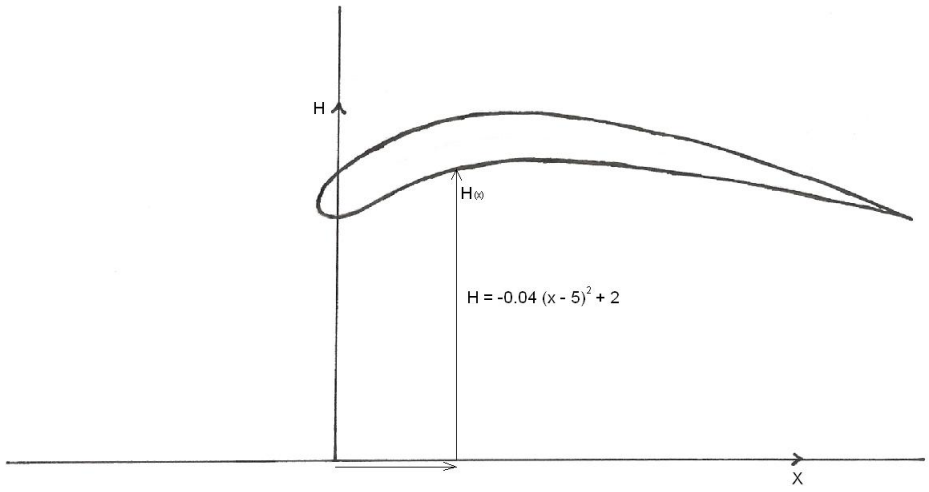

Figure 3.1: Model geometry

3.1.2 Lift Results

The calculated lift results from a simple streamtube analysis.

Comparative speed vehicle			Presented tunnel section					Standard catamaran				
	Mach no.	U in Knts	U in Km/h	Length	Width	Force KN	Tonnes	Length	Width	Force KN	Tonnes	
	0.015071	10	18.52	10	10	0.99364	0.101288	10	10	-2.0351	-0.20745	
				100	10	9.936448	1.01289	100	10	-20.351	-2.07452	
				100	100	99.36448	10.1289	100	100	-203.351	-20.729	
High speed ferry such as Condor	0.060283	40	74.08	10	10	14.86547	1.515338	10	10	-40.4999	-4.1284	
				100	10	148.6547	15.15338	100	10	-404.999	-41.2843	
				100	100	1486.547	151.5338	100	100	-4049.99	-412.843	
Proposed design speed	0.105495	70	129.64	10	10	46.11368	4.700681	10	10	-125.815	-12.8252	
				100	10	461.1368	47.00681	100	10	-1258.15	-128.252	
				100	100	4611.368	470.0681	100	100	-12581.5	-1282.52	
Seabus-hydaer project concept	0.150707	100	185.2	10	10	95.94853	9.780686	10	10	-266.348	-27.1507	
				100	10	959.4853	97.80686	100	10	-2663.48	-271.507	
				100	100	9594.853	978.0686	100	100	-26634.8	-2715.07	
Current world water speed record	0.376768	250	463	10	10	634.5285	64.6818	10	10			
				100	10	6345.285	646.818	100	10			
				100	100	63452.85	6468.18	100	100			
Ekranoplan	0.452122	300	555.6	10	10	940.1616	95.83706	10	10			
				100	10	9401.616	958.3706	100	10			
				100	100	94016.16	9583.706	100	100			
Boeing 747	0.783678	520	963.04	10	10	3751.672	382.4334	10	10			
				100	10	37516.72	3824.334	100	10			
				100	100	375167.2	38243.34	100	100			

Table 3.1: Table of results

3.2 Simplified Drag Evaluation

An estimation of the total drag D_T for a hybrid aero/hydrodynamically supported craft can be calculated as follows:

$$D_T = D_{Va} + D_{induced_a} + D_{Vw} + D_{Wh} + D_{Wac} + D_{induced_w} \tag{3.11}$$

However, for the present evaluation, this will be reduced in order to apply simple methods to the most significant factors.

For most modern high-speed sea vessels, operating in calm water, the greatest drag component is the skin friction. This can be estimated from the ITTC line as described earlier. Although not as accurate as Grigson's algorithm the ITTC line is an industry standard and can be applied with ease.

The viscous water drag D_{Vw} can be calculated using the ITTC 1957 model-ship correlation line as follows:

$$D_{Vw} = \frac{1}{2}\rho_w U^2 C_F S_w \tag{3.12}$$

where

$$C_F = C_f + \Delta C_f \tag{3.13}$$

and

$$C_f = \frac{0.075}{(log_{10}R_e - 2)^2} \tag{3.14}$$

and

$$\Delta C_f = [111(AHR \cdot U)^{0.21} - 404]C_f^2 \tag{3.15}$$

Here AHR is the average hull roughness in μm. It is assumed to be approximately $100\mu m$ for a new ship.

A further correction can be made to allow for greater form drag by encompassing a form factor into the ITTC equation as follows:

$$C_{Fff} = (1 + k\frac{d}{d_{stat}})(C_f + \Delta C_f) \tag{3.16}$$

Where k is the form factor, d is the draft and d_{stat} is the static draft. This formula is designed to allow for the effect of aerodynamic lift on the hulls.

The hull wash drag D_{Wh} can be calculated using Michell's thin ship theory[59].

$$D_{Wh} = \frac{4\rho g^2}{\pi U^2} \int_1^\infty (I^2 + J^2) \frac{\lambda^2 \partial\lambda}{\sqrt{\lambda^2 - 1}} \tag{3.17}$$

Where

$$I = \int\int_H \eta_x(x, z) e^{\frac{\lambda^2 gz}{U^2}} \cos\left(\frac{\lambda g x}{U^2}\right) dxdz \tag{3.18}$$

and J is a similar integral involving *sine* instead of *cosine*. H in this case refers to integration around the hull.

However, the drag contribution of hull wash for a suitably thin hull should be very small in comparison to the other terms and is ignored at present for the sake of brevity.

The viscous air drag D_{Va} can be calculated using the well known formula:

$$D_{Va} = \frac{1}{2}\rho_a U^2 C_d S \tag{3.19}$$

Where C_d is the coefficient of drag for the hull exposed to air.

The internal air drag is a different matter, since it is affected by the change of momentum of the air in the diffuser as well as the viscous drag along the wall.

The diffuser drag D_D, or air drag through the duct, is calculated from[60] by using empirical data to predict the total pressure loss along a diffuser. D_D is effectively part of D_{Va} but is calculated separately because equation 3.19 is not designed to cope with momentum losses from ducts.
The process involves the estimation of a pressure loss coefficient C_{pr} from graphical results accounting for duct size, shape, inlet conditions and angle of expansion. The value of C_{pr} is then used to find the total pressure loss coefficient K_t and hence change in momentum and resultant force as follows.

$$K_t = 1.04 \left[1 - \left(\frac{A_1}{A_2} \right)^2 \right] - C_{pr} \tag{3.20}$$

from which total pressure at the exit is calculated via:

$$K_t = \frac{P_{t_{in}} - P_{t_e}}{\frac{1}{2}\rho U_{in}^2} \tag{3.21}$$

and the exit velocity (where α is a turbulence velocity profile factor) is found from:

$$P_{t_e} = P_\infty + \alpha \frac{1}{2} \rho U_\infty^2 \tag{3.22}$$

thus the force is:

$$F_{drag} = \dot{m}(U_e - U_{in}) \tag{3.23}$$

The wash drag from the air cushion D_{Wac} can be calculated from the sum of the free surface pressure distributions through the diffuser by approximating the distribution as a set of regular rectangular areas assumed to have the local average value, see Tuck[61]. However, at higher F_n the wave drag is significantly decreased because the air cushion effectively planes. For such high speed vehicles as ekranocats the sea surface is assumed to be perfectly flat, representing an infinitely high F_n. For the following calculations this condition will be assumed in order to simplify matters.

3.2.1 Combined Lift and Drag Results

Figures 3.2 to 3.4 show graphical results for a 100 m long by 50 m wide duct:

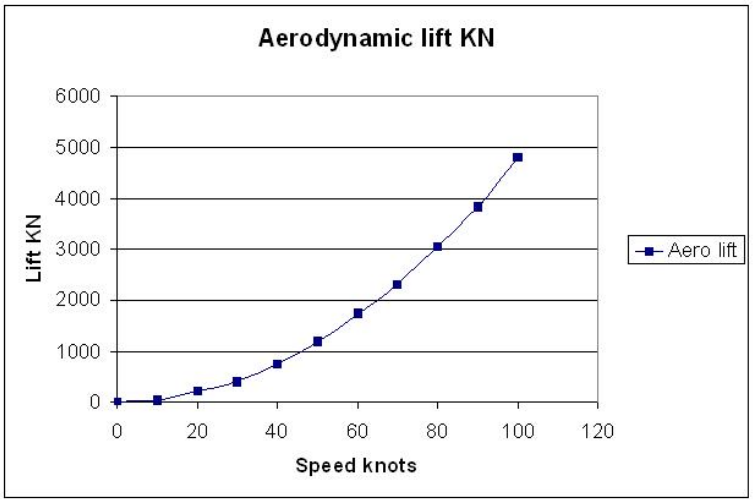

Figure 3.2: Aerodynamic lift

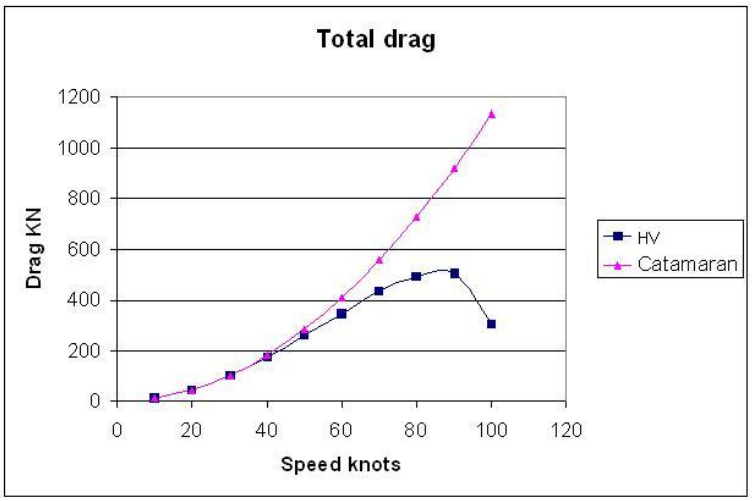

Figure 3.3: Total drag comparison

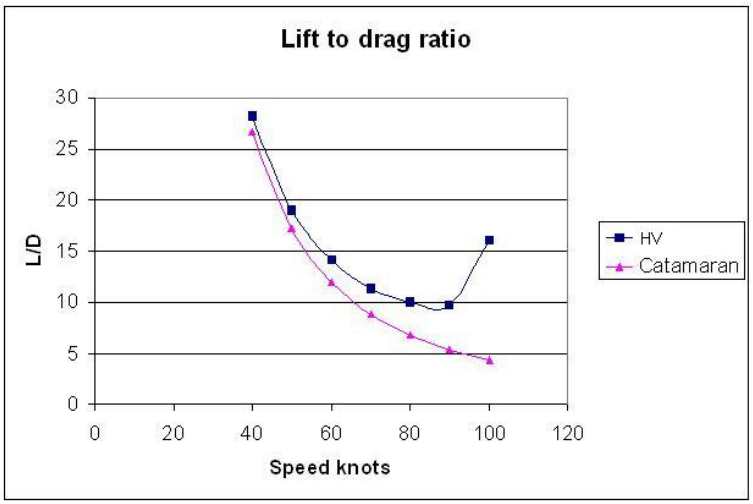

Figure 3.4: Lift-to-drag ratio

3.3 Discussion of Results

The results presented in Figures 3.1, 3.3 and 3.4 form an approximate evaluation of a simplified dynamic air cushion vehicle. They show a proportional relationship between the change in stream tube area, the free stream Mach number and the local static pressure. It can be seen that with an increase of duct area along the hull length there is a significant pressure change and hence resultant force along the duct. This effect is only in the order of a few tonnes or less for small or slow moving vehicles (below 10 knots) however at higher speeds and larger areas the force rapidly increases. For a duct area ratio of 1:2:1 (inlet:middle:outlet) at 40 knots and an upper surface area of $L = 100$ m and $W = 10$ m the lift increases to 15 tonnes, which is not an insignificant load. Furthermore, for the same conditions but with a $W = 100$ m, the lift is 150 tonnes. It must be noted that no attempt to account for the scaling effect from the value of W has been incorporated, thus consideration must be given to the effect of hull separation on the effective lift produced. At very high speeds, such as those of an ekranoplan or cargo jet, the lift

for a large vehicle is in the order of thousands of tonnes. Such speeds, however, are perhaps unrealistic and assumptions for the conditions inside the duct are most likely invalid.

Due to the one dimensional approach, the change in area of the duct appears quite large in the illustration shown in Figure 3.1. It should be noted that this change in area can be spread among the three walls and in some part to the deflected curve of the sea surface caused be the pressure. This makes the walls curve significantly more gently than illustrated and suggests that there would be minimal risk of flow separation.

It is also important to note that the standard catamaran hull presented assumes an area change of 2:1:2 which may be much larger than on many catamarans. However, it is an underestimate for some sea-piercing multihull designs. For this model it is seen that the decrease in duct area causes the flow to speed up and hence, decrease the static pressure resulting in a net down force to the vessel. It is calculated that at 40 knots a $L = 100$ m by $W = 10$ m vessel has 40 tonnes of induced weight from the pressure distribution through the hull. At speeds of over 100 knots the flow in the duct reaches Mach 1 and the approach used fails (N.B. results can be calculated but the automated process used cannot cope with the second solution obtained at Mach numbers higher than 1 in a convergent-divergent duct). However, it is clear that the high velocity flow causes extremely low pressure to form in the duct giving negative lift. This would also lead to high viscous friction along the duct walls.

Although the method presented is simplified to a quasi-one dimensional state in which the flow over the top of the duct is considered to retain free stream conditions, it is predicted that by shaping the top of the duct into a suitably aerodynamic shape such that the upper deck has a cross section similar to a highly cambered airfoil such as a NACA 6406 the pressure above the duct would be de-

creased and the resultant lift increased. Furthermore the effective angle of attack caused by the wing shaped deck would provide an increase in streamtube area from the free stream before entering the duct. This would invalidate the assumption that inlet conditions are free stream conditions but it would actually result in an increased pressure under the wing and hence more lift. Thus, significantly greater lift values can be achieved when the result of shaping the upper deck into a wing-in-ground effect airfoil is included into the calculations.

The drag results show a promising reduction in skin friction as the vessel is lifted from the water. Since this is the largest contribution to friction, the results for a standard catamaran compared to a hybrid vehicle (Figure 3.3) show a marked deviation at higher speeds.

There are, however, many simplifications made during the calculations which must be addressed. Perhaps the most important is the effect of the air cushion wave drag. Although the Quadrimaran team found the air cushion to provide a damping of motion and reduction of the wake size, it is not safe to assume that this is the case. For many air cushion vehicles, the wave drag is very significant and it could be that the hull waves and air cushion interfere to produce a formidable resistance. Without more detailed investigation, any beneficial effect must be ignored and the possibility of added drag may not be ruled out.

Also of concern are the scaling effects and turbulent energy losses. Although the method used from [60] accounts for some effects of separation, turbulence and scaling, from which the maximum divergence of the duct was selected, it cautions against overconfidence in results from turbulent transition areas. That is to say that it is hard to predict the onset of turbulence for multiple conditions. With the assumption that the free surface has not disrupted the inflow, and having increased the duct to a size far beyond the experimental range, the results must be regarded with caution.

The method presented clearly shows that favourable pressure distributions and reduction of drag can be achieved through suitably designed ducted hull geometry. Furthermore, it has been demonstrated that failure to take these effects into consideration with modern high-speed multihull design can result in significant additional dynamic loading, and hence increased wetted area drag at the top of the speed range. Further work must be done however, to provide a more conclusive analysis.

Chapter 4

2D POTENTIAL FLOW BASED APPROACH

4.1 Introduction

For the present chapter it is intended that only the aerodynamics of the hulls will be considered. In order to acquire a better understanding of the flow properties through a ducted hull, some simple two dimensional models will be simulated using potential flow theory. The simplification of the problem into two dimensions is not ideal as the flow is inherently three dimensional. However, a combination of the scarcity of information regarding such flows and a need to test the applicability of these methods to varying shapes makes it necessary to use a simple method at first.

Initially the properties of various hull shapes and the effect of their spacing on pressure distribution will be studied by means of panel codes. A description of the methodology is presented below.

4.2 The Panel Method

Panel methods, first used by Hess and Smith [62] are an extension of potential flow, which is itself a form of field theory, as described by Newton [63]. The principal of potential flow is to define a flow field in terms of the effect of constant strength sources, the influence of which are dependent on the distance from which they are observed. An excellent description of potential flow is given by Kellog [64]. By manipulation of the position and strength of the sources, it is possible to create flow fields which resemble real world flows, such as that about a wing. Simple forms such as the Rankine oval can easily be managed with pure potential theory. For more complex geometry however, a numerical panel method is required. Descriptions of the formulation and implementation of panel codes can be found in 'Low-Speed Aerodynamics' by Joseph Katz [6] and much of the code used in the following section is developed from programs described in his book.

In order to calculate the flow about an arbitrary body using potential flow, the body geometry is discretized into flat or curved panels which can be treated individually. Each panel represents a distribution of either source or vortex singularities, which can be combined. If a source and sink are brought together, they form a recirculating flow called a doublet.

As a result of the flow being inviscid, an artificial circulation must be added to the flow in order to recreate the Kutta condition at the trailing edge. The Kutta condition is the observation that the flow over a foil section always leaves the trailing edge at an angle equal to the bisect of the angles at the trailing edge. This assumption is true for streamlined bodies at moderate angles of attack; but it becomes invalid if flow separation occurs. To achieve this, it is necessary to use either doublets or vortex panels where the strength of circulation can be calculated to meet the Kutta condition.

The degree of accuracy achieved with panel codes can be increased by using a larger number of smaller panels and by using more sophisticated singularity distributions. However, this is done at the cost of additional programming effort and computer run time. It is thus desirable to find the simplest method appropriate to the situation.

The simplest method used for wings is the constant strength doublet panel, which produces reasonable results for a single wing at a low angle of attack. This method is less appropriate though for off body calculations due to each panel being equivalent to a pair of discreet vortex elements placed at either end of the panel.

The panel method can be universally described as the solution of a set of panel source strengths, such that the combination of the free stream flow and the panel flow, are zero perpendicular to the panel. That is, the strength of the panel is solved by ensuring that there is no flow normal to the body surface. This can be described mathematically in general terms as follows:

$$U_{\infty,n} + U_n = \frac{\lambda_i}{2} + \sum_{j=i}^{n} \frac{\lambda_j}{2\pi} \int_j \frac{\partial}{\partial n_i} (\ln r_{ij}) ds_j + U_\infty \cos \beta_i = 0 \tag{4.1}$$

where r_{ij} is the distance from panel i to panel j. This equation can be solved to find the required source strength λ_j for each panel in turn. This is achieved using colocation points, where each panel, or unknown source strength, is calculated in conjunction with a colocation point placed at the centre of the panel. This allows accurate calculation of the flow properties at the collocation point; but it does not account for the flow to either side of it. In the case of a doublet panel this can be misleading as the flow is concentrated at the ends where there is in effect a vortex. As a result, the flow is calculated correctly at the collocation points; but tends to fluctuate between them as shown in fig 4.1. This causes a problem

if the off body velocities are required, or if two bodies such as a wing and aileron or the hulls of a boat, are modelled close together.

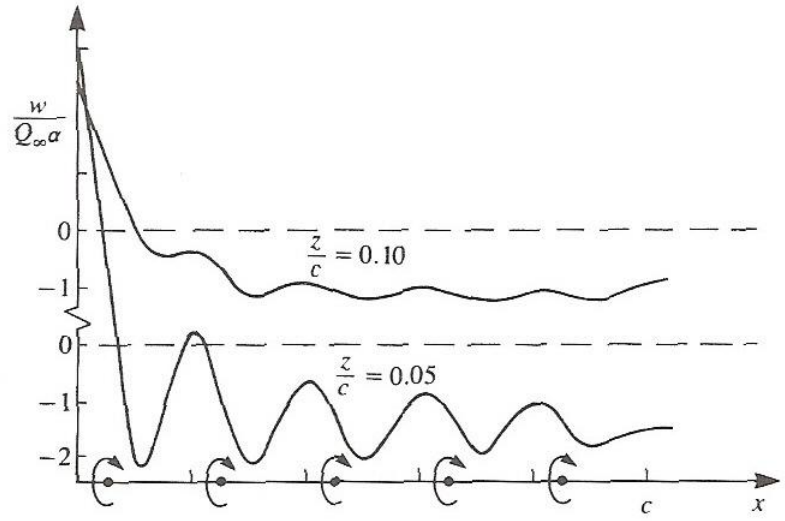

Figure 4.1: Calculated flow between discrete doublet points in potential flow. Reproduced from [6]

This problem can be smoothed by using a greater number of panels, but as mentioned above, this requires more computational time. Alternatively a more sophisticated singularity distribution can be used. The use of constant strength vortex panels would alleviate this problem to some extent because each panel has a continuous distribution of vortices rather that a single vortex at either end and thus less of a potential jump as the flow passes from one panel to the next. The constant strength vortex panel method is slightly harder to implement than the doublet method but should yield more accurate results.

4.2.1 Description of Constant Strength Vortex Code

The constant strength vortex method, as with any panel method, may be broken down into discreet stages for the purpose of implementation. The first stage is the definition of the geometry and requires that the shape be discretized by a finite number of points placed around the body. In general they are not evenly spaced and form a concentration around areas of interest or irregularities, such as the leading and trailing edges or a discontinuity on the surface. These points are read into the computer program (MATLAB 7.1); from which the start and end points of the panels are calculated and the associated panel angle. A collocation point is then assigned to the center of each panel and the geometry is fully defined.

The next step is to determine the influence coefficient matrix. This is the effect that each panel has on every other panel in the calculation. Thus n panels produce an n by n matrix representing the individual effect that each panel has on all of the other panels and itself. This influence coefficient is based entirely on geometry and is independent of the panel's strength.

Once the matrix is formed, the potential flow at any point, such as a collocation point, can be specified in terms of the geometry, which is specified via the influence coefficient and the panel strength γ. The flow at the collocation point, normal to the panel can thus be defined as the sum of the contributions from all of the panels plus the free stream. This can then be equated normal to the panel and set to zero in order to define a no flow condition through the panel surface.

Thus the problem is reduced to a set of linear algebraic equations in the form of a matrix, depicted in Figure 4.2. The solution to which can be found by solving for the inverse and multiplying by the right hand side. Where the right hand side represents the contribution due to the free stream.

$$\begin{pmatrix} a_{11}, & a_{12}, & \ldots, & a_{1N} \\ a_{21}, & a_{22}, & \ldots, & a_{2N} \\ \vdots & \vdots & & \vdots \\ a_{N1}, & a_{N2}, & \ldots, & a_{NN} \end{pmatrix} \begin{pmatrix} \gamma_1 \\ \gamma_2 \\ \vdots \\ \gamma_N \end{pmatrix} = \begin{pmatrix} \mathrm{RHS}_1 \\ \mathrm{RHS}_2 \\ \vdots \\ \mathrm{RHS}_N \end{pmatrix}$$

Figure 4.2: Matrix of influence coefficients for solving potential flow. a is the influence coefficient, N is the number of panels, γ is the vortex strength and RHS is the right hand side, which represents the contribution from the free stream. From [6]

In order to simulate the Kutta condition an additional consideration must be made to specify the flow leaving the trailing edge. This is achieved by setting the circulation at the trailing edge to zero, that is, the influence coefficients must produce a zero value of γ at the trailing edge. This is achieved by adding a further equation to the matrix which specifies the values at the trailing edge and a stagnation point via a zero value for the right hand side and a coefficient of one on the two trailing edge panels, with all others set to zero. This additional equation renders the matrix uneven and hence, unsolvable. The solution is therefore to remove one of the existing equations in order to produce a square matrix again. The choice of which panel to discount is tricky and some trial and error is necessary to check that the choice is not affecting the results. However, it is usual to use a panel situated on a flatter part of the surface such as mid way along a wing, where the flow is quite linear.

In the case of vortices, the influence of a panel on itself is zero, this produces a zero diagonal throughout the matrix. A pivoting scheme of some form is thus required to prevent the division by zero during a Gaussian style solution.

Once the matrix is solved and the values of γ are found, the velocities around the body surface can be calculated as well as the corresponding pressure coefficients.

4.2.2 Results from Constant Strength Vortex Panel Method

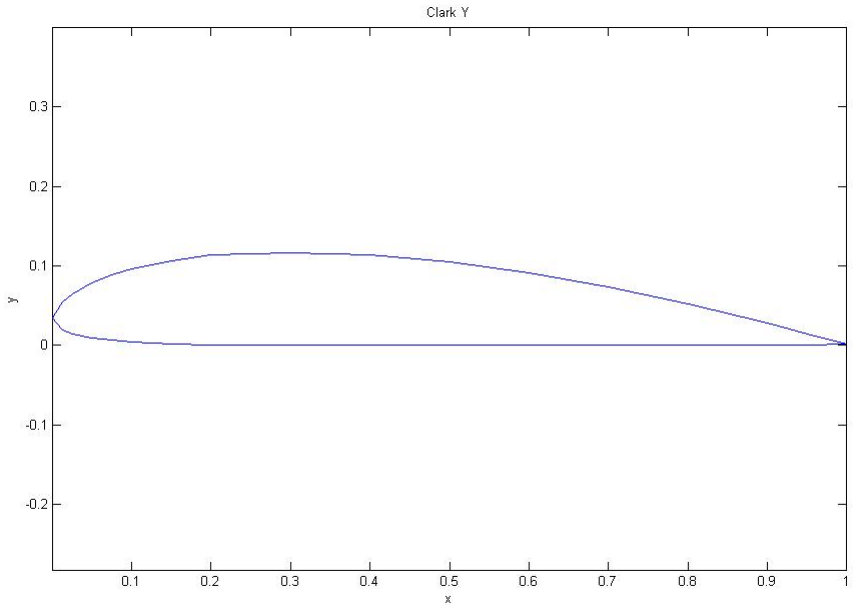

Figure 4.3: Clark Y foil shape.

A set of shapes, shown in Figures 4.3 to 4.5 was tested using this method and the results for a single wing were validated against wind tunnel data for a Clark Y foil taken from reference [7], and depicted in Figure 4.3. The method was implemented with ease for a single foil shape and shown to have satisfactory results. The comparison with wind tunnel results for a Clark Y foil is given in Figure 4.6. The potential flow results are inviscid and hence over predict the lift, that is they neglect viscous losses as the angle of attack increases. At zero lift however, the results are very similar and this suggests that the code is functioning correctly. It must be remembered that the wind tunnel results will contain experimental errors and equally that the shape of the Clark Y foil may be slightly different for the two experiments.

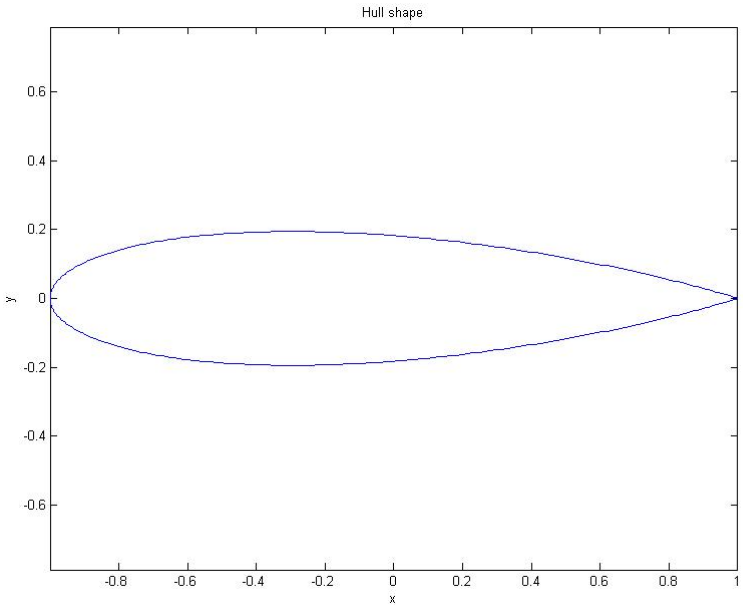

Figure 4.4: 'Hull shape', symmetric foil shape.

The adaptation of this method to the simulation of a pair of hulls requires some modifications. Firstly the geometry for the second hull must be included along with a routine to allow the hull spacing to be specified. Secondly, the matrix must be expanded to include the new coefficients. This involves making the matrix four times greater in size due to the influence of the first hull on the second, the second on the first and the second on itself. Lastly a second Kutta condition must be set for the second hull, this is done as above. The results for the symmetric hull shape are given in Figure 4.7.

Although the method worked satisfactorily for a single wing, it was not suitable for the hull shapes tested and produced highly fluctuating results. It should be noted that even for the Clark Y shape a smoothing technique was employed to reduce the effect of potential jumps experienced between panels as it has been described above. However, for the single Clark Y the fluctuations were stable and easily removed. For the hulls they were more pronounced and random in

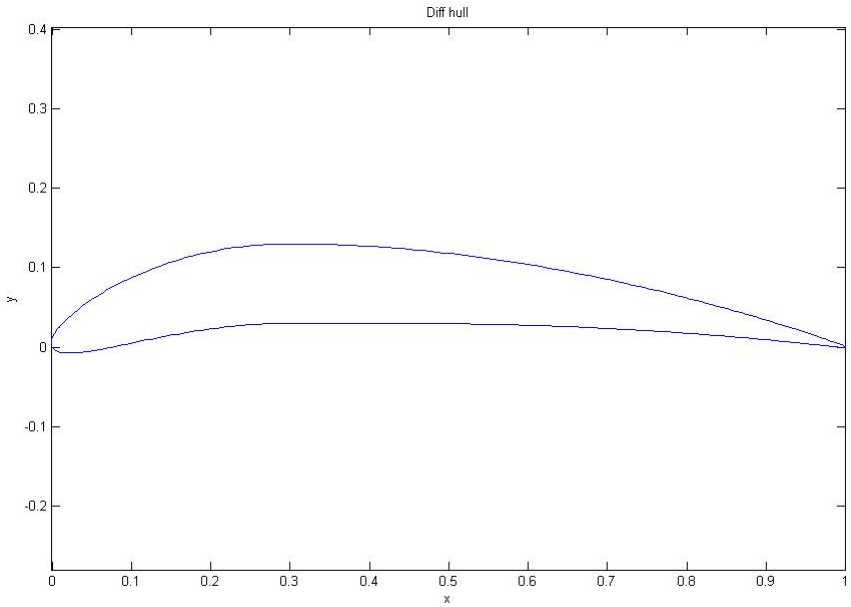

Figure 4.5: 'Diff hull' based on a NACA 8310. This shape is designed to create a divergent-convergent diffuser in order to expand the flow between the hulls.

nature. Upon inspection it was found that the incorporation of the second hull resulted in an extremely ill-conditioned matrix. From comparison of the matrix condition number (the ratio of the largest singular value to the smallest) it was found that the second hull caused the condition number to rise by many orders of magnitude, to as high as 10^{12}, a clearly unacceptable level of instability. This in turn produced wildly varying values of γ in order to satisfy the flow conditions. It is probable that this was a result of the proximity of the bodies to each other. As discussed earlier, problems often arise when the fluctuations along one panelled surface interfere with those of another. This is often remedied by aligning the panels, which was already the case in this situation due to the symmetry. A further cause may have been the inclusion of a second Kutta condition, which necessitated the removal of a further equation from the matrix. Equally, there is

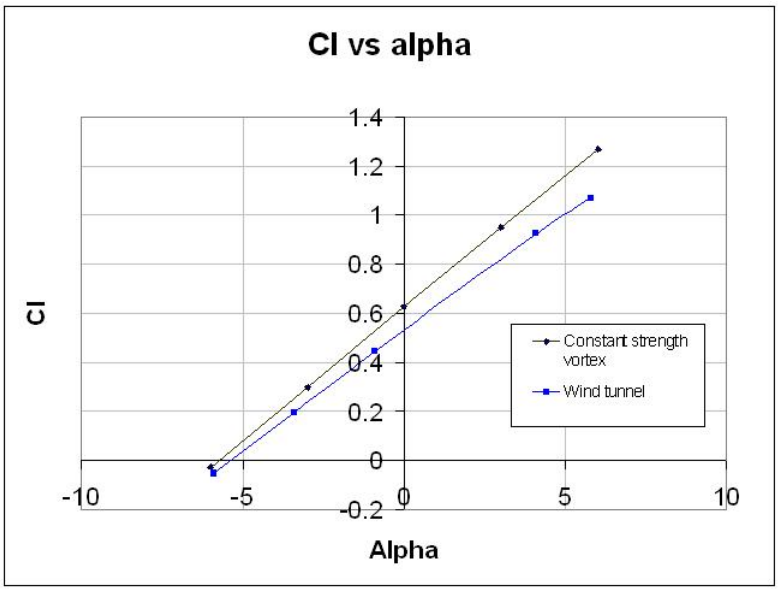

Figure 4.6: Comparison between constant strength vortex method and wind tunnel results for Clark Y foil from [7]. Angle of attack in degrees.

the possibility that the solution of the matrix, due to the need to shuffle the order to avoid division by the zero diagonal, was resulting in numerical errors.

The possibility of numerical errors was tested and found to be an unlikely cause. Although the number of calculations was quite high, the number of iterations undergone while shuffling and solving the matrix was not directly linked to the stability of the results.

It was found that the results for large spacings agreed well with those for a single airfoil; but that at spacings with an aspect ratio of one or less, the results became more erratic. A general curve however was obtained to suggest that the hull shape tested would, as hypothesised, produce a low pressure between the hulls. However, it was felt that a more accurate method would be required.

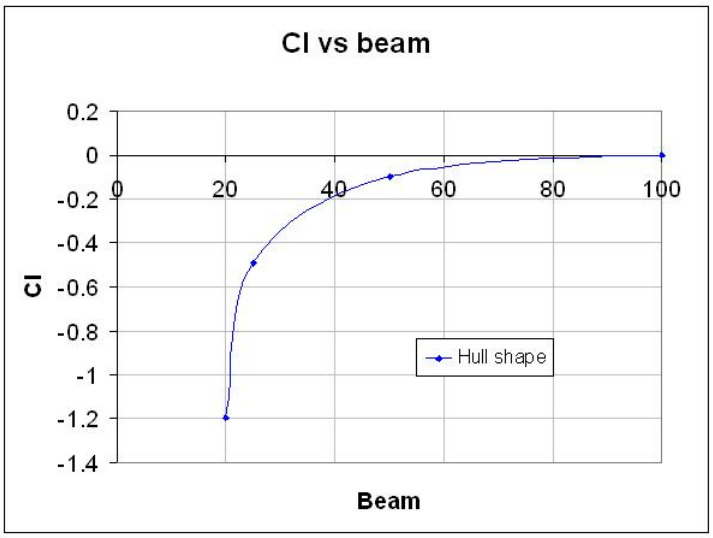

Figure 4.7: C_L vs beam (m) for constant strength vortex method

4.2.3 Linearly Varying Vortex Panels

The use of linearly varying vortex panels can help to solve the problems encountered earlier in a number of ways. As a consequence of using a varying source strength, the panels can be made to match strengths at the edges. This results in a far lower potential jump from one panel to the next and facilitates the use of fewer panels. This in turn may help alleviate numerical problems, if they were a contributing factor. Furthermore, there is no longer a zero diagonal in the coefficient matrix which avoids the need for a pivoting scheme. Most importantly however, the varying strength results in each panel being associated with two values of γ and hence, the matrix is not square until the Kutta condition is added. This prevents the need to remove equations, which it was felt was a likely cause of instability in the previous model.

This method provided very stable results for the single wing as shown in Figure 4.8 and was also able to produce a stable solution for a set of wing shaped hulls in

close proximity. The single wing, Clark Y foil produces the same over estimation of lift with angle of attack as before, except that the results are slightly lower giving a better average fit. The similarity to the previous results is encouraging and the fit against the wind tunnel results is still as it is expected to be.

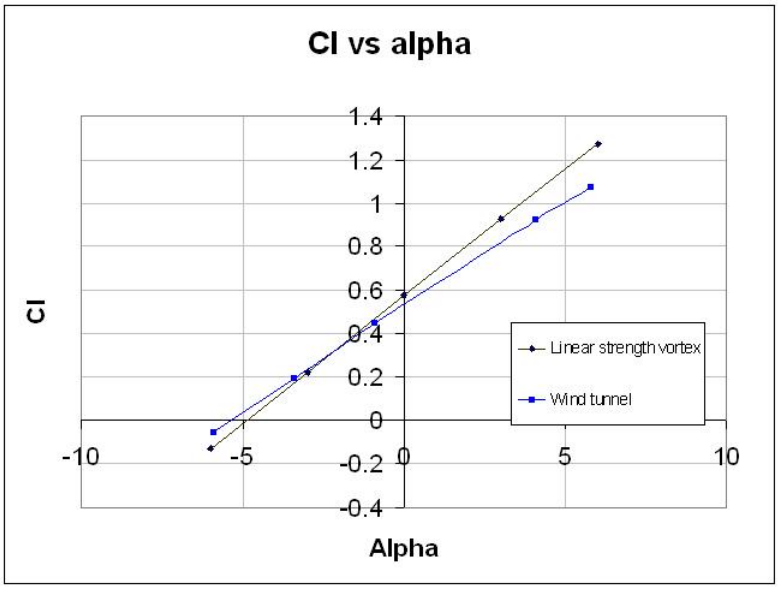

Figure 4.8: C_L vs alpha (deg) for linear strength vortex method, comparison to wind tunnel data [7]

The results for C_L with beam for the symmetric hull were qualitatively in agreement with previous results but showed a less dramatic decrease in pressure with decreasing hull spacing. Figure 4.9 shows the results for Hull shape, Clark Y and Diff hull with comparison to the constant strength method and wind tunnel results where possible.

It is clear that the results for the symmetric hull are very different. It is encouraging that the general trend is the same and that it follows the predicted pattern, however, the variation in magnitude of the results at closer spacings renders the

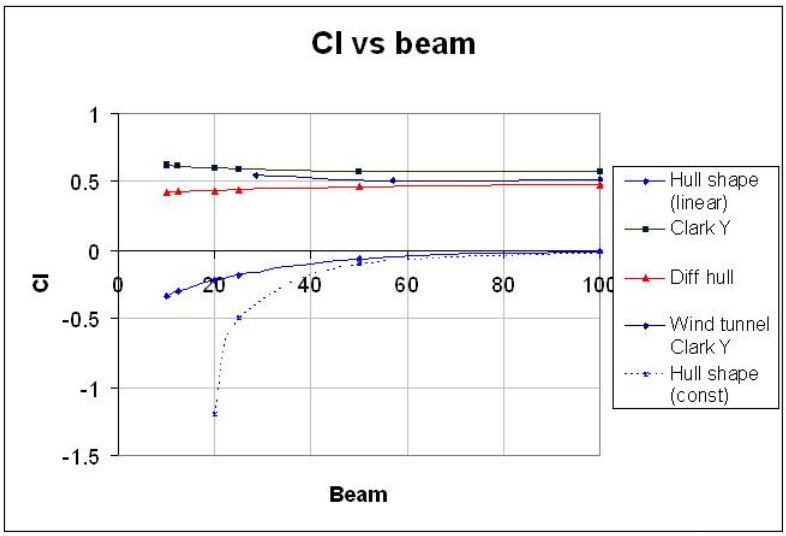

Figure 4.9: C_L vs beam (m) for linear strength vortex method, showing comparison to constant strength method and wind tunnel results

results almost unusable. Looking at the comparison with wind tunnel results however, it can be seen that the Clark Y results are quite similar. Accepting the inevitable over prediction from ignoring viscosity, the results rise in a similar manner. By ignoring the results at closer spacings than the wind tunnel, the results for both both Clark Y and the symmetric hull become more encouraging and the difference between the results is much smaller. Certainly it can be seen that the symmetric foil has a tendency to create a significant negative pressure as it is brought together and that the Clark Y produces greater lift when brought together. Meaning of course that the symmetric hulls would detract from a wing suspended between them and would suck a non-lifting hull down, where a Clark Y shaped hull would aid lift. The results for the Diff hull are less encouraging. The results begin lower than for the Clark Y which is contrary to intuition since it is highly cambered and should produce greater lift. Equally, as the hulls are brought together, the only slight change is a negative one where a positive would

have been anticipated. From observation of the pressure plots it was clear that the results where not stable. Large spikes had formed near the leading and trailing edges which crossed over each other and became more pronounced as the hulls got closer together. This suggests that the program was not able to cope with the shape. It is possible that this was caused by the way in which the geometry was set up, since both the symmetric and Clark Y hulls where formed using conformal mapping, meaning that the points where very evenly spaced. Where as for the Diff hull, the geometry was taken from a separate data set for a NACA 8310 which did not have such a high resolution at the nose and tail. An attempt was made to increase the resolution, which was typically 300 to 600 panels for the other shapes and could be specified in the conformal mapping program; but this was unsuccessful and very time consuming since the intermediate points had to be calculated by hand.

The method was also unable to cope with sharp nosed shapes such as the Wigley hull, which is a mathematically defined parabola often used for simple hull drag calculations. These results were again roughly in agreement with predictions; but had severe discontinuities in the pressure curve near the sharp edges. This effect is often observed in flat plate analysis or thin foil calculations and is considered to have little effect on the overall result; but is less than satisfactory and without further results for comparison, casts doubt over their validity.

A further concern arises when attempting to model hulls such as the quadrimaran, which has a flat stern. This makes the implementation of the Kutta condition both difficult and unrealistic due to the separated flow which would appear in reality. In combination with the sharp bow this makes it difficult to accurately model such a flow. Furthermore, since a simple analysis (such as the stream tube approach used earlier) would predict that the deceasing area of the space between the hulls would result in low pressure, yet the experimentation [4] shows an associated lift,

there is clearly a problem. It is presumed that the lift is generated in part by the slight angle of attack of the lower wetted deck of the quadrimaran, but also by some form of ram air due to viscous effects. If this is the case then a viscous model must be used to check the quadrimaran results. Equally, although the flow around the simple hull shapes is largely inviscid and the results show the predicted trend, it is clear that at some point the hulls will become close enough to choke the flow and change the properties. Research done on wing in ground effect [34], [42] and spheres in close proximity [38] show that the forces can be reversed as the boundary layers start to interact, or as the flow becomes channelled. According to Paulson [42], this reversal of force occurs at values of $h_0/b \leq 1$, where h_0 is the ground clearance and b is the wing span. These results are for a wing alone and it is not at all clear how the results would differ for a ducted configuration. This is clearly an important issue. It has been seen that the ducted effect only becomes significant at length to beam ratios of one or over. This is about the standard aspect ratio for a catamaran as structurally it is difficult to produce a strong vessel of higher aspect ratio. As a result, many multihulls such as the quadrimaran are much lower, hence it is critical to know how the force will change as a result of close spacings and indeed, what defines a close spacing in these circumstances. Paulson notes that the vortex lattice panel methods used were not able to predict this effect, only more complicated versions such as the full Hess surface panel method gave any indication of this phenomena. They were however, not a very good fit to the experimental data. It is of course possible that the experimental data was itself in error due to the difficulty of modeling boundary layers on scale models, however the data is unlikely to be far out.

It is possible to incorporate a boundary layer analysis into a panel code, but they are not well adapted to flow separation and it has already been seen that sharp edges cause a problem. It is considered that the incorporation of boundary layer analysis and higher order panel methods, which may solve the sharp nose problem,

would be a considerable effort and may well out weigh the initial advantages of panel codes, namely there simplicity.

Given the present information, it would appear that a simple analysis with potential flow will not provide further answers and that a more complete approach to the problem should be adopted. It is suggested that some CFD models be considered for comparison.

Chapter 5

2D CFD SIMULATIONS OF DUCTED HULLS

5.1 Introduction To CFD

Computational Fluid Dynamics (CFD) may be thought of as analogous to a numerical wind tunnel. It can be used to perform simulated flow experiments within the specified boundaries of the computational domain. CFD is often used alongside wind tunnel results in automotive and aerospace design. There are many distinct advantages of using CFD, namely that it can provide an enormous amount of very detailed data without the need to run a large and expensive wind tunnel. CFD also has the advantage that once the solution has converged, the data for pressure, velocity, turbulence etc, can be analysed at leisure, with detailed graphical interfaces and animations often allowing for insights and explanations which may have been impossible in a wind tunnel, without the need to rerun the experiment, or produce a new model suitable for the next set of results. In addition, the main problems faced by CFD users during its development have significantly decreased, that is the speed and expense of computers and the amount of evidence (validation and verification) to provide industry confidence in the codes.

The speed of computers and the price per CPU has changed dramatically over the past ten years and looks set to continue. The advances made with parallel processing have allowed even relatively small companies to combine a network of standard office computers into a 'super computer' which can be left to run over night or at weekends. This reduction in computation times has allowed CFD to perform far more as a design tool, where several models can be run and compared, allowing rapid evolution of designs without the time and expense of wind tunnel models. However, it should be noted that CFD suffers in just the same way as a wind tunnel does if the simulation is not set up correctly. Insufficient attention to the boundary conditions and oversimplification of the model can easily result in incorrect physical modeling. Therefore it is important to understand the limitations of the models and to verify and validate the model wherever possible. For this reason, wind tunnel tests are still widely used along side CFD as a safety check.

5.2 Verification and Validation

In CFD the term verification is specifically used in reference to the establishment of the level of agreement between numerical predictions and the specific mathematical model [65]. Ideally this would mean comparison with the exact solutions to the mathematical equations, however this is rarely ever feasible. If this can be achieved then we are provided with the precise level of numerical inaccuracies caused by approximations in the model and solution method as well as computational phenomena such as numerical diffusion. Numerical diffusion being the cumulative effect of rounding errors caused by the finite storage space for each of the millions of calculations. For codes such as FLUENT 6.2, the verification is assumed to be done by the authors and is known to provide an extremely high

level of accuracy when correctly applied.

Validation is the comparison between numerical predictions and actual physical flow data, such as that from a wind tunnel. This is a far more reasonable method and is used throughout industry with CFD models. Of course it is important to recognise the inevitable inaccuracies of wind tunnel tests and to account for these during comparisons. One example might be the effect of obstacles upstream of the experiment, or the effect of measuring equipment on the flow. A systematic validation of CFD code would be desirable. However, due to time and financial constraints, it is more usual to have a specific case verified with wind tunnel experiments and then to expand on these with various CFD models which can be considered as accurate providing they use the same method and, model suitably similar geometry and physical conditions.

5.3 The RANS Method

CFD literally means computational fluid dynamics and is thus not restricted to any particular method. However, it is generally meant to refer to the numerical solution of the Navier-Stokes equations. The complete solution of the Navier-Stokes equations is extremely expensive computationally and as a result some simplifications are made. The simplest is to use an inviscid model such as the potential flow model described earlier, but this is inadequate for dealing with more complex flow patterns or separation.

The Reynolds averaged Navier-Stokes equations (RANS) were developed to provide a more thorough solution without solving the full set of equations. The method used in Fluent[10] is Reynolds (ensemble) averaging. In this method, the solution variables of the exact Navier-Stokes equations are decomposed into the

mean (ensemble-averaged or time-averaged) and fluctuating components. Thus for the velocity components:

$$u_i = \bar{u_i} + u_i' \tag{5.1}$$

where $\bar{u_i}$ and u_i' are the mean and fluctuating velocity components ($i = 1, 2, 3$). Likewise for pressure and other scaler quantities:

$$\phi = \bar{\phi} + \phi' \tag{5.2}$$

where ϕ denotes a scalar such as pressure, energy or species concentration.

By substituting these expressions for the flow variables in the instantaneous continuity and momentum equations and taking a time average yields the ensemble-averaged momentum equations. These equations are shown in Cartesian tensor form and the overbar on the mean velocity v has been dropped. The continuity equation is thus:

$$\frac{\partial \rho}{\partial t} + \frac{\partial}{\partial x_i}(\rho u_i) = 0 \tag{5.3}$$

and the momentum equation becomes:

$$\frac{\partial}{\partial t}(\rho u_i) + \frac{\partial}{\partial x_j}(\rho u_i u_j) = -\frac{\partial p}{\partial x_i} + \frac{\partial}{\partial x_j}\left[\mu\left(\frac{\partial u_i}{\partial x_j} + \frac{\partial u_j}{\partial x_i} - \frac{2}{3}\delta_{ij}\frac{\partial u_l}{\partial x_l}\right)\right] + \frac{\partial}{\partial x_j}(-\rho\overline{u_i' u_j'}) \tag{5.4}$$

Equations 5.3 and 5.4 are the Reynolds-averaged Navier-Stokes equations. The RANS equations are essentially the same as the standard Navier-Stokes equations, but with the solution variables representing a time (or ensemble) average.

The final term in equation 5.4 differs from the instantaneous equations and represents the Reynolds stresses $-\rho\overline{u_i' u_j'}$. This is a three by three symmetrical tensor, representing six unknowns which must be solved in order to model the turbulence effects. The Boussinesq approach, used in Fluent, assumes that these unknowns can be linked to the mean velocities of the fluid via the turbulent viscosity, which

is the constant μ_t. Thus the Reynolds stress can be related to the mean velocity gradient as:

$$-\rho\overline{u_i' u_j'} = \mu_t \left(\frac{\partial u_i}{\partial x_j} + \frac{\partial u_j}{\partial x_i} \right) - \frac{2}{3} \left(\rho k + \mu_t \frac{\partial u_i}{\partial x_i} \right) \delta_{ij} \tag{5.5}$$

Although more complete methods such as Large Eddy Simulation (LES) and Direct Numerical Simulation (DNS), which calculate the full Navier-Stokes equations, are possible, they require substantially more computer time and can be much harder to implement correctly. Such simulations are necessary when the exact flow properties are required, particularly with respect to turbulent wakes. However, the RANS model can produce highly accurate results at drastically lower costs where the flow is not dominated by large eddies and the exact properties of the turbulent wake are not required. For this evaluation, although some highly turbulent wakes are expected to form behind the transom hulls, it is considered of secondary importance to accurately model the exact time dependent shape of the wake. The main effort is toward determining the time averaged pressure distribution between the hulls. Which, providing the phenomena of turbulent vortex shedding is faithfully recreated should be little affected by the exact pattern of the wake. The RANS model should certainly be adequate for streamlined bodies and with careful use and an appropriate viscosity model it should provide accurate enough data for the bluff bodies as well.

5.4 Viscous Models

As is often the case with modelling, there is no single correct method and the choice of which turbulence model to use is as much dependent on the geometry and the Reynolds number as the available computing facilities, time constraints and accuracy requirements. It may be that for much of the modelling the choice of

turbulence model is not the most significant factor. However, for the bluff bodies it may be more critical and a model capable of handling all of the geometries presented here would be desirable as it would lend consistency to the results.

An excellent description of the available turbulent models and their properties can be found in the Fluent documentation [10], however more detailed discussions are provided by Drikakis et al [66]. A brief description of the models considered is provided below.

5.4.1 Spalart-Allmaras

This model, proposed by Spalart and Allmaras [67], uses the transport variable $\tilde{\nu}$ which is essentially the turbulent kinematic viscosity. However, for the near-wall viscous affected region, the transport equation for $\tilde{\nu}$ becomes

$$\frac{\partial}{\partial t}(\rho\tilde{\nu}) + \frac{\partial}{\partial x_i}(\rho\tilde{\nu}u_i) = G_\nu + \frac{1}{\sigma_{\tilde{\nu}}}\left[\frac{\partial}{\partial x_j}\left\{(\mu+\rho\tilde{\nu})\frac{\partial\tilde{\nu}}{\partial x_j}\right\} + C_{b2}\rho\left(\frac{\partial\tilde{\nu}}{\partial x_j}\right)^2\right] - Y_\nu + S_{\tilde{\nu}} \tag{5.6}$$

where G_ν is the production of turbulent viscosity and Y_ν is the destruction of turbulent viscosity occurring in the near-wall region due to blocking and viscous damping. The values $\sigma_{\tilde{\nu}}$ and C_{b2} are constants and ν is the molecular kinematic viscosity. $S_{\tilde{\nu}}$ is a user defined source term. It is noted that since the turbulent kinetic energy k is not calculated in the Spalart-Allmaras model, the last term in Equation 3.5 is ignored when estimating the Reynolds stresses.

The Spalart-Allmaras model is a relatively new and simple one equation model. It solves a modelled transport equation for the turbulent kinematic viscosity in which it is not necessary to calculate the length scale. The S-A model has the advantage of being specifically adapted to aerospace applications and has shown good results for boundary layers in adverse pressure gradients, such as is typical of

aerospace and turbines. However, it was originally built as a low Reynolds number model and is sometimes noted for inaccuracies when modelling rapid transitions in length scale. As this is precisely the case with a transom stern it may be necessary to use a model better suited to step transitions.

5.4.2 k-ϵ Model

The k-ϵ model, originally proposed by Launder and Spalding [68] & [69], uses two transport equations to independently determine both the turbulent velocity and length scale. It has become an industry standard due to its robust nature in a large variety of flow situations as well as its relative economy and accuracy. Part of the success of this model may be attributed to the empirical and phenomenological nature of its construction.

For the k-ϵ model, the turbulent kinetic energy, k and its rate of dissipation, ϵ, are obtained from the following transport equations:

$$\frac{\partial}{\partial t}(\rho k) + \frac{\partial}{\partial x_i}(\rho k u_i) = \frac{\partial}{\partial x_j}\left[\left(\mu + \frac{\mu_t}{\sigma_k}\right)\frac{\partial k}{\partial x_j}\right] + G_k + G_b - \rho\epsilon - Y_M + S_k \quad (5.7)$$

and

$$\frac{\partial}{\partial t}(\rho\epsilon) + \frac{\partial}{\partial x_i}(\rho\epsilon u_i) = \frac{\partial}{\partial x_j}\left[\left(\mu + \frac{\mu_t}{\sigma_\epsilon}\right)\frac{\partial \epsilon}{\partial x_j}\right] + C_{1\epsilon}\frac{\epsilon}{k}(G_k + C_{3\epsilon}G_b) - C_{2\epsilon}\rho\frac{\epsilon^2}{k} + S_\epsilon \quad (5.8)$$

In which, G_k represents the generation of turbulent kinetic energy due to the mean velocity gradients, where the exact term is

$$G_k = -\rho\overline{u_i' u_j'}\frac{\partial u_j}{\partial x_i} \quad (5.9)$$

However, the term is redefined in accordance with the Boussinesq hypothesis as

$$G_k = \mu_t S^2. \tag{5.10}$$

The terms G_b and Y_M respectively, are representative of the production of turbulence due to buoyancy and fluctuating dilatation in compressible turbulence. These terms are less significant in purely air flows, at low Mach numbers. The C's are constants where $C_{1\epsilon} = 1.44$, $C_{2\epsilon} = 1.92$. σ_k and σ_ϵ are turbulent Prandtl numbers for k and ϵ and have the values 1.0 and 1.3 respectively. S_k and S_ϵ are user-defined source terms. It should be noted that all of these values can be changed, however, they have been widely tested and show good results across many applications, as discussed below.

The turbulent viscosity, μ_t, is computed by combining k and ϵ as follows:

$$\mu_t = \rho C_\mu \frac{k^2}{\epsilon} \tag{5.11}$$

where C_μ is a constant of value 0.09.

The k-ϵ turbulence model would seem the most appropriate choice due to its wide acceptance in industry and its ability to handle a variety of turbulent flows. In particular the rapid length scale changes associated with backwards facing steps, such as the transom of a ship's hull. It is true that for specific cases it may be better to use more computationally expensive methods such as Reynolds Stress Model (RSM) or a simpler method such as Spalart-Allmaras, but in order to lend consistency to the results, it is desirable that only one model, for which the limitations are well understood, should be used. Accepting that the drag is likely to be slightly over predicted due to the k-ϵ model's inability to account for transitions from laminar to turbulent flow, there will at least be a uniform

over-prediction for all cases, allowing for a fair comparison. That is to say, we may choose accuracy over precision. The accuracy of the k-ϵ model however, has proved to be more than adequate throughout much of industry. The k-ϵ model is considered to be robust, stable, versatile and accurate, and as such, will be used for all of the computations in this analysis.

5.5 Geometry and Setup

5.5.1 Mesh Generation

The geometry was set up in two dimensions, in the same manner as for the potential flow calculations. The pair of demi-hulls will be viewed as though from above with the water surface and upper deck assumed to act as end plates allowing the two dimensional analysis. Once again this is not ideal, however it does allow for comparison of the relative effects of hull shape and spacing on an arbitrary wing covering them. The free stream will be approaching the hulls at zero angle of incidence, that is, no cross wind, and with a speed of 36 ms^{-1}, which is about 70 knots. This speed is chosen as about the highest currently achievable by large high-speed marine vehicles and a reasonable estimate of future cruise speeds. The hull shapes chosen for analysis are shown in Figures 4.3, 4.4 & 4.5 and are hoped to roughly approximate a wide selection of current and future designs.

The geometry will be defined as a series of vertex points which can be imported into Gambit (version 2.2.3) for pre-processing. The vertex points can then be joined to create a series of lines and thus a face. The face is then removed from a 2-D computational fluid plane and the boundaries are set up. The boundaries form a computational wind tunnel, with a velocity inlet, a pair of parallel moving walls (set to move with the free stream in the manner of a rolling road) the hull

shapes as stationary walls and a pressure outlet. This set up is shown in Figure 5.1. The empty space, or 'air' is then divided into finite areas bound by a series of nodes, which create the computational mesh which can be exported to Fluent (version 6.2).

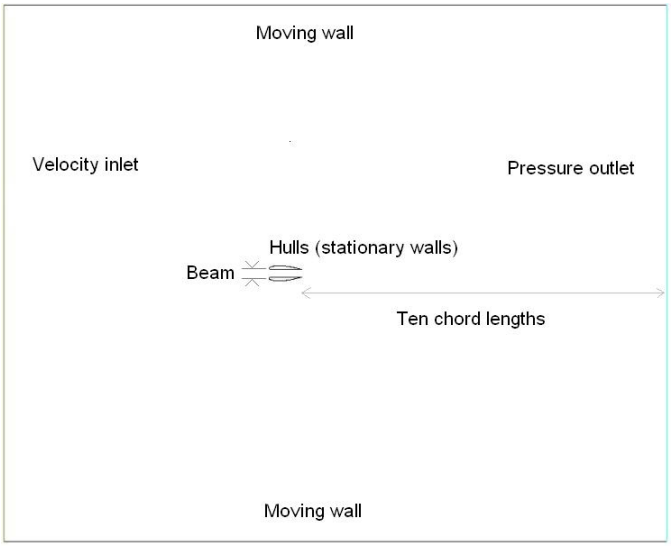

Figure 5.1: Illustration of the Gambit setup for a pair of Clark Y hulls.

5.5.2 Mesh Refinement and Grid Convergence

The generation of computational grids is something of an art and the creation of a good grid can be vital to obtaining accurate results. Fluent is an unstructured solver, which means that unlike many finite difference solvers the mesh does not need to be conformally mapped. However, the density and skewness of the grid remain important. The density is roughly equivalent to the accuracy, since each grid point represents a point at which the flow will be calculated, hence the density must be high enough to 'notice' all of the features of the flow. Unfortunately, the combined effects of computational errors and the associated cost in time, warrants the use of as few nodes as possible. Hence the user must make an educated guess

as to which parts of the flow will be important (such as the leading edge, boundary layer and wake on a wing) and which will be largely unchanged over significant areas and therefore less important, such as the free stream at a distance from the wing; excluding the wake region. There is a further source of error in regard to the size and position of nodes in that their skewness, the size ratio of one element to its neighbour, can affect the results. The results are calculated from averaging nodal values throughout the computational domain, this means that if too larger elements are placed in a region which results in them having an inaccurate value, they will also throw out the smaller neighbouring elements by forcing them to take an average value. Likewise a string of small elements bound by a large element may be forced to take on an average gradient which is misrepresentative of their actual values.

Much can be achieved through experience of building and solving meshes, however it is still necessary to show that the resulting mesh is correct by proving mesh independence. For the majority of problems it is possible to obtain a correct result from a large band of mesh densities. Once a suitable geometry and mesh pattern has been set up, it is possible to produce a range of meshes from the very coarse to the very fine. By running these and plotting the results as a function of the number of nodes, it should be possible to see the value, of C_l for instance, converge on a single value as the density increases. It should then remain on this value until numerical errors cause it to divert. For very advanced computations this flat region can become very small and extremely difficult to find conclusively. In the case of simpler computations however, it should be easy to show that using the pattern of skewness chosen and between a pair of defined mesh densities, the value of C_L is independent of the exact mesh geometry .

5.5.3 Fluent Setup

Fluent version 6.2 will be used for the computation and post-processing of the data and unless stated otherwise the default values have been left unchanged. Fluent will be run in two dimensions, segregated steady state solver using the k-ϵ turbulence model as described above. The velocity inlet is set to 36 ms^{-1} and the walls are set as moving walls at the same speed as the free stream and with zero roughness. Standard wall functions are used for the hull walls which are accounted for via the k-ϵ model with default roughness setting and the residual monitors are set to 10^{-4} in order to increase accuracy.

5.6 Validation of Results

Data for a mock two-dimensional wind tunnel test of a Clark Y airfoil section in ground effect using the mirror image method [7] provides a suitable comparison for checking mesh independence. The data uses a pair of Clark Y foils mirrored about an imaginary ground plane. The data is compared from readings of zero angle of attack for the three height settings, H_0 = infinite, H_0 = 160 mm and H_0 = 80 mm, where H_0 is the distance from the tip of the leading edge to the plane of symmetry or 'ground'. The section has a chord length of 280 mm and the free stream velocity is 36 ms^{-1} with an artificially disturbed flow from a regular network of 2 mm diameter cords giving an effective Reynolds number of 2×10^6.

By setting up this geometry in Gambit, a series of meshes of varying density can be constructed and computed in Fluent as described above. The results are shown below in Figures 5.2, 5.3 and 5.4.

It can be seen that the results converge satisfactorily as the mesh density increases

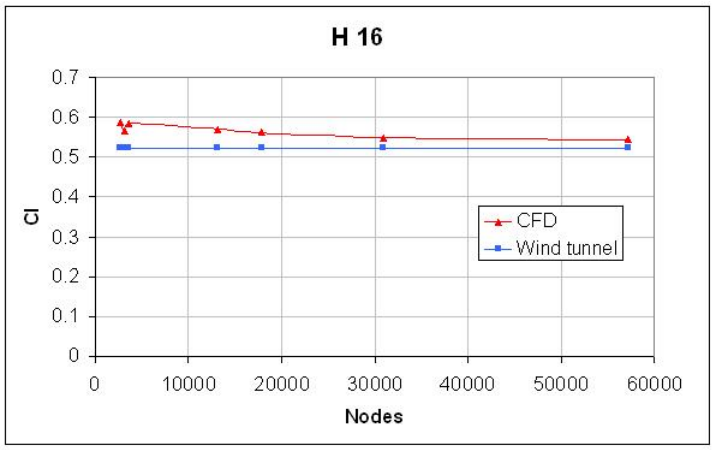

Figure 5.2: Mesh independence at $H_0 = 16$ vs wind tunnel data from [7]

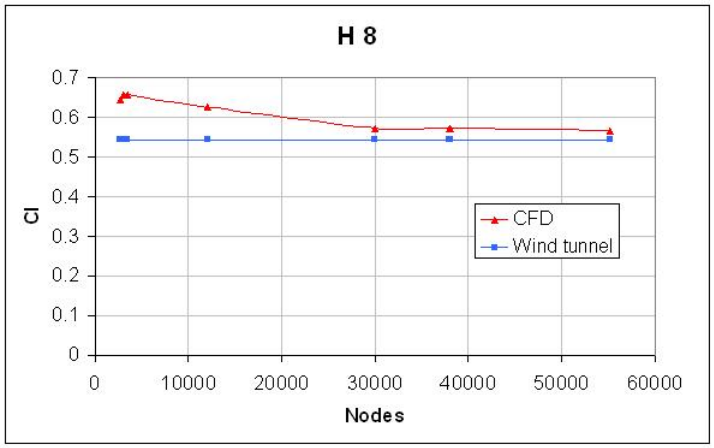

Figure 5.3: Mesh independence at $H_0 = 8$ vs wind tunnel data from [7]

and that it converges on much the same value as that obtained by the wind tunnel tests in every case. For meshes of 3×10^4 to 6×10^4 nodes, there is almost no change in the value of C_L and we can therefore assume that this region represents mesh independent results. It is interesting to note that although the error for an infinite wing is less than one percent, the error increases to around five percent as the foils approach each other. There is little reason to suggest which method has produced

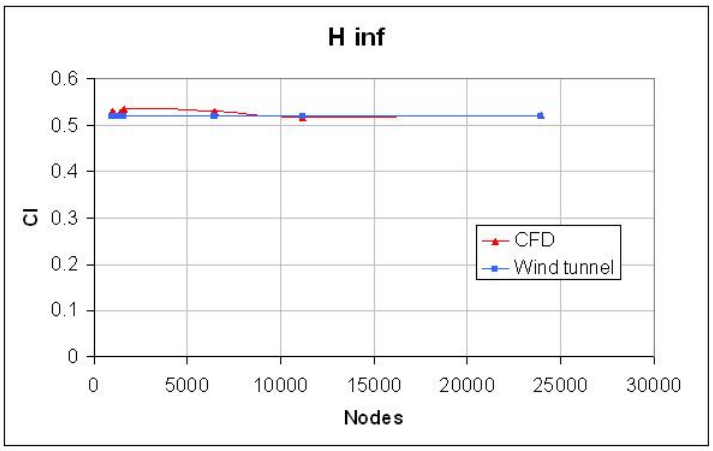

Figure 5.4: Mesh independence at $H_0 = \infty$ vs wind tunnel data from [7]

the more accurate result other than to note that boundary layer interaction at close spacings is a notorious problem in wind tunnels, the important point is that the agreement is still suitably close, but to note that as with the potential flow model, small hull spacings may be a more problematic area to solve.

A further series of computations was done for the single wing at infinite height and varying angle of attack in order to compare the wind tunnel, CFD and potential flow results, shown in Figure 5.5. It can be seen that the wind tunnel and CFD results lie almost exactly on top of each other, where the potential flow results diverge as the coefficient of lift increases. This over prediction of lift is evidently due to the fact that the panel method used does not take viscosity into account and will thus ignore viscous losses. Both of the CFD models used produce essentially the same result, which is encouraging because the main reason to use Spalart-Allmaras over the k-ϵ model would have been increased accuracy for more standard wing shapes.

5.7 Results

The hull sections tested are shown in Figures 4.3, 4.4 & 4.5 and have a uniform chord length of 50 m. As described earlier, they are placed in a free stream of $u = 36\ ms^{-1}$ between moving walls. By integrating the forces around the hull the coefficient of lift C_L can be calculated for each hull for a range of separations. Here the beam B is the distance between the two leading edges, or twice H_0. The results are shown in Figure 5.6.

It can be seen that the modulus of the coefficient of lift $|C_L|$ increases as the distance between the hulls decreases. It can also been seen from the plots of coefficient of pressure C_P that the pressure around the hull changes significantly as the beam is changed. There is little change however, at large separations. The points plotted as $B = 100$ are actually the results for $B = \infty$, plotted as such for obvious reasons of space. However, it can be seen from the trend line shape

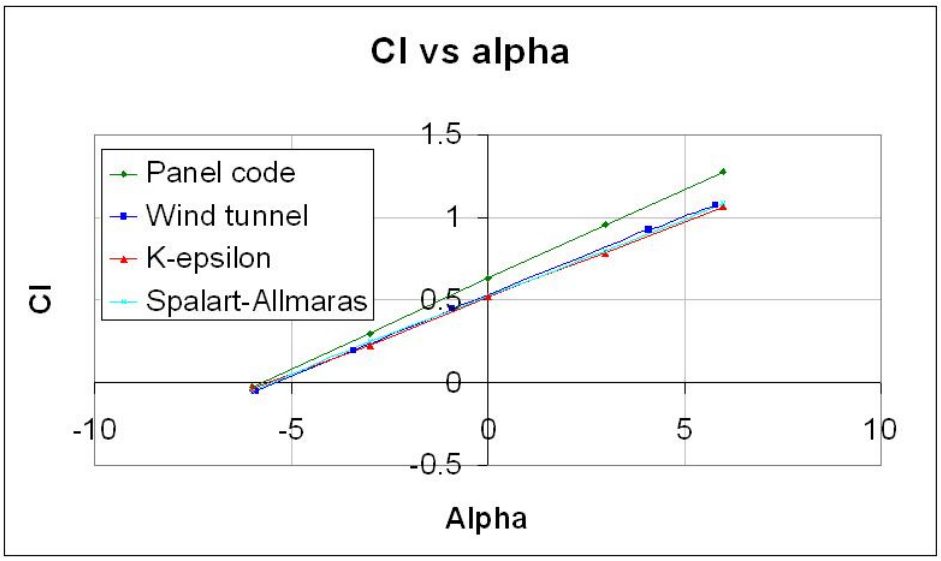

Figure 5.5: Cl vs alpha (deg) for various methods

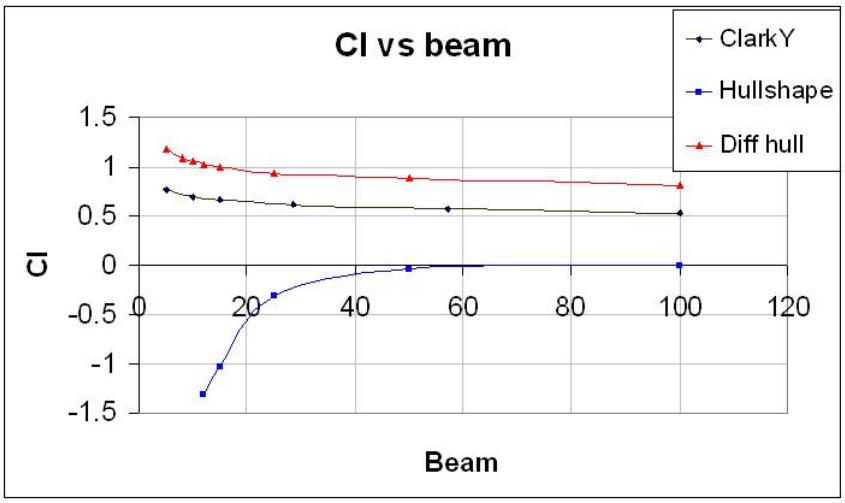

Figure 5.6: C_L as a function of hull spacing (m)

that this modification of scale has little affected the slope of the graph, and as such, there is very little effect on C_L from infinity to spacings of fifty or under. As the hulls are fifty metres long this means that no significant hull interaction occurs at length to beam ratios L/B of one or lower. As it is highly unusual to find a boat with a length to beam ratio lower than one we can assume that the hull interaction will always be of some significance. For reasons of stability, ships are ideally kept close to an L/B of one, however, due to the effects of wave resistance, a mono hull is made as long and thin as possible without encountering unacceptable structural problems or instability. For this reason at least, it is preferable to have a catamaran whose hulls can cut through the water with a high L/B ratio, while separating the hulls such that the stability is based on a much lower L/B ratio which is usually closer to one.

The most significant feature of the results in Figure 5.6 is the discrepancy in the magnitude of force for the different hull shapes. Perhaps most interestingly in the hull called 'hull shape', which was designed to approximate a simple aerodynamic shape. That is, it was designed to represent a shape which might arise if the

designer where simply trying to make a bluff shape more aerodynamic. The fact that such a significantly negative coefficient of lift has been generated by a 'non-lifting' body, suggests that simply designing a ship to be more aerodynamic, in accordance with the rules of streamlining, could have a serious and negative effect on the ships performance. At the other extreme we have a very high coefficient of lift produced by the Clark Y and Diff hull. These positive coefficients are, of course, in the horizontal plane and literally represent a force pressing the hulls outwards. However, the C_L is a fair representation of the pressure around the hull and thus the pressure through the tunnel hull. This simple analysis allows us to view the general effect of hull geometry and spacing on the surrounding pressure field.

It is interesting to note at this point, that there do not appear to have been any significant effects of boundary layer interaction between the hulls at very close spacings. It was discussed in section 4.2.3 that for extreme ground effect Paulson [42] found that thick wing shapes began to produce a negative lift. However this effect is not observed for the Clark Y foil despite being tested at spacings equivalent to an H_0 of only $2.5m$ for a chord length of $50m$. For tests done on spheres [38] it was found that the suction encountered as the initially non-lifting spheres were brought together actually became a repelling force at even smaller spacings. It would seem that in the case of the spheres the flow is symmetric at large spacings and hence there is no force. As the spacing decreases, the flow becomes channelled and speeds up creating a low pressure suction between the spheres. However, eventually the spheres become so close that their respective boundary layers interact and the flow is slowed once more to a high pressure. In the case of Paulson's wing the suction is presumably due to the same effect of channeling as the spheres and indeed the results shown for the 'hull shape'. The fact that the Clark Y foil did not experience suction at small separations can be explained by considering the position of the stagnation point and the behavior of

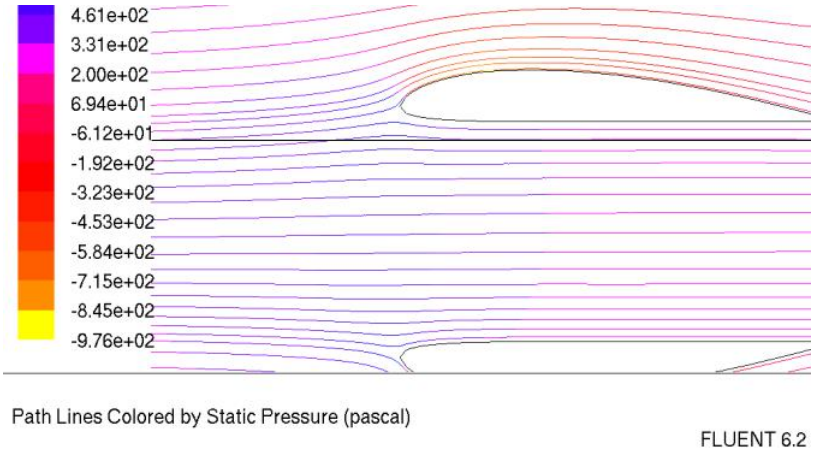

Figure 5.7: Streamlines for a Clark Y foil at $H_0 = 8$

the free stream ahead of the leading edge. Figure 5.7 illustrates the flow around a Clark Y foil at an H_0 of 8. The black line is a reference line of $y = constant$ to show the direction of the undisturbed free stream. It is clear that although from the stagnation point the flow is channeled inwards, it is by less than the amount by which the free stream has diverged due to the induced angle of attack and hence the pressure is still high.

By plotting the lift results vs height for the Clark Y foil at various angles of attack, as shown in Figure 5.8, it can be seen that for an angle of $\alpha = -3$ the foil starts with a C_L of 0.226 which then decreases to 0.165. From observation of all of the results it is clear that the thickness of the foil does indeed induce a channeling of flow which is the cause of a lowering of pressure within the duct. However this effect is counterbalanced by the camber of the wing which moves the stagnation point and induced angle of attack as previously discussed. This is to suggest that the thickness of the hulls should be kept to a minimum and that any thickness should be accounted for by a minimum amount of camber in order to prevent adverse suction between the hulls. The lack of a corresponding high pressure at

extremely small separations is attributed to the effect of Reynolds number. For the full size hulls the Reynolds number of 1.22×10^8 is many orders of magnitude in excess of that used in the spheres experiment, in which the increasing Reynolds number was seen to have a diminishing effect on the fluctuation of force with respect to distance. The high ratio of inertial forces to viscous forces is most likely the reason why no boundary layer interaction and hence flow stagnation was observed even at unrealistically small spacings.

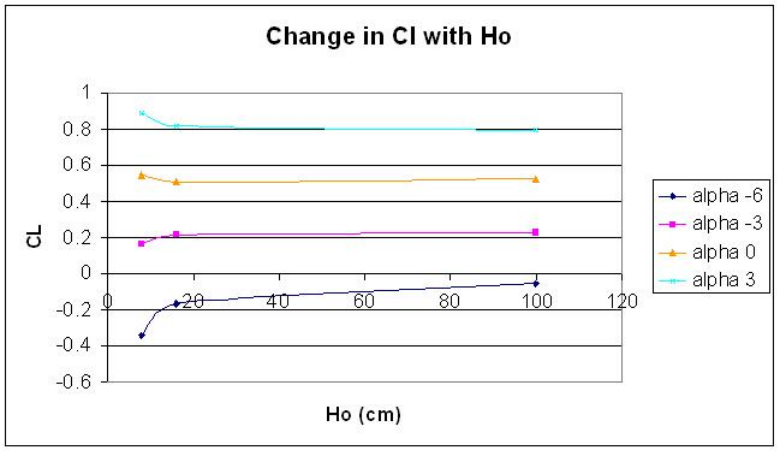

Figure 5.8: Change in C_L for a Clark Y foil with respect to height for various angles of attack

The second set of results, shown in Figure 5.9, represents a more accurate analysis of the lift, derived from the averaged pressure throughout the tunnel. By plotting the pressure at all points between the hulls as colour contours, the average pressure and hence force for any discrete area ΔS_w can be calculated as

$$F_{L(x,y)} = p_{(x,y)} \Delta S_w \tag{5.12}$$

where $F_{L(x,y)}$ is the lift force, $p_{(x,y)}$ is the average pressure and ΔS_w is the discrete area at the point (x, y). For this, it is assumed that the upper deck of the tunnel

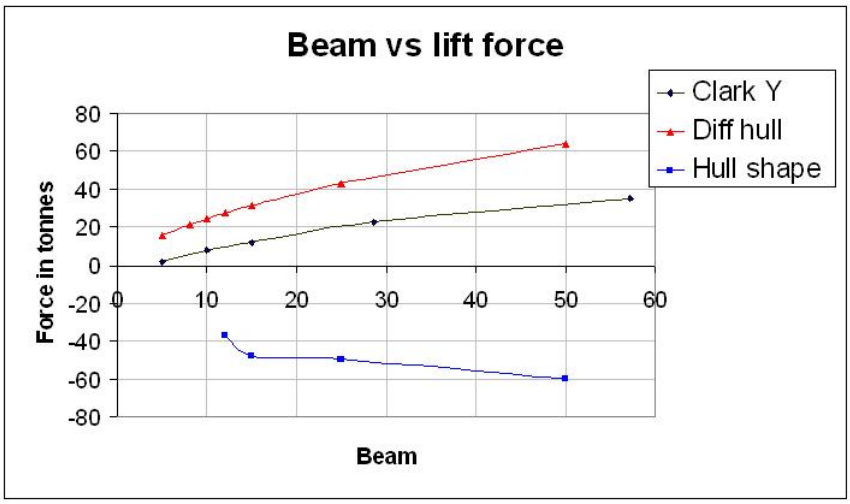

Figure 5.9: Force in tonnes as a function of hull spacing (m)

is experiencing standard atmospheric conditions. As it happens the upper deck will most likely be a wing shape and will therefore have a lower than atmospheric pressure and thus more lift force, however a fair comparison between the hull shapes can be achieved by ignoring this extra force, since it is uniform across the board.

For these results the trend has changed and the force is observed to increase as the hulls separate. However, as we have already discussed, the upper limit for hull separation is around fifty metres. At this separation we can see a significant variation in the results. From studying vehicles of a similar size and role as our assumed vessel, an estimated total vehicle weight of two hundred tonnes is adopted for comparison. Here we see that the 'hull shape' at a spacing of fifty metres produces a down force of around sixty tonnes, nearly 30% of the vehicle weight! Conversely the 'diff hull' has a positive lift of just over sixty tonnes, again accounting for 30% of the vehicle weight. Graphs and contour plots for these hulls are provided at the end of the chapter, Figures 5.10 to 5.27.

5.8 Discussion of Results

From comparison of the two graphs presented above (5.6 & 5.9), it can be seen that although the modulus of both the coefficient of lift and the pressure increases as the hulls are brought together, the decreased surface area of the wetted deck is more significant and that overall there is a decrease in the magnitude of force. At L/B ratios of around one there is a considerable force from the hulls; but even at L/B ratios of as high as five the force is still as much as 10%, which is far from negligible. For multihull vehicles travelling at speeds in excess of sixty knots it is apparent that aerodynamic analysis could prove critical to the vessels performance.

The analysis thus far has only considered streamlined bodies, from which it can be seen that as a general rule the C_L for an infinite spacing can be used to estimate the comparative lift force of a given hull shape. It is clear that the highly cambered and thus high C_L shapes have the most effect. This is inline with earlier predictions made using stream tube analysis. The difference is from the symmetrical bodies, which have a C_L of zero. In this case, the negative pressure is due to the effect of the two negative pressure fields combining between the hulls, which alone would have been equal in magnitude. For such shapes then, an approximation of their effectiveness may be gauged from their finesse ratio. Shapes of greater width will have a lower pressure and experience greater force. It is clear then that the 'hull shape' is perhaps an upper limit, representing a rather wide foil. The approach of stream tube analysis may be more conducive to thought for this purpose since unlike a regular foil where the pressure difference across the foil itself is responsible for the lift, the hulls are only useful if they create high pressure within the tunnel, regardless of the pressure outside. In this respect it is clear that the C_L is not the best approximation of effectiveness. The most promising results are achieved by expanding the area of the tunnel and thus slowing the flow. Hence a highly

cambered and thin foil should provide the most lift.

The interesting exception to this theory are the results published by Hockberger for the Quadrimaran[4]. The shape, called 'quad' and shown in Figure 6.2 is a long thin triangle with the short base as the transom. Four of these hulls were placed next to each other and joined by a wetted deck. The Quadrimaran was briefly discussed in chapter two, and is depicted in Figures 2.5 & 2.6. Hockberger tells us that the Quadrimaran experiences lift from air trapped under its hulls and that the effect was first noted due to the vessels ability to achieve higher speeds in a strong head wind! Use of simple stream tube analysis would predict a low pressure; but in reality it is high. The discrepancy is likely to come firstly from the difficulty of predicting where the stagnation point of the stream tube will be on the body and how the free stream will curve before it meets the body; but more significantly, from the effect of flow separation from the flat stern. In order to simulate this, the model will have to be adapted to cope with flow separation.

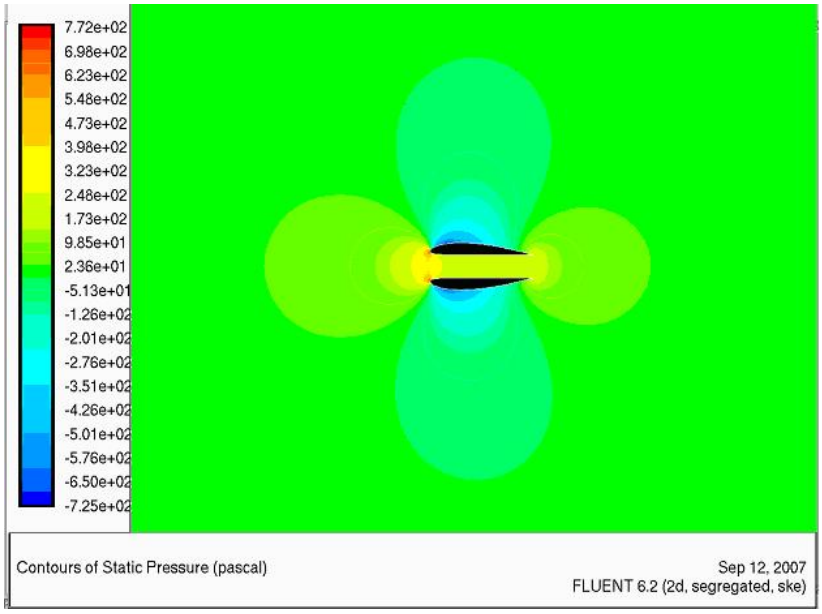

Figure 5.10: Contours of static pressure for Clark Y hulls at $B = 15$

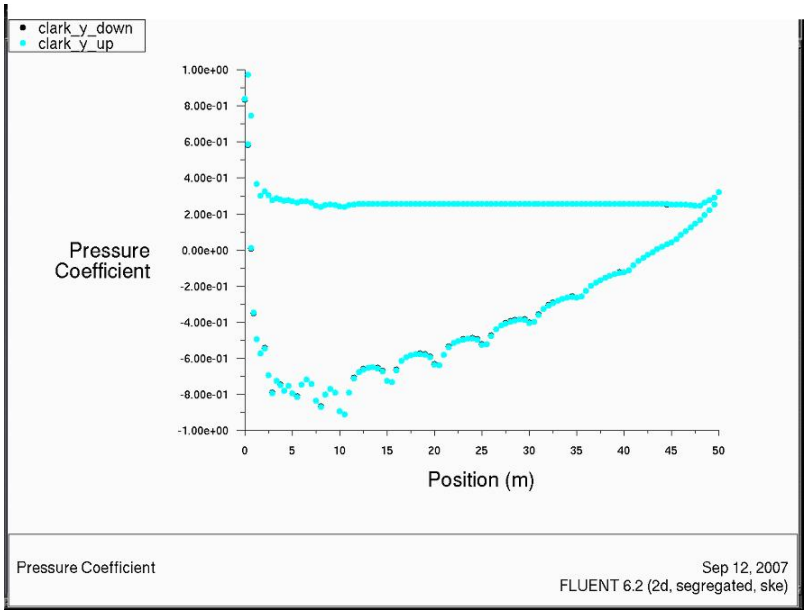

Figure 5.11: Plot of C_p for Clark Y hulls at $B = 15$

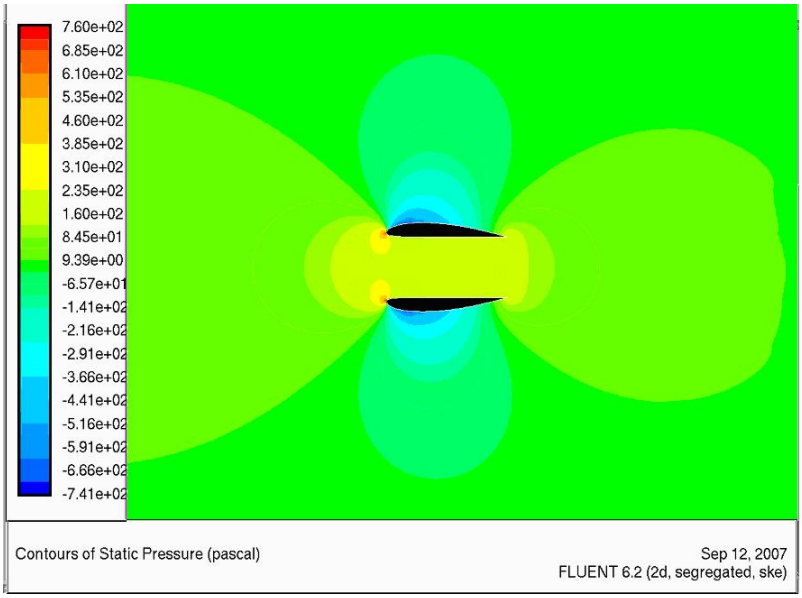

Figure 5.12: Contours of static pressure for Clark Y hulls at $B = 28.57$

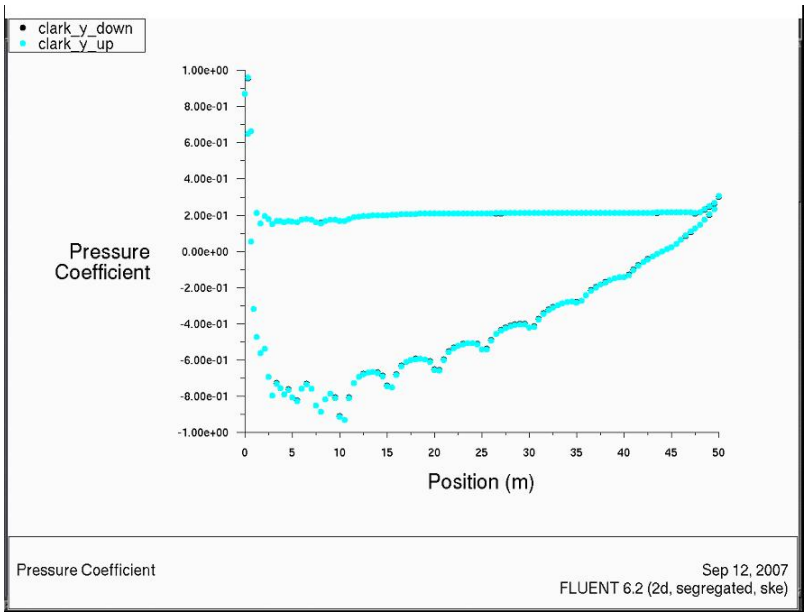

Figure 5.13: Plot of C_p for Clark Y hulls at $B = 28.57$

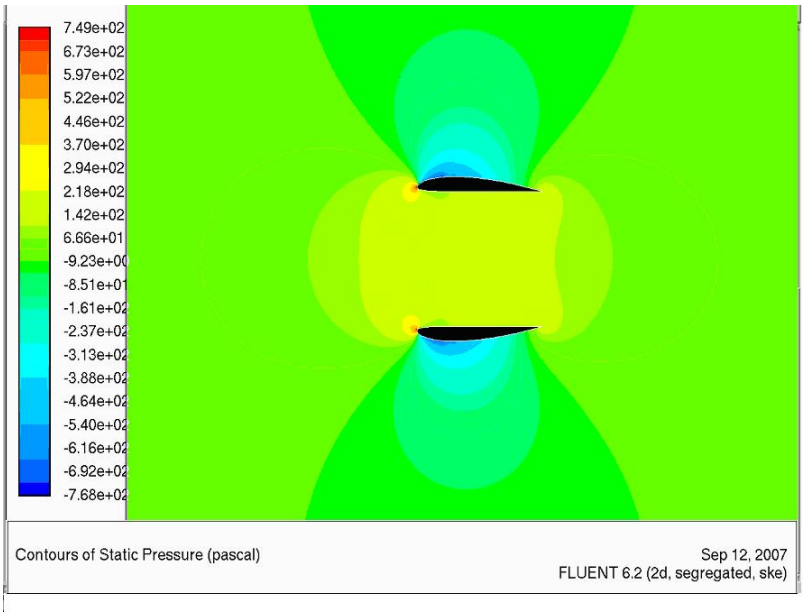

Figure 5.14: Contours of static pressure for Clark Y hulls at $B = 57$

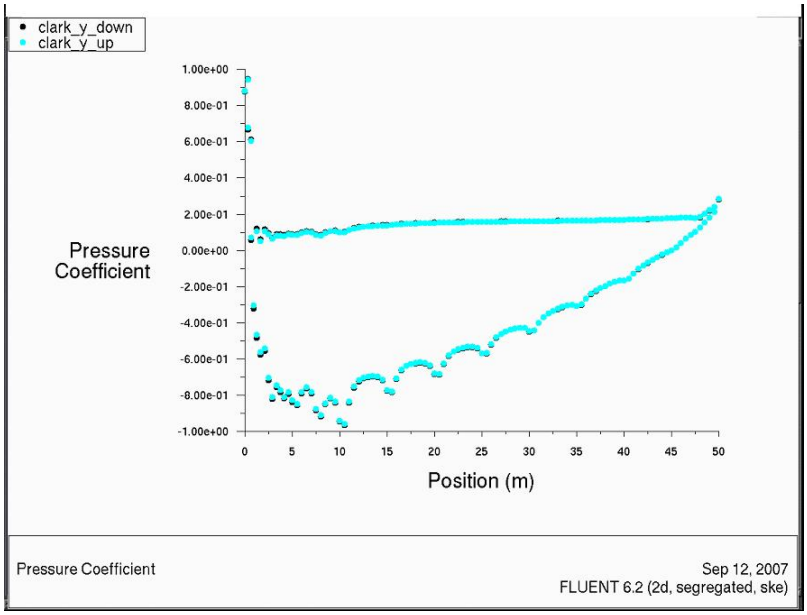

Figure 5.15: Plot of C_p for Clark Y hulls at $B = 57$

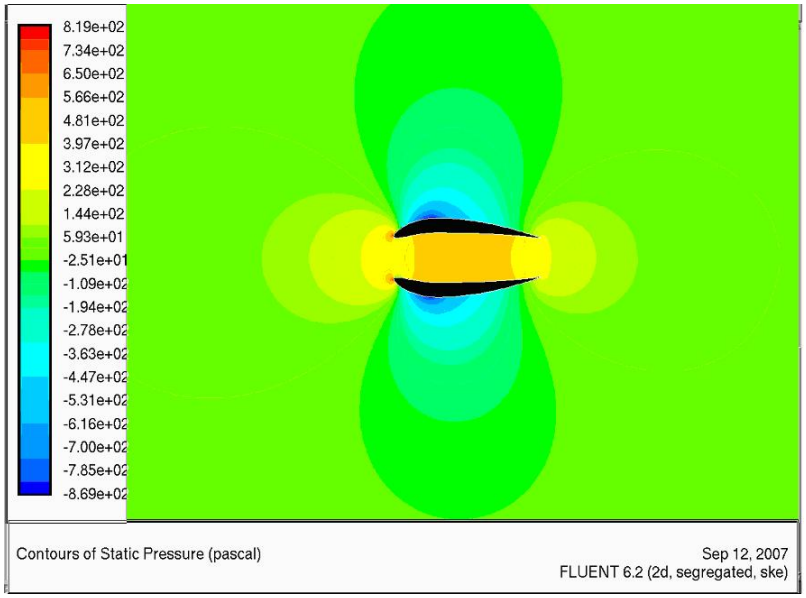

Figure 5.16: Contours of static pressure for Diff hull at $B = 15$

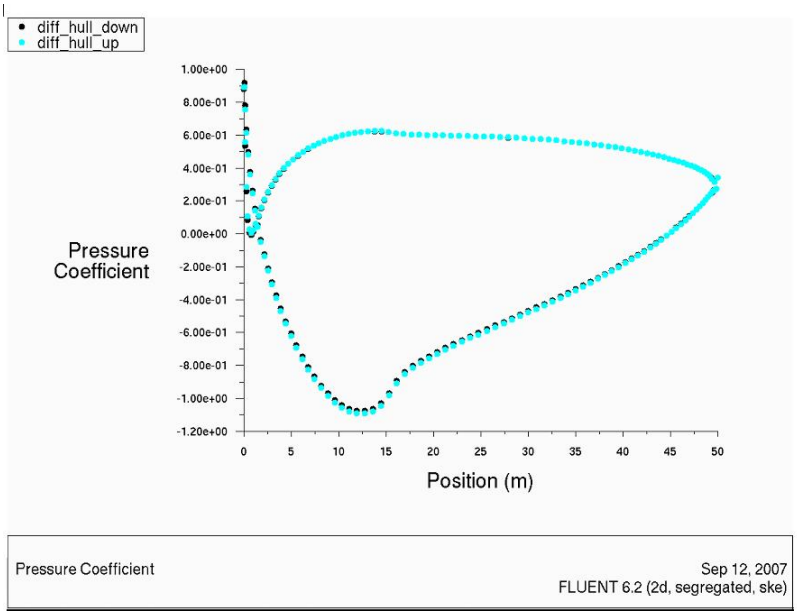

Figure 5.17: Plot of C_p for Diff hull at $B = 15$

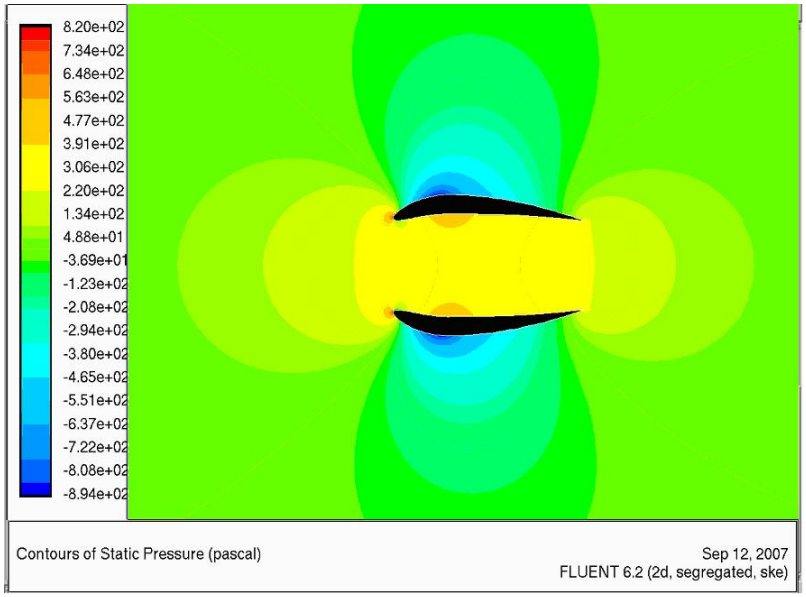

Figure 5.18: Contours of static pressure for Diff hull at $B = 25$

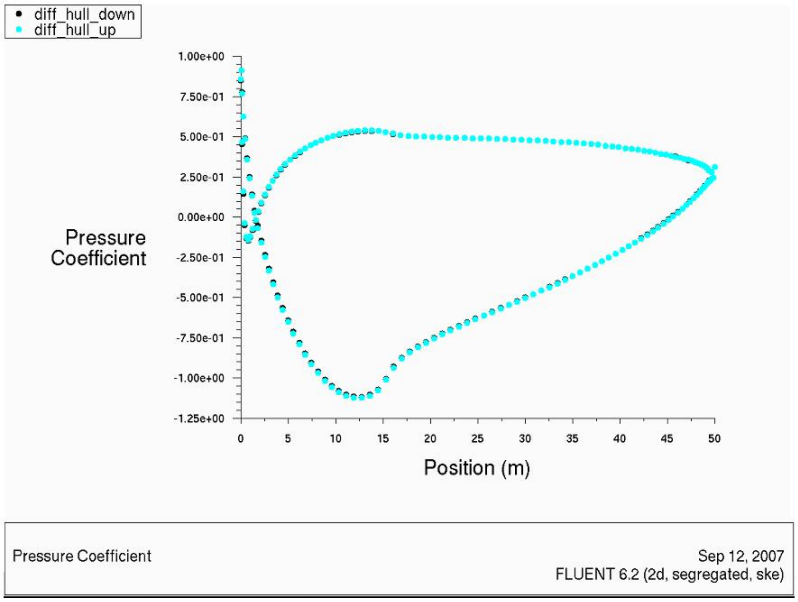

Figure 5.19: Plot of C_p for Diff hull at $B = 25$

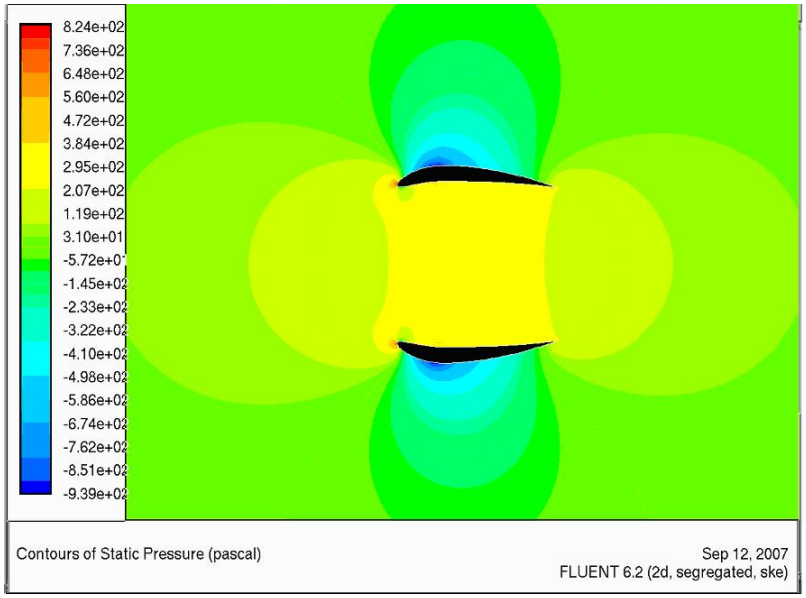

Figure 5.20: Contours of static pressure for Diff hull at $B = 50$

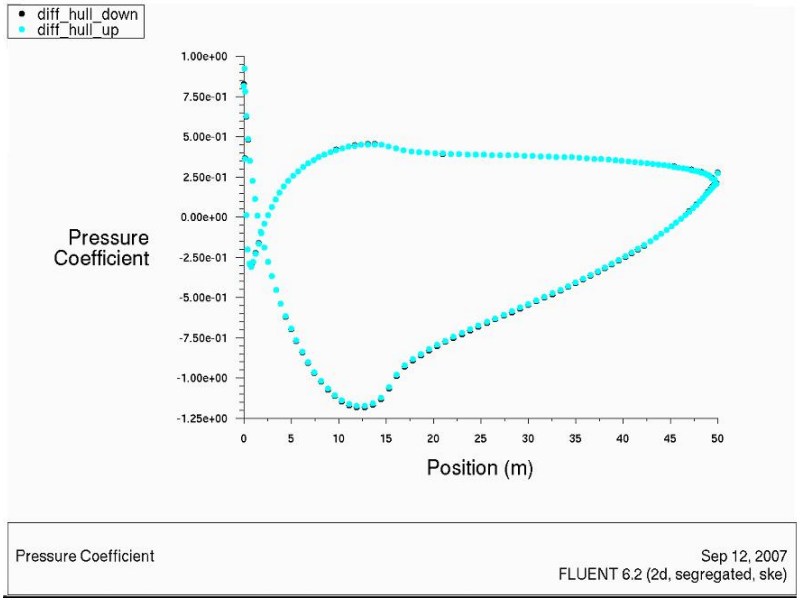

Figure 5.21: Plot of C_p for Diff hull at $B = 50$

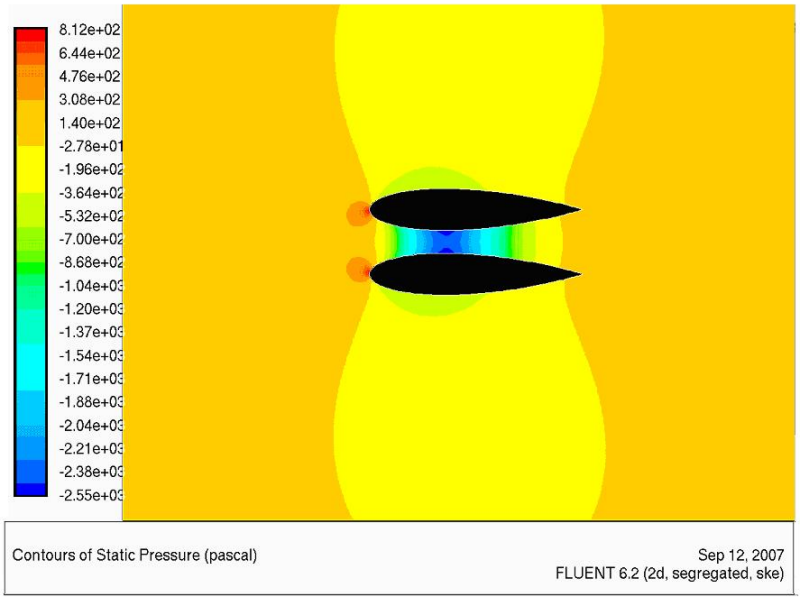

Figure 5.22: Contours of static pressure for Hull shape at $B = 15$

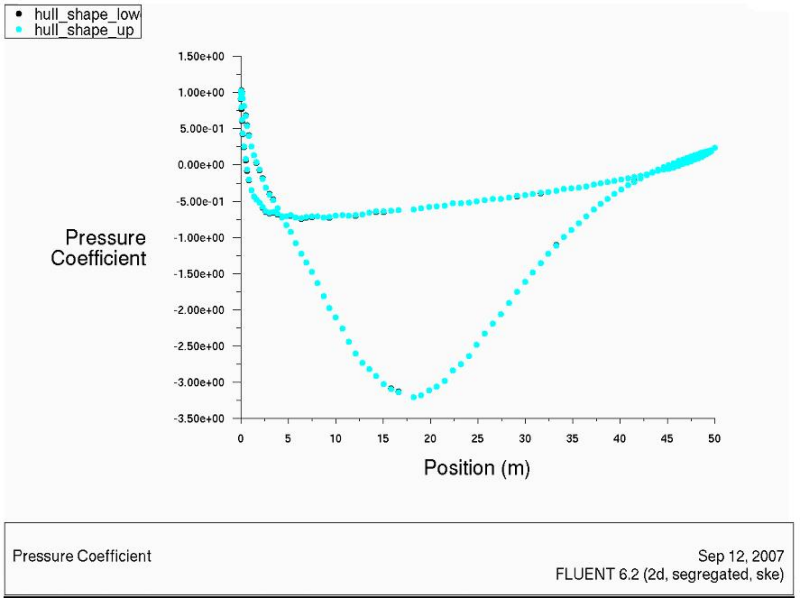

Figure 5.23: Plot of C_p for Hull shape at $B = 15$

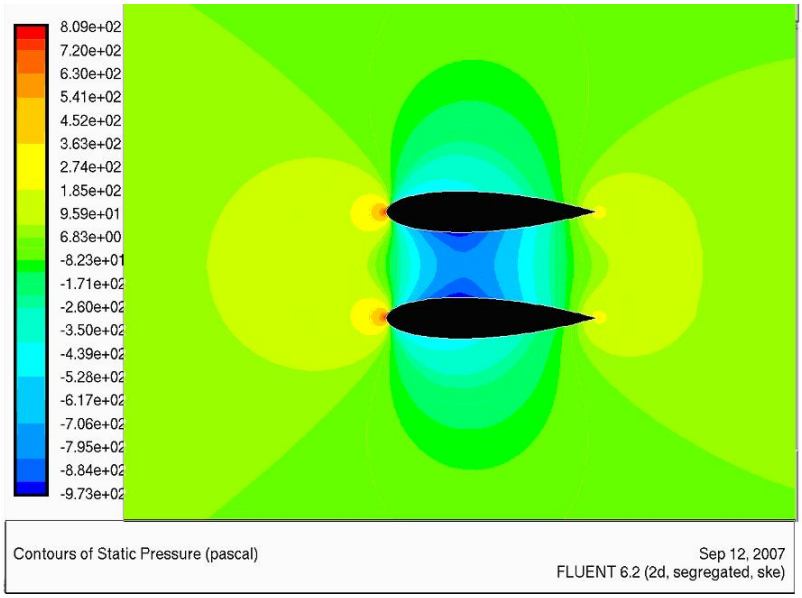

Figure 5.24: Contours of static pressure for Hull shape at $B = 25$

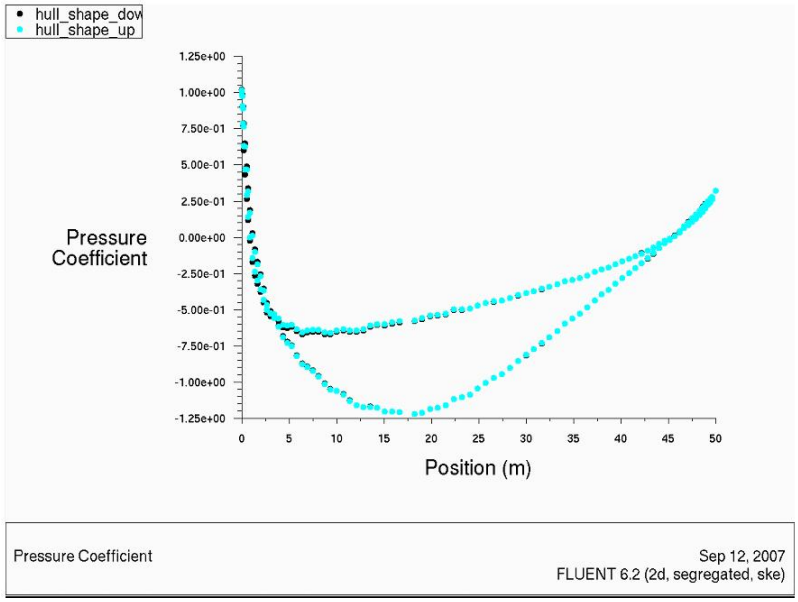

Figure 5.25: Plot of C_p for Hull shape at $B = 25$

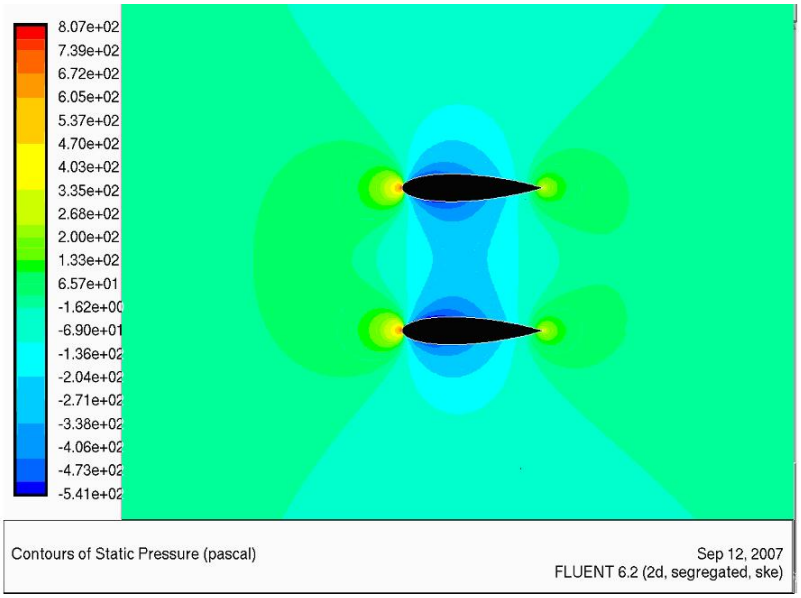

Figure 5.26: Contours of static pressure for Hull shape at $B = 50$

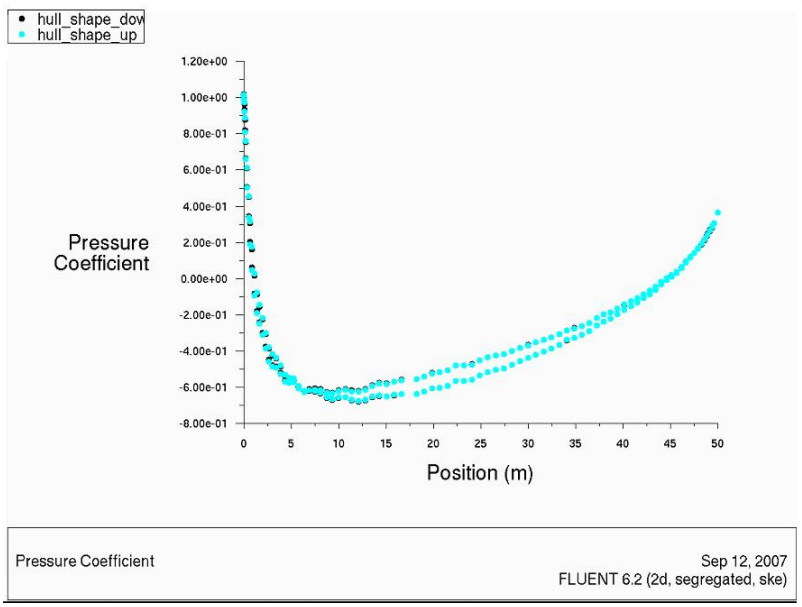

Figure 5.27: Plot of C_p for Hull shape at $B = 50$

Chapter 6

UNSTEADY MODELLING OF FLOW SEPARATION ON TRANSOM HULLS

6.1 Introduction

The previous chapter demonstrated the importance of hull design for aerodynamically alleviated multihulls. All of the shapes considered however, had streamlined sterns and were thus not typical of planing hulls. The flat transom at the rear of a planing hull is necessary in order to separate the water flow and prevent adverse pressure gradients. However, the air flow will also be separated at this point, which generally results in a loss of pressure and reduced efficiency. This chapter will focus on the aerodynamics of more conventional ship hulls.

Of particular interest is the Quadrimaran, described by Hockberger [4] and illustrated in Chapter 2, Figures 2.5 & 2.6. The Quadrimaran has four identical hulls, each of triangular shape with a transom. The upper deck is relatively flat and no effort was made to design the ship for aerodynamic alleviation, yet it was found to

produce some lift at high speeds. Since the hulls are symmetrical and the upper deck flat, it is not immediately obvious how the lift is produced. No attempt is made by the author to describe how the lift is achieved, other than that it appears to be 'trapped' by the hulls. In this section the Quadrimaran hulls will be analysed for their aerodynamic properties in order to ascertain their contribution to the lift and their potential use for other aerodynamically alleviated multihulls.

6.2 Description of Problem

The aerodynamics of shapes such as the Quadrimaran hull, are not easily modeled due to the flow separation which occurs at the sharp edges of the transom stern. As with all flows the exact nature of the flow around and behind the body is determined by the shape of the body and the Reynolds number of the flow. However, the variation in flow pattern with Reynolds number for bluff bodies is quite dramatic. As the speed of flow increases for a given body submerged in fluid, the flow ceases to follow the contours of the body and starts to separate. Initially the separation is symmetrical, but it is soon imbalanced by turbulence in the free stream causing one eddy to become larger and eventually break free. This in turn causes the remaining eddy to grow as a new one forms resulting in an alternating pattern of vortex shedding called a Von Karmen vortex street. For many objects, such as a cylinder, there is a critical Reynolds number where the flow will stop shedding vortices.

It is evident that the nature of the pressure distribution around the hull will be affected by the turbulent vortex shedding occurring behind the hull. It is thus important to correctly model this phenomena in order to achieve a fair prediction of the forces on and around the hull.

6.3 Method

The first crucial difference which has to be made to the modelling is that it can no longer be time independent. Since the pressure will change with time due to the vortex shedding, a stable solution cannot be achieved though the previous method. The flow must now be resolved with respect to time as well. As a result, we need not only to prove mesh independence, but time-step independence as well. That is, we must show that the time-steps, or intervals at which the flow is measured are sufficiently small to give accurate results without becoming prohibitively slow to compute. Since the onset and type of vortex shedding are determined largely by the Reynolds number, it is prudent to check this against relevant data. Based on the ship length the Reynolds number for all of the hulls is 1.22×10^8 which is well into the turbulent vortex shedding region for comparable shapes.

The frequency of vortex shedding is related to the flow speed and geometry by the Strouhal number S_n, which is defined as

$$S_n = \frac{f_s D}{u_\infty} \tag{6.1}$$

where f_s is the frequency of vortex shedding and D is the characteristic length, usually the diameter or width. Unfortunately the Strouhal number is usually calculated from experimental results and there is little data for shapes that resemble those presented here, or indeed at such high Reynolds numbers. It is possible however, to form an estimate based on the results provided by experimental data such as that from Blevins [70]. From the many shapes tested, the Strouhal number is usually restricted to values of 0.15 to 0.3 and judging from the more similar shapes the value should remain more or less constant; especially at higher Reynolds numbers. From observation of the data in [70]an estimate for

the Strouhal number may be placed at 0.2 to 0.26. By calculating the frequency for these two limits, a value of between 1.5 and 1.875 Hz is obtained. Hence one cycle will take approximately two thirds of a second. In order to allow a full wake to propagate down stream of the body, assuming the turbulent wake speed to be marginally less than that of the free stream and allowing for a wake length seven times that of the hull, requires a total physical run time of about ten seconds. In order to check this the flow results are recorded at a physical time of five and ten seconds and the results compared.

Fluent 6.2 allows for an adaptive time-stepping scheme and its use is highly recommended, particularly during the first set of iterations. In the fully developed turbulent flow, the motion (as calculated by the frequency of the vortex shedding) is relatively slow. Since one cycle is about 2/3 of a second, each vortex is formed in about 1/3 of a second and might therefore be captured by time-steps of perhaps 1/30. However, in that time the free stream has moved 1.2 m. This is not a problem in fully developed flow since the pressure patterns will not have changed much, but for the first iterations it can prevent the continuity equation from converging due to the flow 'jumping' 1.2 m away from the body at a time. This will remain a problem until the flow is more developed and hence correctly aligned. As a result, it is convenient to start with much smaller time-steps and gradually allow them to grow as the flow develops in order to reduce run times. It should be mentioned that for each time-step the flow solution must converge in much the same manner as for the time independent method (except that the result are unique to the time-step) and hence the solution is far more time consuming.

The magnitude of the time-steps chosen where partly down to intuition, in the sense that the flow can be calculated to move at a certain speed from which an estimate of the tolerable amount of movement per time-step may be estimated. A certain amount however, is simply a matter of trial and error. In most cases,

if the time-step is too large the solution simply will not converge and this soon becomes apparent from observation of the residual monitors. The result was an adaptive time-stepping sequence beginning with time-steps of 1×10^{-4} seconds rising by a minimum factor of 0.5 and a maximum factor of 5, to a maximum time-step size of 5×10^{-3} seconds.

6.3.1 Validation

A series of meshes for the Quadrimaran hull at an infinite spacing were produced, ranging in node size from very coarse to very fine, in the same manner as for the previous validation. By running the meshes as time dependent codes and taking an average result from a series of time intervals as in the method described above, a set of results can be obtained to show how mesh size affects vortex shedding. From previous analysis it is known that the pressure distribution can accurately be captured by meshes of 4×10^4 nodes or more. Figure 6.1 shows the estimated Strouhal number for the series of meshes. For mesh densities of less that 5×10^4 the mesh is not fine enough to capture the effect of vortex shedding and only small areas of recirculation appear. For mesh densities of 1×10^5 and above the turbulent wake is fully captured. This sudden transition is clearly seen in Figure 6.1. Once the wake has appeared, an estimate of the Strouhal number can be made by calculating the frequency based on the wave length and the wake speed. It is seen that the Strouhal number is almost independent of the range of grids once vortex shedding has begun. This is very useful since it allows relative faith to be placed in the results provided that the grid is above 1×10^5 and vortex shedding has been observed. It must be remembered that the exact position and properties of the wake are of secondary importance to the pressure distribution around the body, which is affected far more by the immediate vortex shedding and hence the frequency of shedding.

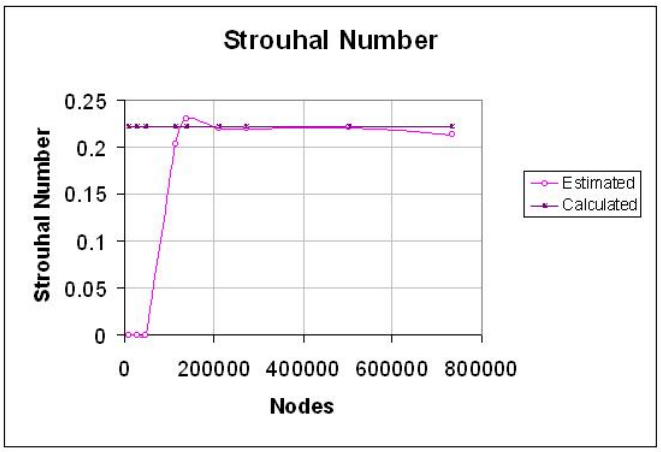

Figure 6.1: Mesh independence for Strouhal number.

6.4 Results

The two shapes chosen are illustrated in Figures 6.2 & 6.3. The Quadrimaran hull, labeled 'Quad' is an estimation of the hull shape taken from diagrams supplied in the paper by Hockberger [4]. The Quadrimran has already been observed to provide aerodynamic lift in scale tests, including a 17.5 m manned version on open water. However, since it was not originally designed to create lift by these means it is not completely understood what all of the contributing factors are. The suggestion by Hockberger is that the positive angle of attack of the upper and wetted deck create lift pressure which is simply trapped by the hulls. It is therefore of interest to the present study to examine the effect of just the side hulls on the airflow.

The second model is that of the KUDU II, which is taken from Ward *et al* [8]. This design utilises exactly the sort of design considered by Doctors when describing an ekranocat. The vessel consists of two demi-hulls joined by a modified wing and was designed as a racing power boat. The hulls are illustrated in [8] and

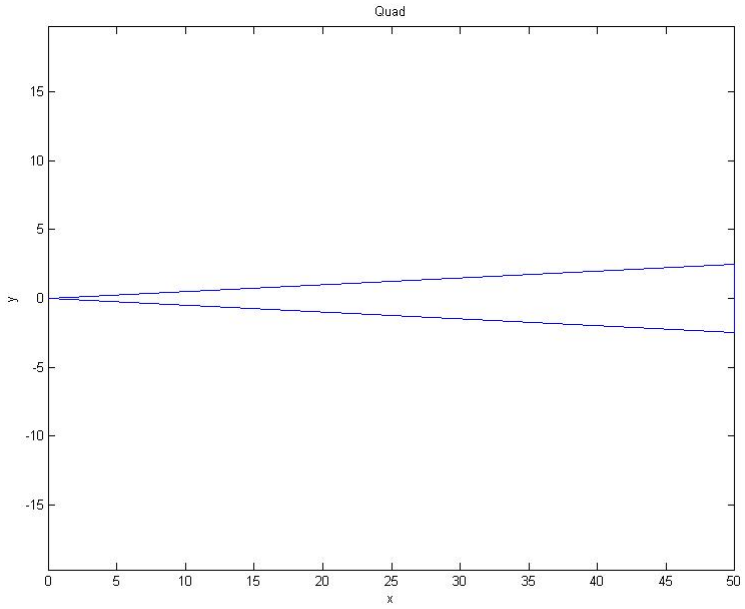

Figure 6.2: The 'Quad' hull is an estimation of the single hull geometry used on the Quadrimaran Alexander.

an estimate of their dimensions was used to reproduce the geometry of the hull labeled 'KUDU'.

Figures 6.4 and 6.5 show the results for these two shapes included with those for streamlined bodies discussed before. The hull called Quad 4x4 has four quad hulls placed side by side. The beam is taken as the distance between the leading edge of the outer hulls, thus the total craft beam and the separation of each hull from the next, being uniform is therefore a third of the total beam.

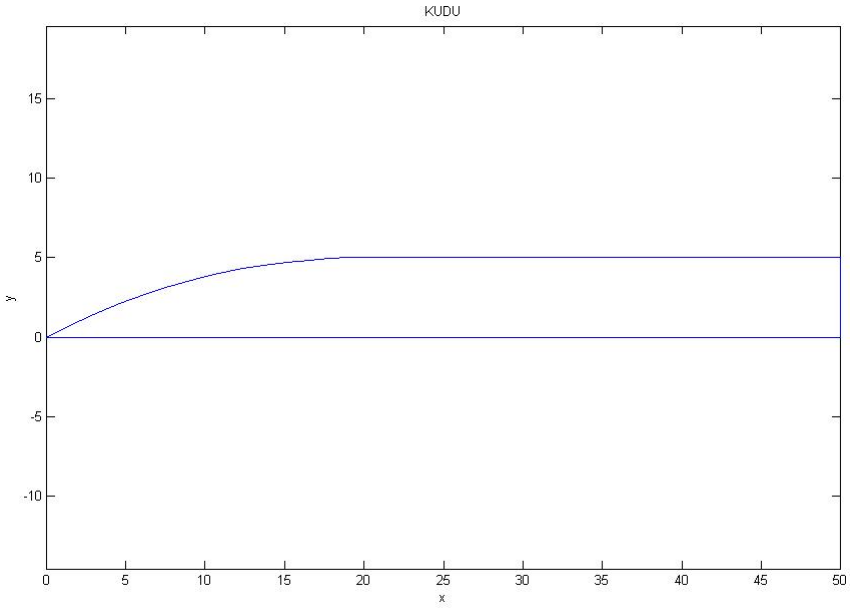

Figure 6.3: The Kudu is an estimation of the single hull geometry used on the KUDU II vessel [8].

6.5 Discussion of Results

The difference in pressure distributions created by the two new hull shapes is considerable. The KUDU has created some negative pressure but it is known that it was an effective craft and indeed, won the race for which it was designed. This is not too surprising since the negative pressure created for an equivalent length to beam ratio (which would scale to about eight metres on a fifty metre craft) is very small. In comparison the wing, which had an angle of seven to ten degrees and which was in extreme ground effect, would more than likely have acted as a RAM wing and compensated for the hulls. In fact it is quite likely that the ram effect would have considerably slowed the flow speed under the hulls and also changed the angle of incidence on the hulls, this would certainly diminish the

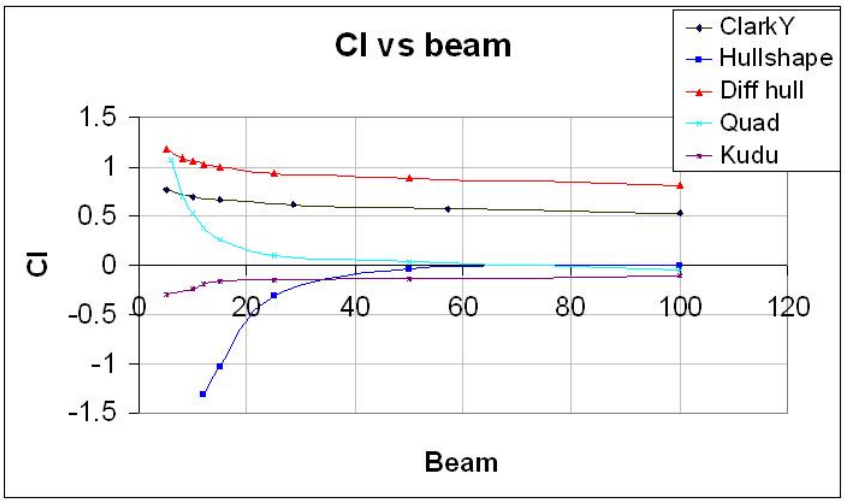

Figure 6.4: C_L as a function of hull spacing (m) for various hull configurations

channeling effect of the hulls if not stop it altogether. Such a shape may well seem a suitable design for a larger vessel if the upper deck were not close enough to allow choking of the flow, especially if the designer were not overly concerned by the hulls aerodynamic properties above and beyond their estimated drag coefficient. This would appear to be a mistake since they can create a significant low pressure, although much less than for large symmetrical bodies. The expectation that such hulls may appeal to ship designers does not seem unreasonable since they are already used on other ships and are almost exclusively used on SESs.

For the Quad shape shape the C_L is effectively zero for L/B ratios lower than two and it is only after this that a dramatic increase in lift is seen. The curve in Figure 6.4 rises sharply to a value of 1.07, just under that for the diff hull. This maximum value was obtained at an L/B of $8.\dot{3}$ which is much higher than had been considered a feasible design. However the Quadrimaran has a unique feature, in that being symmetrical it can be stacked. Unlike the cambered foil shapes which would attempt to cancel each other out in close proximity the quad can be stacked with high pressure created between each pair of hulls. The results for a set of four

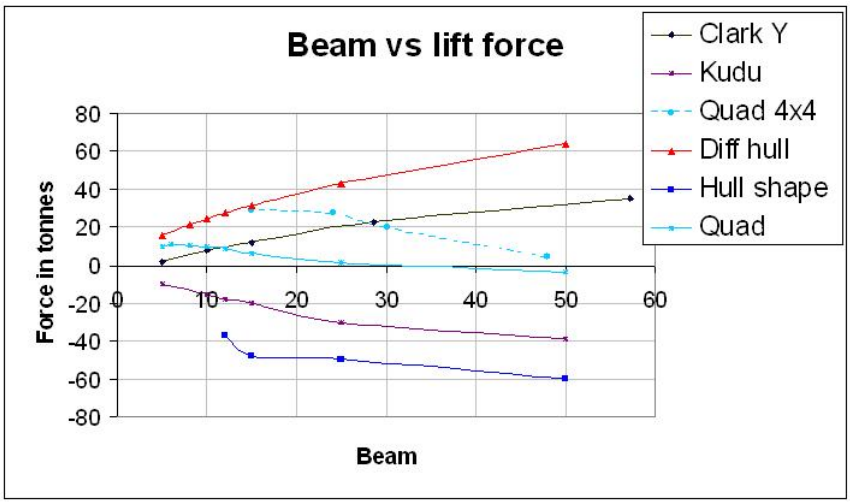

Figure 6.5: Force converted into equivalent tonnes, as a function of hull spacing (m) for various hull configurations

evenly spaced hulls are shown on Figure 6.5. Both the Quad and Quad 4x4 are the only hulls to have an increased force with decreased beam, which is a result of the rise in pressure, corresponding to the rise in C_L, being greater than the reduction in deck area. As mentioned before, the consequence of additional hulls is simply to multiply the force, which is scaled from the twin hull version, noting that the beam will be the distance separating the leading edges of the outer hulls. It can be seen that for the minimum spacing the result is approximately three times higher for the Quad 4x4 than the Quad as a catamaran. It should be noted that the final result for the Quad 4x4 was done at an individual hull spacing of five metres which, from the geometry of the craft, makes it a closed shape, or 'ram wing'. For this case, the flow reaches stagnation pressure, $1/2\rho v^2$, and thus no higher pressure can be obtained, however the area is now the smallest. Also, since the air is stagnating, the flow has to pass around an apparently square body, with a width of about twenty metres. This, in comparison to the two streamline

diff hulls which create approximately the same pressure would suggest that the efficiency of the Quadrimaran would be much lower, even before the extra skin friction from air and water is accounted for from the additional hulls. However, there are structural and stability benefits to the Quadrimaran which make it well worth further investigation. How the Quadrimaran hulls create high pressure and thus how it can be optimised poses an interesting question, one which does not appear to have been answered in the paper by Hockberger [4]. The effect of lift produced by the hulls was initially attributed to the slope of the upper deck. "The underside of the upper hull (the 'wet deck') has a constant slope of its own from bow to stern, and air pressure on these surfaces between the lower hulls produces an aerodynamic lift as the Quadrimaran moves ahead." He goes on to say that "This was not an expected effect, but once recognised, aerodynamic lift was treated as a major component of total lift" and from wind tunnel tests and observation from the scale prototype he concludes that "The effect was not simply the pressure on the underside of the wet deck causing lift. The tunnels were pressurised throughout.....riders saw a sea surface flattened by the pressure in the same way as occurs beneath an ACV or SES" although no explanation of how this is achieved has been provided.

From observation of the CFD results for both the Quad and Quad 4x4, it can be seen that the side hulls contribute substantially to the lift produced. Indeed for a speed of seventy knots, a hypothetical 56 m Quadrimaran is estimated to have 60 tonnes of aerodynamic lift. By comparison the 50 m Quad 4x4 of similar beam has an estimated lift of 30 tonnes just from the pressure created by the hulls.

In order to understand how the side hulls of the quadrimaran create lift, it may be beneficial to first consider the case of a symmetrical foil in more detail. In this case, the foil in free air at H_∞ will have a stagnation point on the centre of the leading edge, from which high pressure radiates. As the flow curves around the

front of the nose the pressure decreases sharply and this low pressure continues along the body, varying according to the thickness, until reaching the trailing edge, where the flow leaves at atmospheric pressure. As the foil is brought toward its mirror image, the high pressure field created by the stagnation point on the nose will start to combine with its opposite number. Although the high pressure field is very small, the combination of the two fields between the foils results in a greater pressure than around the edges, where the flow will tend to be diverted. This in turn will move the stagnation point on the leading edge of both foils slightly in towards the line of reflection, thus increasing the pressure further. However, since the nose is round, the stagnation point is very small and the flow soon starts to curve around the wing resulting in a much more significant low pressure, which combines between the foils as discussed earlier. In the case of the Quadrimaran hull, the flow behaves in much the same way, except that since the nose is sharp, the stagnation point will begin much smaller than for the foil. Once the hulls are close enough for the high pressure interference to move the stagnation point around to the inside however, the flow will no longer meet the sharp nose but will hit the side of the hull straight on. This increases the size of the stagnation point considerably, and as the hulls move closer, the effect is compounded in the same manner as for the symmetric foil. Vector diagrams of the flow around the leading edge of these hulls is shown in Appendix A. As the flow moves along the hull however, the thickness of the hull causes the flow to reduce pressure, this is clearly seen in the pressure plots, Figures 6.12 to 6.17, where the stagnation point at the leading edge has the highest pressure, which reduces along the length of the hull, ending in a low pressure due to the turbulence behind the transom hull. As the hulls get closer, the stagnation value increases (toward the total $1/2\rho v^2$) and spreads down the hulls. Although the pressure always decreases along the length of the hull, the starting pressure soon increases to a point where the vast majority of the length is in high pressure. Since it is the case that the hulls have

to be close to each other before the minimal stagnation pressure pushes the flow around the hulls and hence moves the stagnation point in, as well as the fact that the substantial pressure reduction along the length produces a net zero pressure until the hulls are very close, it easy to see why the force changes so dramatically with the beam.

Since the quadrimaran requires twice as many hulls to achieve the same lift as the diff hull and it has substantial turbulent losses, it is likely that the efficiency is much less, due mainly to the extra drag. However the ability to stack consecutive hulls may make it a very important design. With this in mind, the question of how to optimise the hull shape becomes tricky, since it would appear that the hulls are effectively acting like a pair of flat bottomed wings in close proximity. The suction noted by Paulson [42] for wings at an angle of attack in extreme ground effect is clearly also a problem here since the narrowing of the duct, which is accentuated with angle of attack will decrease the pressure just as the same increase in angle will increase the stagnation region and hence pressure. As for the turbulent losses, any attempt to reduce turbulence by streamlining the shape would either render it a symmetrical foil (at zero angle of attack) or else would result in asymmetry which prohibits stacking. Thus it would appear that the symmetric triangular shape of the Quadrimaran hull is a special case, only the length to beam (base width) ratio of the individual hulls can be changed, where an increased beam will result in higher drag and higher stagnation region, but also a greater channeling effect and reduction of pressure along the hull.

Equally there is the question of numbers of hulls. Common sense may limit the ship to at least single figures, however up to six hulls might not seem too unreasonable if the hulls were long and thin. From looking at the Quad 4x4 pressure plots however, it seems that the effect of stacking is not quite uniform. That is, the two central hulls experience less lift than the outer ones. This appears

to be the result of the apparent angle of attack of the hulls. As discussed earlier, once the hulls are close enough, the high pressure around the leading edge causes the flow to divert around the hulls. Since the flow is diverting around the central line, the divergence is accentuated as it passes the second hull. This can be seen in the vector plots of Figures A.5 & A.6, where the flow is clearly hitting the outer hull at a much greater angle. It is likely then, that the more hulls there are the more uneven the stacking will be, with much greater pressure in the outer hulls then in the inner ones. This may also lead to flow separation on the opposite side to the flow, which in turn could create low pressure and further turbulent losses.

It may be that the use of Quadrimaran style hulls allows other asymmetrical hulls to be spaced, that is a Quadrimaran hull may be used to create a trimaran out of a diff hull configuration. However , since the central hull would have no angle of attack it would not contribute to the lift. If two were used however, it may be a more beneficial configuration.

6.6 Conclusion

From the results, it is clear that for a catamaran configuration a cambered foil shape is the best for producing a high pressure throughout the hulls, and that a significant force can be produced at speeds which are already being reached by large vessels at sea. Likewise the Symmetric foil produces significant suction and could seriously diminish the performance of a craft. The KUDU, although not as problematic as the symmetric shape, still creates negative pressure in comparison to the foils. The Quadrimaran is an interesting case because despite its symmetric shape it still produces high pressure, which is a great benefit for ships with more than two hulls. However, it appears to have large turbulent losses and could have far greater drag. Certainly the results suggest that for greater beams the

cambered foil is more effective than the Quadrimaran. Further study is required in order to fully understand the potential of the Quadrimaran configuration.

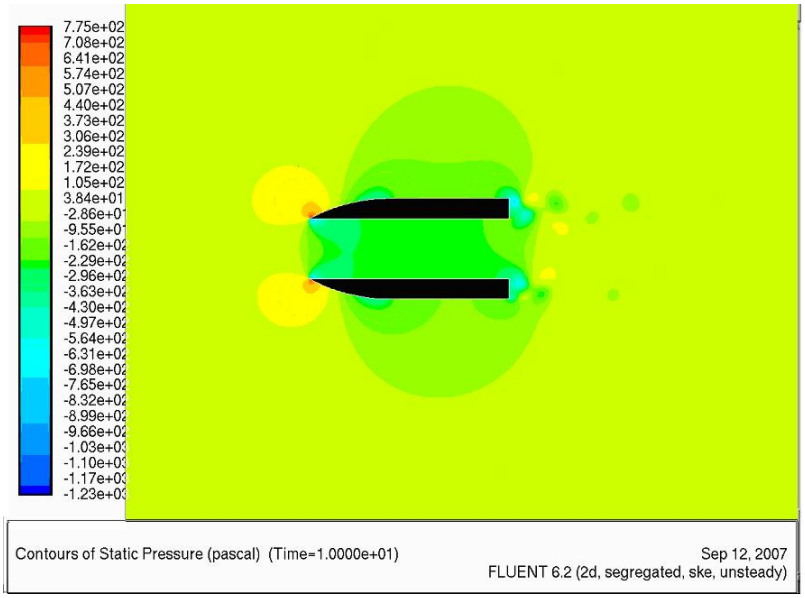

Figure 6.6: Contours of static pressure for the Kudu hull at $B = 15$

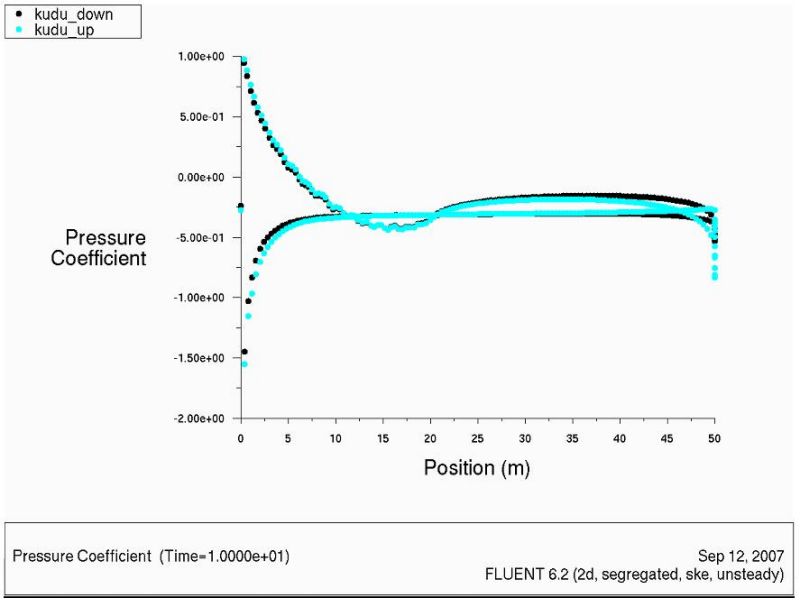

Figure 6.7: Plot of C_p for the Kudu hull at $B = 15$

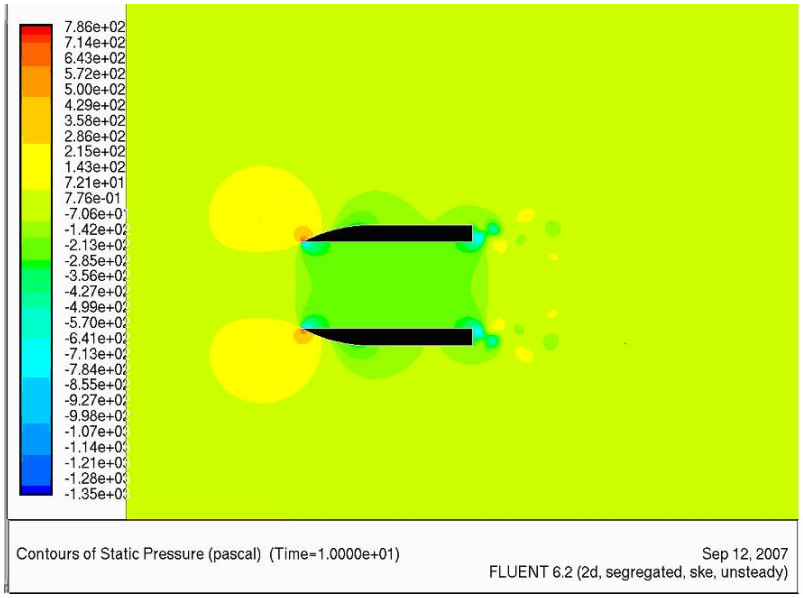

Figure 6.8: Contours of static pressure for the Kudu hull at $B = 25$

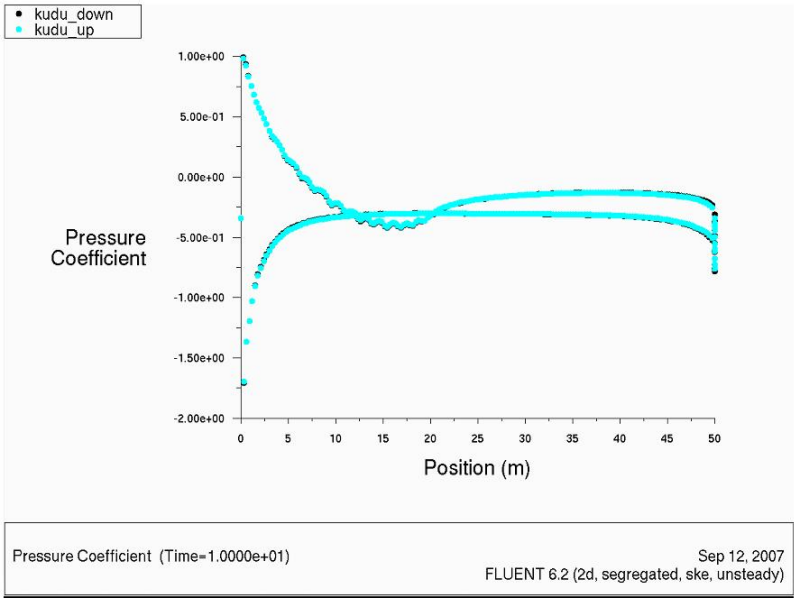

Figure 6.9: Plot of C_p for the Kudu hull at $B = 25$

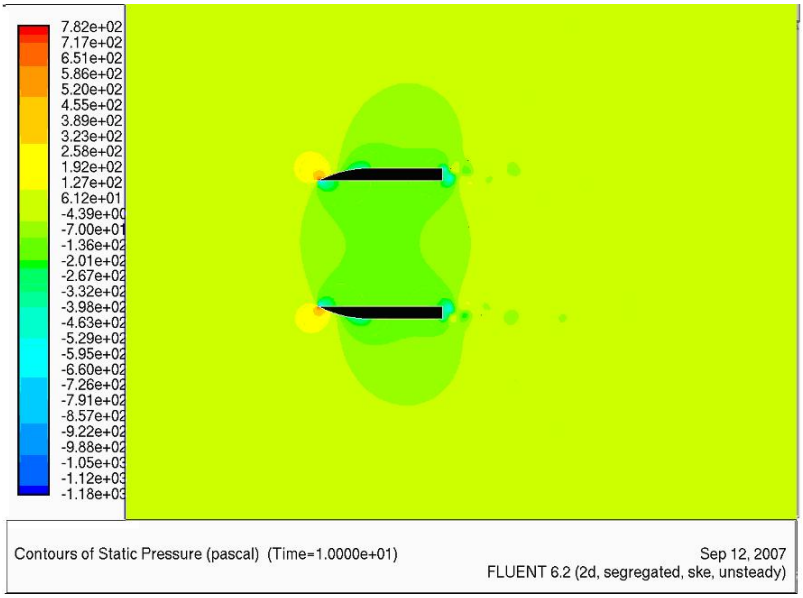

Figure 6.10: Contours of static pressure for the Kudu hull at $B = 50$

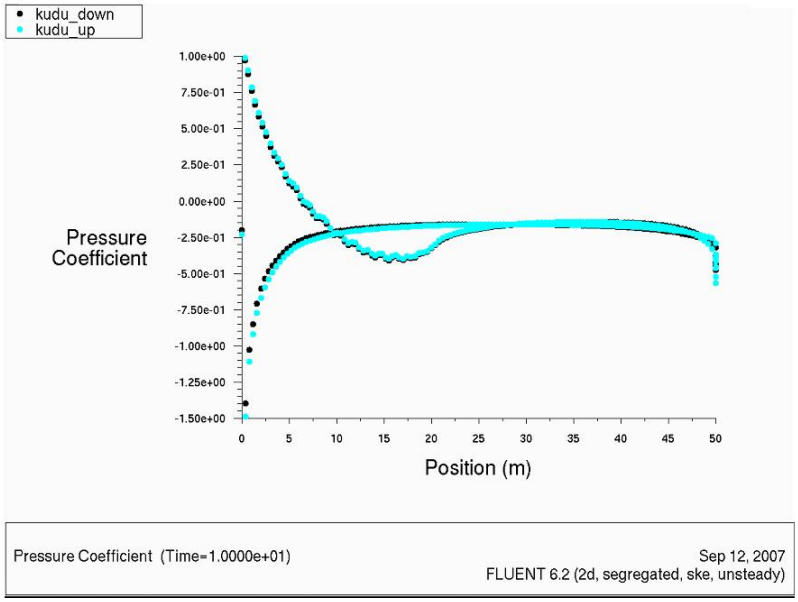

Figure 6.11: Plot of C_p for the Kudu hull at $B = 50$

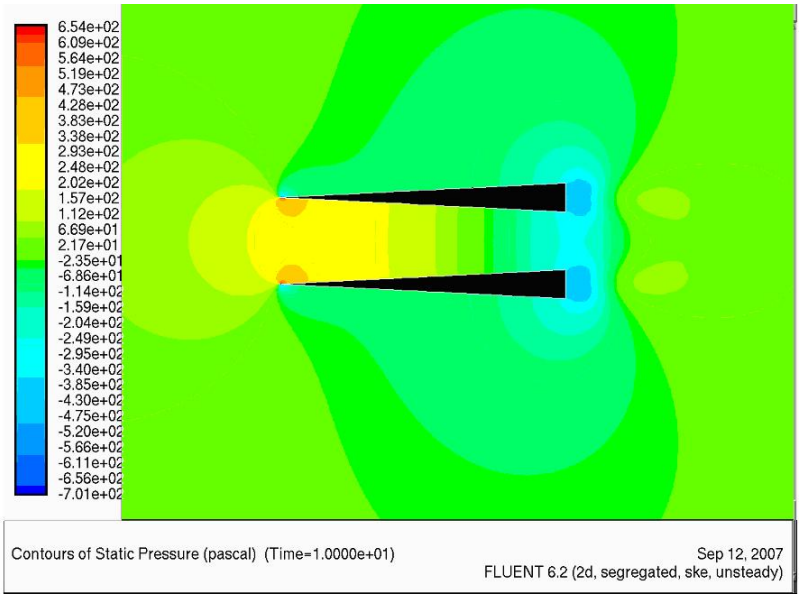

Figure 6.12: Contours of static pressure for the Quad hull at $B = 15$

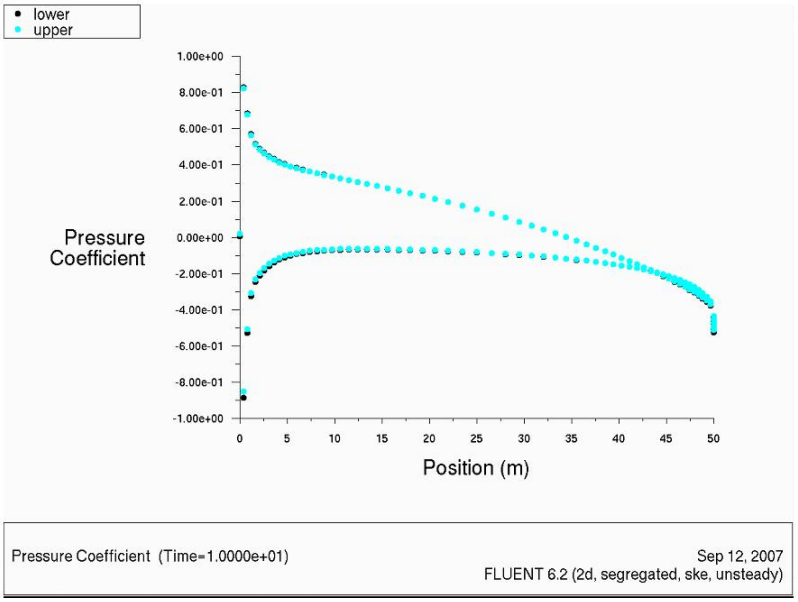

Figure 6.13: Plot of C_p for the Quad hull at $B = 15$

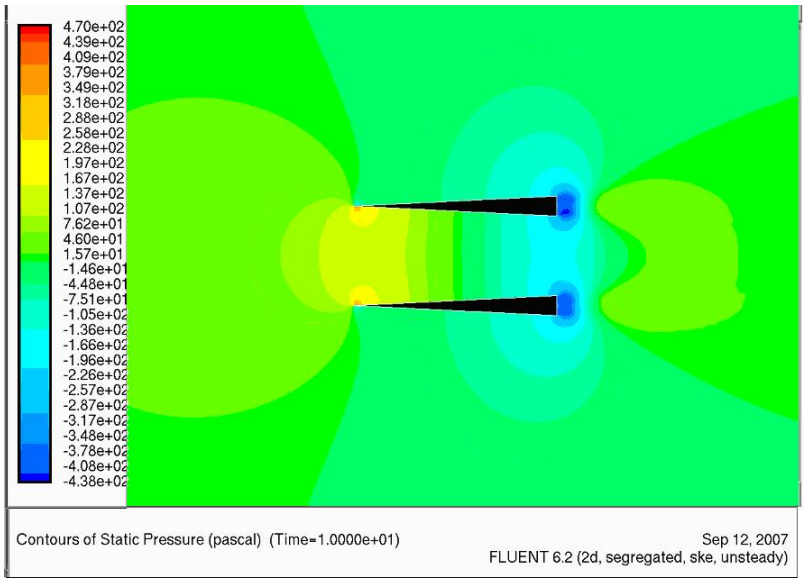

Figure 6.14: Contours of static pressure for the Quad hull at $B = 25$

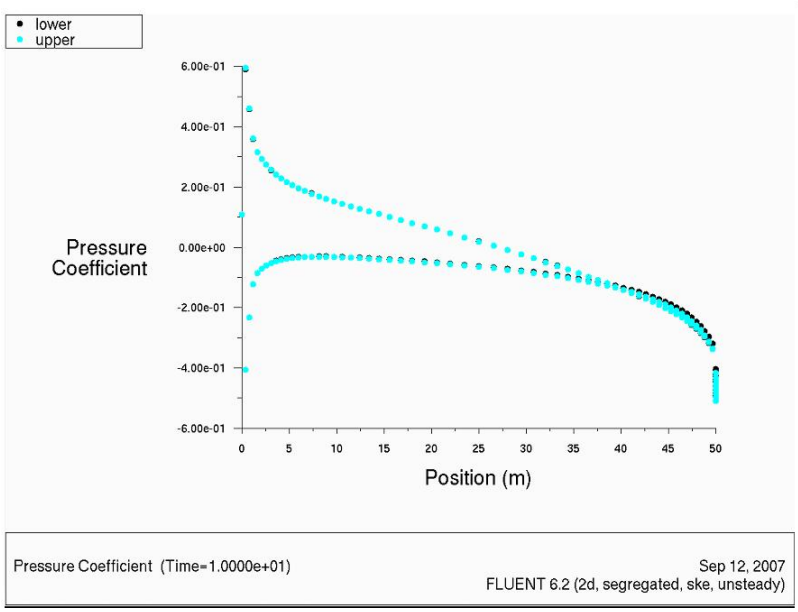

Figure 6.15: Plot of C_p for the Quad hull at $B = 25$

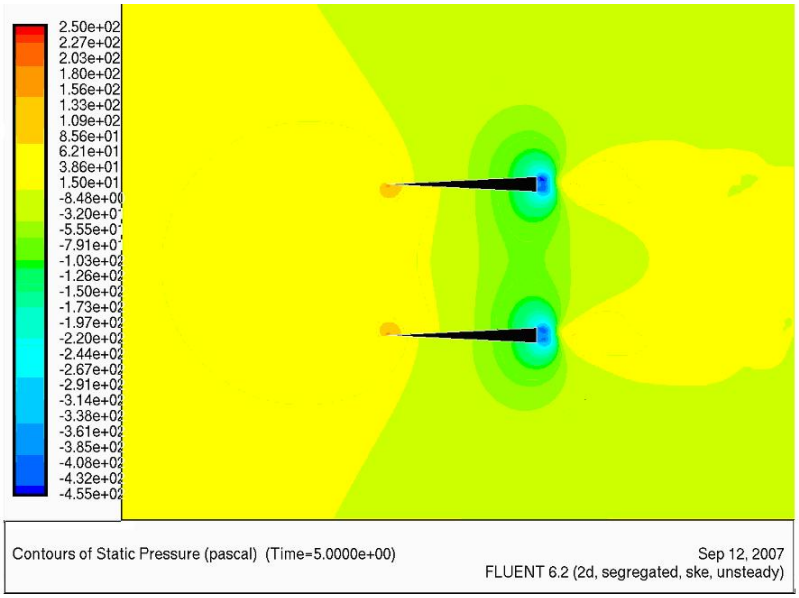

Figure 6.16: Contours of static pressure for the Quad hull at $B = 50$

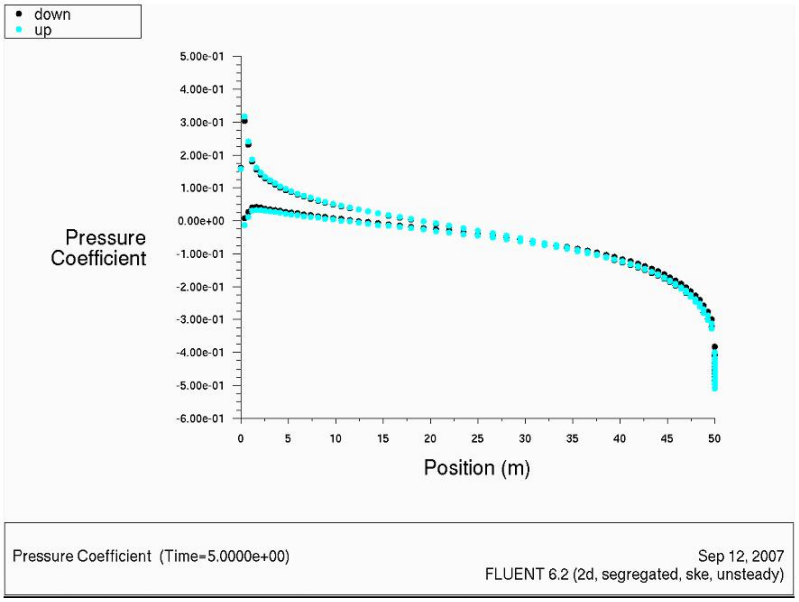

Figure 6.17: Plot of C_p for the Quad hull at $B = 50$

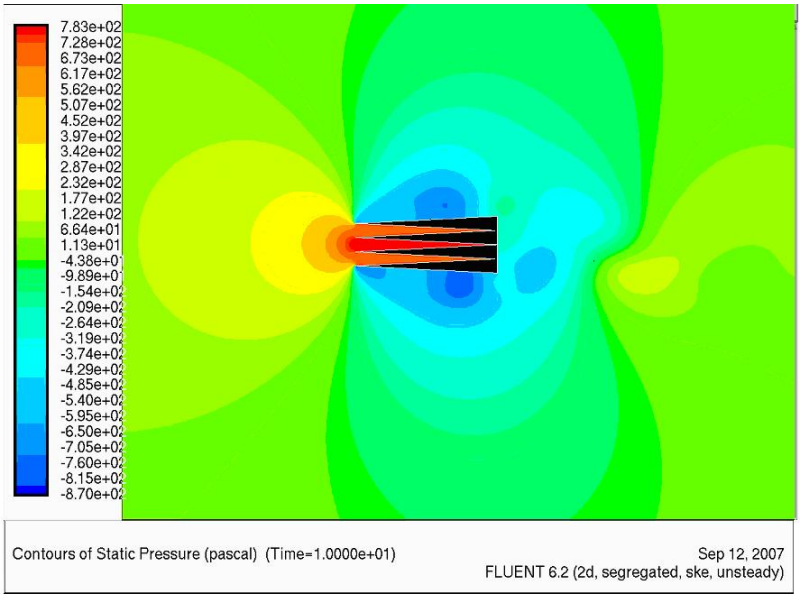

Figure 6.18: Contours of static pressure for the Quad 4x4 hull at $B = 15$

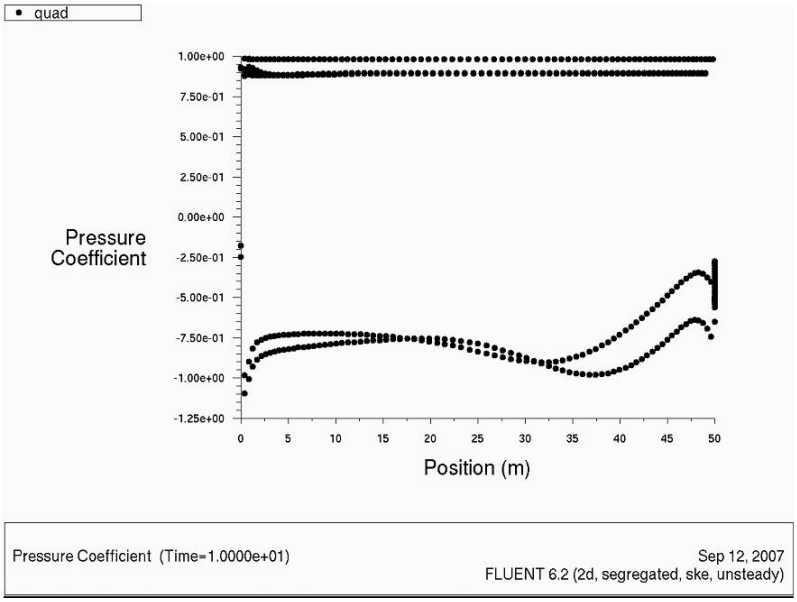

Figure 6.19: Plot of C_p for the Quad 4x4 hull at $B = 15$

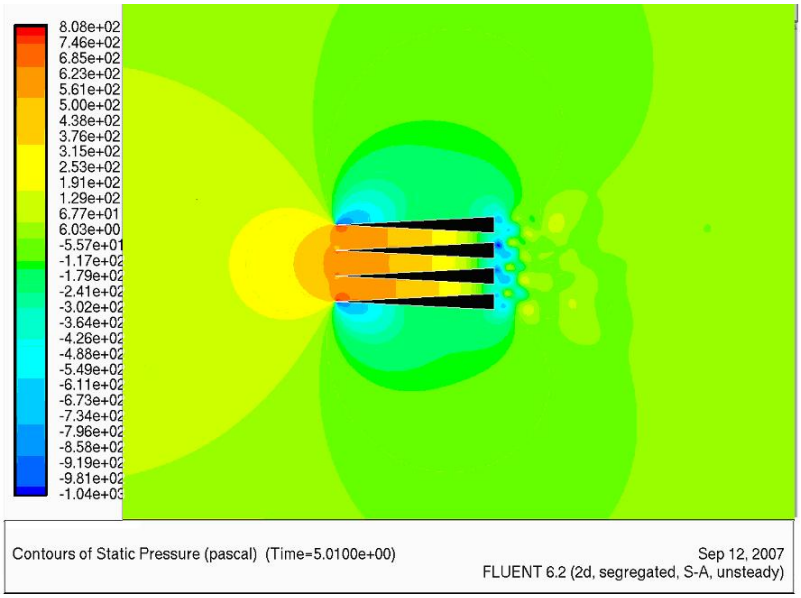

Figure 6.20: Contours of static pressure for the Quad 4x4 hull at $B = 24$

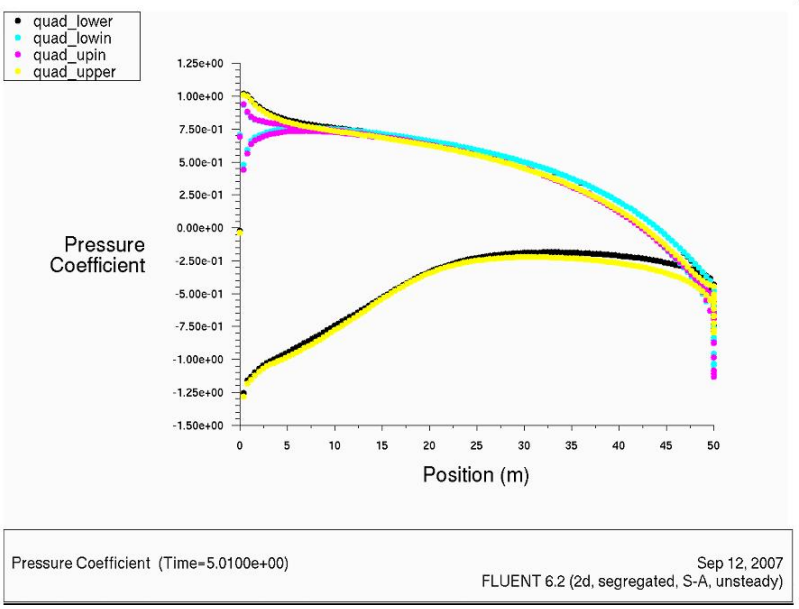

Figure 6.21: Plot of C_p for the Quad 4x4 hull at $B = 24$

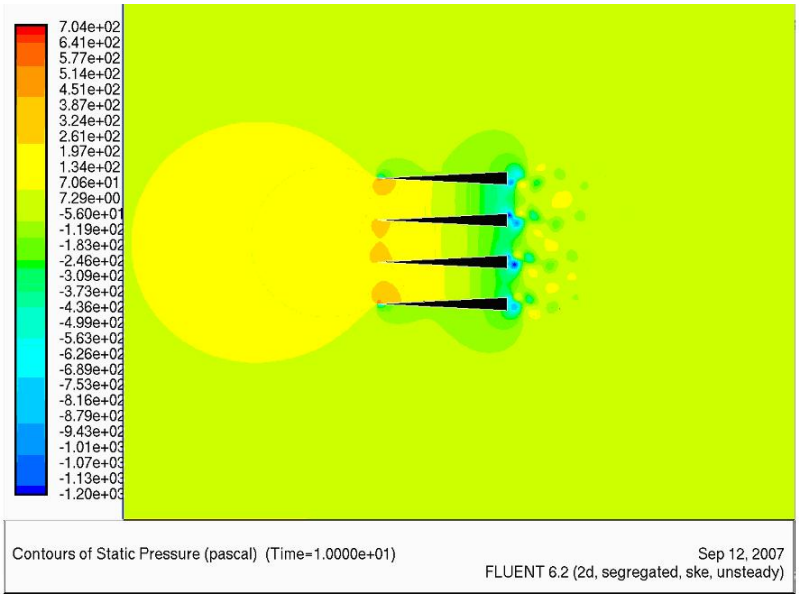

Figure 6.22: Contours of static pressure for the Quad 4x4 hull at $B = 48$

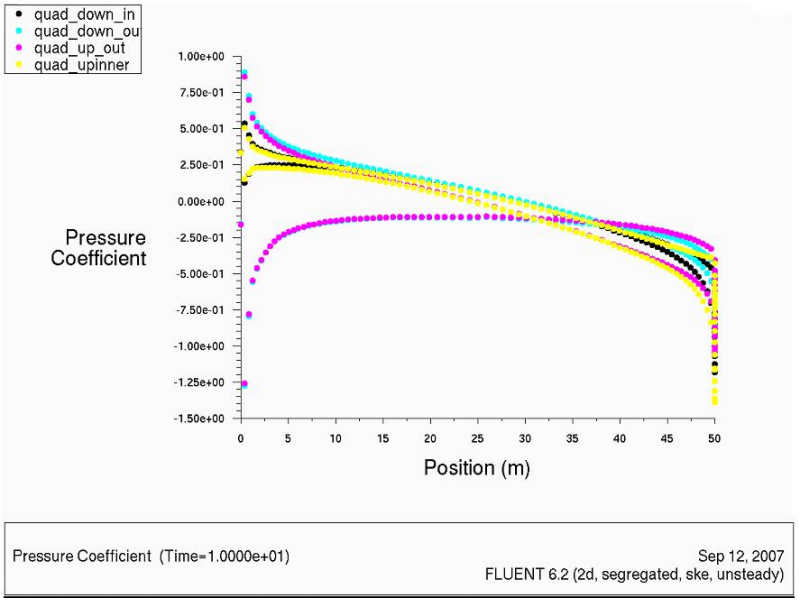

Figure 6.23: Plot of C_p for the Quad 4x4 hull at $B = 48$

Chapter 7

3D MODELLING

7.1 Introduction

Using a Computer Aided Design program (SolidWorks 2004), the airfoil sections studied in two dimensions were extruded to produce a 3D wing. It was then possible to loft the chosen hull shape to the wing tips, forming a complete structure. It was decided that the Clark Y wing profile should be used as the general case, since it has a flat underside which can be more easily lofted with a variety of side hulls. Due to the variety of shapes under consideration and the constraints on time, the models have been kept as simple as possible, particularly in regard to the air water interface. It is obvious that the aerodynamic profiles suggested will differ greatly from the optimum hydrodynamic shape and that some compromise to the aerodynamics must be made along the water line. However, at this stage of the research the priority lies in identifying the most useful aerodynamic properties, from which a more realistic ship may be designed.

An example of the shapes used for testing is shown in Figure 7.1. The shapes are derived from a combination of the 'Clark Y' wing with 'hull shape', 'Clark Y' and 'Diff hull' side walls. Once a suitable meshing technique and model has been

chosen the effect of height, beam and profile on static pressure and drag can be evaluated for the chosen shapes.

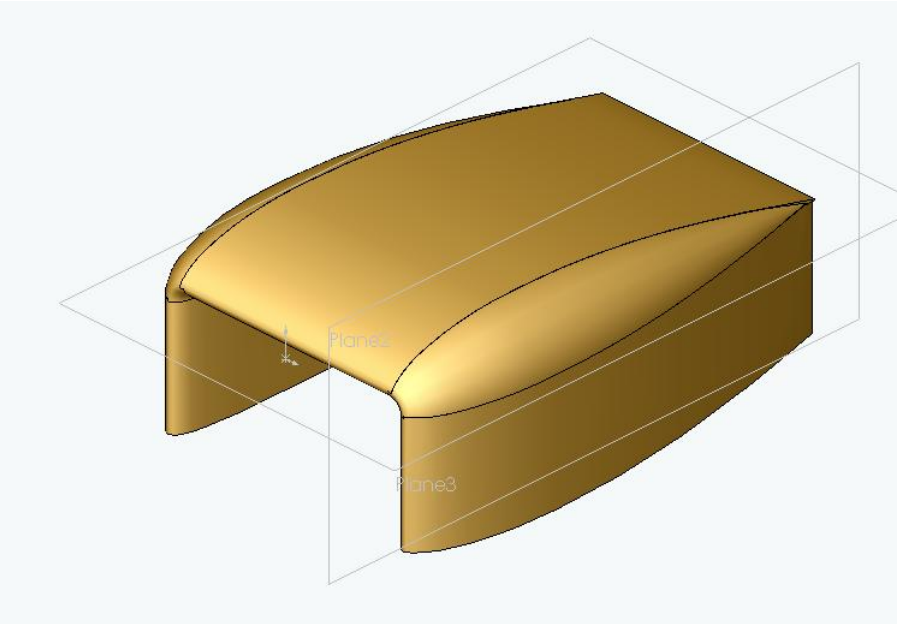

Figure 7.1: Solid model of the Clark Y wing-hull combination.

7.2 Validation

As the experimental results for the Clark Y wing do not cover the same enclosed shape that is tested here, it is not possible to directly compare the results. However, it has been estimated that the 3D Clark Y tunnel will act in much the same way as an infinite, or 2D wing and as such, can be compared to the earlier results. Further validation comes from the more standard procedure of mesh refinement, or mesh independence, as has been described above.

Two cases were chosen for mesh refinement, a Clark Y wing of aspect ratio 0.5 and a Clark Y wing with Clark Y side hulls. Both were 50 m long, 25 m wide, at

zero angle of attack and with the leading edge 15 m from the rigid ground plane. The tests were run at 36 ms^{-1}, the same as for the 2D cases. A series of simple meshes were produced ranging from 20,000 to 200,000 nodes, a diagram of the setup and typical mesh are shown in Figures 7.2 and 7.3.

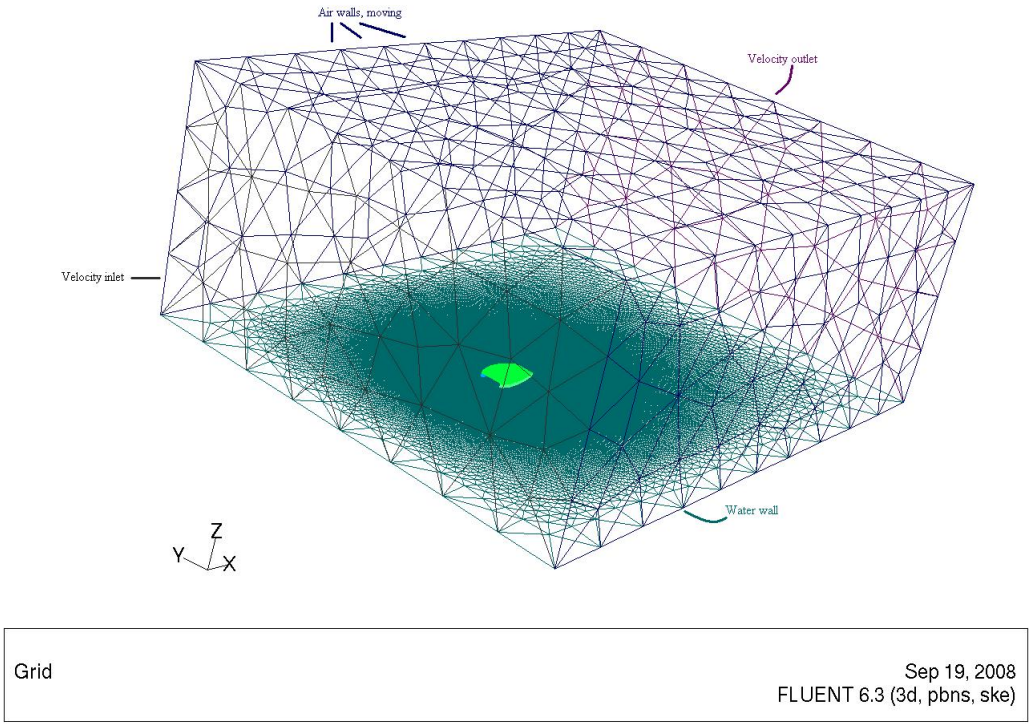

Figure 7.2: Detail of three dimensional grid setup

Fluent was setup is a similar manner to the 2D case, using the K-epsilon model with standard wall functions. The velocity inlet having a flow speed of 36 ms^{-1}, with the air walls set to move parallel to the flow at equal velocity, with zero roughness. The water surface was also set as a moving wall, but given default roughness. The rear wall was set as a pressure outlet, this setup is shown in Figure 7.2.

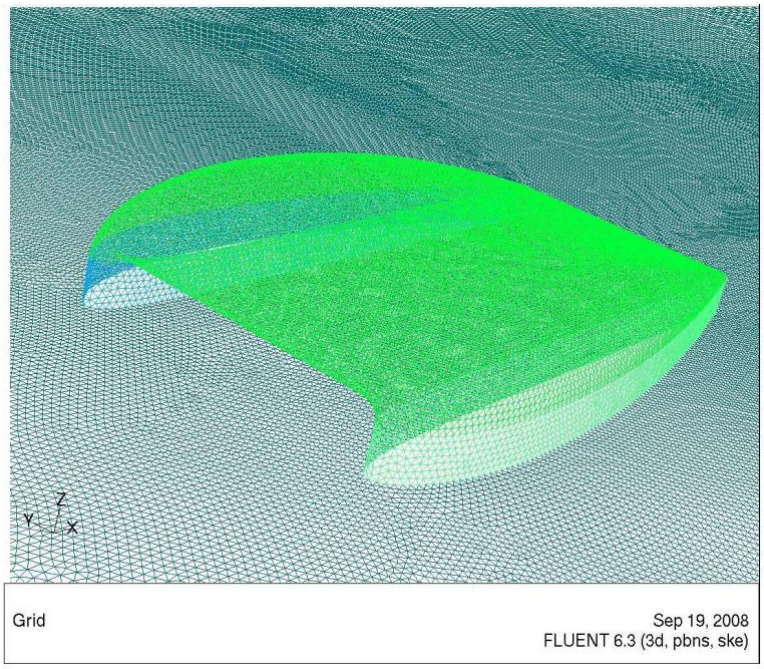

Figure 7.3: Surface mesh on Clark Y wing/hull combination

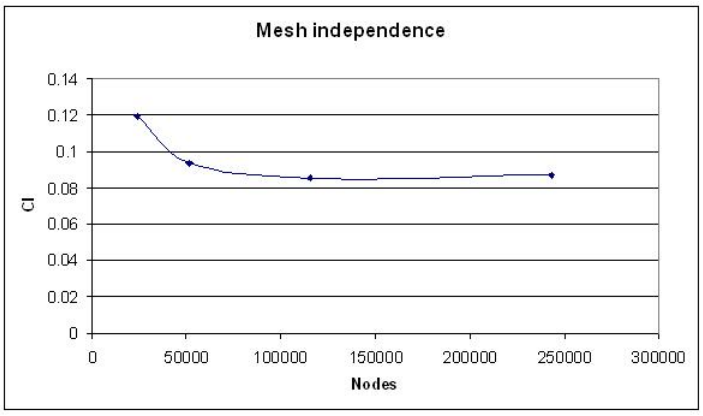

Figure 7.4: Mesh independence for a low aspect ratio wing of beam 25m

From the graphs in Figure 7.4 it can be seen that the main flow properties of the wing are captured for meshes of above 100,000 nodes. Below this the mesh is

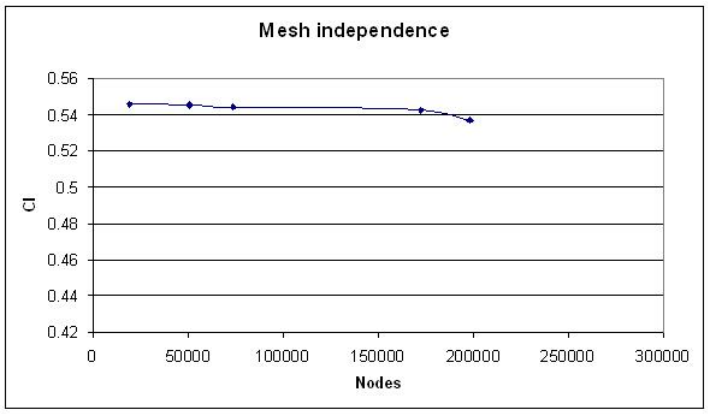

Figure 7.5: Mesh independence for tunnel hull of beam 25m

too coarse to allow the vortices to form and the lift is over predicted. It is most likely that a much finer mesh would be needed to accurately capture the wake pattern. However, the static pressure can usually be found to a reasonable degree of accuracy provided the physical properties of the flow, such as the vortices, have been modeled. For the wing and side hulls, shown in Figure 7.5, the results are much more stable, decreasing only very slightly as the mesh is made considerably finer. This is probably due to the lack of vortices, which in turn is the result of the wing tips effectively going into the ground. This produces both a better flow aerodynamically, since the high pressure does not recirculate on top of the wing, and a simpler flow to compute. The static pressure appears to be reasonably captured even before the coarse 20,000 node mesh first used. Static pressure plots for the two wings are shown in Figures 7.13 and 7.14.

It is immediately obvious from comparing the pressure plots shown in Figures 7.13 and 7.14 that the side hulls (made transparent in Figure 7.14) have resulted in a significant increase in pressure throughout the duct. This is certainly the difference in end effects and illustrates the importance of the side hull design

when dealing with such low aspect ratio wings.

The lack of vortices on the tunnel shape could be a major advantage to the design, as such, it is important to check that the program was not missing them due to inadequate meshing. It may be that the vortices could still form at the corners of the trailing edge of the wing, or at the base of the side hulls. If this is so, failure to account for them could seriously effect the results.

7.3 Investigation of Possible Vortex Formation

By cutting the model in half about the Y plane and using the symmetry function available in Fluent and Gambit, the computational space can be significantly reduced. Furthermore, the space around the hull can be diminished, this may slightly effect the pressure field if any reflection occurs from the surfaces. However, the walls were still kept at a sufficient distance to allow a wake or vortex to form. By doing this the computational domain is dramatically reduced, allowing more detailed meshes to be built around the side hulls, trailing edge and wake region. Although this may effect the results slightly, it is necessary since a fine grid may be required to notice the vortices and such a grid in a full size domain would take a very long time to build and run, if indeed it did not prove too much for the desk top processor to construct.

A series of very fine meshes, concentrated around the side hulls, trailing edge and wake region, were used to test the Clark Y tunnel section. The value of C_l only changed by about 6% and the drag by around 12%. No obvious vortices formed about the corners or trailing edge of the side hulls or wing. The largest degree of vorticity was found around the trailing edge, which showed only the small amount of turbulence expected at the trailing edge of such a large wing.

Figures 7.15 to 7.17 show the vorticity magnitude around the trailing edge. Some small amount of vorticity extends quite far down stream of the side hulls near the ground, however they do not exhibit any noticeably uniform rotation and are more likely the result of the wake interacting with the ground friction. That is, the ground is still moving at 36 ms^{-1} however, the wake will have slowed and this shear force may help to maintain the turbulence of the wake near the free surface for greater lengths down stream. Figures 7.18 to 7.20 show the Y velocity around the trailing edge. If there were any distinct vortices, the y component of flow would be equal and opposite above and below the axis of rotation. From the figures however, it is clear that the flow is running slowly parallel to the wing surface on both sides.

It is concluded that the tunnel shape does not have obvious vortices and as such, the flow properties will most likely be adequately captured by the coarser mesh. However, meshes of around 100,000 to 200,000 nodes were used in all the subsequent cases since they offer a slightly higher level of accuracy, particularly with regard to viscous drag.

7.4 Results

In this section the models are all run at zero angle of attack. This is partly to reduce the number of runs required, but equally due to the consideration that the deck wing must carry cargo and as such, should not be at extreme angles of attack during cruise if it can be avoided. Running at a very low angle would allow for the best use of space, particularly with reference to car ferries.

The first set of models run were based on a combined Clark Y wing and hull section. The models were run at constant beam $B = 25\ m$ and for a range of

heights H_0 from 5 to 20 m. All models where again tested at 36 ms^{-1}. The results for lift, drag and L/D are shown in Figures 7.6 & 7.7 below.

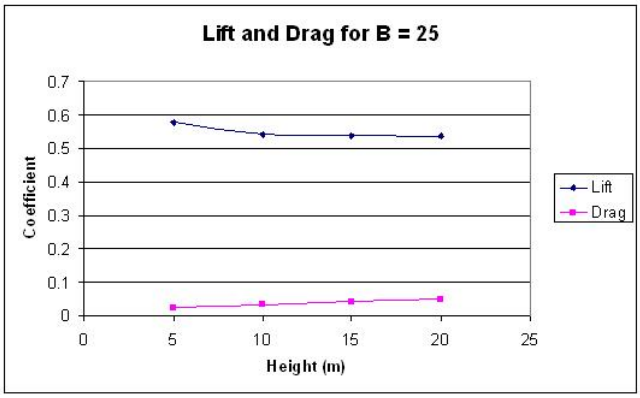

Figure 7.6: C_L and C_D as a function of hull height (m)

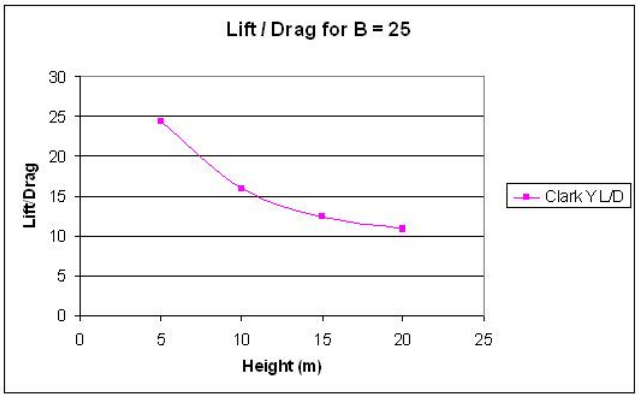

Figure 7.7: Lift-to-drag ratio as a function of hull height (m)

It is clear from the results that the lower height is significantly better for both lift and drag. This is likely to be a combination of the ground effect and the extra drag caused by the hull rising out of the water. As such, it is beneficial to have the wing as close to the water as possible. However, if the wing is too close, there is a

danger of wave impacts. From observation of comparably sized catamaran ferries, it would appear that a clearance of around three metres should be acceptable. This corresponds to a leading edge height H_0 of 5 m and this is the height which will be used for the remaining tests in this section.

Having ascertained a feasible height, the models can be run at a range of hull spacings in order to study the effect of beam on lift and drag. The results are shown below in Figures 7.8, 7.9 & 7.10.

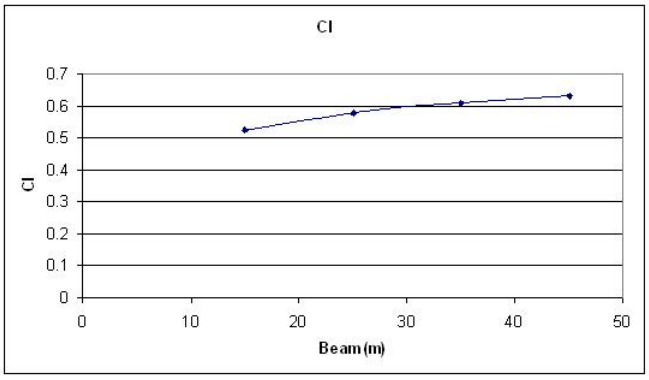

Figure 7.8: C_L as a function of beam (m)

Again, it is evident that the beam has a considerable effect on the lift and drag. Just as for the two dimensional case, increasing the beam increases the lift, but by a diminishing amount as the side hulls begin to interfere to a lesser extent. Equally, the increased beam reduces the drag. This would suggest that a wide beam would be best, however, in reality a ship with such a wide beam would be unable to enter most ports and may suffer from structural problems due to bending moments across the deck. A beam of 25 m is chosen as the largest plausible beam, but it is noted that much better performance can be gained where larger beams are possible.

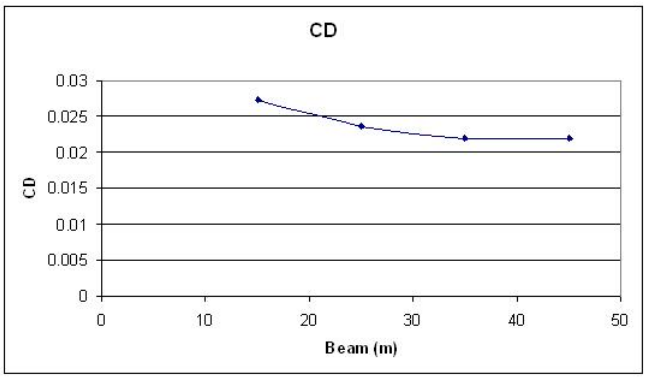

Figure 7.9: C_D as a function of beam (m)

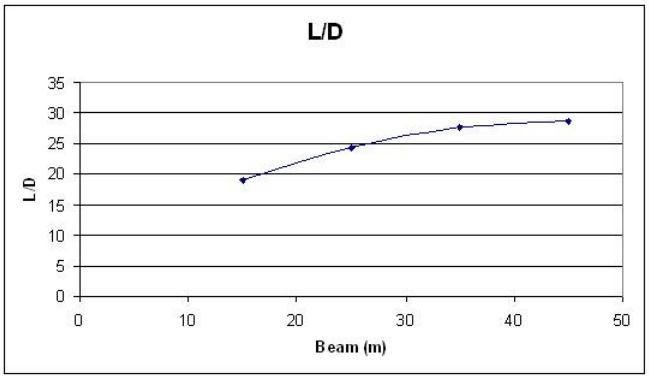

Figure 7.10: Lift-to-drag ratio as a function of beam (m)

Using the same 25 m beam and a height of 5 m, the Clark Y wing model can be run with any number of hulls designs and directly compared. The results for the Clark Y in combination with the Hull shape, Clark Y and Diff hull sides are shown in Figure 7.11 below. In addition, the results for a complete diffuser hull are also shown. This being the combination of the Diff hull shape with an upper wing of the same highly cambered profile.

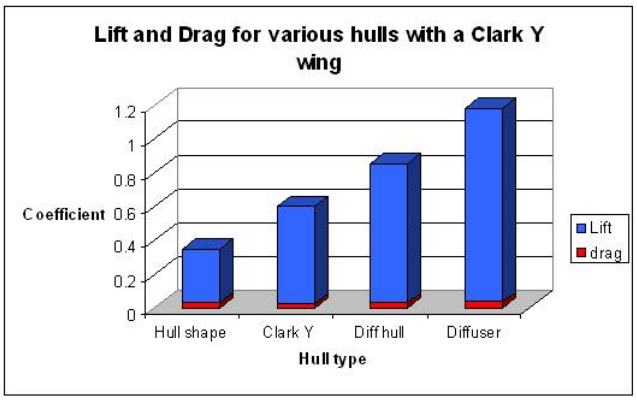

Figure 7.11: Lift and drag for various hull configurations

7.5 Discussion

The three dimensional results show the same trends as for the two dimensional tests. The lift coefficient is improved by lowering the height of the wing and by increasing the beam. As mentioned before, it is necessary to impose restrictions on both the height and beam due to the constraints of open ocean waves and harbour conditions.

The results for the different hulls in conjunction with the Clark Y wing clearly show that the shape of the hull has a dramatic effect on the pressure distribution between the hulls. The calculated pressure distributions are shown graphically in Figures 7.23 to 7.28. The results for coefficient of lift and drag demonstrate the change in performance clearly. Figure 7.11 shows the lift and drag for the various hulls in combination with the Clark Y as well as the complete diffuser shape. From this it can be seen that although the drag remains nearly constant, the lift varies dramatically from 0.31 up to 1.15. Figure 7.12 shows the effect of the various hulls as a percent change from a theoretical two dimensional wing. In

previous papers, such as that by Doctors [55], the hulls are assumed to act as end plates and allow two dimensionality to be applied to the aerodynamics. Figure 7.12 shows the percentage error compared to the hull data from two dimensional data of a Clark Y wing at infinite height and at a height of 5 metres. It can be seen that the effect of the symmetrical Hull shape is extremely detrimental and that assuming the effect is two dimensional and still in ground effect leads to an error of around 55%. By shaping the hulls as Clark Y foils however, the assumption of two dimensionality becomes more reasonable. The actual value lies between that of the ground effect and infinite height, that is to say, the end plate effect of the hulls has not produced as higher value as for an infinite wing in ground effect, but it is better than that of an infinite wing out of ground effect. This is a considerable achievement, since end plates do not usually have such a pronounced effect. They are of course not usually airfoil shaped or in contact with the ground, and this must account for much of the difference. In the case of the diff hull, the hulls have improved the coefficient of lift of the low aspect ratio wing in ground effect beyond that of an infinite wing in ground effect by nearly 18%! This means that the assumption of two dimensionality and dismisal of the effects of the side hulls on a low aspect ratio wing can lead to errors of over 100%. Indeed, since much of the dismissal of aerodynamically alleviated catamarans is based on the proposed difficulty of providing sufficient lift with a low aspect ratio wing in ground effect, which, it is suggested, will not achieve the two dimensional lift proposed, may in fact be an under estimate if the hulls are designed properly. It is confirmed that the standard hulls will not allow the assumption of two dimensionality by quite a margin, but the adapted hulls presented here are able significantly out perform the 2D wing.

The final test, using the complete diffuser shaped hull, gives a total C_l of 1.151 and a lift-to-drag ratio of 35.9, this can be compared to a low aspect ratio wing of the same dimensions where the C_l is only around 0.07 and the L/D as low as

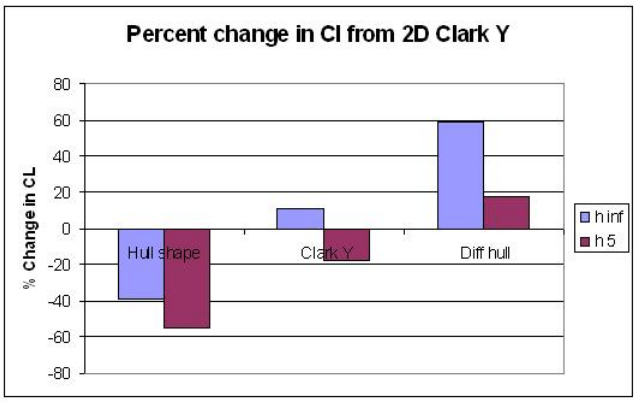

Figure 7.12: Effect of hull shape on lift for a Clark Y wing as a percentage

3. This clearly illustrates the importance of hull design in conjunction with wing design when considering aerodynamically alleviated hull designs.

7.6 Conclusion

The potential for realising very high coefficients of lift and lift-to-drag ratios, makes the ducted hull design a far more viable contender than many of the designs previously suggest for aerodynamic alleviation. With such high values it is perhaps more reasonable to suggest that a dynamic version of the SES craft, with a substantial portion of the weight supported by air, could be produced through the forward motion of the craft. The question remains however, of what the effect of the hydrodynamic shaping of the hull will be? And even if the hydrodynamics do not greatly effect the aerodynamics, will the increase in lift proposed here be enough to make the technology worth pursuing?

Since it is highly unlikely that the hydrodynamics will improve the aerodynamics (although it is hoped that some further improvements will be made to the aerodynamics as well) it is perhaps best to assume that this is the optimum design

and to compute its effect on the performance before continuing. If the improvements are of negligible effect to the over all performance then there is little hope that further iterations will make proportionally larger improvements to the design. However, from previous investigations, such as Doctors [55] it is seen that suitable aerodynamic alleviation can have a significant effect.

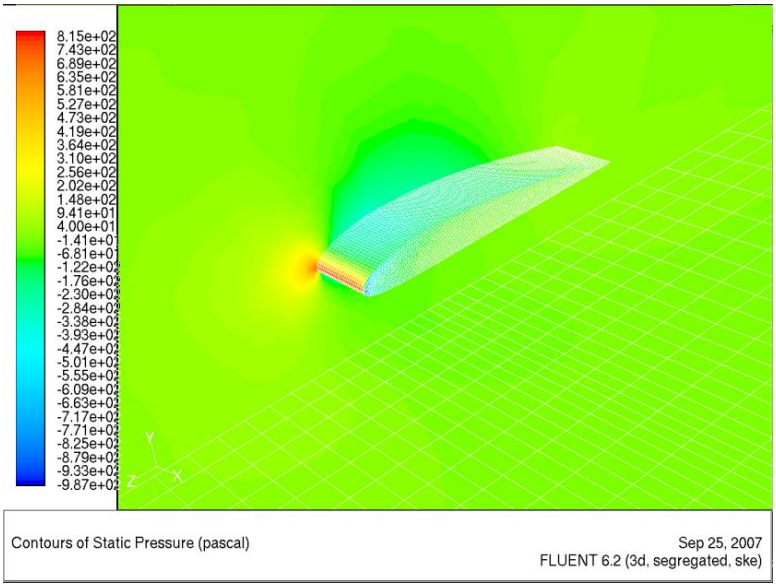

Figure 7.13: Low aspect ratio Clark Y wing static pressure plot, H = 15

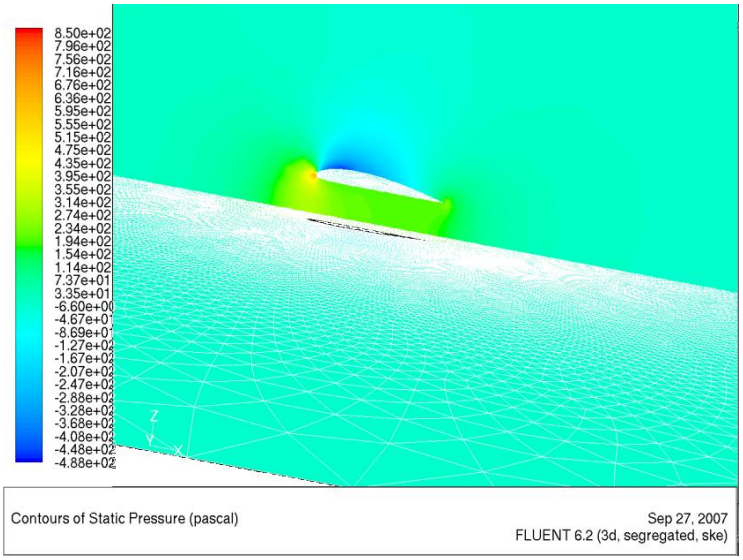

Figure 7.14: Clark Y wing/hull combination, showing static pressure as seen from the side, hulls not shown, H = 15

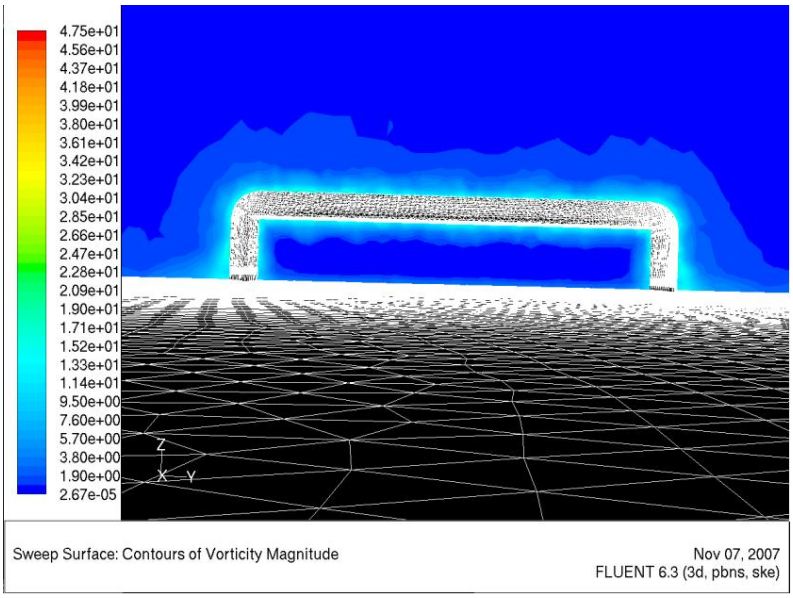

Figure 7.15: Vorticity magnitude at a short distance before the trailing edge

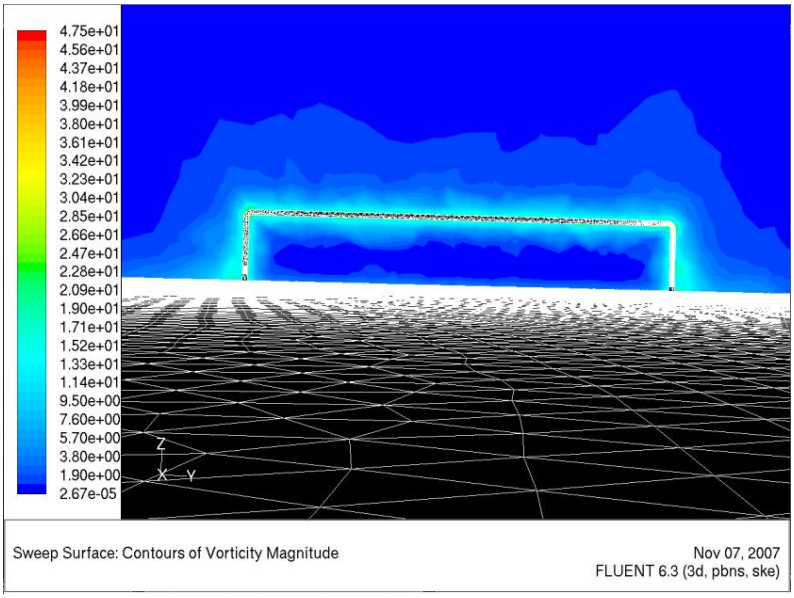

Figure 7.16: Vorticity magnitude at the trailing edge

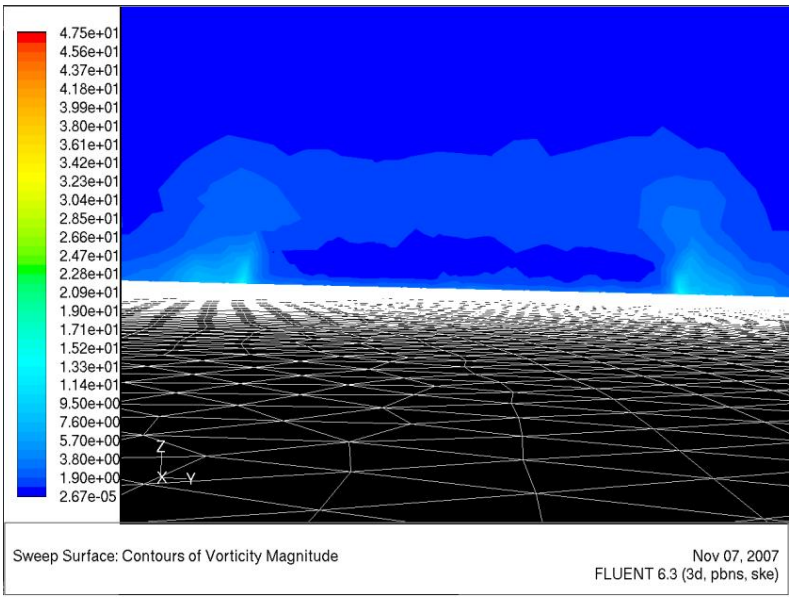

Figure 7.17: Vorticity magnitude at a point just beyond the trailing edge

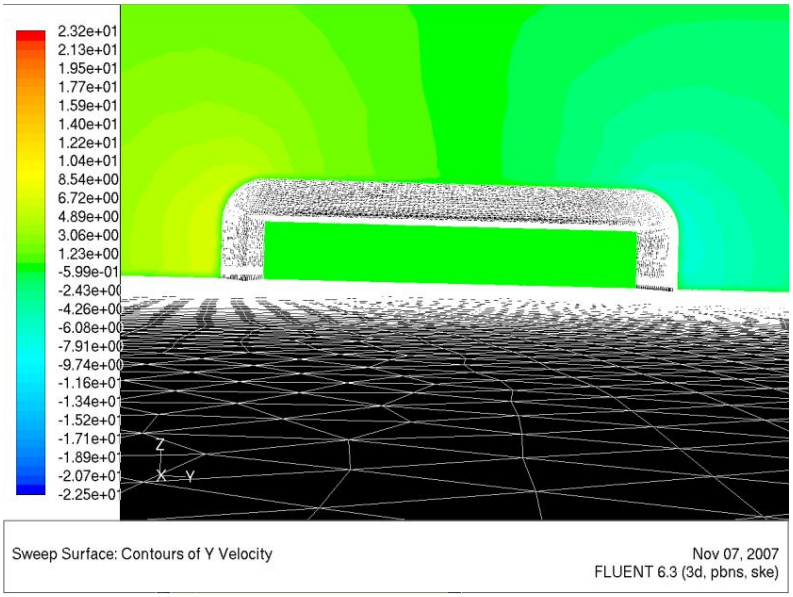

Figure 7.18: Y velocity half a chord before the trailing edge

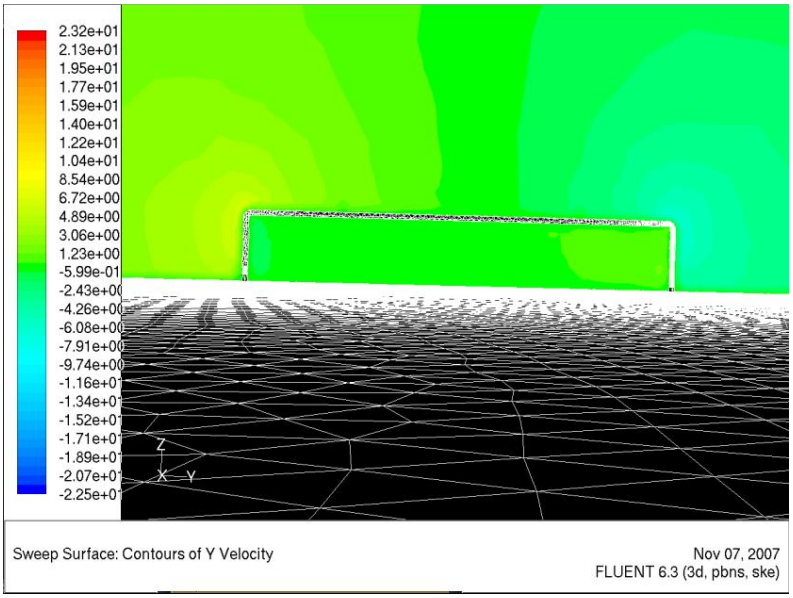

Figure 7.19: Y velocity at a point just before the trailing edge

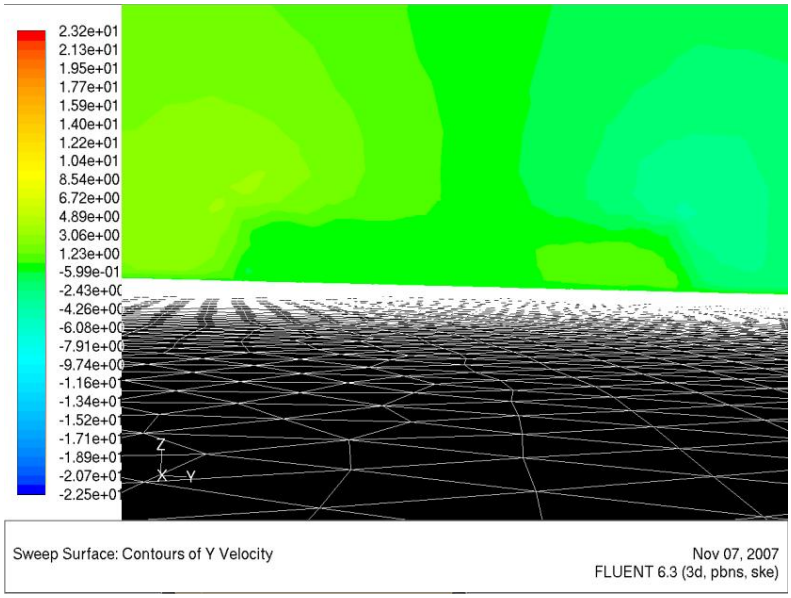

Figure 7.20: Y velocity at a point just beyond the trailing edge

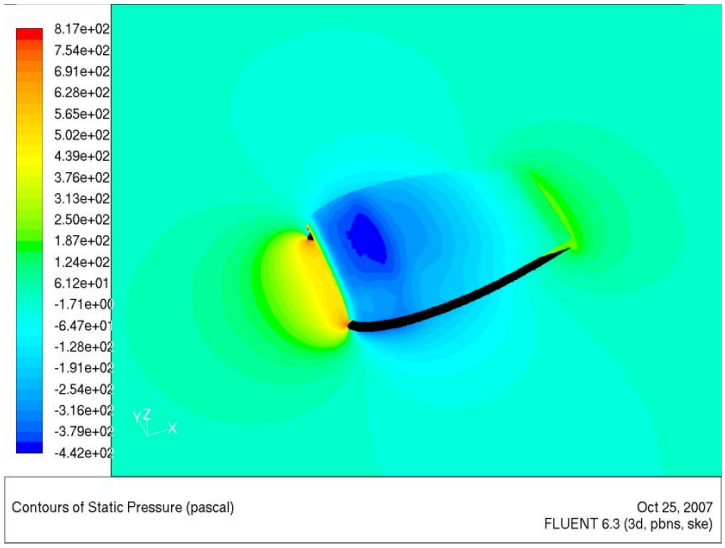

Figure 7.21: Clark Y wing/hull combination, showing static pressure as seen from above, H = 5

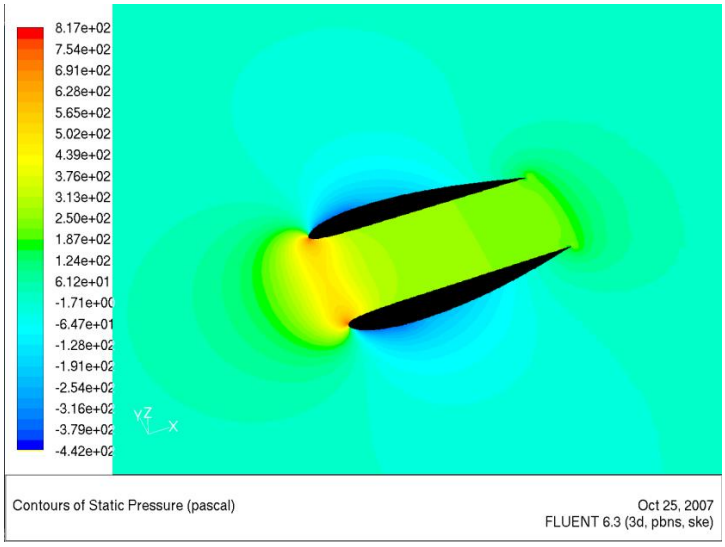

Figure 7.22: Clark Y wing/hull combination, showing static pressure as seen from above, with wing removed, H = 5

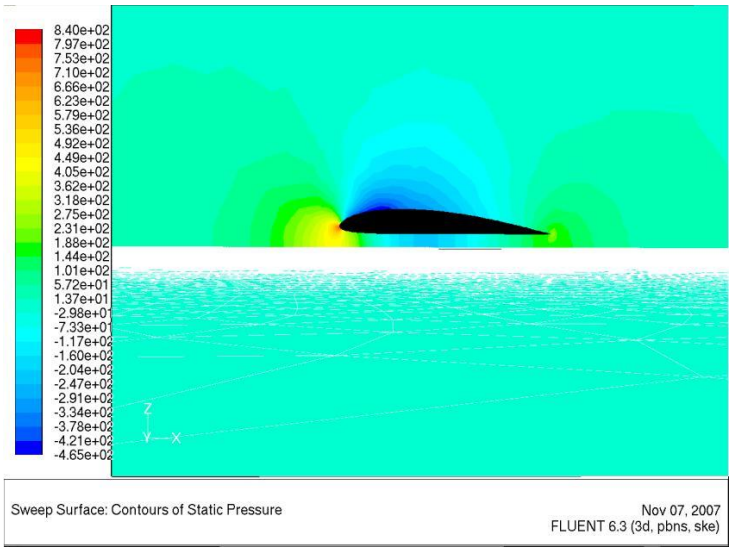

Figure 7.23: Pressure coefficient for Clark Y wing and 'hull shape' combination showing wing plus port and starboard hulls, H = 5

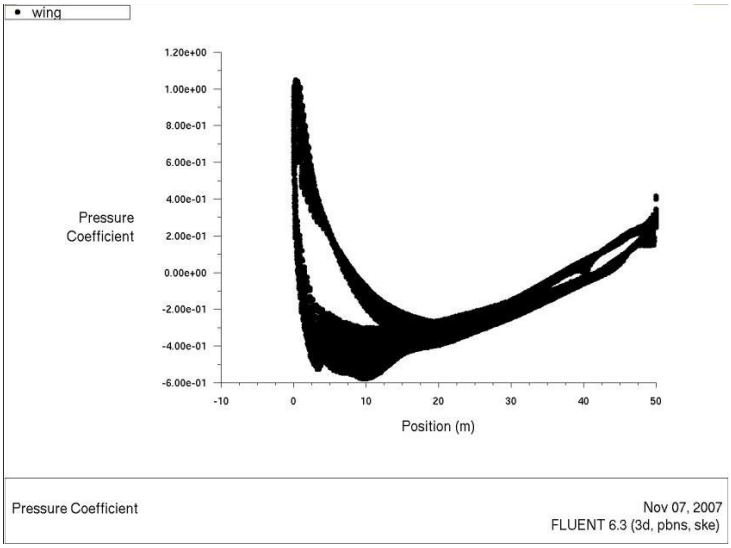

Figure 7.24: Pressure coefficient for Clark Y wing and 'hull shape' combination showing wing plus port and starboard hulls, H = 5

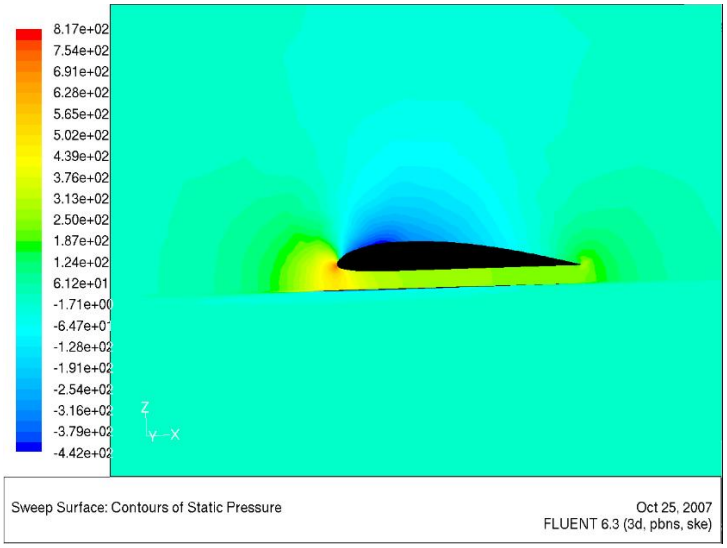

Figure 7.25: Clark Y wing/hull combination. showing static pressure, H = 5

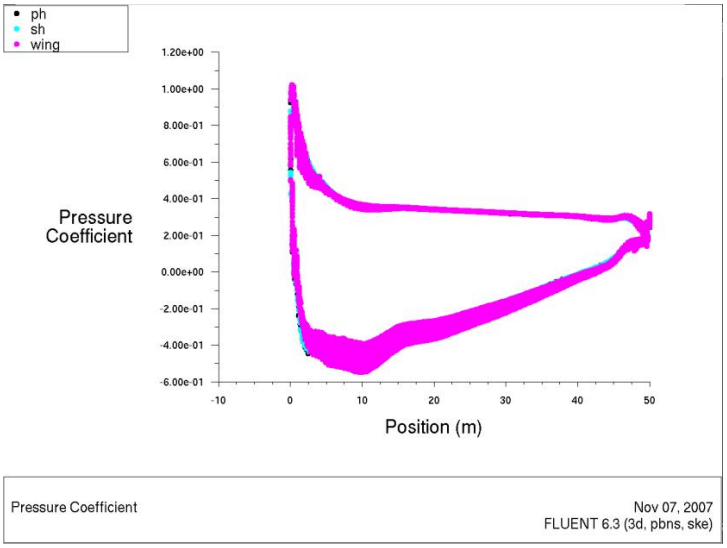

Figure 7.26: Pressure coefficient for Clark Y wing/hull combination showing wing plus port and starboard hulls, H = 5

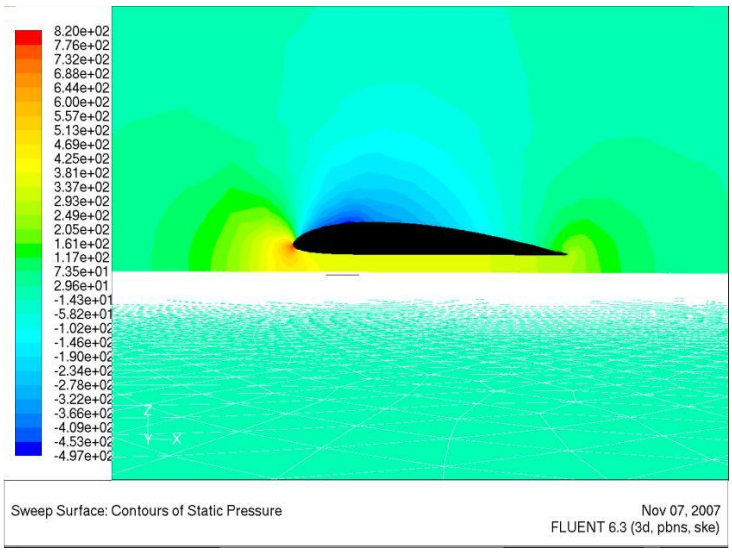

Figure 7.27: Clark Y Diff hull

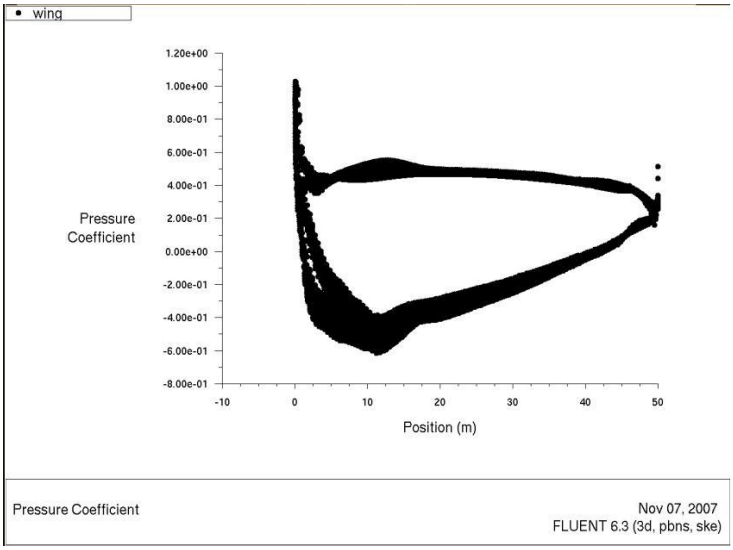

Figure 7.28: Clark Y Diff hull

Chapter 8

INTERPRETATION OF HULL PERFORMANCE USING A HYBRID SAVITSKY MODEL

8.1 Introduction

Although it has been shown that through appropriate shaping of a ducted hull it is possible to achieve significantly greater levels of lift than previously predicted, the extent to which this greater lift will affect the performance of the craft must be established in order to ascertain the true benefits of such design alterations. This chapter aims to investigate the performance characteristics of a hybrid catamaran vessel, having aerodynamic and hydrodynamic support. As mentioned in the introductory chapter, this research is undertaken as part of a wider project. The work of Collu [71] focuses on the stability of these hybrid craft, and it is in conjunction with his work which the following analysis is done.

The model constructed by Collu, uses a Savitsky planing hull, upon which the hydrodynamic loads are altered via the aerodynamic forces calculated for a given

wing at the current velocity and angle of attack. This allows the total lift, drag and moment to be calculated for the vehicle from both the planing hull and wing. By comparing the hull with no wing to various wing configurations, the benefit of each can easily be seen.

8.2 Savitsky Method

The essence of the exercise is to increase the performance of a catamaran planing hull through aerodynamic alleviation. It is therefore necessary to have a good planing model from which to assess the effects of aerodynamic forces. The simplest and most robust method for analysing planing hulls is the Savitsky model [9]. Savitsky's method is based on extensive experimental data for simple prismatic hull shapes, however it has been found to give a useful description of the properties of many more complicated hull geometries within the constraints of speed, length and trim angle. An example of such data comparison, for hard chined hulls, is given by Ikeda *et al* [72].

Savitsky calculates the lift coefficient for a prismatic planing hull as:

$$C_{L\beta} = C_{L0} - 0.0065\beta C_{L0}^{0.60} \tag{8.1}$$

Here $C_{L\beta}$ can be found experimentally in the usual manner, hence

$$C_{L\beta} = \frac{F_{L\beta}}{0.5\rho U^2 B^2} \tag{8.2}$$

and

$$C_L0 = \frac{F_{L0}}{0.5\rho U^2 B^2} = \tau_{deg}^{1.1}(0.012\lambda_w^{0.5} + 0.0055\lambda_w^{2.5}/Fn_B^2) \tag{8.3}$$

where

$$\begin{aligned}
C_{L0} &= \text{Lift coefficient for zero deadrise angle } (\beta = 0) \\
C_{L\beta} &= \text{Lift coefficient} \\
F_{L0} &= \text{Lift force for zero deadrise angle } (\beta = 0) \\
F_{L\beta} &= \text{Lift force} \\
\lambda_w &= \text{Mean wetted length-to-beam ratio} \\
\tau_deg &= \text{Trim angle of planing area in degrees} \\
\tau &= \text{Trim angle of planing area in radians} \\
\beta &= \text{Deadrise angle of planing surface} \\
B &= \text{Beam of planing surface} \\
Fn_B &= \text{Beam based Frounde number } U/(gB)^{0.5}
\end{aligned}$$

We note that the Froude number is based on the beam. This is due to the fact that the length of the hull is dependent on the trim angle and running attitude of the planing surface, and cannot therefore be known prior to the calculation of the equilibrium equations for vertical displacement and moment at a given speed.

Further, it is important to know that the equations are only valid for values of $2 \leq \tau_{deg} \leq 15$ and $\lambda_w \leq 4$. Figure 8.1 shows the geometry for a single planing hull. The mean wetted length-to-beam ratio λ_w is calculated as the average between the actual water line and the spray root as follows:

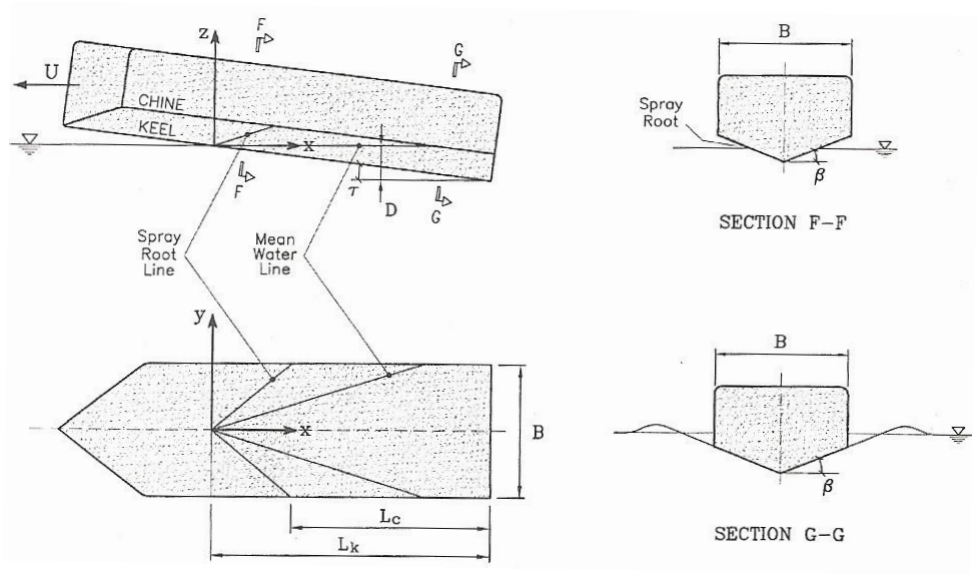

Figure 8.1: Coordinate system (x, y, y) and symbols used in a prismatic planing hull analysis [9]

$$\lambda_w = \frac{0.5(L_k + L_c)}{B} \tag{8.4}$$

The lift force $F_{L\beta}$ will act perpendicular to the planing hull at the longitudinal centre of pressure l_p, which is defined as the distance from the transom hull at the stern, and is expressed as:

$$\frac{l_p}{\lambda_w B} \tag{8.5}$$

The drag is calculated from the separate components of pressure drag R_p and skin friction drag R_f. The pressure drag component is calculated as:

$$R_p = F_{L\beta}\tau \tag{8.6}$$

The frictional component can be calculated using a number of methods, however, the ITTC 1957 model-ship correlation line is the most commonly used and is calculated as:

$$R_f = \frac{1}{2}\rho_w U^2 C_F \lambda_w \tag{8.7}$$

where

$$C_F = C_f + \Delta C_f \tag{8.8}$$

and

$$C_f = \frac{0.075}{(log_{10}R_e - 2)^2} \tag{8.9}$$

and

$$\delta C_f = [111(AHR \cdot U)^{0.21} - 404]C_f^2 \tag{8.10}$$

AHR is the average hull roughness in μm, and is given as approximately 100 for a new ship.

The Savitsky equations are designed to implicitly include the effects of wave formation and hydrostatic forces on the hull. Although they are very simple and make little effort to account for these complex phenomena, the results give reasonable agreement with far more detailed numerical calculations and dramatically simplifies the solution.

It can be see from Figure 8.1 that the prismatic hull is a very simple shape, having constant deadrise along its length. This is not a shape commonly adopted in practical hull design, however, many of the differences are related to the initial low speed stages of motion or the impact of waves and for calm water cruise the area of hull in contact with the water is often quite similar to the constant deadrise model shown here. Furthermore, as mentioned above, the model has been found to give a reasonable description even for hulls with non-constant deadrise or hard chines. As such, Savitsky's model should provide a good description of the behavior of a planing hull, from which the effects of aerodynamic alleviation can be measured.

8.3 Hybrid method

The adaptation of the Savitsky model for hybrid vehicles was done by Collu [71], the model uses a modular, iterative approach to solve for the equilibrium state of a Savitsky hull under the influence of aerodynamic loading. The model uses Savitsky's method to calculate a hull trim angle and sinkage (being the height of the centre of gravity from the mean free surface) for a given hull at a chosen speed for a chosen total displaced weight. From this the trim angle and height of the wing can be deduced and the aerodynamic forces and moments calculated. The hull sinkage and trim are then re-evaluated based on the direction of the forces and moments applied by the wing, and the process is repeated with a new estimation of the hull position. This process is continued until either the difference in sinkage and trim become negligibly small, indicating stability, or the values of sinkage and/or trim go outside of the constraints set by the programmer, which indicates instability and, most likely, a crash.

The aerodynamic forces and moments used for this model are based entirely on coefficients, that is, the lift force is given by:

$$F_{L_{aero}} = \frac{1}{2}\rho U^2 C_{L_{aero}} S_{aero} \tag{8.11}$$

and drag is

$$F_{D_{aero}} = \frac{1}{2}\rho U^2 C_{D_{aero}} S_{aero} \tag{8.12}$$

and the moment is

$$M_{aero} = \frac{1}{2}\rho U^2 C_{M_{aero}} S_{aero} \cdot mac \tag{8.13}$$

where mac is the mean aerodynamic chord.

The data for C_L, C_D and C_M would usually be taken from experimental or numerical calculations for a wing in ground effect. However, it has been shown that WIGE data is not necessarily suitable for describing such hybrid vehicles as these and that the shape of the airborne portion of the hull will dramatically effect the Coefficient of lift produced. By running a range of models in Fluent the data for C_L, C_D and C_M can be produced for use in this model, and the effects of this hull design on a standard Savitsky hull can be observed.

8.4 Input Data

The tests were run on the same 50 m Clark Y wing and hull combination used in previous tests and is illustrated in Figure 7.1. The same meshing technique and Fluent setup was used as for the previous tests since this was found to be reliably accurate whilst economical on both meshing and run time. This is particularly important due to the number of models required. The data range for the hybrid Savitsky model requires at least three different heights, each of which require at least three different angles of attack. This is to allow a trend line to be fitted to the various data sets which can be used to estimate the coefficients at the intermediate values. The Fluent model was run for four different heights (2.5m, 5 m, 7.5m and 10m) and at three different angles, the values of which are dependent on the range of motion available at the given height as a result of the possible collision of the trailing edge with the free surface. This means that at lower heights the angles are closer together than for greater heights above the free surface. This is acceptable because the effect of height on angle of attack is most noticeable at lower heights, which necessitates the smaller increments of angle during testing. At greater height the change in C_L with angle is less substantial, particularly over small angles of attack and it is therefore not worth spending time running extra models.

8.5 Results

The results for the coefficients of lift, drag and moment along with lift-to-drag ratio are shown in Figures 8.2 to 8.5.

The aerodynamic results obtained for the Clark Y hull combination provides a very useful data set. The effect of height and angle of attack can clearly be seen

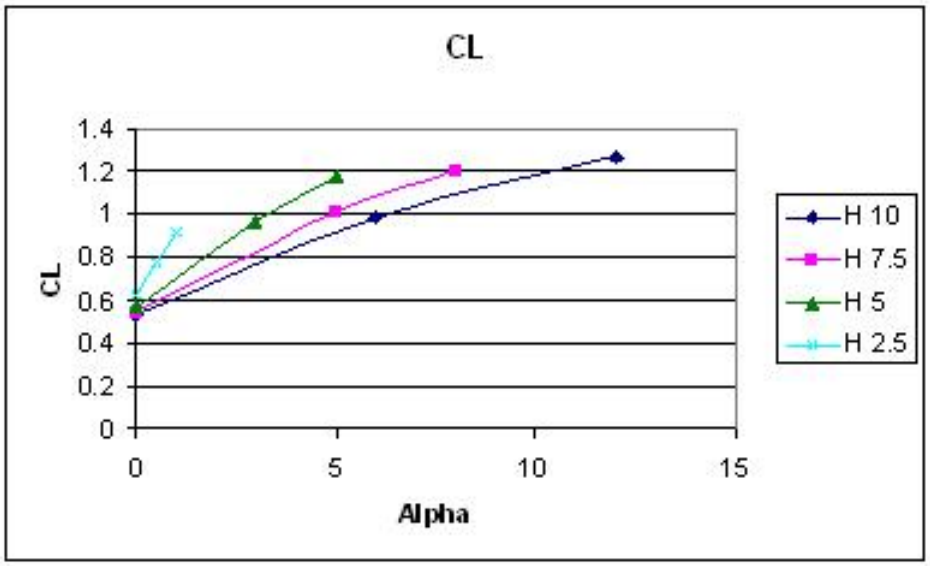

Figure 8.2: C_L versus Alpha for the Clark Y model over a range of heights

and the simple correlation allows trend lines to be developed for use with the hybrid model stability program. As before, decreasing the height has a beneficial effect on the lift and drag of the vehicle whilst increasing the height has an adverse effect. The angle of attack also has a dramatic effect on the lift, as one would expect, increasing the angle increases both lift and drag. Interestingly, the change in lift with angle is more notable at smaller angles and lower heights, whilst the drag is effected to a greater extent at larger angles and relatively unaffected by the change in height at larger angles. This suggests that the craft will function best at lower angles particularly at lower heights, which are also preferable. This is advantageous since, as mentioned before, a larger running angle will complicate the incorporation of a wing as a deck area and necessitate more complex internal structural design as well as possibly limiting the capacity in comparison to a lower angled deck. Although the larger angles produce more lift, the lift-to-drag ratio is greatly reduced. Equally, the lower heights are restricted to lower angles due to the geometrical constraints of the wing and free-surface interaction. It is likely

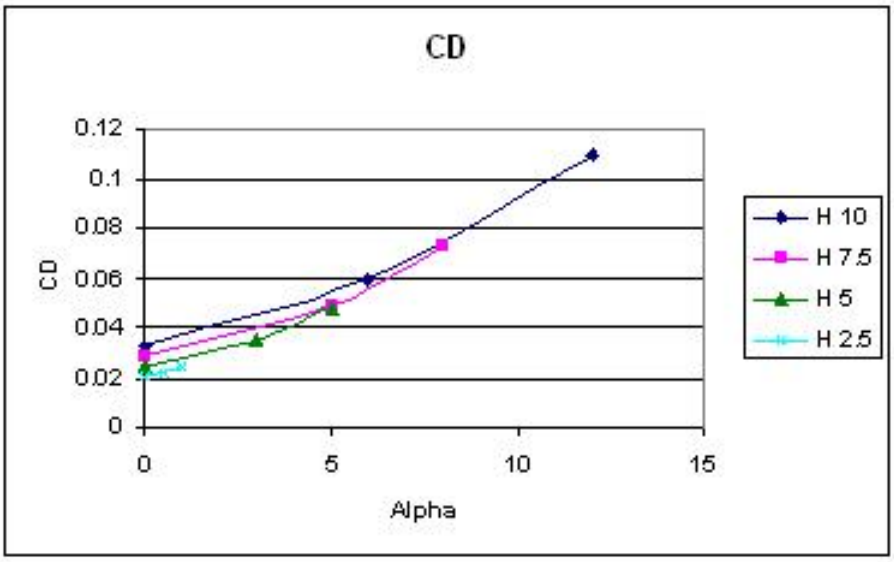

Figure 8.3: C_D versus Alpha for the Clark Y model over a range of heights

that the lower heights will be desirable during cruise since they provide by far the best efficiency. A single degree at lower heights will provide a C_L equivalent to that of several degrees at greater heights and for considerably less drag.

Having analysed the aerodynamic data and found trend lines for them, this data can be imported to the hybrid Savitsky model and further analysed in conjunction with the planing hull. The tests were carried out on the Clark Y wing-hull combination with length of 50 m and a beam of 25 m. The vehicle was tested up to around 70 knots, but the exact value was dependent on the equilibrium state reached. The deadrise angle β was set at either 5 or 10 degrees during initial testing, with a final value of 10 degrees used for the results presented below. The vehicle weight was set at 200 tonnes, this is approximately the value for an SES of around 40 m and is the estimated value of the 56 m quadrimaran ferry proposed in [4]. The results for two test cases are shown below, Figures 8.6 to 8.12.

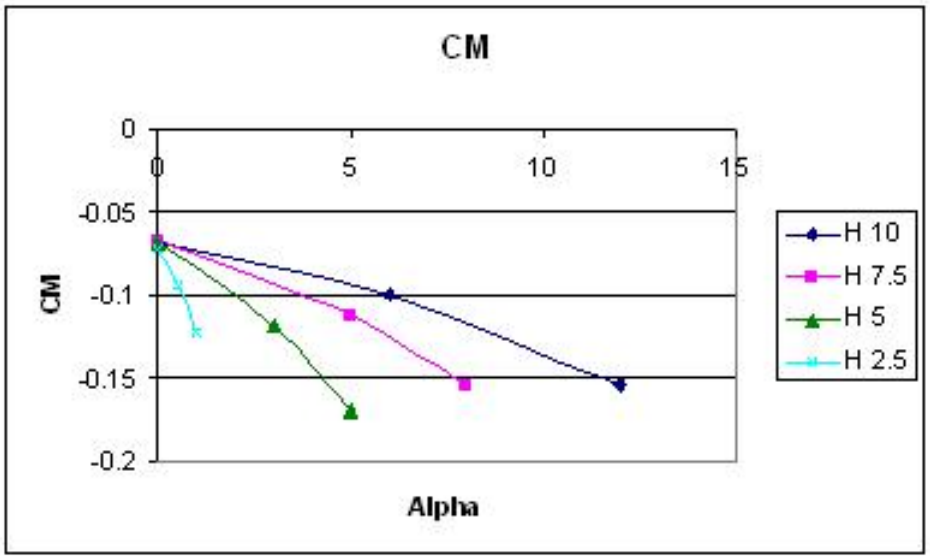

Figure 8.4: C_M versus Alpha for the Clark Y model over a range of heights

8.6 Discussion

The hybrid vehicle stability model was run extensively in order to gain an understanding of both the behaviour of the computer program and the hybrid vehicle. The first set of results, shown in Figures 8.6 to 8.8, shows the data obtained for the first stable solution. It is noted that the program relies on iteration to find a solution and uses guess work to home in on the stable values. It is therefore necessary to have some idea of the realistic running conditions of the craft at the chosen speed in order minimize the time taken for calculation and the chance of an unstable solution forming.

Figure 8.6 shows the lift components for the Clark Y hybrid vehicle from eighteen to seventy knots. Below seventeen knots the vehicle will not plane and a stable solution cannot be found. It can be seen that as the vehicle speed increases the aerodynamic lift increases and the hydrodynamic component of lift decreases.

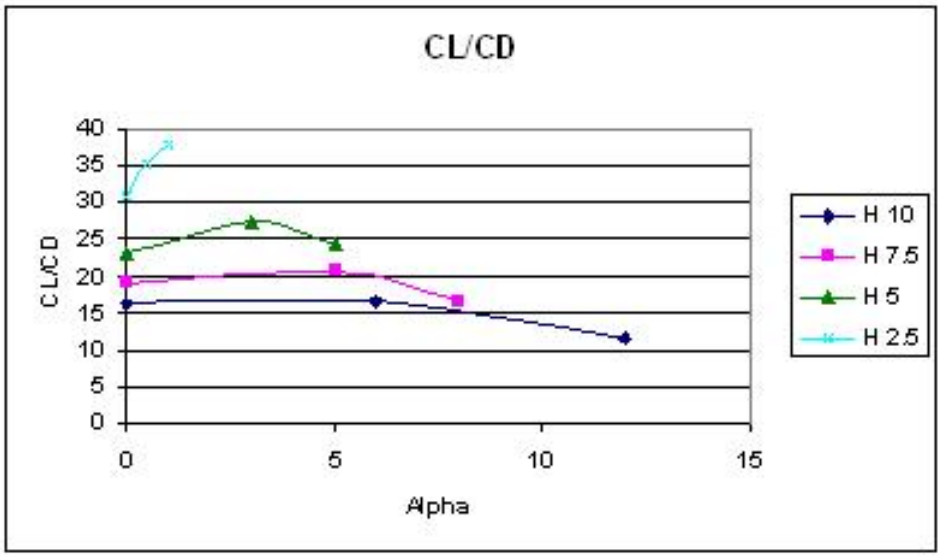

Figure 8.5: Lift-to-drag ratio versus Alpha for the Clark Y model over a range of heights

The aerodynamic contribution is very small below twenty knots, which is to be expected since it was predicted that the forces would not become comparable until at least forty knots. At this speed the aerodynamic contribution accounts for about ten percent of the vehicle weight. At the maximum speed tested, 70 knots, the aerodynamic force accounts for thirty percent of the total lift. This is not an insignificant amount, however, the important factor is to what degree the drag is effected by this lift.

Figure 8.7 shows all of the components of drag for both a 200 tonne planing craft and hybrid vehicle. The planing hull is labeled as 'no wing' and appears in the lighter purple colour whilst the hybrid vehicle is dark blue. The most significant pair of lines are the 'total' drag lines for the wing and no-wing vehicle. From this it can be seen that at low speeds the drag is effectively the same, but that as the speed increases beyond twenty knots the drag of the hybrid vessel becomes

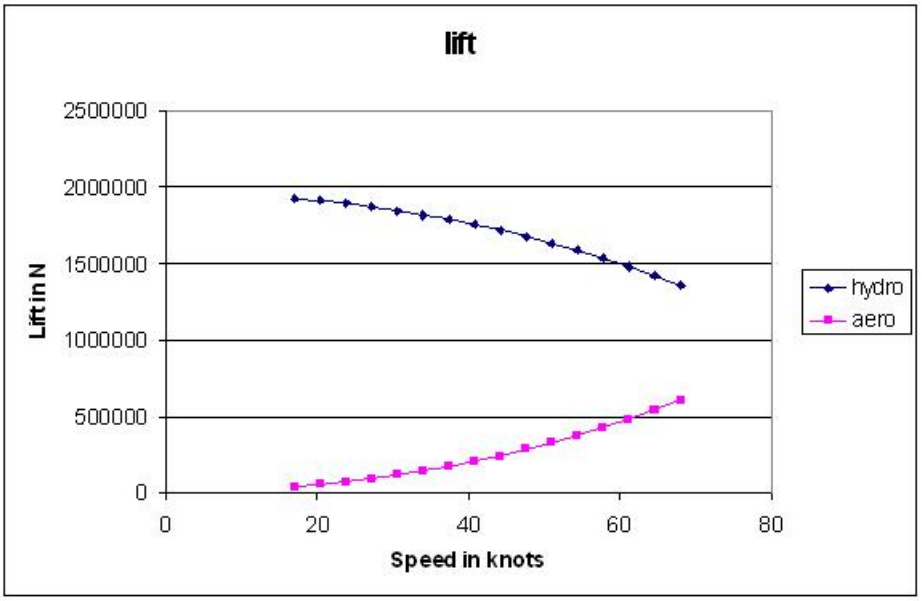

Figure 8.6: Lift components for a 200 tonne hybrid vehicle

significantly lower. The planing hull drag follows a classic upward curve which is composed mainly of the planing hull drag with a small amount of aerodynamic drag added. The hybrid vehicle drag however drops away from the line forming an 's' curve. Again, this is clearly made up almost entirely of the hydrodynamic component of drag with an even smaller component of aerodynamic drag. It is interesting to note the marked difference in aerodynamic drag between the two vehicles. It may have been assumed that the hybrid vehicle, with added wing area would have a greater drag due to induced drag. However, the wing profile is designed to be as streamlined as possible and thus has a very low profile drag and quite a small induced drag. It is also designed to replace the existing superstructure, not to be added to it. In contrast, the above water portion of the planing hull drag is based on a bluff body coefficient used in the estimation of ship wind resistance calculation (values of which can be found in Hoerner [73]) and is distinctly inefficient aerodynamically. This is a fair value based on previous

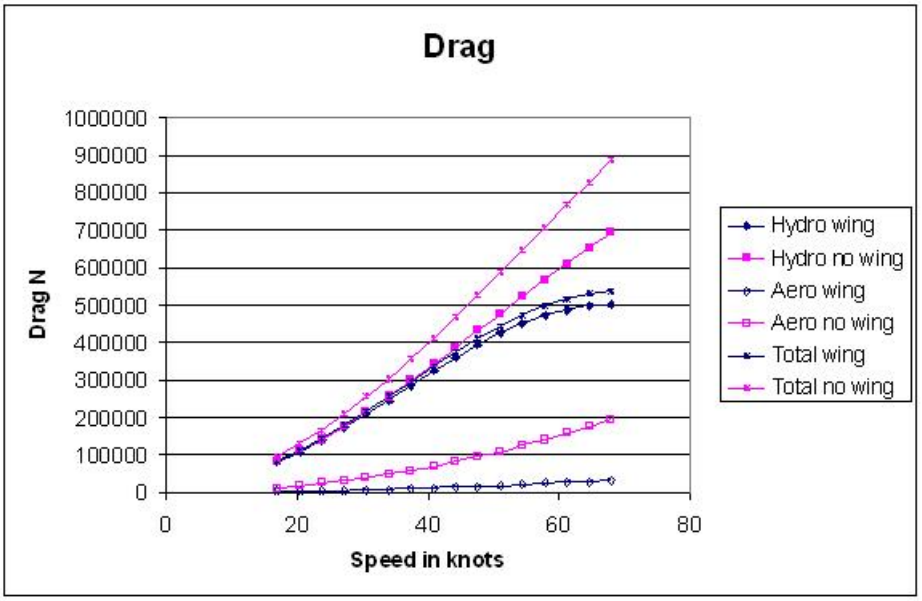

Figure 8.7: Drag components for a 200 tonne planing craft and a hybrid vehicle

ship designs, however, it would be unfair to assume that future high-speed planing craft will not take better account of aerodynamic drag. In which case, the total planing hull drag will lie closer to the hydrodynamic line. It is perhaps worth remembering though, that SES ship have been built, and indeed continue to be built, with the aerodynamic properties of a brick.

These results suggest that a significant amount of drag can be removed simply though aerodynamic shaping of the above water portion of a high-speed vehicle for speeds of around thirty knots and above. The effect of aerodynamic alleviation however, is less pronounced until speeds of over forty knots. The problem is that although the aerodynamic force accounts for over 30% of the lift, the aerodynamic drag accounts for only 6%, with the remaining 94% being hydrodynamic drag. It can be seen from Figure 8.8 that the lift-to-drag ratio, although improved for the hybrid vehicle, still falls dramatically and reaches unacceptably low levels before forty knots. Such a low value is not unrealistic for a planing hull, but it should be

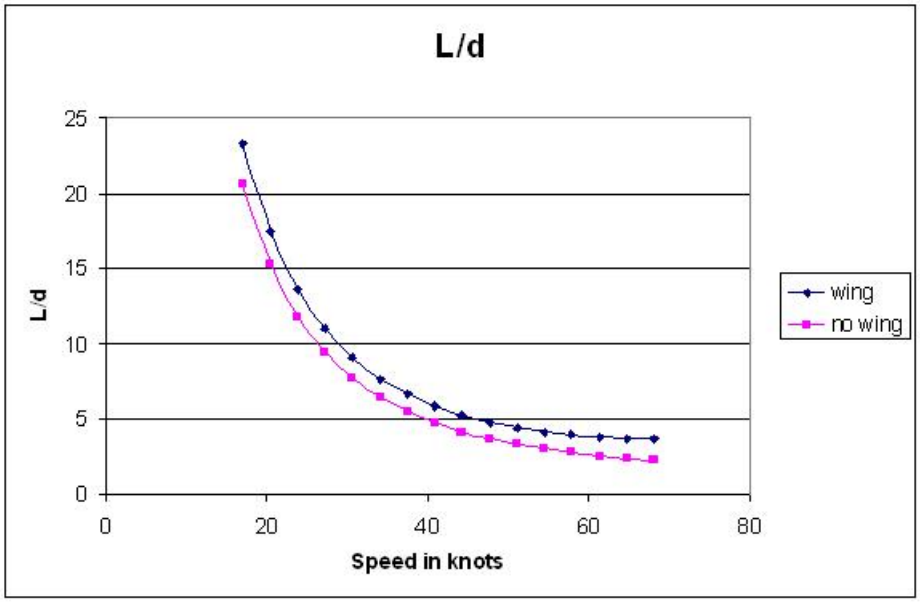

Figure 8.8: Lift versus drag for a 200 tonne planing craft and a hybrid vehicle

possible to achieve much better results. As such, the hydrodynamic hull design must be well below optimum. On closer inspection of the model, this appeared to be largely due to poor location of the centre of gravity. It was chosen that the centre of gravity would be near to the centre in order to maintain level running throughout the speed range. This was a reaction to the concern that positive feedback may result in the vehicle flipping over backwards at higher speeds. This has been a major problem for tunnel hull racing craft where the leading edge of the wing lifts a little and creates more lift, resulting in a further increase of angle and so on, until the vehicle flips. However, the aerodynamic results in Figure 8.2 show that if the vehicle begins to lift it will loose some lift force and unless the angle of attack augments rapidly the rise in height will reduce the lift and the vessel will stabilize. Furthermore, the moment is strongly negative about the quarter chord point, meaning that there is a nose down pitching moment. A wing usually has a centre of pressure near the leading edge due to the greater pressure

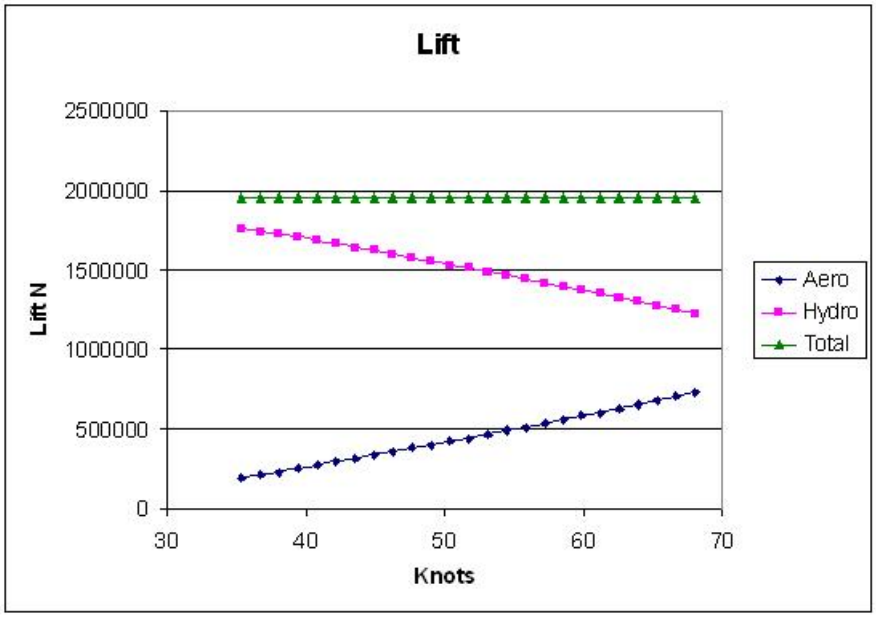

Figure 8.9: Lift components for a modified 200 tonne hybrid vehicle

difference created around the nose. Figure 7.13 shows the pressure plot for a Clark Y in free air. Figure 7.14 shows the pressure throughout the duct of the Clark Y wing-hull combination, and it is clear that the camber experiences an almost uniform pressure throughout. This moves the centre of pressure rearwards and accounts for the nose down moment about the quarter chord point. As a result the hybrid model, with its weight almost central, tended to run at extremely low angles of attack, sometimes less than a degree. This is acceptable for the wing, however, it should be remembered that the Savitsky model is only valid for trim angles of $2 \leq \tau_{deg} \leq 15$. This is because at zero angle the lift goes to zero and hence the hull tends to sink. Since the hybrid model only requires a small amount of hydrodynamic lift, the hull flattens out in response, this however, results in a large increase in the wetted length of the hull and hence hydrodynamic drag. Most planing vessels, including SES ships, have their weight about one third forward of the stern. This balances the planing hulls significantly better. The results for

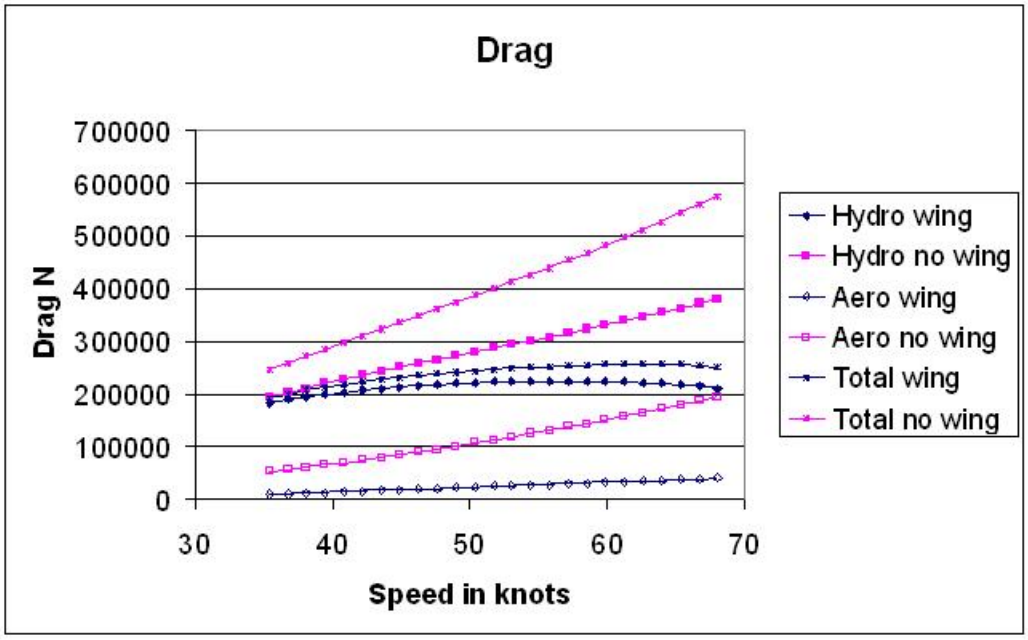

Figure 8.10: drag components for a 200 tonne planing craft and a modified hybrid vehicle

the hybrid vehicle and planing hull with modified center of gravity are presented in Figures 8.9 to 8.12.

The results for the various components of drag are shown in Figure 8.10. It is observed that the vehicles both behave in a similar manner to before, but with lower drag, and the 's' curve begins much sooner for the hybrid vehicle. The drag of the planing hull is reduced 35% and the total drag of the hybrid vehicle is reduced by 53% for the modified center of gravity. This is a substantial difference and results in the proportion of hydrodynamic drag dropping from 94% to 83%. Equally, the aerodynamic loading is increased from 30% to 38%. The second configuration is evidently a far better choice. The second hybrid vehicle having 56% less drag than the equivalent planing hull at the top speed of 68 knots. These

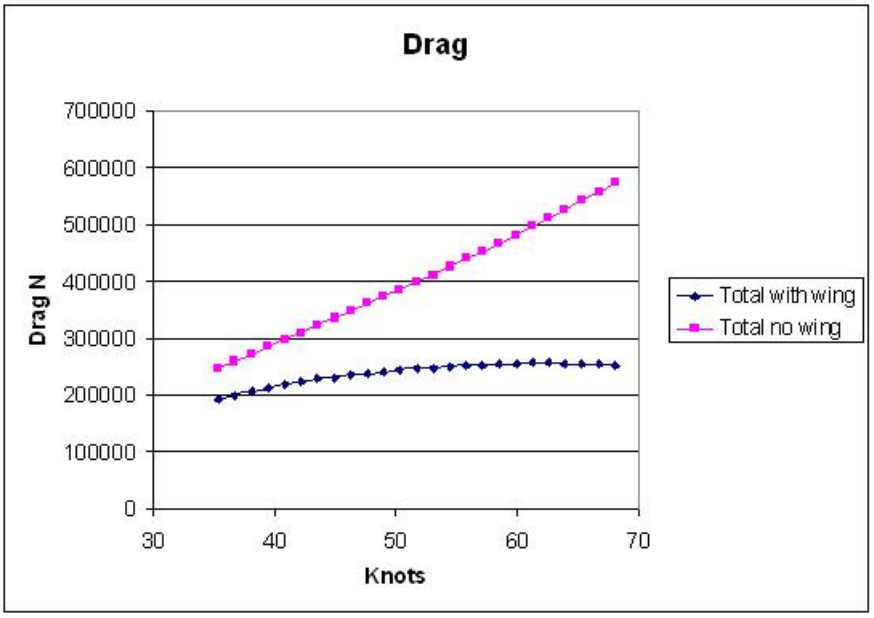

Figure 8.11: Drag comparison of a 200 tonne planing hull and a modified hybrid vehicle

results can be compared to the Quadrimaran which was estimated to achieve around 18% aerodynamic lift at 60 knots for an equivalent vehicle, having four planing hulls. Figure 8.11 clearly shows the difference in total drag for the hybrid vehicle, however, it is interesting to note that the 's' curve is now more of a defined peak. The 's' curve is a phenomenon familiar to other vehicles having transitory lift phases, such as hydrofoils and sea planes. The effect is caused by the transition between two drag curves, for example that of a planing craft and a hydro foil, and the resultant shape is referred to as the 'hump' drag. In this case the planing hull drag increases until the speed is sufficient to create aerodynamic alleviation, this being at around 30 knots for this example, at which point the rate of increase of drag diminishes. That is, until the aerodynamic drag increases to a comparable rate and the drag increases once again. It is the first high point,

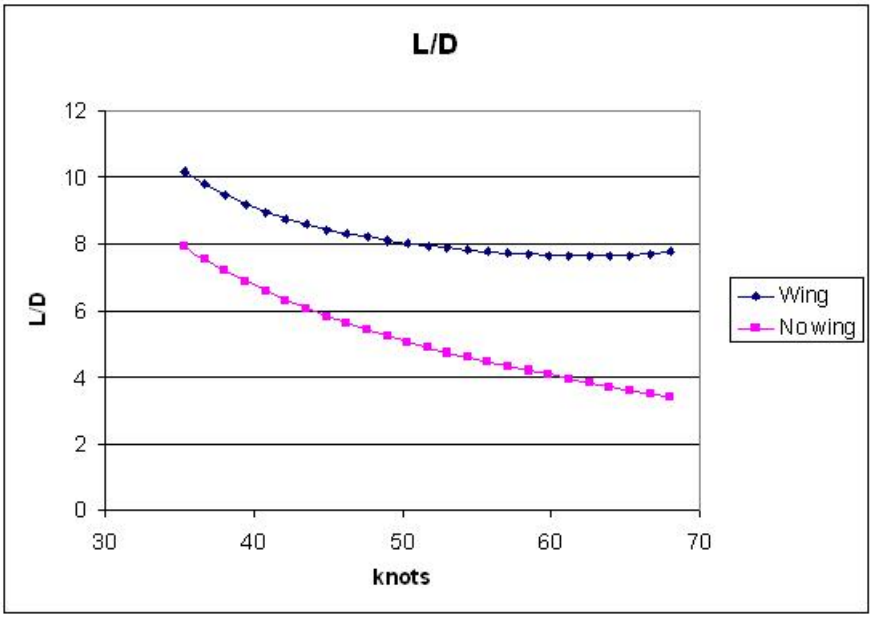

Figure 8.12: Lift versus drag ratio for a 200 tonne planing hull and a modified hybrid vehicle

as the hydrodynamic drag reaches a maximum, that is referred to as the hump drag.

For the first hybrid vehicle, the hump drag was not reached, however, it appeared to be at about eighty knots. The second hybrid vehicle has evidently reached the hump drag at around sixty knots, where the drag can be seen to start decreasing. This is significant since it suggests that if the vehicle can reach sixty knots it should have the power to reach much greater speeds because of the lower total drag. If we assume that our planing hull is capable of reaching forty knots, a fast but not unreasonable speed for such a craft, then the first hybrid would in theory be capable of extending the speed to forty eight knots for the same drag. This is the sort of speed increase experienced by the Quardrimaran and is indicative of the pre-hump drag phase. The second hybrid vehicle however, would be able to

achieve at least seventy knots and in theory could reach much higher, since the drag has not yet reached the same value as that of the planing hull at forty knots.

8.7 Conclusion

It has been shown that the hybrid vehicle can theoretically sustain stable running at speeds of up to seventy knots whilst achieving over 56% less drag than that of the equivalent planing hull. It has been found that the position of the centre of gravity has an extremely large effect on the performance of the vehicle, implying that a combination of careful loading and control surfaces may be essential to maintain performance. In the latter case, it is suggested that trim tabs on the transom may make a significant difference to performance as discussed by Mosaad *et al* in [74], along with the obvious advantages of aerodynamic control surfaces.

The model shows considerable improvement over conventional aerodynamic alleviation, with substantial aerodynamic loading at more realistic speeds. However, the aerodynamics are still simplified. They may be improved though more extreme camber, as seen by the improved results of the Diff hull model in the previous chapter, but equally, the effects of the incorporation of hydrodynamic surfaces into the aerodynamic model may reduce the effectiveness of the model. In particular, the reduction in drag of the second model was largely due to the increased running angle, which, although still only a few degrees at most, resulted in a dramatic reduction in wetted hull length. This reduction brought the hull length well short of the wing, meaning that much of the tunnel must have had some gap along the bottom wall. This gap could result in vortex formation and end effects, dramatically reducing the effective lift.

In order to solve this problem the effect of incorporating hydrodynamic surfaces

into the aerodynamic modeling, and the effect of the hulls leaving the water must be studied. The next chapter will therfor focus on this task.

Chapter 9

COMPLETE AERODYNAMIC HULLFORM ANALYSIS

9.1 Geometric Considerations

To achieve a complete aero-hydrodynamic design for the hybrid vehicle it is necessary to consider the transition states of the vehicle. That is, the at rest requirements, the take-off requirements and the cruise requirements. The static requirements are that the vehicle must float! But beyond this it must float such that the hydrodynamic and aerodynamic surfaces are able to perform once motion has begun. From basic calculations of a prismatic hull using the Archimedean principle of displacement, we can find that a 200 ton planing hull will rest at a maximum draft of about 1.5 m. This is based on the 10 degree dead rise and 2 degree trim angle predicted from the hybrid stability model used in the previous chapter. It may be beneficial to consider the possibility of greater loading, since the aforementioned model gives us reason to believe that a greater load may be supported if correctly designed. As such, a maximum draft of 3 metres is suggested to accommodate greater static loading.

The transitory, or take-off stage, will require the hull to have a good water piercing bow for low speeds as well as a greater trim angle in the bow section to encourage the hull out of the water at lower speeds. The precise design of such a hull is beyond the scope of this thesis, and indeed, it is only the intention of this section to consider the hydrodynamic constraints and study their effect on the aerodynamics of the hull. As such, the design will most likely be far from hydrodynamically optimized. It should however, include the most important features of the planing hull in order to provide a more realistic aerodynamic profile.

The cruise state will require very little hydrodynamic surface, with a draft of less than 1 m and a wetted length of just 14 m predicted by the hybrid stability model. The result being that most of the 3 m of hull depth designed originally for the static and take-off stages will be dry and must now function efficiently in the aerodynamic stage. This means that the hull must be optimized to function both hydro and aerodynamically. The hydrodynamic constraints during full cruise will be that the hull must conform to the simplified prismatic hull shape of the Savitsky model in order to validate the planing results. During the displacement stage there is little requirement other than relatively smooth lines, which should fit easily with the aerodynamic criteria. The take-off stage however, is more complicated. Since a larger proportion of the hull is still wetted, and must function hydrodynamically, it requires minimal curvature in the aft section of the hull since bulges tend to create low pressures which suck the hull into the water. Further, the hull must incorporate a sufficiently flat planing area of appropriate deadrise, which should ideally be between 10 and 20 degrees, and must terminate in a transom, where the water is released, or separates without forming adverse pressure gradients. However, this section of hull must also conform to the aerodynamic requirements, that is, there must be a smooth divergence throughout the front of the duct and a smooth convergence throughout the rear of the duct. There must be no large or sharp angles which might promote flow separation, and all bodies must terminate

in a sharp point via small changes of angle so that the flow remains attached and the drag is minimized. Evidently there are some contradictions here and some compromises will have to be made, particularly with reference to the transom hull and trailing edge of the wing. In this case however, it should be remembered that the transom height is unlikely to move considerably since it forms the rotation point about which the trim angle is dictated. Indeed the hybrid model predicted a change of depth of less than half a metre for the transom, and as such, the loft between the trailing edge and the transom may only account for a small area of flow separation.

The hull designs considered draw largely from SES ships, which have similar hydrodynamic requirements, if somewhat less awkward aerodynamic constraints. Examples of many SES hulls are given by Lavis *et al* in [32]. One notable factor is that they are asymmetric, having what appears to be a single planing hull split down the middle. This is due to the air pressure forcing the water down between the hulls so that it is about level with the base of the hulls. This makes the bottom of the craft effectively one large planing surface, consisting of two solid planing edges bounding a planing air cushion. Higher up the inside wall of the hull however, there is a knuckle designed to prevent slamming of waves into the wetted deck and minimize sinkage whilst operating off cushion. This hull type may well be appropriate for the hybrid vehicle design, since it will also have an air cushion at higher speeds. The knuckle will be extremely important at the trailing edge due to the danger of the wing hitting the free surface. By incorporating a suitable knuckle this risk could be dramatically reduced without additional hydrodynamic drag during normal cruise conditions. The knuckle could equally help during lower speeds, which are equivalent to off-cushion conditions for an SES.

For the purely aerodynamic portion of the hull the highly cambered ‘Diff hull’ wing profile was chosen. This profile has consistently provided the greatest lift

and should be ideal for creating the divergent convergent diffuser shape which is predicted to achieve the largest amount of lift.

9.2 Method

In order to realize this design, the wing data for the Diff hull was imported into a CAD (computer aided design) program as a series of coordinate points. The CAD package used was a solid modeling program called SolidWorks 2004. With the wing coordinates imported it is then possible to form a profile which can be extruded along the beam and rotated about the wing tips to form the upper, purely aerodynamic part of the vehicle. This section was given a depth of three metres so that at full submergence of the lower hydrodynamic section the wetted deck would still have a clearance of three metres in order to prevent wave collisions with the trailing edge of the wing. The hydrodynamic portion of the hull was shaped in accordance with the criteria set out above, using a series of planes along the length of the hull to specify the required cross sections from bow to stern. These sections were then lofted to the aerodynamic portion of the hull. The final solid model is shown graphically in Figures 9.1, 9.2, 9.3 and 9.4 below.

9.2.1 2d Boundary Layer Testing

For the previous sets of aerodynamics data it was deemed necessary to provide a large number of solutions in a relatively short period of time. This required coarse grids and precluded the possibility of solving for the complete boundary layer. Since the models were quite simple, and used in conjunction with the robust and well understood k-ϵ model with wall functions, the results appear to be perfectly adequate for the task. However, the model currently under consideration

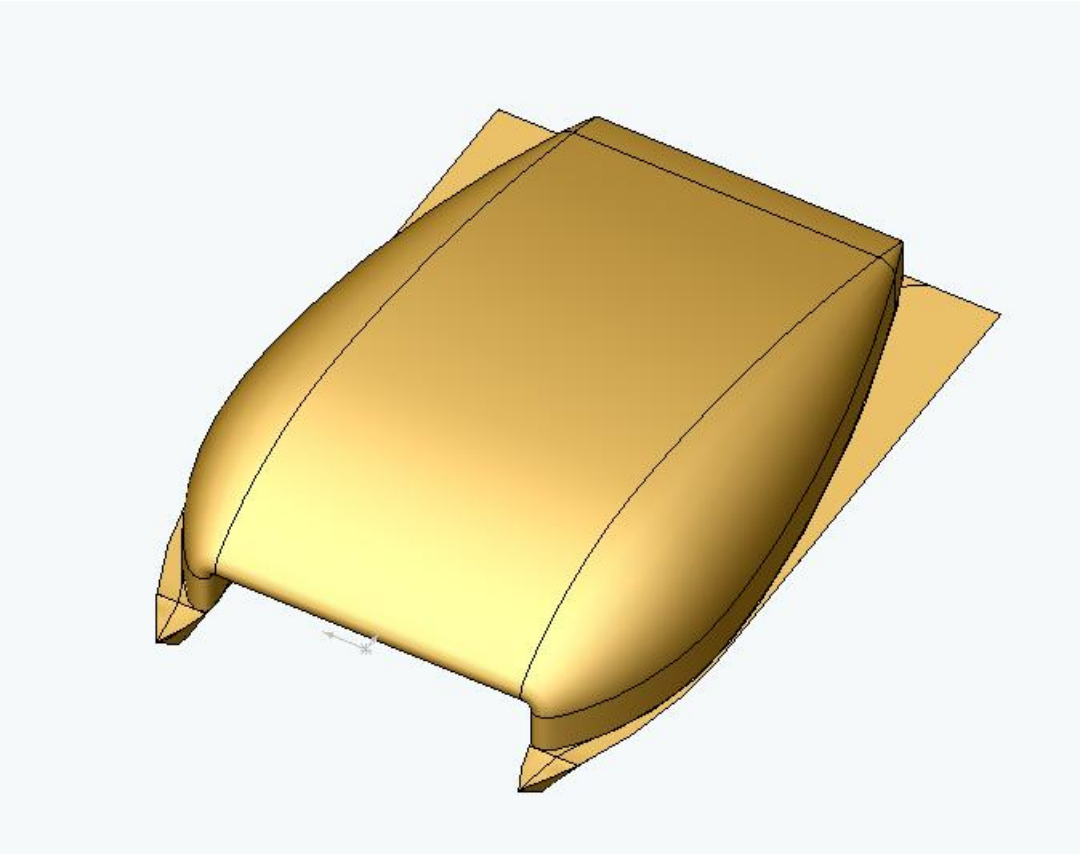

Figure 9.1: Solid model of final hull form.

has a few major differences. Firstly it has a transom hull and a flat topped bow section, which may well produce vortex shedding, but will at any rate produce unstable turbulence, necessitating the use of a time dependent solver. Secondly, the model will be tested at angles of attack and heights which result in a gap forming beneath the forward section of the hull, which could produce either vortices or flow separation. As a result, more sophisticated turbulent modeling techniques might be required and it may no longer be suitable to rely on wall functions to solve for the boundary layer.

The first problem to consider is the boundary layer, since the other turbulence

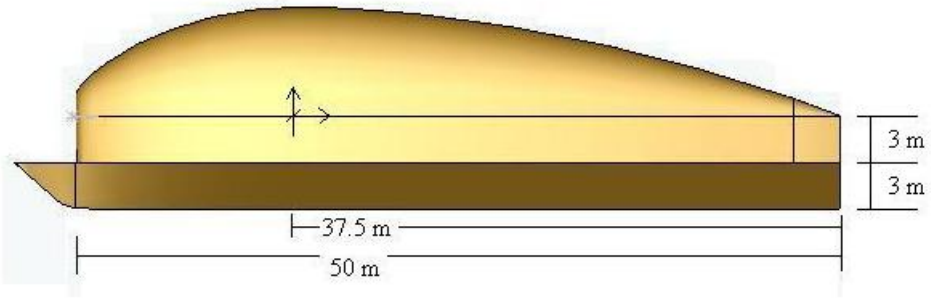

Figure 9.2: Solid model, showing position of axis and dimensions.

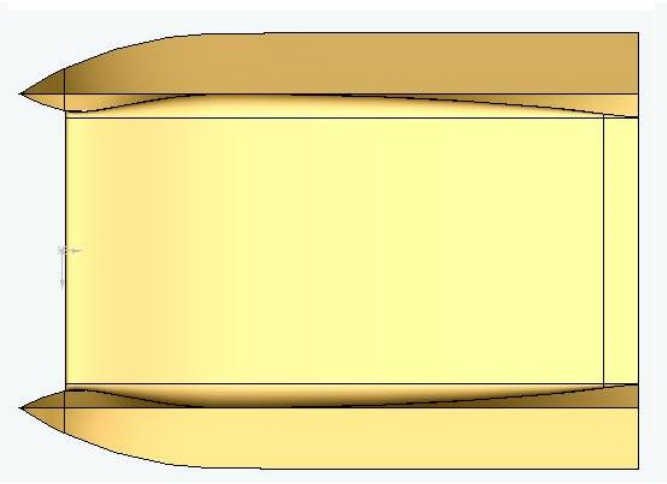

Figure 9.3: Solid model showing hydrodynamic hull area.

modelling issues can be dealt with in the solver, whereas the boundary layer solution is a function of the grid spacing used within that region. In essence the boundary layer is a transition layer between the friction of the hull surface, at which point the flow must travel at the same speed as the hull, and the turbulent free steam conditions found at a greater distance from the hull. The issue is determining the thickness of the boundary layer and the effect it has on the surrounding flow. The height of the boundary layer is a function of the Reynolds number, which in turn is a function of the size of the wing and the speed of the

Figure 9.4: Solid model viewed form the front, showing the planing hull area.

craft. The boundary layer is usually broken down into three sections, which are illustrated in Figure 9.5. The various layers are characterized by their y^+ value, which is defined as:

$$y^+ = \frac{u_* y}{\nu} \tag{9.1}$$

Where y is the distance from the wall, ν is the kinematic viscosity and u_* is the friction velocity at the nearest wall, given as:

$$u_* = \sqrt{\tau_w / \rho} \tag{9.2}$$

where ρ is the fluid density at the wall and τ_w is the wall shear stress and

$$\tau_w = \mu \left(\frac{\partial u}{\partial y} \right) \tag{9.3}$$

where μ is the dynamic viscosity, u is the flow velocity parallel to the wall and y is once again the distance from the wall.

The first layer is called the viscous sublayer and has almost laminar flow, with a y^+ of between 0 and 5. The second layer is called the buffer layer or blending region and has a y^+ of between 5 and 60. The final layer is called the fully turbulent or log law region and has a y^+ of 60 up to around 500, however the value is

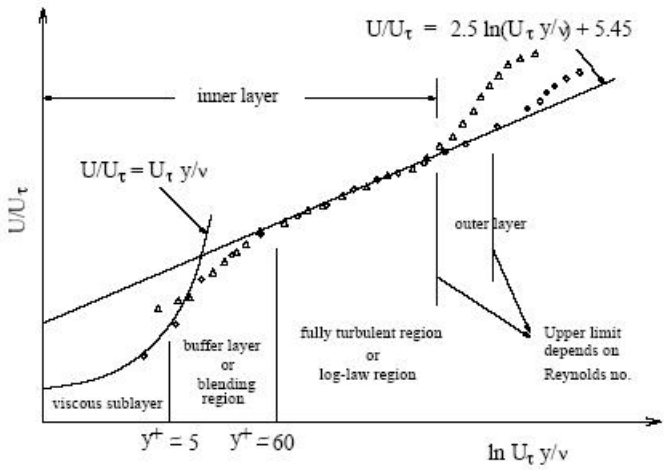

Figure 9.5: Graphical representation of the boundary layer transition flow in the near wall region, from [10].

largely dependent on the Reynolds number. Beyond this region is the free stream. The importance of the boundary layer can be difficult to judge, since many fluid problems can be accurately modeled by inviscid flow. However, boundary layer formation and interaction can have a large effect on the overall flow, particularly in ducts, as discussed in [60] or between objects in close proximity such as in [38] where the forces were reversed when the boundary layers began to interact between two spheres being brought closer together in a flow field.

There are two methods of dealing with the boundary layer in Fluent, shown in Figure 9.6. The first is to solve the flow in two regions using wall functions. This method, used for the earlier calculations, is robust and efficient, however it does not solve the flow in the boundary layer, it models the flow based on semi-empirical formulae. The second method uses a fine mesh to solve the flow right through

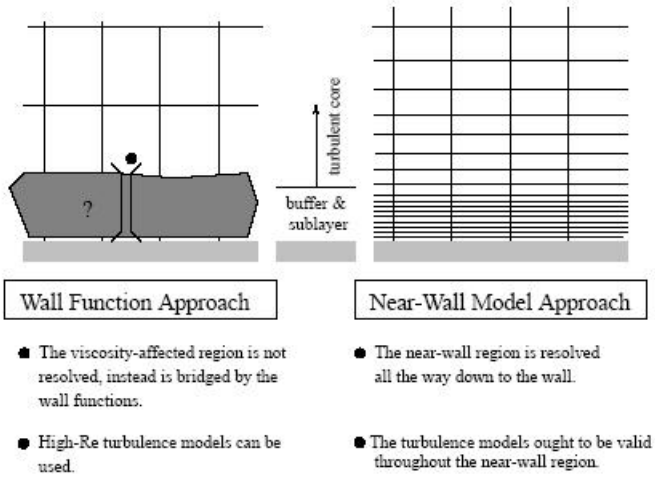

Figure 9.6: Near-wall treatments used in Fluent, [10]

the viscous sub layer and laminar layer to the wall. Figure 9.7 shows the detail of such a mesh. This requires a solver that can handle the low Reynolds number calculations in the sublayer as well as the turbulent free stream. In addition it requires a highly structured mesh in the boundary layer zone.

The mesh within the boundary layer must capture all of the elements of the flow. To do this it is recommended that the first element in the mesh (adjacent to the wall) should have a y^+ value of around 1, and that there be at least ten elements within the boundary layer. The determining factors for achieving a y^+ value of 1 in the first cell are the Reynolds number and the cell height. It is therefore critical to determine the correct cell geometry for the mesh before attempting to calculate the boundary layer flow. An excellent resource is available from NASA *(http://geolab.larc.nasa.gov/APPS/YPlus/)* which will calculate the required cell height for a geometry to attain the desired y^+ value.

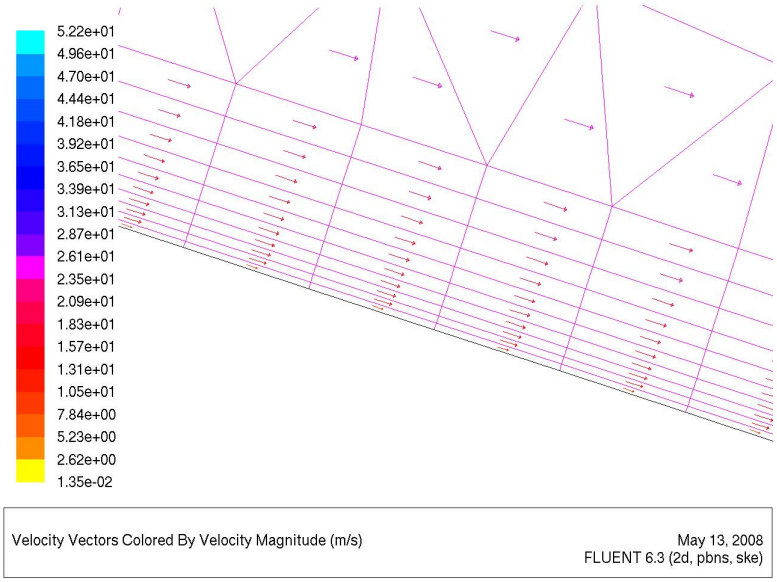

Figure 9.7: Detail of a boundary layer on 50 cm wing, y^+ 1

Some initial attempts to capture the full boundary layer proved unsuccessful, and it was decided that the problem should be studied in two dimensions first so that an understanding of the grid requirements could be gained. In addition, it was suspected that the scale of the hybrid vehicle, having a reference length of 50 m, was also effecting the boundary layer resolution. To investigate this a pair of two dimensional wings were studied, one of 50 m and the other of 50 cm so that the effects of scaling could be observed. Both models were tested in a free stream flow of 36 ms^{-1} using the k-ϵ turbulence model with enhanced wall functions, allowing for full boundary resolution where the grid resolution is fine enough. Table 9.1 below shows the information calculated for both the 50 m and 50 cm wings.

Both wings are in a free stream flow of 36 ms^{-1} but due to their size difference they have dramatically different Reynolds numbers. As a result the boundary layer conditions are different and the cell height has to be adjusted accordingly. It can be seen that for both wings the first layer of the grid must be extremely

Ref. Length (m)	50	0.5
Re	1.23E+08	1.23E+06
y+	1	1
Cell height (m)	1.37E-05	9.6E-06
h as % of L	2.74E-05	0.00192

Table 9.1: Cell height requirements for near wall mesh with a y^+ of 1

small, which is the main reason for the popularity of wall functions, since they remove the necessity for such fine and computationally expensive grids in the near wall region. Fluent (version 6.1) is equipped with enhanced wall functions. This allows the program to solve the full boundary layer problem where the grid is fine enough, whilst using wall functions in areas where the resolution of the grid is insufficient. This technique was employed for the testing of the 2d sections. The details of the grids are given in Table 9.2 and the results shown in Figure 9.8.

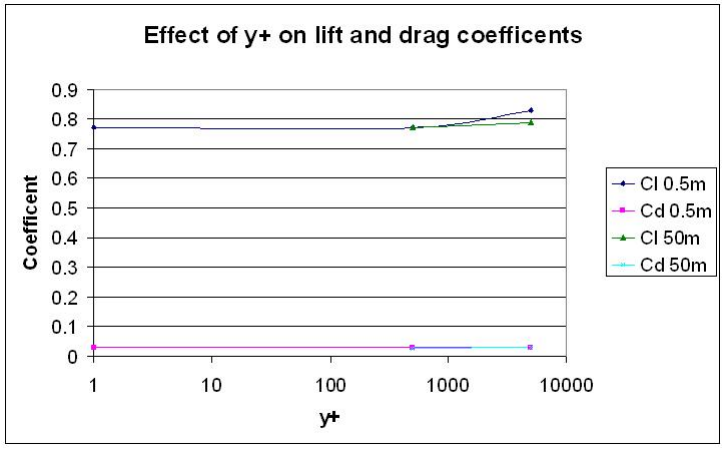

Figure 9.8: Graph of effect of y^+ on C_L and C_D for the 50 m and 0.5 m wings

The most significant result from this numerical experiment is the conspicuous

Ref. Length 0.5(m)			
y+	First cell (m)	cl	cd
1	0.0000096	0.77253	0.0276
500	0.00483	0.77168	0.0281
5000	0.0483	0.82881	0.0286

Ref. Length 50(m)			
y+	First cell (m)	cl	cd
1	0.0000137	NA	NA
500	0.00685	0.77226	0.0268
5000	0.06854	0.78944	0.027913

Table 9.2: Comparison of the effect of the y^+ value on C_L and C_D for the 50 m and 0.5 m wings

absence of a value for the 50 m wing with a y^+ of 1. This is because it proved impossible to construct a sufficiently fine grid. From Table 9.1 it can be seen that although the 0.5 m wing requires a smaller first cell than the 50 m wing, as a percentage it is significantly bigger, by two orders of magnitude in fact. This means that the grid must be much finer around the 50 m wing, despite their apparent similarity on the computer screen. Unfortunately, the desktop processor used for building the grids was not capable of generating such fine grids. This instantly precludes the possibility of resolving the full boundary layer on a full size three dimensional model since it will have an even larger grid, being a volume not an area. However, from observing the results it can be seen that the wall functions appear to provide an accurate solution for the 50 m wing, with stable results from both the medium and coarse grids. In comparison the boundary layer for the smaller wing can be resolved fully. This result compares well with the medium grid, however the coarse grid result is less similar. This is because although the

wall functions are compensating for the lack of resolution in the near wall region, the extremely coarse mesh has artificially enlarged the boundary layer. It must be remembered that volume of fluid solvers such as Fluent, solve the flow for individual elements, or grid cells, the centre of which is called the node and takes on the average value for the cell. This means that if a cell experiences a shear flow, such as in the near wall region, it will have an average value for the flow gradient across it. Thus if the cell is too large it can artificially extend the flow gradient into the rest of the flow and alter the results. In order to avoid this it is necessary to keep the first grid cell (in which the wall functions will be used for coarser meshes) to a similar size to the boundary layer. From Figure 9.5 it can be seen that the upper limit of the boundary layer is at a y^+ of between 100 and 1000. This corresponds to to the findings in Figure 9.8 which show the results beginning to deviate after these values with the 50 m wing having acceptable results up to 5000.

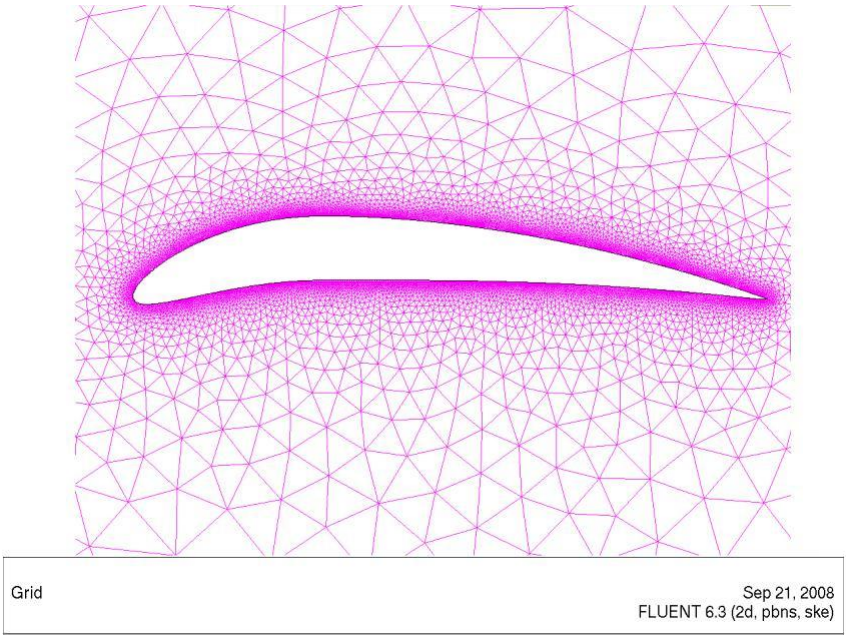

Figure 9.9: Mesh for 50 cm wing with y^+ 1

It has been shown that it will not be feasible to resolve the full boundary layer problem. However, providing the grid is kept sufficiently small the wall functions give an accurate description of the flow around a wing. It could be that in areas of flow separation the wall functions do not give an adequate result. If the flow proves to be highly separated it may then be necessary to conduct further tests on sections of the model so that the grid size is kept within the computational limits.

9.2.2 Grid Generation and Fluent Setup

It was decided that nine grids should be constructed, comprising three different heights, at which three different trim angles would be tested. The grids were generated in Gambit by importing the model in the form of a .STEP file as before. The models used a lateral symmetry, that is, they were split about the vertical plane between the hulls in order to half the number of nodes. The grids were all constructed around a semi-stuctured grid due to the complex geometry. However, the near wall meshes were kept uniform with a maximum cell height of 0.1 m and a growth rate of 1.4 in the near wall region. The maximum cell height of 0.1 m gives a maximum y^+ of 7000, however, the mesh was structured such that the cell size decreases around areas of greater curvature such as the leading and trailing edges and consequently the majority of the wing has lower y^+ values. Examples of the grids are given in Figures 9.10 and 9.11.

9.3 Turbulent Model Analysis

From the two dimensional boundary layer analysis it is clear that although a complete low Reynolds number solution may provide better results in certain

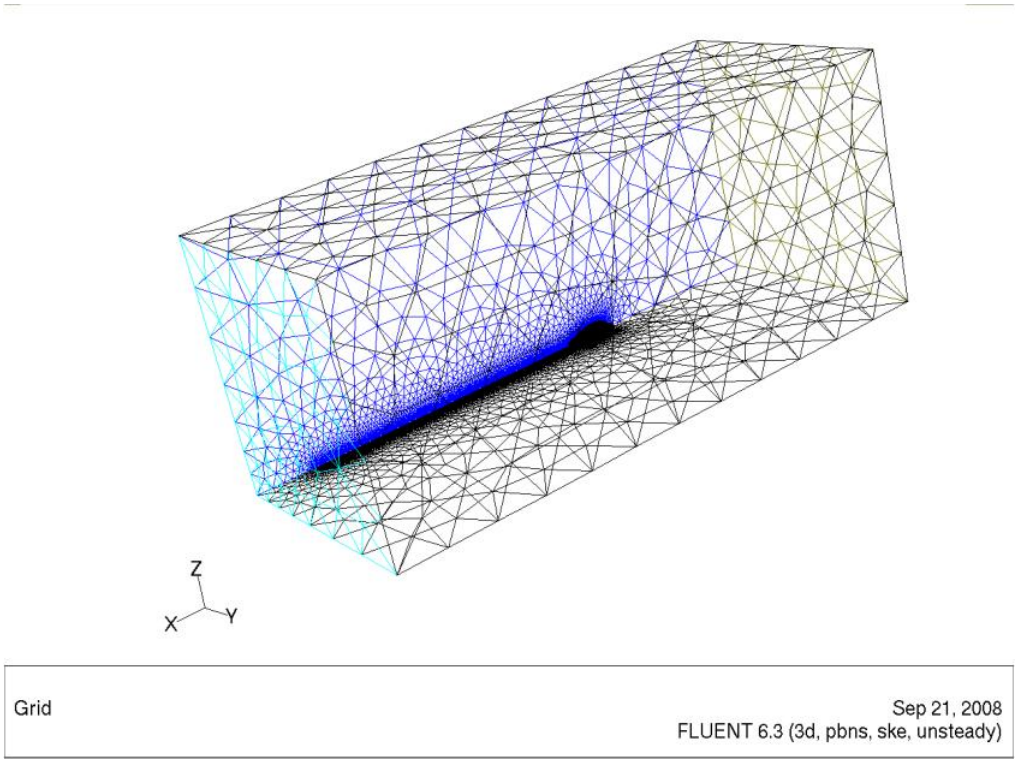

Figure 9.10: Mesh for complete hydrodynamic surface model, H = 5 $\alpha = 4$

circumstances, it would not be practical for the current situation due to insufficient computational power. This removes the necessity for low Reynolds number solvers such as the Reynolds Stress Model (RSM), however it does not mean that such a model would not be advantageous. The RSM model is the most sophisticated turbulent model available in Fluent and requires the solution of seven additional transport equations in comparison to the k-ϵ model. This is because the RSM model does not assume isentropic eddy viscosity in the same way as the k-ϵ model, but instead solves the full turbulent transport equations. This can lead to better results in areas driven by the production of anisotropic turbulence, such as in regions of vortex shedding. However, according to the Fluent documentation [10] this is not always evident and unless there is specific interest in the vortex motion, not always worth the additional computational expense. For the current

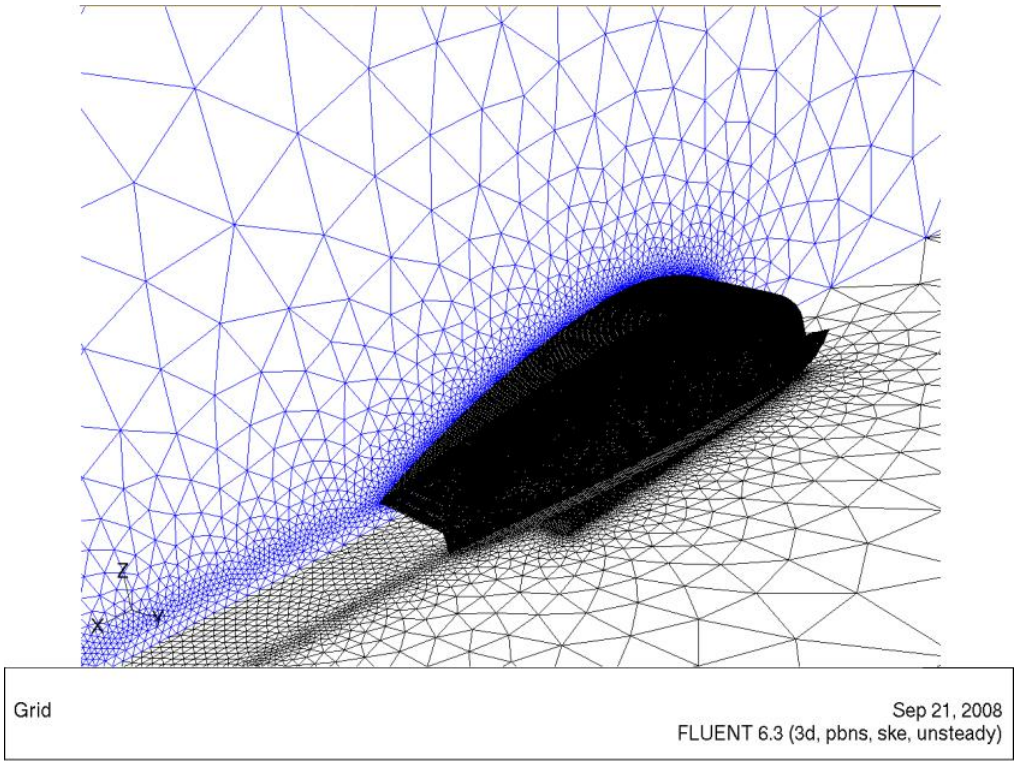

Figure 9.11: Mesh detail for complete hydrodynamic surface model, H = 5 $\alpha = 4$

application it is likely that the turbulence will be limited to small regions and that there will not be any well defined vortex shedding. This is because the area of turbulent separation, namely the transom stern, is quite small and immersed in a high Reynolds number flow. As a result it may not be worth the additional computational effort of using the RSM model over the k-ϵ model, particularly in light of the use of simplifying wall functions, themselves necessitated by limited computational resources. However, it was decided that a comparative test should be done on a single mesh so that the difference between the two models could be evaluated.

The test mesh used was that of $h = 5$ and $\alpha = 2$ and was run for a flow speed of 36 ms^{-1} using both the RSM and k-ϵ models with enhanced wall functions.

This mesh was chosen because it exhibits all of the difficulties of the model, that is, the partially submerged transom hull, the gap beneath the leading edge of the hull and a sharp angle around the front of the upper deck area of the hulls, which is inclined at an angle of attack to the flow. Experience gained from computing the two dimensional time dependent flows showed that starting at a much smaller time-step and gradually increasing in size gave the most stable and rapid solution. This approach was adopted for the three dimensional study as well. The maximum time-step size is equal to the smallest node size divided by the free stream velocity, that is:

$$Tstep_{max} = \frac{\Delta x}{U_\infty} \tag{9.4}$$

For an average minimum cell size of around 0.05 this gives a maximum time-step size of 0.00139 seconds. It was therefore chosen to start at a time-step size of 0.0001 seconds and increase to a maximum of 0.001 seconds as the solution stabilized. Furthermore, it was decided that the models should be run up to a minimum of fifteen seconds so that the flow could form a stable wake. This gives at least ten chord lengths of down stream wake based on a chord of 50 metres and a free stream flow of 36 ms^{-1}.

During the testing, the RSM model was found to be quite unstable and crashed easily in comparison to the highly robust k-ϵ model. From observation of the residual monitors for both models, it was seen that the k-ϵ model formed a stable solution in fewer iterations. Most significantly however, the k-ϵ model was able to provide the solution in substantially less time. For example, to calculate the first physical second of flow time (ΔT) using the k-ϵ model required around a day, whilst the RSM model took nearly three. It should be remembered that the first second takes longer due to the adaptive time-stepping, however, at $\Delta T = 15$ the

RSM will have taken around 25 days as opposed to around 10 for the k-ϵ model. Since nine complete runs of 15 seconds each are required this would lead to around 225 days of computer time for the RSM model. Admittedly it is possible to run up to three models at once on the Cluster grid facility at Cranfield, but multiple processors are not always available. This in conjunction with the instability of the RSM model encountered during initial testing, which could lead to a significant number of repeat runs for individual grids, leaves the RSM model with the distinct possibility of not providing the complete data set within the time frame. This makes the k-ϵ model the only feasible option. This should not be a problem however. In light of the reliable results previously gained and its industry wide application, it is perhaps a better choice for providing comparisons, and there is little reason to believe that the RSM would provide more detailed results. If however, there appears to be significant flow separation or vortex shedding within critical regions of the flow, it may be necessary to re-run some models (for instance those at higher angles of attack) using the RSM for comparison.

9.4 Results

The results obtained from CFD are presented in Figures 9.12 to 9.15, which represent the likely data range for the hybrid vehicle during take-off and cruise. It should be noted from Figure 9.2 that the height above the water of the origin at zero angle of attack is the total ground clearance of the wing. Since the origin is located at the quarter chord point it is possible to use trigonometry to calculate when the trailing edge will interfere with the water surface. The following choice for alpha and height are made assuming that a clearance of at least one metre is required and that the hull must always touch the water. Hence at a height of seven metres the minimum angle is two degrees and at a height of three the maximum

angle is three degrees. The results are kept within these constraints, with consideration to earlier results from the stability model which show characteristically low trim angles and a tendency toward shorter wetted length.

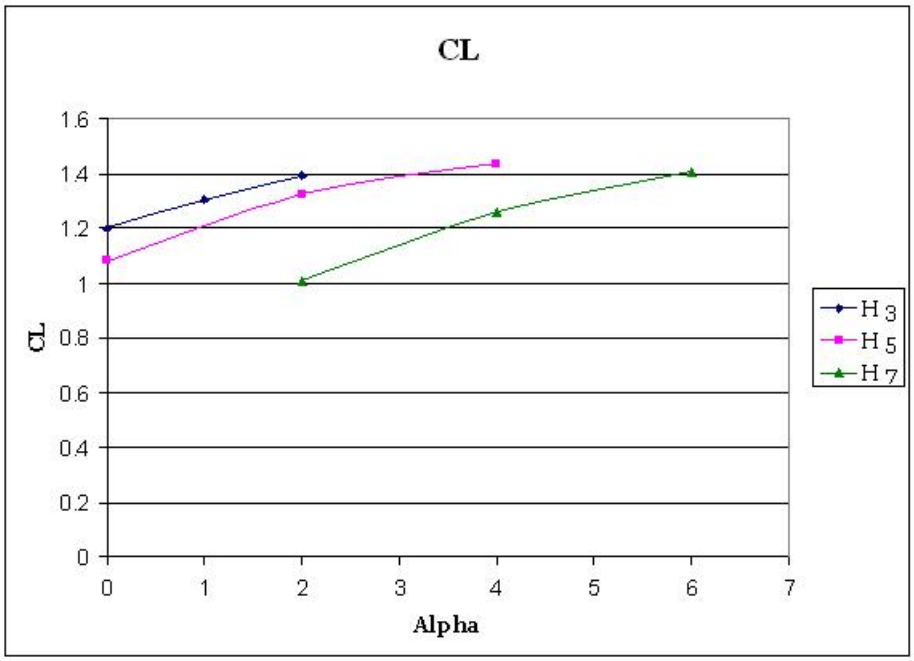

Figure 9.12: C_L as a function of angle of attack at various heights

9.5 Discussion

Figure 9.12 shows the lift coefficient at various heights as a function of angle of attack. One notable feature is the maximum value of C_L, which is around 1.4 for all heights. This is in excess of the previous set of results, despite the lower angles of attack used in this set, and shows that the aerodynamic modifications were wholly justified. Indeed, the results are entirely superior at all heights and angles. This is particularly pleasing since it was presumed that the inclusion of hydrodynamic surfaces would have a considerable and detrimental effect on the

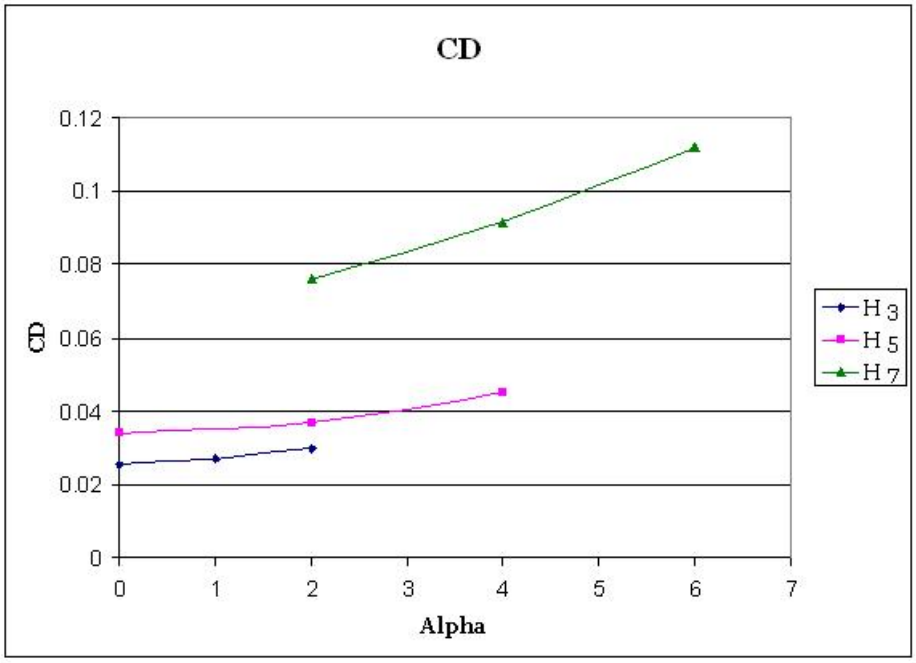

Figure 9.13: C_D as a function of angle of attack at various heights

aerodynamic performance. It appears however, that the effect is quite small, and more than compensated for by the improved aerodynamics.

Figure 9.13 shows the results for drag. From the graph, it can be seen that although the results are similar for lower heights and angles, that is, whilst the hydrodynamic portion of the hull is submerged, the drag is significantly increased at greater heights and angels of attack. This must be the result of the hydrodynamic surfaces. The transom hull must account for some of the increased drag at the greatest height, but it is submerged at a height of five metres, and hence, the forward portion of the hull must contribute to the drag at this attitude. Since the hydrodynamic portion of the hull has a flat upper deck, it is likely that there is some flow separation around its edges when they are inclined against the flow. This was observed in the three dimensional flow plots for the model, where low pressure formed behind the forward bow section. Relatively little of the transom

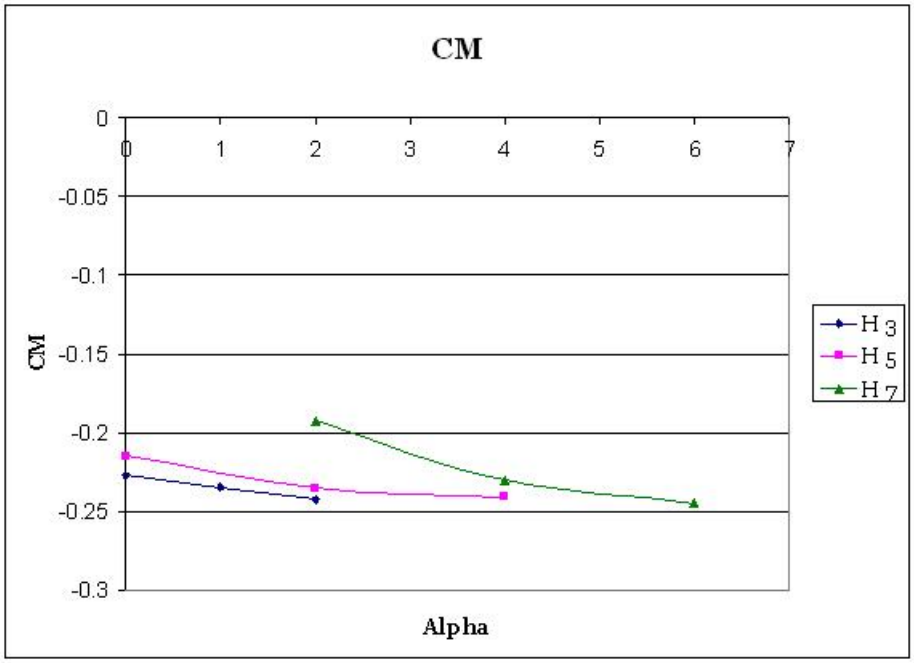

Figure 9.14: C_M as a function of angle of attack at various heights

hull was ever exposed and as such, little flow separation appeared except at high ground clearance and low angles of attack. The effect of the hydrodynamic surfaces on the pressure can be seen from comparing the previous 3D pressure plots with those presented at the end of the chapter, Figures 9.16 to 9.33. From the discontinuous curve of the pressure plots it is clear that the flow is interrupted by the hydrodynamic surfaces, and that although the effect on lift has been minimized, the drag has been increased significantly.

The results for the coefficient of moment are shown in Figure 9.14 and are markedly different from the previous set. Firstly, although the moment is still negative, being nose down about the quarter chord point, the magnitude is far greater. This is partly due to the increased lift, but also the new wing profile, which is highly cambered. This has the effect of creating a more even pressure distribution on both the inner and outer surfaces of the hull and results in a more equidistant

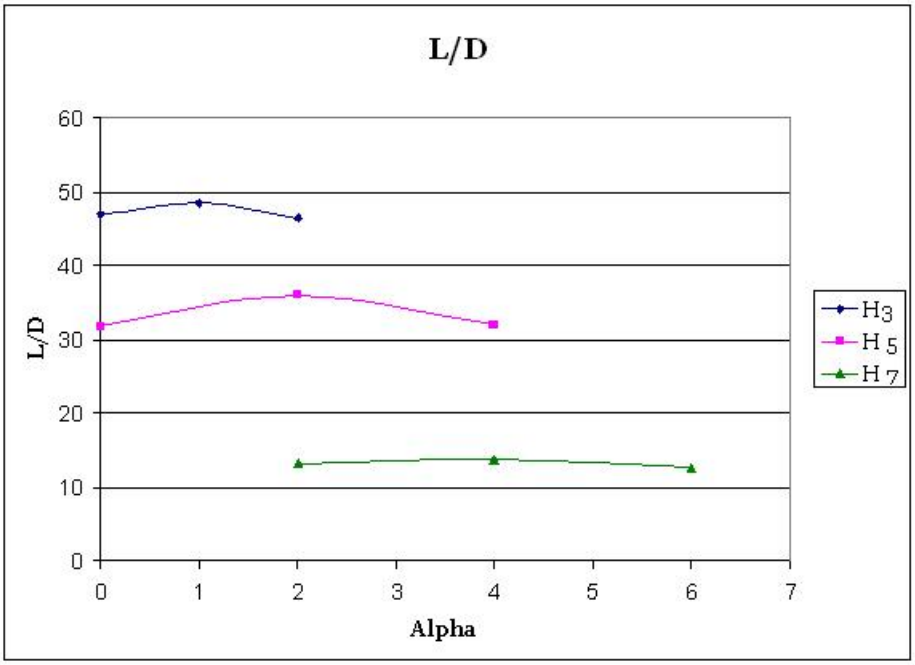

Figure 9.15: Lift-to-drag ratio as a function of angle of attack at various heights

centre of pressure, as opposed to the nose biased centre of pressure associated with more conventional wings. Secondly the curve of the graph is reversed. That is, although the moment increases (albeit negatively) with the increase of angle in both cases, the differential, or rate of change of moment with angle is opposite. In the first case the rate of change of moment increases with increased angle of attack, which is quite normal behavior. In the second case however, the rate of change decreases. This is probably the result of the moment being quite central to start with. That is, since the highly cambered wing creates quite an even distribution of pressure, the change in angle does not cause the high pressure on the underside of the wing to move back like it would on a normal wing. This results in a far more gentle change in moment with angle and one which diminishes with increased angle.

Figure 9.15 shows the results for lift-to-drag ratio. With values of nearly fifty at

the lowest height it is apparent that the configuration is capable of considerable aerodynamic efficiency. However, at this point the hydrodynamic portion must be completely submerged, meaning the vessel is moving very slowly and is heavily loaded. At more reasonable attitudes, such as a height of 5 m, the lift-to-drag ratio is between thirty and forty, which is not as good, but still very high. Unfortunately, the value decreases rapidly at a height of seven to a value of around thirteen. Although this is significantly lower it is worth remembering that it is still quite a high value and that it is largely reduced by the increased drag, not any loss in lift. It is quite reasonable to assume that a significant reduction in drag could be achieved through modifications to the hull. It should be remembered that the hull form tested here is more a proof of concept than an attempt at optimization. Although much effort has gone into the wing design, the aerodynamics of the hydrodynamic part of the hull have only survived their first analysis and are thus likely to be far from ideal.

It is interesting to note that although some losses occurred through high pressure escaping under the raised hulls, the effect was quite small and no noticeable vortices formed as a result. This could well be because the hulls, although partially removed from the water, where never fully removed and remained always with the rearmost portion submerged. Since vortices form at the leading edge and grow as they move rearwards, having the transom of the hull in contact with the water would prevent the complete formation of vortices. This means that although some pressure can escape, there will never be the efficient transportation of pressure associated with fully formed vortices.

The vehicle appears to be self stabilizing, in that the moment tends to move rearwards and become more nose down as the angle of attack increases. This would tend to keep the vessel quite level, which is very useful, especially considering the instability of previous RAM wing craft. Equally, it would appear that if the craft

did become fully airborne, the lift would significantly decrease due to the hull becoming more akin to a wing with end plates. This would allow the formation of complete wing tip vortices, and hence, lower the pressure. It may be speculated that in addition the centre of pressure may move forward, in accordance with more conventional wing shapes. It is difficult to determine at this stage which factor will prove dominant, the shift in centre of pressure, which would cause a nose up moment and tend to destabilize the vessel, or the resultant decrease in lift as the efficient ducted wing becomes a highly inefficient low aspect ratio wing, which would tend to cause the vehicle to lower and stabilize. This can only be found through continued aerodynamic analysis and stability modeling, however, it may well be irrelevant since the aerodynamic portion of lift may not be capable of supporting the entire vehicle weight. Indeed, maximum efficiency is often obtained for SES ships at around eighty percent cushion support, and the hybrid vehicle may be designed to run at a lower aerodynamic support.

9.6 Conclusion

The results appear to be very promising, with lift-to-drag ratios of nearly fifty achieved and very high lift coefficients. It is true that the drag is increased at greater heights due to the hydrodynamic design. However, it is very unlikely that the aerodynamic contribution to drag will be as great as the hydrodynamic contribution which it replaces. The data must be analysed with the stability model and compared to existing craft so that the potential benefits of the increased aerodynamic efficiency can be gauged.

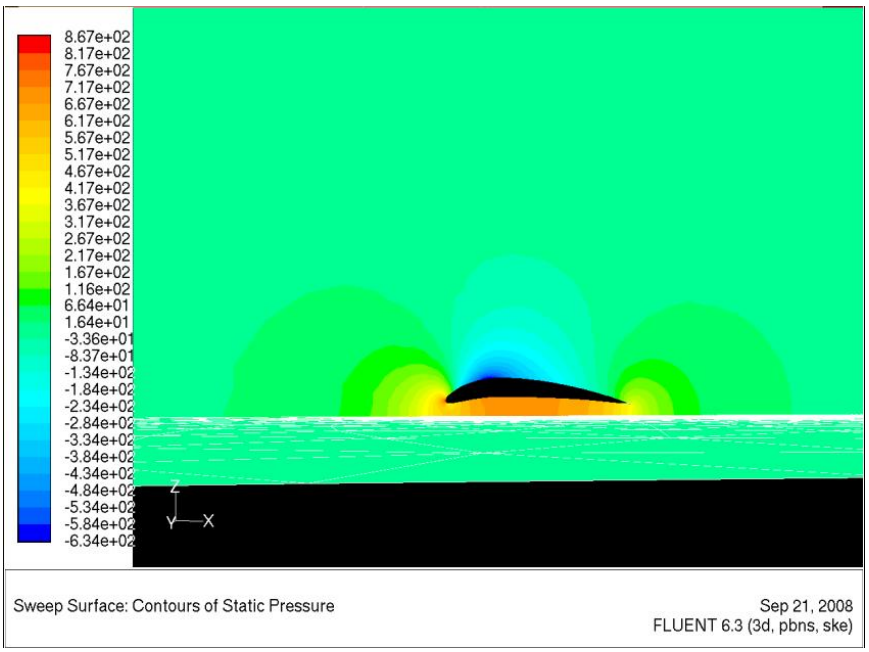

Figure 9.16: Pressure coefficient plot, H = 3 $\alpha = 0$

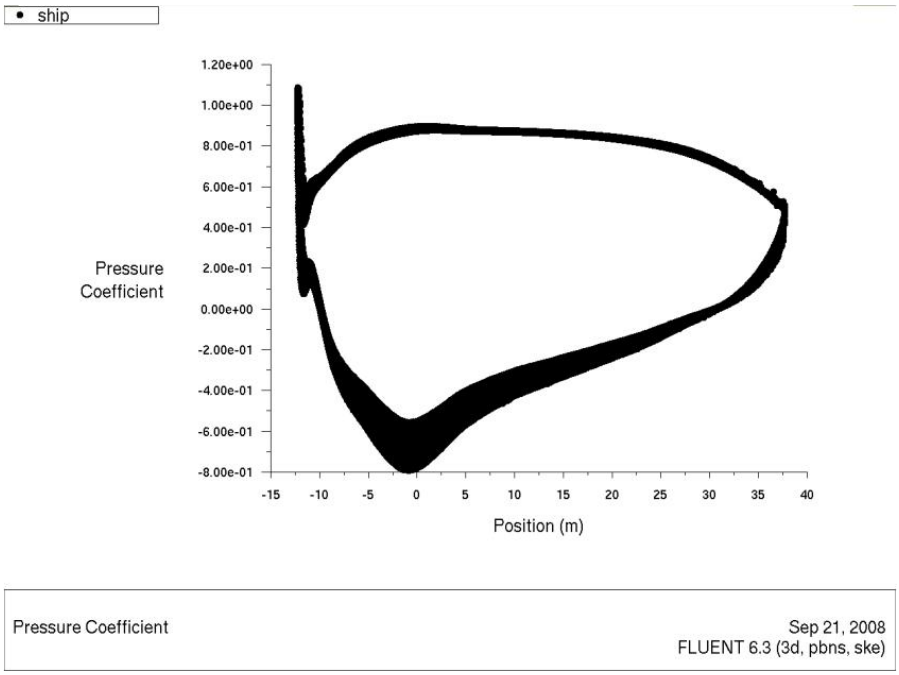

Figure 9.17: Static pressure, H = 3 $\alpha = 0$

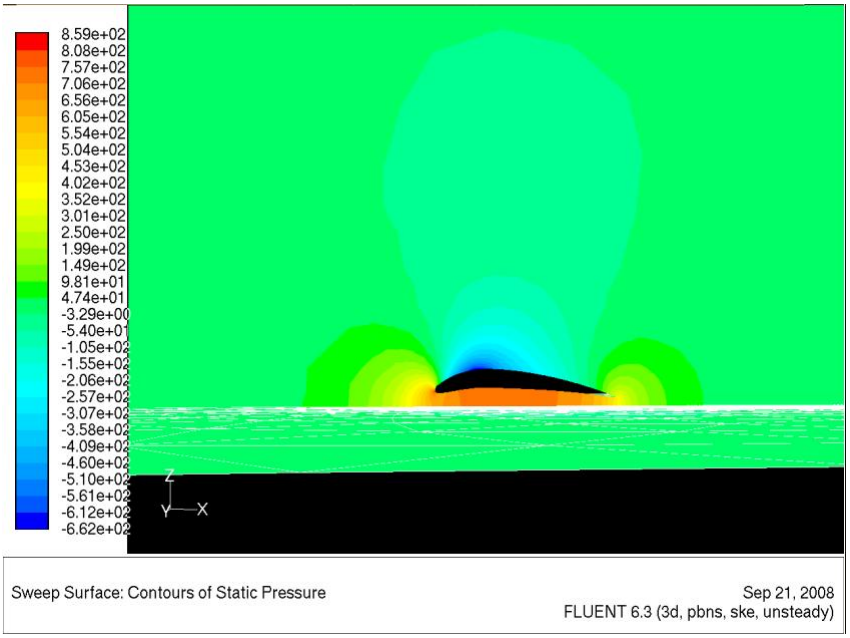

Figure 9.18: Pressure coefficient plot, H = 3 $\alpha = 1$

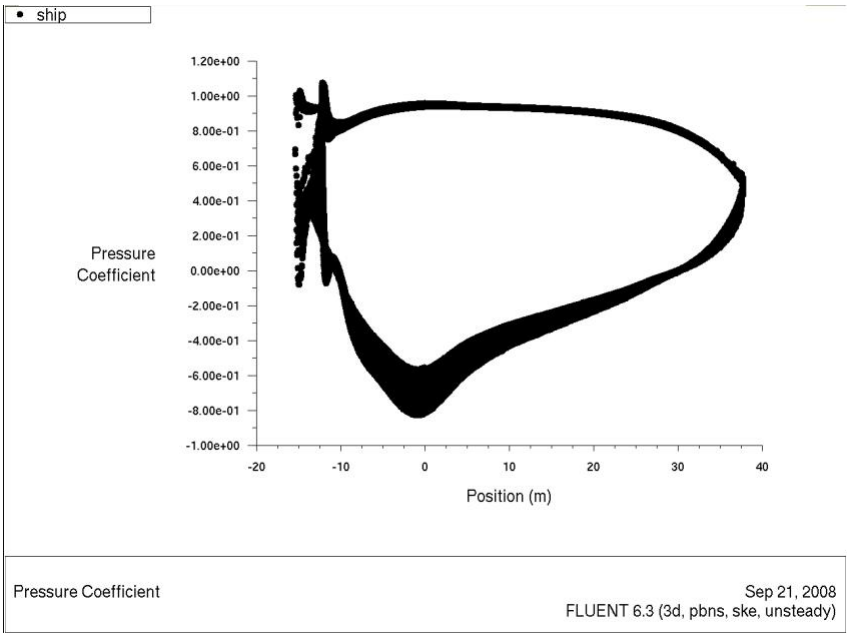

Figure 9.19: Static pressure, H = 3 $\alpha = 1$

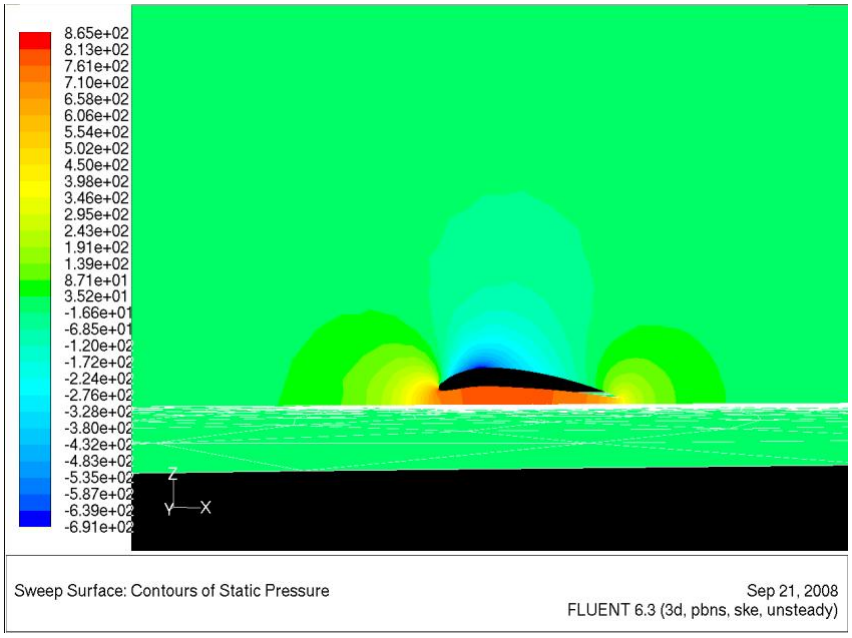

Figure 9.20: Pressure coefficient plot, H = 3 $\alpha = 2$

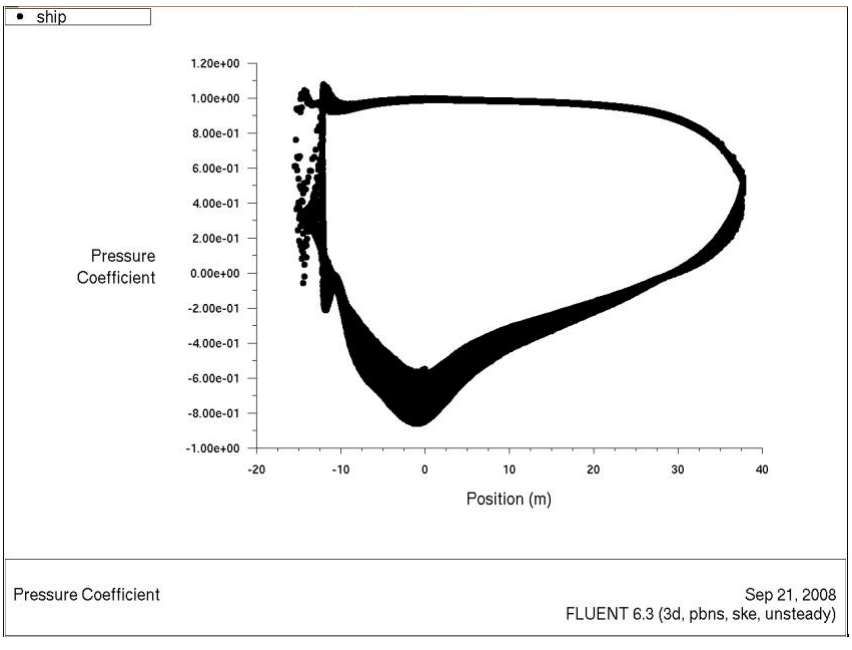

Figure 9.21: Static pressure, H = 3 $\alpha = 2$

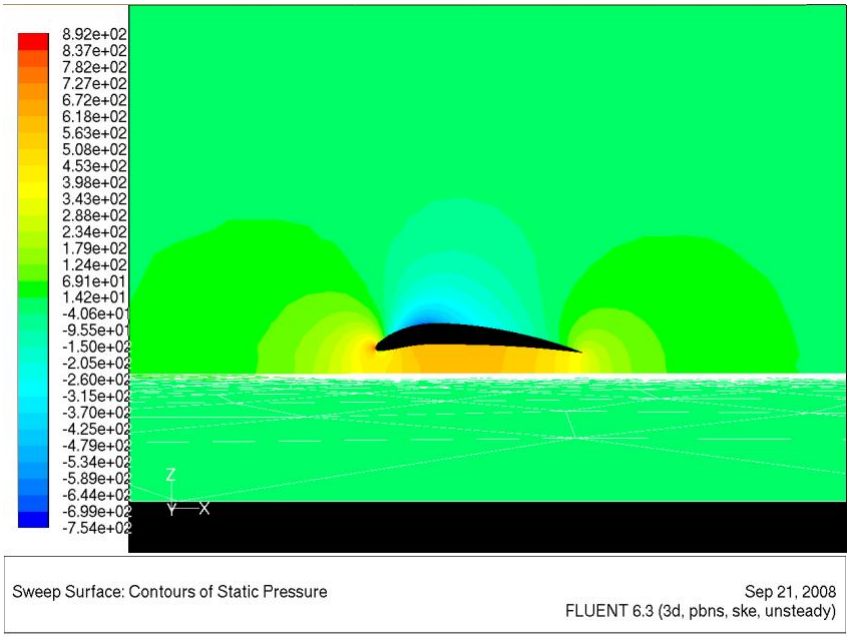

Figure 9.22: Pressure coefficient plot, H = 5 $\alpha = 0$

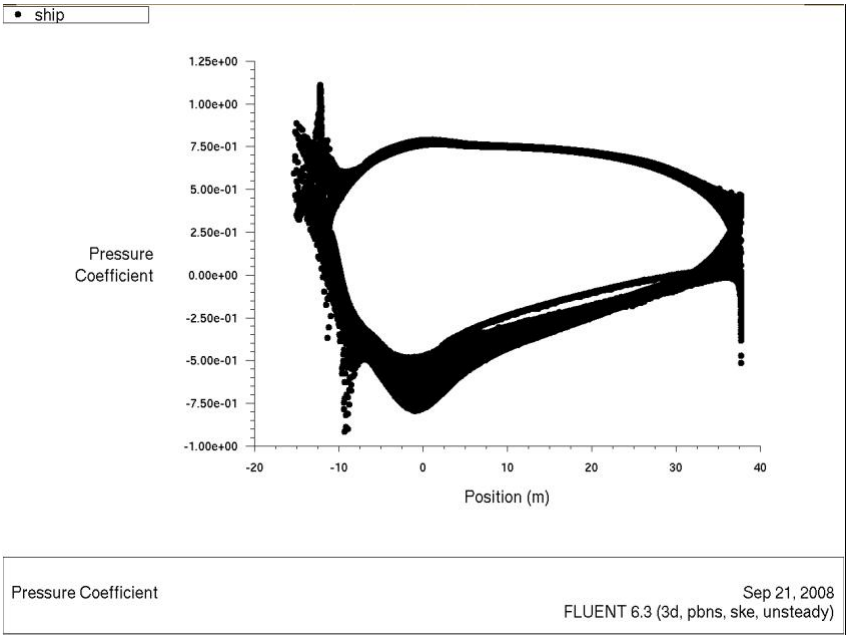

Figure 9.23: Static pressure, H = 5 $\alpha = 0$

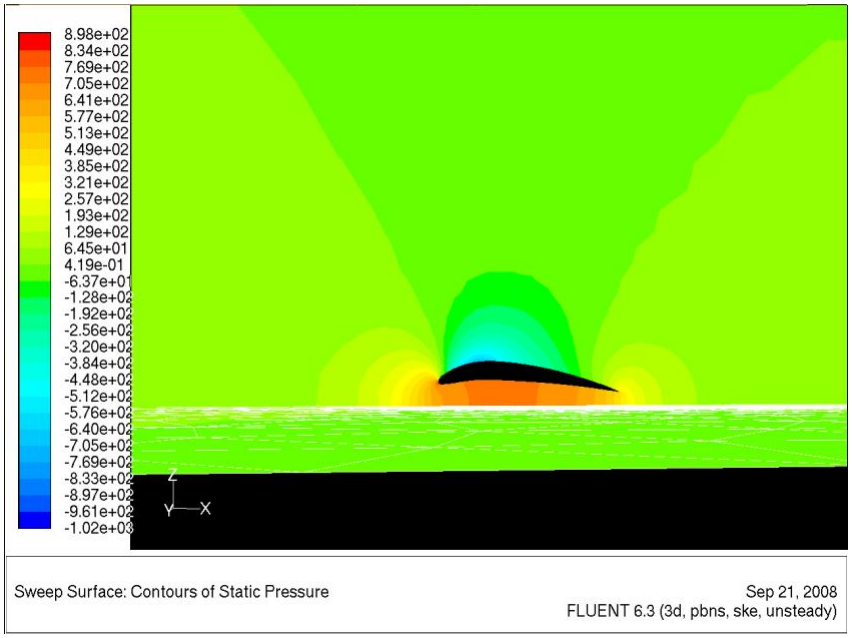

Figure 9.24: Pressure coefficient plot, H = 5 $\alpha = 2$

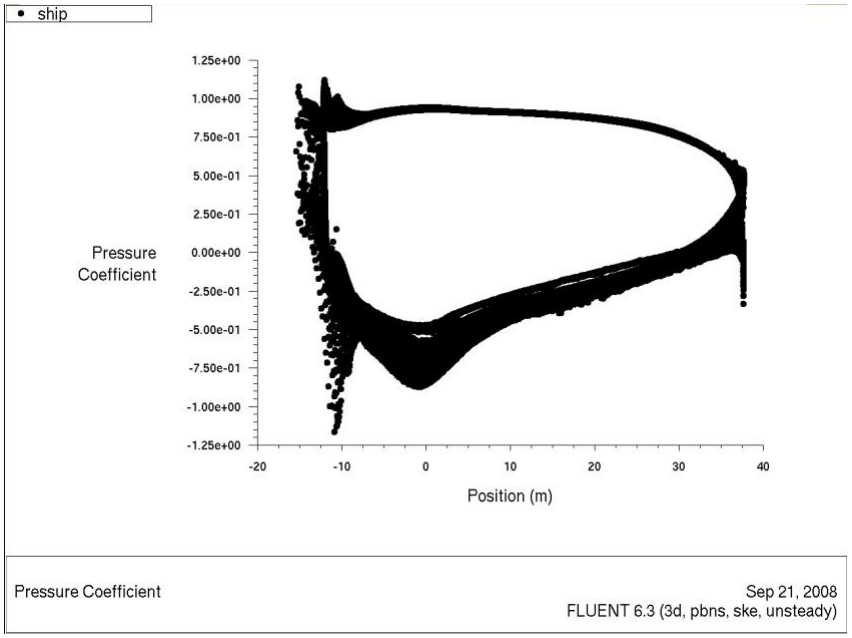

Figure 9.25: Static pressure, H = 5 $\alpha = 2$

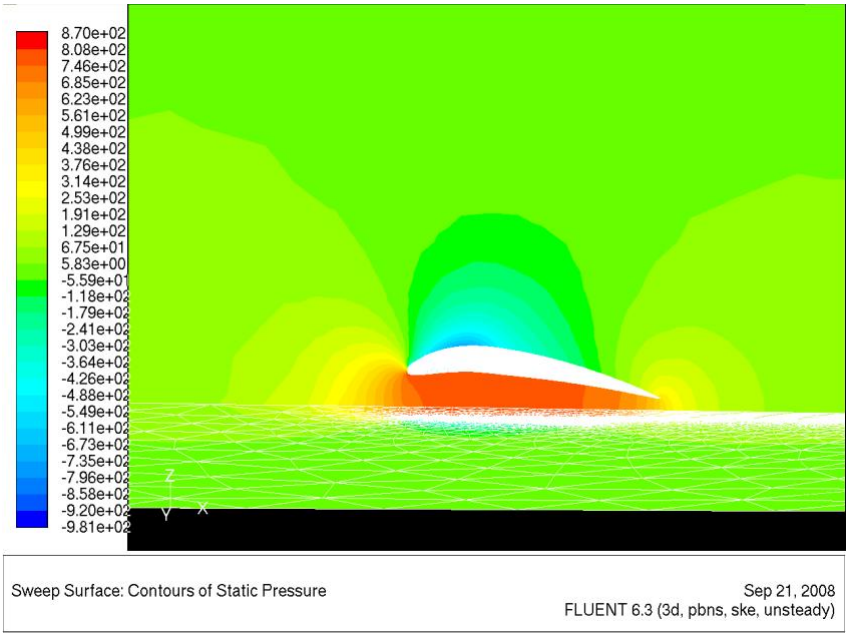

Figure 9.26: Pressure coefficient plot, H = 5 $\alpha = 4$

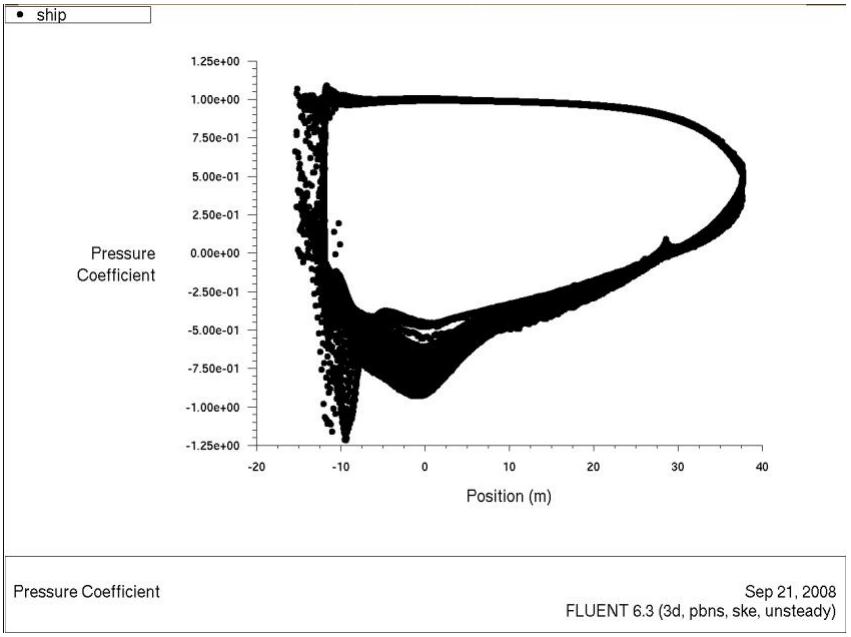

Figure 9.27: Static pressure, H = 5 $\alpha = 4$

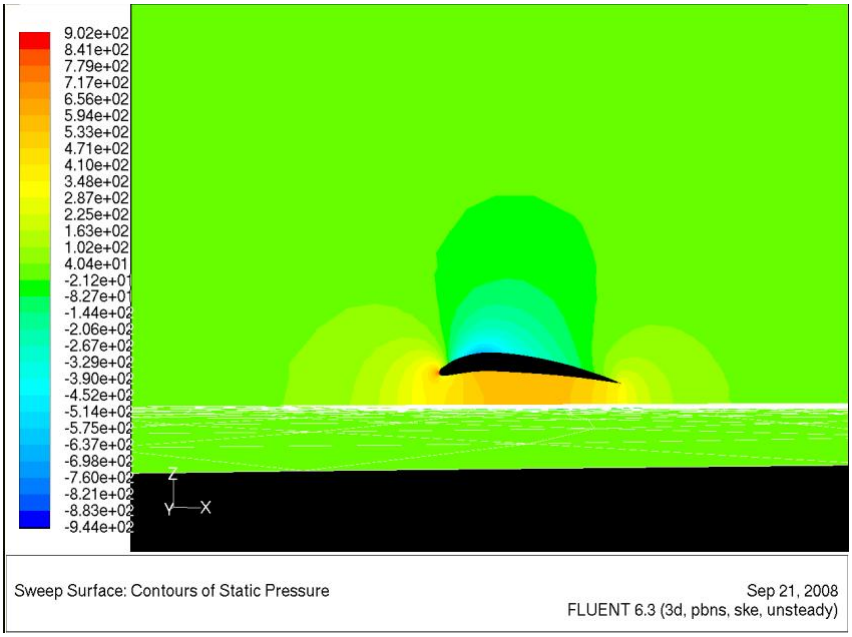

Figure 9.28: Pressure coefficient plot, H = 7 $\alpha = 2$

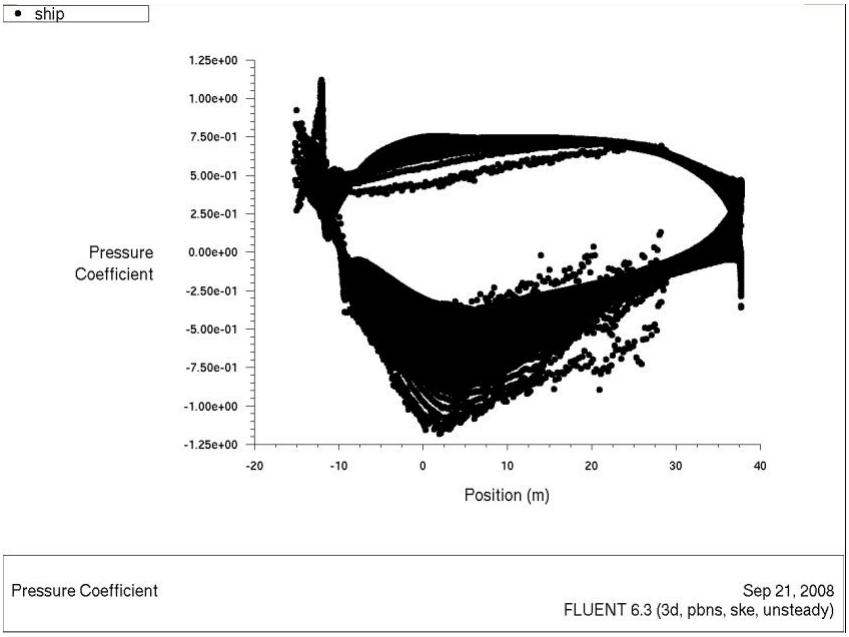

Figure 9.29: Static pressure, h = 7 $\alpha = 2$

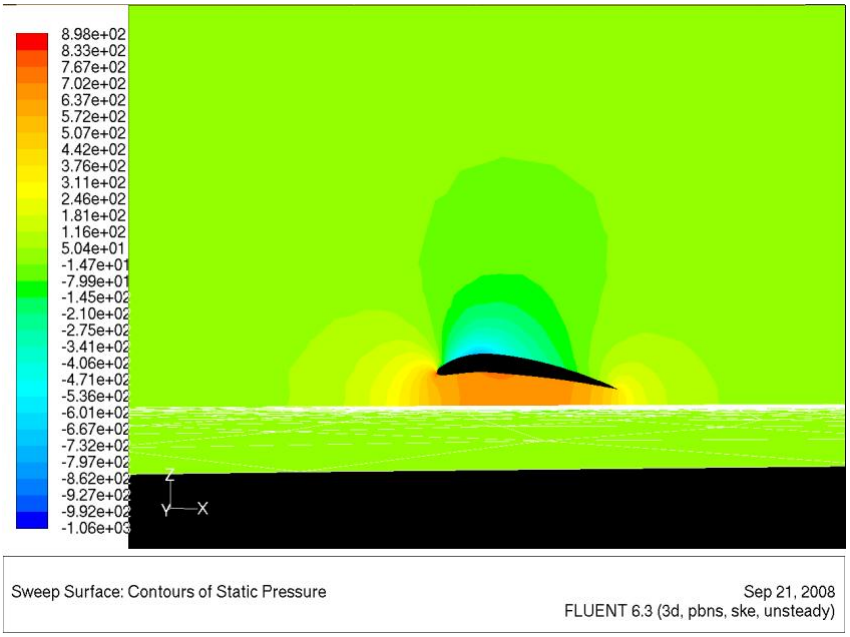

Figure 9.30: Pressure coefficient plot, H = 7 $\alpha = 4$

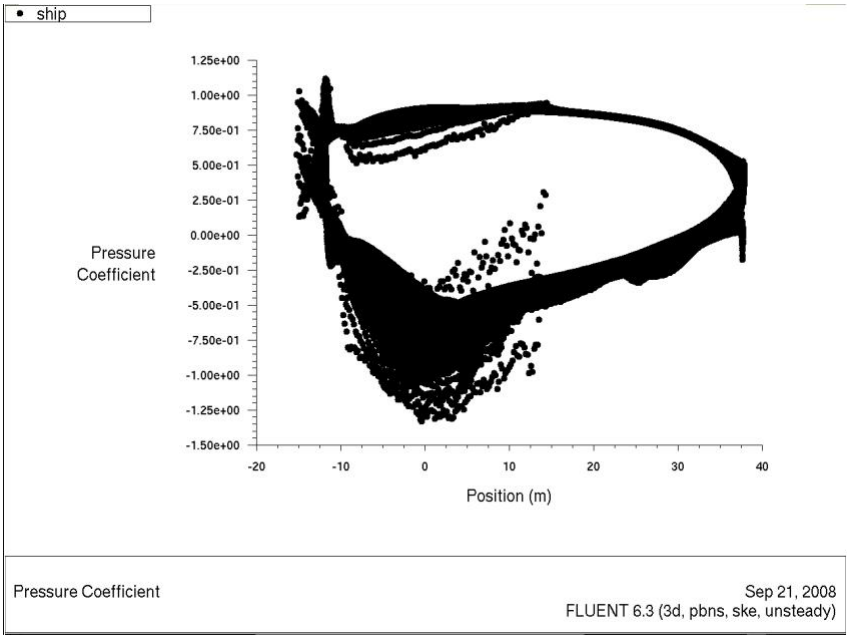

Figure 9.31: Static pressure, H = 7 $\alpha = 4$

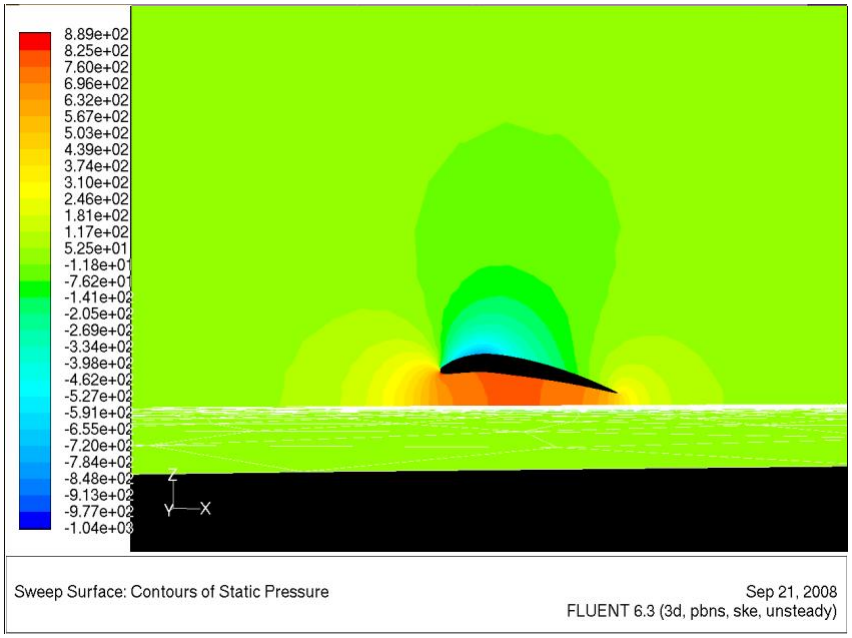

Figure 9.32: Pressure coefficient plot, H = 7 $\alpha = 6$

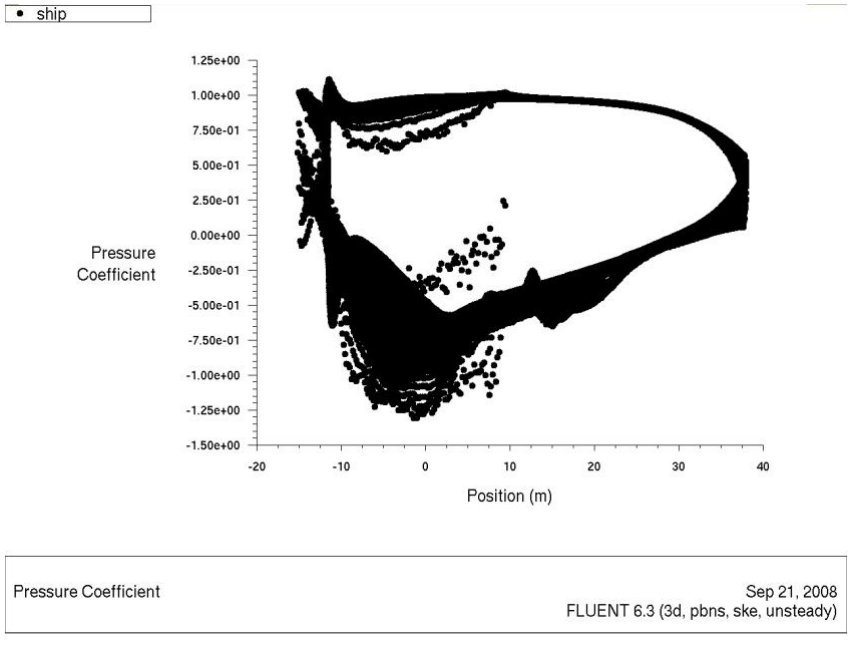

Figure 9.33: Static pressure, H = 7 $\alpha = 6$

Chapter 10

INTERPRETATION OF RESULTS

10.1 Introduction

The results from the full three dimensional analysis in the previous chapter show extremely promising results and conclusive evidence that a ducted hull can provide a significantly improved aerodynamic lift over a standard low aspect ratio wing in ground-effect. Lift-to-drag ratios of nearly fifty were obtained under optimum conditions. However, at higher elevations, the efficiency was considerably reduced. This was shown in part to be the result of the high pressure escaping under the raised hulls, but largely the increased drag on the hydrodynamic surfaces, particularly at higher angles of attack. As a result the running attitude of the vehicle will greatly determine the performance. The vehicle will therefore be analysed using the hybrid stability model in order to obtain results for the sinkage and trim as well as power requirements.

Once the vehicle has been evaluated using the hybrid stability model, a comparative parametric analysis can be performed. This is in order to examine the relative performance of the vehicle in comparison with other vehicles, with regards to their size, speed and payload. This should identify the likely market potential of the

hybrid vehicle.

10.2 Hybrid Vehicle Stability Model Results

10.2.1 Data

The same method was used with the hybrid stability model as described in Chapter 8. The data used is shown in Figures 10.1 to 10.4. These results are the ones obtained in Chapter 9, but interpolated and extrapolated for a wider range. This is necessary due to the nature of the stability model, which relies on iterative approximations in order to home in on a stable solution. This means that although it is known that the vessel is likely to operate in a relatively confined range of trim angles and heights, the program requires data for a wider range to facilitate the approximation process. Hence, the results are extrapolated beyond the reasonable trim angles and elevations. It is possible that the vessel will stabilize outside of the original CFD data, and if this occurs it will compromise the accuracy of the results. However, obtaining the full CFD solutions is very time consuming and since it is likely that the range of data has been well covered, extrapolation is a far more economic method of providing the 'edge' data for the program to use. When the final results are examined, the trim angle and height will be observed to check that they are within the CFD data range. If they are not, further CFD runs may be required to provide accurate data.

10.2.2 Results

Figures 10.5 to 10.8 show the data obtained for the complete hybrid vehicle using the hybrid vehicle stability model. The data for an identical planing hull with

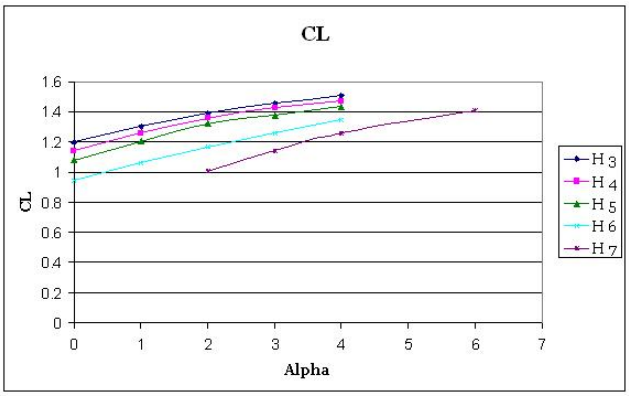

Figure 10.1: Lift coefficient for hybrid vehicle stability model

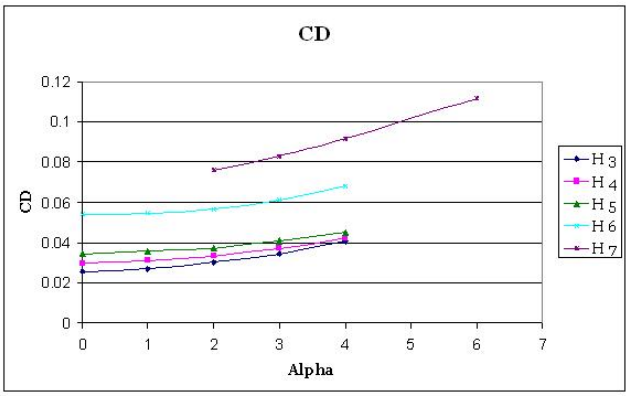

Figure 10.2: Drag coefficient for hybrid vehicle stability model

non-lifting aerodynamic body is also presented for comparison. The aerodynamic data is taken from the model shown in Figure 9.2, with the planing hull geometry being the same for both the hybrid and standard model. The model is once again 50 m long and 25 m wide, weighing three hundred tonnes in this case and having a centre of gravity approximately one third of the ships length from the transom; being a distance of 17 m from the stern.

Figure 10.5 shows the percentage contribution of lift for the aero and hydrodynamic components of the hybrid vehicle as a function of speed. As before, the

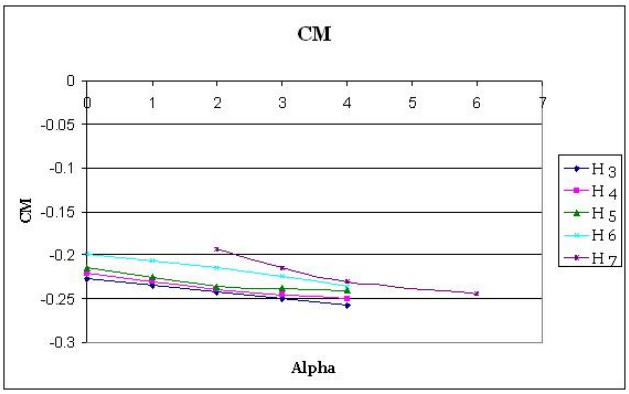

Figure 10.3: Moment coefficient for hybrid vehicle stability model

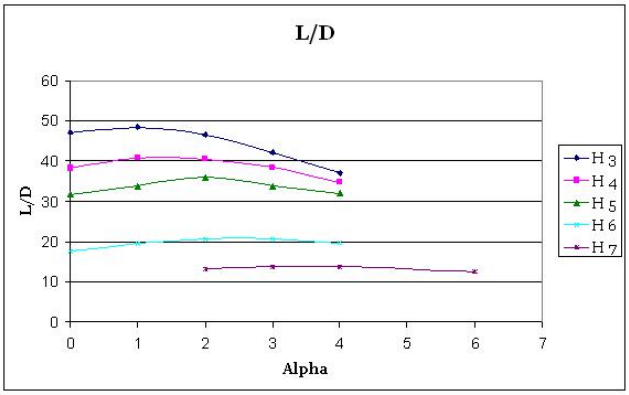

Figure 10.4: Lift-to-drag ratio for hybrid vehicle stability model

aerodynamic contribution increases rapidly beyond thirty knots and reaches a fifty percent contribution at around seventy six knots. At the top speed recorded, eighty four knots, the aerodynamic lift contributes sixty percent of the lift.

Figure 10.6 shows the drag components for both the hybrid vehicle and an equivalent planing hull without aerodynamic support. The results are similar to those obtained for the first run, shown in Figure 8.3, with a dramatic reduction in drag for the hybrid vehicle at speeds over forty knots.

The lift-to-drag ratio, presented in Figure 10.7, once again shows the significant

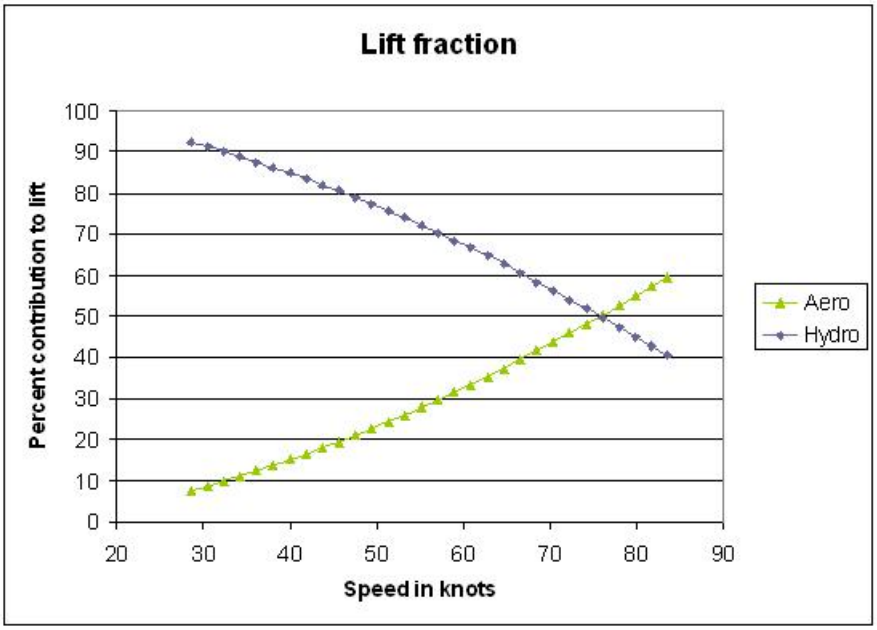

Figure 10.5: Percentage contribution of lift for the hybrid vehicle

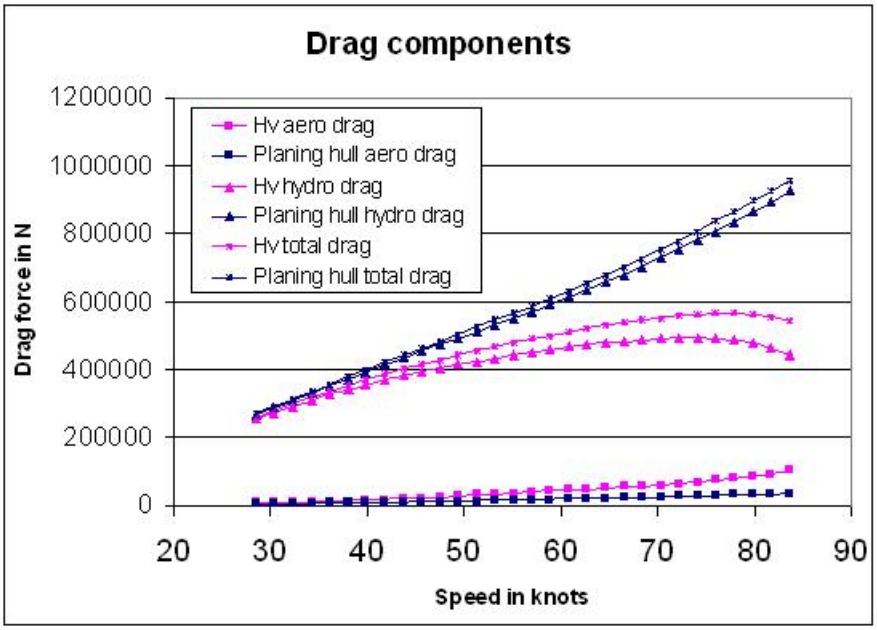

Figure 10.6: Drag components for the hybrid vehicle and planing hull

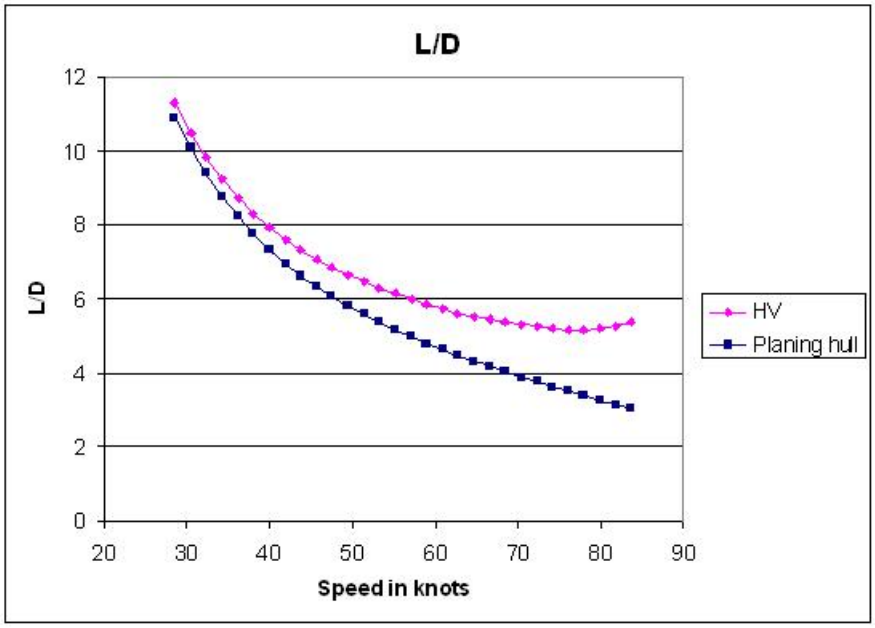

Figure 10.7: Lift-to-drag ratio for the hybrid vehicle and planing hull

increase in lift-to-drag for a hybrid vehicle when compared to a standard planing hull.

Figure 10.8 shows the resistance divided by weight, as a factor of ship speed. This is a useful indication of efficiency and clearly shows the advantages of aerodynamic alleviation when compared to the standard planing hull. In this case, the reduction of resistance over weight at the top end of the speed range is forty four percent, and appears to be continuing to improve beyond the measured range.

Figures 10.9 and 10.10 show the running attitude of the hybrid vehicle and planing hull. The important point to draw from this data is that the trim angle respects the limits of the Savitsky model as well as the data range obtained from CFD, without settling on a solution within the extrapolated data. It is also interesting to note the difference in running attitude caused by the aerodynamic forces. In particular the draft of the transom, which is clearly the result of the planing hull

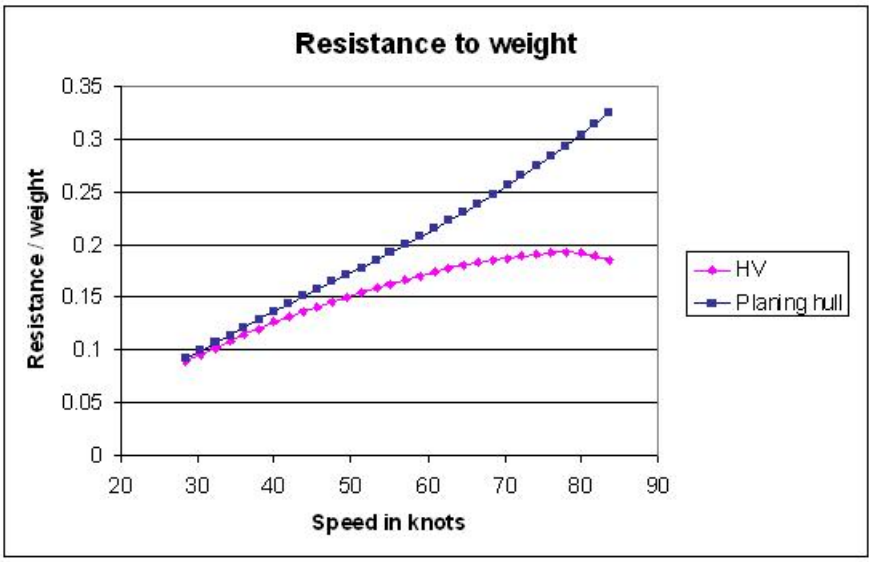

Figure 10.8: Resistance over weight for the hybrid vehicle and planing hull

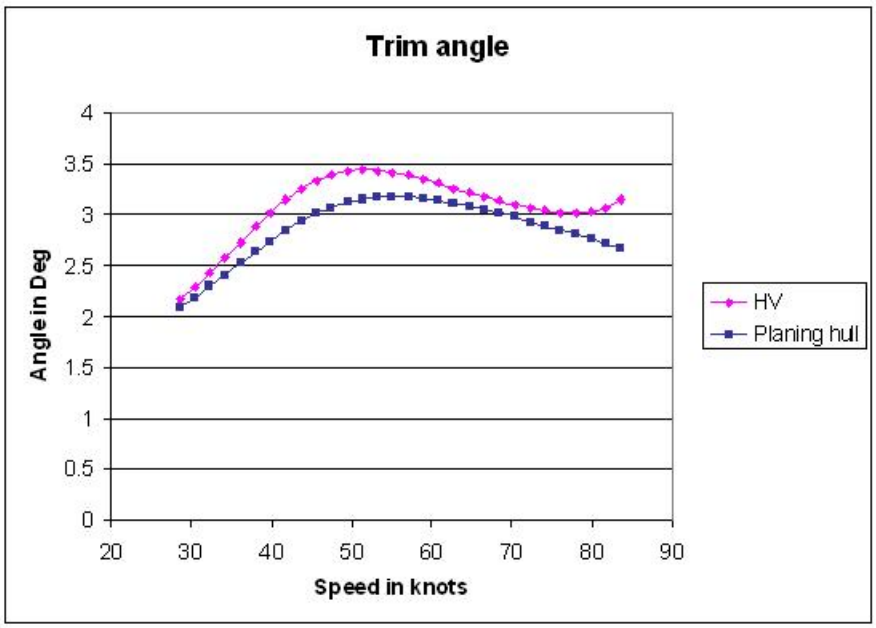

Figure 10.9: Trim angle in degrees for the hybrid vehicle and planing hull

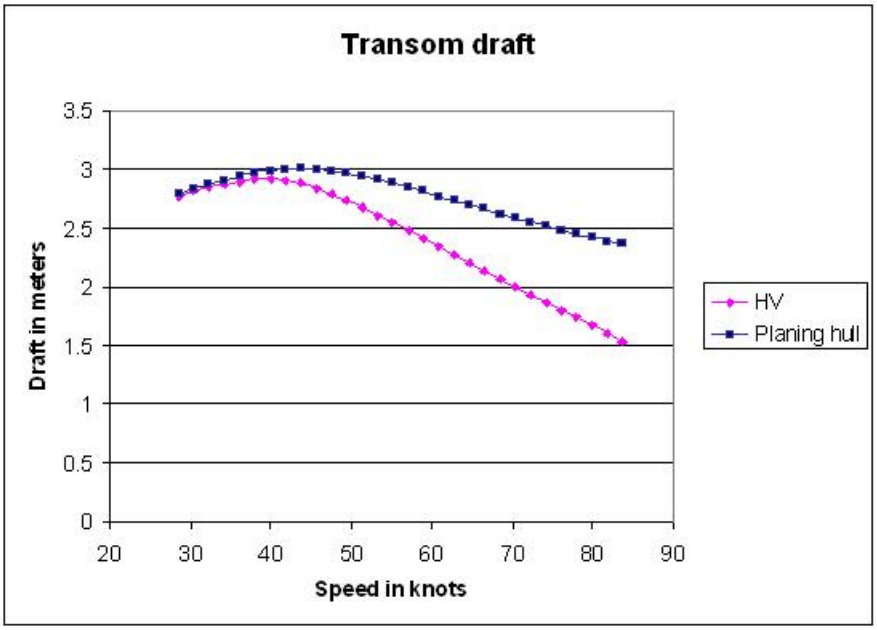

Figure 10.10: Draft of transom hull for the hybrid vehicle and planing hull

rising out of the water and accounts for the reduction in hydrodynamic drag. It should also be noted that the transom does not exceed a depth of three metres, which is the size of the transom used for the aerodynamic model. One noticeable change in the running attitude is the rather sharp increase in trim angle for the hybrid vehicle at the top end of the speed range. It should be noted that the actual change in angle is significantly less than one degree, but the change is nose up as opposed to the nose down motion of the standard planing hull.

10.2.3 Discussion

These results are very similar to the last set for the hybrid vehicle, once again showing that a considerable reduction in drag can be achieved through aerodynamic alleviation. This also shows that the effect of incorporating the hydrody-

namic surfaces is not overly detrimental to the performance of the vessel. Although the aerodynamic resistance has been increased a little, it is still a small proportion of the total drag, and crucially, the aerodynamic lift remains high. The aerodynamic drag could well be improved when better knowledge of the hydrodynamic requirements allows for a more careful design. However, this will not be the most significant factor since the main influences are clearly the hydrodynamic drag and the aerodynamic lift.

The peak of the hydrodynamic drag occurs at a fifty percent aerodynamic loading. Indeed, once the aerodynamic forces are dominant, the drag decreases rapidly. It is seen that even at the peak drag for the hybrid vehicle the drag is still some forty four percent less than that of the planing hull. Once the aerodynamic forces become dominant however, the stability becomes a serious issue. The main reason for this is the difference between the aerodynamic centre and the centre of gravity, and this is also the reason why no results are obtained beyond eighty five knots. The aerodynamic centre is calculated from the quarter chord point, being thirty seven and a half metres forward of the transom. From the moment coefficient data shown in Figure 10.3 it can be seen that the moment is nose down about this point, meaning that the actual centre of lift is further aft. This can also be deduced from the pressure plots shown at the end of Chapter 9, which show a rather uniform pressure throughout the hull. The precise location of the centre of lift is dependent on the running angle of the wing, but it has been found to be just forward of the central point for most cases. This means that if a vessel has its weight placed behind the central point, the aerodynamic force causes a nose up motion.

The centre of gravity is located seventeen metres from the transom, which is about a third of the length, this being the position found to be optimal in previous tests. The hydrodynamic centre tends to be similarly placed nearer the back of the hull

since the front is often lifted out of the water during cruise. This results in a balancing act where the aerodynamic force near the centre and the hydrodynamic force nearer the rear must balance the weight, which is usually between the two. The hydrodynamic centre moves rearwards as the speed increases which balances the increase in aerodynamic force, until the aerodynamic force becomes too large. At this point the aerodynamic force will lift the nose up, rotating the ship about the centre of gravity and causing a greater aerodynamic loading as a result of the increase in angle of attack. This effect can have a positive feed back and result in the ship flipping over, which is of course extremely undesirable! It is not however, necessarily an indication of poor design, since the ship currently has no control surfaces and therefore cannot reasonably be expected to remain stable through such a dramatic shift in loading; at least not without a considerable amount of careful design study. It is possible to solve the problem by changing the position of the centre of gravity, however this is likely to prove impractical. The simple solution would seem to be the addition of control surfaces, such as trim tabs and ailerons or a tail plane. The addition of a trim tab in particular would allow the centre of lift of the planing hull to move rearwards and increase in strength, which would help counter the aerodynamic forces. This however, may result in much higher levels of drag than aerodynamic control surfaces, which could equally be used to stabilise the craft.

The most disappointing result is the hydrodynamic drag and its effect on the lift-to-drag ratio and resistance-to-weight curve. Although both graphs show the benefit of aerodynamic alleviation, the actual values are quite low. The important point, is that the hydrodynamic drag is very large on both the hybrid vehicle and the planing hull, showing that it is the hydrodynamic design, and not the hybridisation, which has resulted in the below average results. The planing model is simplistic, but not inaccurate, meaning that the effect of aerodynamic alleviation such as a prediction of a forty four percent decrease in drag, should be fair. The

value of total drag in contrast is probably very high. This may be attributed to two main factors. The first is the simplistic prismatic hull design, which is a far cry from the current state of the art. The second is the choice of deadrise angle, which was found to be thirty one degrees. This was not a specific choice and arose as a result of the geometry produced for the aerodynamic testing. Although consideration was given to the hydrodynamic requirements, the main aim was to produce a model as a demonstration that such combined features could be achieved. In hind sight, a lower deadrise of around ten degrees would have been a better choice. Indeed most modern hulls have a highly variable deadrise, with a sharp bow flattening out to a stern with perhaps only a few degrees of deadrise. This would make the rear portion considerably more efficient than the constantly moderate deadrise angle used.

Allowing for the poor hydrodynamic drag experienced by both vessels, the hybrid vehicle shows considerably improved performance over an equivalent planing hull. The model used in the above tests was fifty metres long with a ship weight of three hundred tonnes and a possible cruise speed of eighty knots without the need for control surfaces. There is clearly a realistic potential for hybrid vehicles with suitably shaped aerodynamic hull forms to achieve efficient cruise with significant levels of aerodynamic support. This analysis has highlighted the important relationship between the percentage of aerodynamic loading and the total resistance. The next section is concerned with using this information in conjunction with existing vehicle data to assess the relative performance and most suitable configuration for the hybrid vehicle.

10.3 Parametric Analysis

The primary focus of the research thus far, has been to ascertain the degree of aerodynamic lift which can realistically be achieved for a ducted multihull. The data has shown that a considerable amount of lift can be generated whilst retaining enviable efficiencies for the most part. Since the aerodynamic drag is very small in comparison to the hydrodynamic drag, the efficiency of the aerodynamic lift is less critical than the magnitude of the aerodynamic lift, although the high efficiency is certainly a benefit. The question now becomes that of determining the potential of this form of aerodynamic alleviation with regards to current vehicle technologies.

Previous analysis has shown that the peak drag occurs at about fifty percent aerodynamic support, but that at this speed the vessel has around forty percent less drag than an equivalent planing hull. The problem is therefore to consider what combinations of weight, size and speed could prove realistic. As McKesson [11] points out, if an aerodynamically supported vessel has an equivalent foot print to an SES, for instance 150 m x 40 m, with a ship weight of 6000 tonnes, according to Doctors' model [55] a 100 m catamaran would need to travel at 116 knots to achieve 50% aerodynamic support. This is clearly an ambitious speed for such a catamaran. However, Doctors' model uses less effective aerodynamics that those presented here. Furthermore, 6000 tonnes is an extremely heavy vehicle, a lighter vehicle would achieve a 50% loading at a lower and perhaps more achievable speed. There is also the size to consider, in that a 150 x 40 m SES ship may compare more favourably to a 150 x 75 m hybrid vehicle.

Figure 10.11 shows the lift coefficient used by the hybrid stability model. The value remains above and around 1.3 for most of the speed range. At the peak it has a value of nearer 1.4. The maximum value of lift coefficient for the hybrid vehicle, shown in Figure 10.1, is 1.5, but a value of 1.4 can be achieved for a

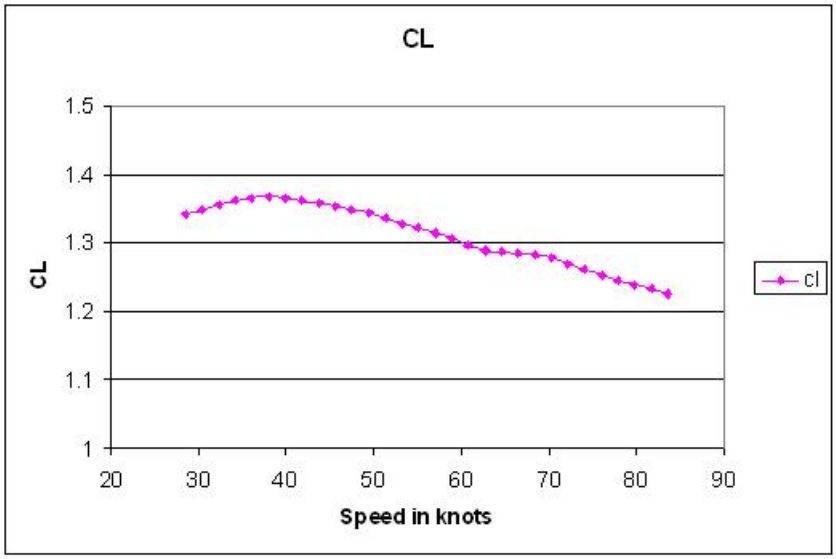

Figure 10.11: Calculated lift coefficient used by the hybrid stability model for the hybrid vehicle

range of heights if the angle of attack is carefully managed. In theory, with the use of trim tabs and a trailing edge flap, the wing could produce significantly higher values of C_L. Certainly the work of Trillo [75] and later Walker *et al* [56], suggests large gains from various trailing edge flaps or deflectors. For the present calculations a maximum C_L of 1.4 will be used since this seems well within reach for future designs.

Having established the lift coefficient and a maximum drag at 50% aerodynamic support, the relationship between ship speed, size and weight can be analysed via the standard aerodynamic equations. The ship speed required to provide a 50% aerodynamic support is calculated as follows.

Since the aerodynamic support must be half of the total support, F_{aero} must equal $F_W/2$, where F_W is the the ship weight converted to Newtons. Thus the ship speed

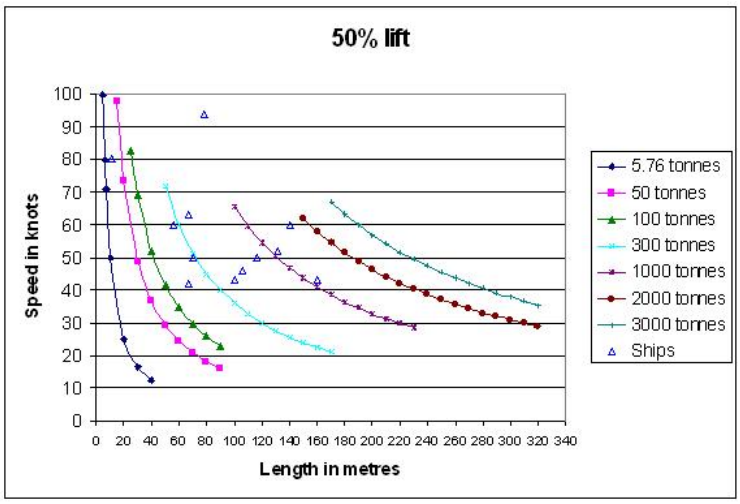

Figure 10.12: Comparison of the effect of size and speed on a hybrid vehicles of a chosen weight

is calculated as

$$U = \sqrt{\frac{F_W}{\rho_a C_L A}} \tag{10.1}$$

where A is the reference area and is taken as $L^2/2$ since $B = L/2$ for the present configurations.

Figure 10.12 shows the results for this equation plotted for a variety of ship weights. Also included in the figure are a selection of comparable craft, displayed as the hollow triangles and marked 'Ships' in the legend. Table 10.1 gives details of the vessels shown.

The results show the important relationship between the size, weight and speed of the craft. The figure represents a design space and allows us to consider the potential of various configurations. A comparison can be made between the hy-

Ship	Length in metres	Speed in knots	Ship weight in tonnes
KUDU II	11	80	5.76
Quad (56)	56	60	200
Destriero (full)	67	42	1100
Destriero (light)	67	63	550
Hisho	70	50	1500
SES 100b	78	94	93
Westpac express	100	43	2200
CIRR-105p	106	46	120
CIRR-120P	116	50	157
WESTAMARIN 4000	131	52	180
Quad (140)	140	60	3500
SES-200A	160	43	244
Savitsky	457	50	55000

Table 10.1: Details of ships shown in Figure 10.12

brid vehicles and the various craft presented. The KUDU for instance is 10.97 m long, weighs 5.76 tonnes and achieves 20% aerodynamic support at the top speed of 80 knots. A hybrid vehicle of the same weight and traveling at the same speed is calculated to achieve 50% aerodynamic support for a hull length of only 6.25 m. This makes it not only a reasonably realistic possibility, but a considerable improvement. Of course any such suggestion is purely speculative until it is actually demonstrated on open water. However, the lift coefficient for the hybrid vehicle is far higher than the KUDU, being around 1.4 as opposed to 0.84 and with far greater efficiency since the KUDU has an aerodynamic lift-to-drag ratio of only 3.2. Although this has been seen to be less critical during hydrodynamically dominated cruise, it will certainly become important once the aerodynamic forces are dominant. There is little reason to suspect that the hydrodynamic lifting surfaces used for the KUDU could not be married to the hybrid vehicle to produce a vehicle capable of the same very high speeds, but with perhaps greater load capacity, in this case presumably used for fuel in order to increased the range, since the vessel

would have little appeal for cargo transport. The largest unknown would then be the stability of the vehicle, particularly if it attempted to go beyond the 80 knot speed and 50% aerodynamic loading discussed here. This problem is beyond the scope of the current work, but has been studied by Collu [71] in conjunction with this research project and will be addressed further in future efforts.

Table 10.2 shows a comparison of some existing vehicle designs with a few hybrid vehicle configurations. The SES 200A was built as a demonstrator model and the Destriero, a planing monohull, holds the Blue Ribband award for crossing the Atlantic in record time without refueling. The chosen hybrid vehicle configurations show that comparable designs could be achieved. The HV 90 and 160 for instance, are both able to achieve similar load capacity to the SES 200A. The HV 90 achieves similar speeds for a shorter vessel; however, unlike the SES this would have to be done without the aid of lift fans at lower speeds. In comparison the HV 160 requires only 22 knots to achieve 50% aerodynamic loading for a similar size and weight. This should be quite attainable and offers the possibility of operating at higher speeds on almost full air support, but without the need for lift fans and with a much reduced air profile. In addition, the seals are not required to keep contact with the water and hence the friction drag should equally be reduced by the lack of front and rear skirts, as well as a reduced wetted lengths as the hulls tilt out of the water. The benefit in rough seas is hard to gauge; but the potential for drag reduction, given the much reduced frontal impact area, is substantial, and there is certainly a potential to sustain greater speeds in rougher seas.

The Destriero is labeled as light due to the report of its speed change over the crossing. It was stated that the vessel left with a weight of 1100 tonnes (full) and a speed of 42 knots. Upon completing much of the journey however, the speed began to increase. It was found that at the end the weight was 550 tonnes (light) and the speed was 63 knots. This vehicle has no aerodynamic alleviation,

Vehicle	SES 200A	HV 90	HV 160	Destriero (light)	HV 60
Length in metres	160	90	160	67	60
Speed in knots	43	40	22	63	60
Weight in tonnes	224	300	300	550	300

Table 10.2: Medium

but it demonstrates the real world advantages of weight reduction very clearly. Equally, if a 67 m planing hull weighing 550 tonnes can achieve 63 knots, it is perhaps reasonable to assume that the 60 m HV weighing only 300 tonnes could be made to achieve the same thing. Especially considering that it would by this stage already have 50% aerodynamic support, and of course the associated reduction in drag. This should allow for a vessel capable of continuing on to even greater speeds without excessive drag penalties. This is significant since 300 tonnes represents something of an upper limit for aircraft and hence anything below this value could not be considered high-payload. It is of course a difficult matter to accurately determine the feasibility of such a craft, let alone the payload. However, it is encouraging to see that similar sized vehicles have achieved these speeds with greater loads. Assuming that such a design is therefore achievable, a fair payload might be up to 40% of the ship weight (a discussion of ship size, weight and potential load fraction is given by Ritter *et al* in [76]) this gives a payload of 120 tonnes.

For a ship to be considered high-payload, it must go significantly beyond the capacity of aircraft. Table 10.3 shows a few vessels with weights of 1000 to 2000 tonnes, which equates to a payload of around 400 to 800 tonnes. This is enough to carry armoured vehicles or significant amounts of passengers and cargo. In the case of the Westpac express, a military catamaran currently in operation, the load is described as 970 troops with either 153 HMMWV's (High Mobility Multi-

purpose Wheeled Vehicles, quarter ton military jeeps also known as 'humvees') or 12 AAV's (Amphibious Assault Vehicles, about, 22 tonnes) and 20 LAV's (Light Armored Vehicles, around 10 tonnes). Since this speed is achieved without any aerodynamic alleviation, it should be possible to achieve a similar speed given the reduction in drag for an HV. The equivalent hybrid vehicle however, is just over twice the length. This is not necessarily a problem for the planing hulls, since they are lifted from the water at quite low speeds resulting in a water line length considerably shorter than the aerodynamic length. In terms of weight though, it could be more of an issue. If the vehicle must be twice the length and also considerably wider due to the lower length-to-beam ratio in comparison with conventional designs, and yet still retain the same overall weight, some compromise must be made. A decrease in payload is obviously highly undesirable, making a reduction in material weight the only option. Advances in material science and the fabrication techniques could well bring substantial reductions in weight over the years, however these will benefit all vehicles. The only reasonable hope is that the structure can be made in a more economical fashion. Since the vessel size is increased for aerodynamic loading purposes only, the increased size should largely be the result of 'wing' material, not the main body and hydrodynamic surfaces, which require far greater strengths. If large portions of the aerodynamic superstructure are built around purely structural needs, the weight could be much reduced compared to the load baring hydrodynamic surfaces and cargo area. It is difficult to speculate, but the weight issue may not be as serious as it would first appear when suggesting a vehicle of twice the length should retain a similar weight.

Consideration of ships beyond the 5000 tonne range becomes very difficult. Such ships are invariably displacement vessels which travel at very low speeds. Unless of course they are very long. Savitsky [12] discusses the design of a 457 m displacement monohull with a weight of 55,000 tonnes and a speed of 50 knots. This

Vehicle	Westpac	HV 210	Destriero (full)	Hisho	HV 150
Length in metres	100	210	67	70	150
Speed in knots	43	44	42	50	44
Weight in tonnes	2200	2000	1100	1500	1000

Table 10.3: Large

Vehicle	Savitsky	HV 460	HV 1k
Length in metres	457	460	1000
Speed in knots	50	45	49
Weight in tonnes	55,000	10,000	55,000

Table 10.4: Extra large

design has been discussed elsewhere, such as by [11], and is generally credited as both achievable and desirable. Figure 10.13 shows the Savitsky monohull added to the design space and Table 10.4 shows the vehicle comparisons.

The Savitsky monohull can achieve fifty knots with a length of 457 m and a weight of 55,000 tonnes. A similar sized hybrid vehicle however, can only achieve 50% air support at 45 knots if the total weight is 10,000 tonnes. if this can be achieved, with a reasonable payload fraction, the vehicle would certainly be high-payload. Such a vehicle could have tremendous advantages, with excellent sea keeping and extremely high speeds for such a large vessel. The difficulty is that such a large vehicle has to weigh so little that it is unlikely to be possible to create even with out the payload.

As a final experiment, a 55,000 tonne vessel with a cursing speed 49 knots, to match the Savitsky monohull design, was considered. The vessel required was found to be 1000 m long, which is perhaps beyond even the most optimistic of speculation.

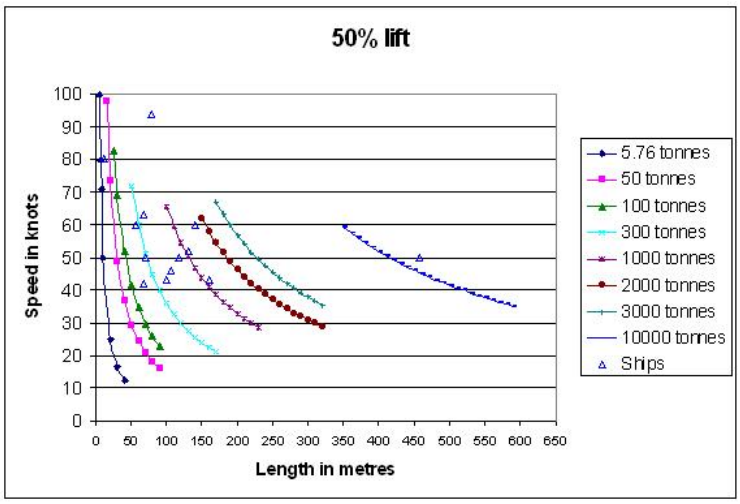

Figure 10.13: Effect of size and speed on hybrid vehicles, including very high payload ships

From the previous analysis it would appear that there is much potential for hybrid vehicles to achieve substantial aerodynamic support at comparable sizes to existing vehicles. Although the best capacity is found at the larger end of the spectrum, the designs are much harder to justify. At the opposite end, small ships seem very feasible and appear to be an improvement on similar designs which have been in operation for a few years. The most promising configuration is the medium to large sized craft, with weights well in excess of aircraft without departing substantially from the size and speed range of modern SES ships and catamarans. The vehicle chosen for study in this section is the 1200 tonne catamaran INCAT86 built by International Catamarans Pty Ltd and used for a comparative study by Lazauskas [5]. The ship is 76.41 m long and 26 m wide with a maximum draft of 3.5 m and has a maximum speed of around 40 knots. An estimated payload for ships of this size would be around 480 tonnes.

Lazauskas uses the INCAT86 catamaran hull for a comparative study of vehicle

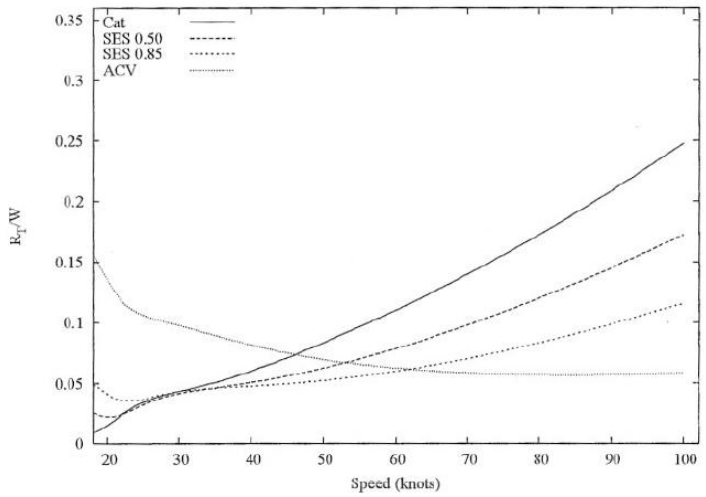

Figure 10.14: Resistance-to-weight ratio for optimised vessels as a function of speed, reproduced from [5]

performance. Versions of the INCAT are in operation around the globe as ferries and have achieved speeds of around thirty to forty knots at sizes of thirty to one hundred metres. Lazauskas applies a theoretical SES cushion to the hull with various pressures to simulate the effect of air cushioning up to 100% at which point the hulls leave the water and the vehicle becomes a pure ACV.

The investigation aims to provide a 1200 tonne vessel capable of 75 knots, the results for resistance-to-weight ratio as a function of speed are reproduced in Figure 10.14, taken from [5]. The graph shows the catamaran, the catamaran as an SES with 50% air cushion support, 85% air cushion support and as an ACV with 100% air cushion support.

It can be seen from the graph that the optimum vessel configuration is very much dependent on the speed of operation. Clearly, below forty knots the optimum

vessel is a catamaran and this is reflected in the number of catamarans in service around the world whose maximum speed is seldom in excess of 40 knots. Above 40 knots the SES ships become the most favourable, with speeds up to about 65 knots. Again this can be seen from observations of current naval designs, where most ships over 40 knots are SES; but few reach speeds of 60 knots. The surprise might seem to be that there are not more ACVs making use of the very low resistance achievable at speeds over 70 knots. However, as discussed earlier, hovercraft are extremely difficult to maneuver at such speeds, and more importantly, rarely get the chance to reach such speeds at all. In reality the sea surface is often too rough to allow hovercraft to operate at all, let alone at 70 knots or over, resulting in inefficient and often uncomfortable cruise at much lower speeds.

The great aim is to achieve a vehicle with the characteristics of a catamaran at low speeds, an SES at high speeds and an ACV at extreme speeds, and this should ideally be achieved without the associated problems of operating ACVs in rough seas. The hybrid vehicle concept certainly appears to offer such a possibility. At low speeds it can be thought of as a standard catamaran, whilst with increasing speed it becomes more akin to the SES and eventually the ACV; allowing for the issue of stability of course. It may also have some other advantages, as discussed before, in that it has no skirt to cause additional drag, particularly in rough seas; the hull wetted length is reduced as the speed increases, unlike SES which must retain cushion pressure, thus keeping the complete hull line submerged; and there is no need for a lift fan to maintain cushion pressure. It is also worth mentioning that there should be no cushion momentum drag and that the aerodynamic profile should be much improved.

The hybrid vehicle evidently embodies a very promising concept, but can it provide the required characteristics? Figure 10.15 shows the ideal percentage of aerodynamic support at a given speed, for a hybrid vehicle, as estimated from

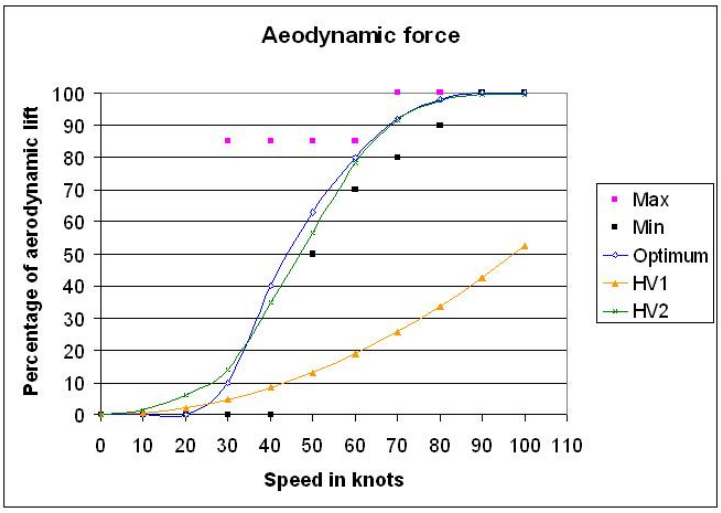

Figure 10.15: Optimum aerodynamic loading with speed

Figure 2.8. The 'max' markers show the maximum level of air cushion support which closely follow the optimum resistance line. The 'min' markers show the minimum estimated air cushion support to follow the optimum resistance line. The optimum line is thus an estimate of the optimum air cushion support for a hybrid vehicle of this type.

The line for HV1 represents the results for the hybrid vehicle of length 76.41 m and weight 1200 tonnes. It is evident that this vehicle falls short of the required aerodynamic load. It may well be an improvement on the catamaran, but with only around 10% cushion support at 40 knots, the improvement is likely to be small.

HV2 shows the results for an altered hybrid vehicle, having the same weight but with a length of 150 m and a variable coefficient of lift. The results closely match the optimum curve, with the cushion pressure at less than 20% at 30 knots, 50% at 47 knots and 85% at around 63 knots. This should follow the optimum curve and in theory keep the resistance low enough to allow the high speeds to be gained.

Speed in knots	CL	cushion pressure %
0	1	0
10	1	1.6
20	1	6.2
30	1	13.9
40	1.4	34.8
50	1.45	56.4
60	1.4	78.4
70	1.2	91.5
80	0.98	97.6
90	0.79	99.5
100	0.64	99.6

Table 10.5: Variable lift coefficient for optimised hybrid vehicle HV2

47 knots is not an excessive speed to have to reach to achieve the 50% cushion pressure, which is the peak drag for the hybrid vehicle, whilst still being very close to the optimum drag value for any of the vehicles. The difficulties are that the vehicle has a variable lift coefficient and must be 150 m long.

As discussed earlier, a variable lift coefficient could be achieved through the use of control surfaces. The range of C_L values used for the HV2 data is provided in table 10.5. The maximum lift coefficient of 1.45 is within the reach of the data obtained for the hybrid vehicle, but would require careful control of the running attitude. Some improvements to the overall aerodynamics in successive design iterations are to be expected and this should make such a value easier to obtain. It is noted that a lower value of $C_L = 1.4$ does not place the curve outside of the minimum value of lift, but does result in a poorer and less continues curve.

The reduced C_L values at the lower speeds could be harder to reach since the lower speeds result in lower running heights and this increases the lift coefficient. A trailing edge flap may well help to solve this problem, however, even the more likely values of 1.3 only cause a cushion pressure of around 20% at thirty knots.

The reduction in the final values are necessary to avoid total 'take-off'. The model

proved unstable for such high cushion pressure ratios and no values were obtained for C_L once the whole vehicle has left the water. It may be that at such a time the C_L drops naturally as the end vortices are allowed to form, although it is not possible to tell without further testing.

During this period of cruise the aerodynamic stability will be crucial and control surfaces will be essential. If stable flight can be achieved however, the vehicle should be able to operate almost entirely on dynamic air cushion support.

The change in vehicle length was by far the most critical departure from Lazauskas's design criteria. Without increasing the length (or fabricating considerably higher values of C_L) the trend line cannot be made to match the optimum. This brings back the old problem of achieving comparable weight for a vehicle of nearly twice the length. Again we can consider that if the vehicles are the same weight, they could have the same hydrodynamic surfaces. This however, would require the aerodynamic surfaces to protrude forward by nearly half the ships length. Interestingly, the hybrid stability model shows that the length of the hydrodynamic surfaces reduces rapidly with forward speed, and that much of the forward part of the hull is only in the water at such speeds where the boat is not yet planing. As with the Savitsky hulls, this has a lot to do with the considerably low speed-to-length ratio during the early stages of take-off. It may therefore be possibly to have much of the forward part of the hull shaped almost entirely for aerodynamic purposes, since the sharp angles required for planing would only be needed on the rear portion. The front and middle sections would then be analogous a displacement and semi-displacement hull shape respectively, and would be tailored toward the lighter weight and aerodynamic construction.

The fact remains that without detailed design weights it is impossible to determine the probability of such a design working. It is possible to conclude that the aerodynamics can be made to produce the desired lift fractions for 150 m 1200

tonne vehicle traveling at up to 100 knots, However, it may not be possible to construct such a ship with reasonable payload capacity within the design weight.

Chapter 11

CONTINUATION OF WORK

11.1 Introduction

The ultimate aim of this research is the production of a hybrid vehicle capable of carrying greater loads than an aircraft at greater speeds than a conventional ship. As such it was always beyond the scope of this thesis to provide a complete design and the aim has been to make progress toward a suitable configuration. This chapter outlines some suggestions for future research, and some progress already made in that direction.

11.2 Direction of Future Research

This research has shown that a great deal of benefit can be derived from the aerodynamics of multihulls. Not just from the possibility of utilising wing-in-ground effect, but from the ducted effect of the complete hullform. In terms of the potential this provides to sea-lift vessels, the hybrid stability model has suggested gains of nearly fifty percent, however, there are some significant unknowns. Perhaps the most important is the stability of the craft during aerodynamically

dominated cruise. Previous models have not been able to provide stable results for the vehicle during this stage of cruise, and it is thought that this is due to the vessel being inherently unstable during the aerodynamically dominated phase. The modeling of control surfaces would be an important step in determining the feasibility of cruise in the highest speed ranges.

The next major unknown is the effect of free surface deformation. Although it has been considered that the free surface deformation will be quite small at low speeds due to the lack of cushion pressure, and quite small at high speeds due to the high Froude number, it is important to check what effect it will have. The deformation will have some associated drag, however, it may also provide increased aerodynamic performance as the water surface is forced into a concave, creating a further diffuser-like surface. Accurate predictions of the free surface deformation from both the air cushion and hull wash, as well as the associated drag, would help to give a clearer picture of the performance of the vessel.

Finally, the hydrodynamic design of the hull is evidently in need of some improvement, and as such, an optimisation of the hydrodynamic surfaces could lead to a significant improvement in performance. It should be remembered that the final model presented here was a proof of concept, and much can still be done to improve the lift and drag of the aero/hydrodynamic interface.

11.3 Scale Model Testing

Much improvement can be made through continued study of the model via CFD and an improved stability model. However, the free surface deformation is very difficult to simulate and a reduced scale model would therefore be desirable to validate the results.

A scale model would provide a great deal of useful information about the design and would certainly help to prove the concept. There are however, many difficulties to overcome when modeling a combined air and water flow. This is due to the need to match both the Reynolds and Froude numbers for the reduced scale tests. It is likely that this will prove impractical and some compromise will have to be made. Data obtained separately for the air and water components would still provide a great deal of useful information, which in turn, could help produce a larger open water model.

Provided the previous tests have produced suitably encouraging results, an open water test would be the next stage of testing. An open water trial should provide enough data to prove the concept and determine its market potential.

Chapter 12

CONCLUSIONS

12.1 Hypothetical Vehicle Configurations

Extensive research of hybrid vehicle designs has led to the concept of the aerodynamically alleviated catamaran, which shows much promise for future transport requirements. Suggestions have been made for optimising the hull shape and one possible configuration has been tested. The results from this test are discussed in Chapter 10 and the potential of such a vehicle is contemplated across a range of vehicle sizes. The following descriptions are intended to outline what is considered to be the most feasible configurations for the hybrid vehicle concept.

12.1.1 Small Scale

Any small scale vehicle, being of only a few metres of length, will naturally lack cargo capacity, and the hybrid vehicle would be no exception. However, as the tunnel hull racing boats have proven, it is possible to achieve extremely high speeds through aerodynamic alleviation of small craft. Since the aerodynamics of this vehicle have proven to be extremely efficient, with lift-to-drag ratios of nearly 50 achieved, it is quite feasible that the ducted hull geometry developed for the

hybrid vehicle could be used for small scale racing craft. The design suggested follows the optimum aerodynamic loading outlined by Lazauskas [5] and discussed in Chapter 10, and would be of comparable size to the KUDU, having a length of 11 m, but with a total vehicle weight of 7 tonnes and a potential speed of perhaps 100 knots. The KUDU has a length of 10.97 m, a weight of 5.76 tonnes and a top speed of 80 knots. Such craft would be useful as military or civilian personnel transport, as well as racing and pleasure craft.

12.1.2 Medium Scale

The medium scale vehicle is supposed to equate to the maximum aircraft size. A large aircraft, such as a Boeing 747, usually weighs about 150 tonnes, but they can have take-off weights of up to four hundred tonnes. A weight of 300 tonnes was chosen to compete with the largest aircraft.

The vehicle proposed would be 70 metres long with a weight of 300 tonnes and is again designed to follow the optimum aerodynamic lift fraction discussed earlier. This vehicle would achieve 50% aerodynamic loading at 50 knots, a speed which according to similar sized craft, such as the Destriero, can be achieved even without aerodynamic alleviation. 300 tonnes is not an unreasonable weight for a 70 m vessel and compares favourably to current designs. If the stability and lift fraction can be controled at speeds above the 50% aerodynamic load range, the top speed could once again reach as high as 100 knots. The estimated payload might be between 100 and 150 tonnes. This vehicle configuration would be extremely useful as a small ferry, carrying medium density loads, such as people and cars, rapidly across stretches of open water. This should appeal to both military and civilian transport markets.

12.1.3 Large Scale

The large scale configuration is both the most exciting and difficult to justify. Potentially, a large hybrid vehicle design could achieve significant high-speed, high-payload transport with considerable efficiency. However, the design suggested is a major departure from conventional design and is therfore not easily comparable to existing ships. This makes it difficult to back up the theoretical configuration suggested without further research. As such, the design proposed is given tentatively, although optimistically, and should be considered a point at which such research is to be aimed.

The large scale vehicle suggested has a weight of 2200 tonnes and a length of 200 m. This is to be compared with the Westpac express, which has a weight of 2200 tonnes, but a length of only 100 m. The Westpac represents a high-payload vehicle and carries a significant cargo of military vehicles and personnel, as discussed in Chapter 10. With a top speed of 43 knots, it represents a state of the art vehicle for its size. The hybrid vehicle would need to achieve 50 knots to achieve 50% aerodynamic loading, which may be possible given that the Westpac achieved 43 knots without the 40% drag reduction which the hybrid vehicle would have. As such, it may be possible for the hybrid vehicle to achieve the much greater speeds predicted by following the optimum drag line for aerodynamic loading discussed earlier. In which case, the vehicle would be a 100 knot, 2200 tonne vehicle, which is certainly high-speed, high-payload. Unfortunately, this must be achieved for a vehicle of the same weight, but twice the length. Is such a ship feasible? Possibly, but it is not possible to determine the likelihood of such as design at the present time.

Designs of greater load capacity were considered in Chapter 10, but were found to require unrealistic size to weight ratios and are thus, not considered a likely area

for the future development of this project.

12.2 Market potential

In all of the above cases it is clear that the vehicle is suited mainly to operation at higher speeds, rather than payloads, when compared to other marine transport. However, with the potential advantages of operating at comparable speeds and efficiencies to an SES, whilst maintaining the sea keeping attributes of a catamaran, there is a clear market potential for a vehicle which can achieve the performance suggested by the hybrid vehicle.

Operation at high speeds in rough seas would be a major advantage to ferry operators and military transport and the hybrid vehicle has the potential to perform this function extremely well. The lack of skirting at the bow and stern should greatly improve the ride through waves, as should the higher ride height achieved by the aerodynamic lift. The size of vehicle will obviously determine the size of waves it can withstand and from this point of view it is a pity that the larger vehicles, which would be less effected by waves, are harder to justify. The sea keeping of the vehicle must be studied in future research.

It is unlikely that the hybrid vehicle can compete with the higher payload displacement ships, due to the shear size of duct area required in order to aerodynamically support a significant fraction of the load at reasonable speeds. In essence, the aerodynamic force is proportional to the area whilst the weight is proportional to the volume. This means that as the vehicle becomes larger it will gain less aerodynamic lift as a fraction of its weight compared to a smaller vehicle at a similar size. Equally, as the ship size is increased, so the structure becomes heavier and a greater amount of the ship's weight must go towards strength rather than payload.

A structural analysis of the ship will therefore be critical in determining the maximum feasible size and payload which can be achieved. However, ship weights of up to 2000 tonnes currently appear plausible, which represents payloads of up to 1000 tonnes. This is considerably beyond the maximum payload of any airplane and with potential speeds well beyond current high-speed ferry designs.

The technology discussed here is far from mature, however, successful implementation of the vehicles discussed would provide a significant advantage in the area of high-speed marine transport, and would therefore, represent an area of considerable interest for future investment.

12.3 Conclusion

Aerodynamic design of multihulled hybrid vehicles has been shown to have a significant effect on their performance. Furthermore, the assumption that hull shape will have little effect on a wing other than that of end plates, and that conventional two dimensional theory for wings in ground effect can be used to analyse ducted hull designs has been shown to be inaccurate. Specifically the side hull design has been shown to have a dramatic effect on the lift coefficient of the complete hull.

Complete aerodynamic shaping of the duct has been shown to increase the efficiency of low aspect ratio wings in ground-effect. The divergent/convergent shaped duct, constructed from highly cambered wing profiles, was found to have the best aerodynamic performance and achieved lift-to-drag ratios of nearly 50 in some cases; a value comparable, and often in excess of, the best high aspect ratio wings.

The effect of incorporating hydrodynamic surfaces into the aerodynamic design

was found to have little detrimental effect on the lift produced. The drag was affected to a greater extent at larger angles of attack; but the overall performance of the craft was not greatly effected. Furthermore, it was considered that a more careful design of the hydrodynamic surfaces could reduce the drag by a significant amount.

Performance analysis undertaken by the hybrid stability model showed a considerable benefit for a planing hull when equipped with aerodynamic alleviation. Specifically, a 40 to 50% reduction in drag was observed for the hybrid vehicle with 50% aerodynamic alleviation. However, the poor hydrodynamic design reduced the overall performance of both the planing hull and hybrid vehicle to unacceptable levels. It is evident that much improvement needs to be made in this area through a better understanding of conventional planing hull design.

A further issue was highlighted at aerodynamic loadings of over 50% where the hybrid vehicle appeared to become unstable. It is assumed that this may be rectified through the use of control surfaces, however, further study is required.

The size of the vehicle was found to be of importance to the fraction of weight which can be aerodynamically alleviated at a given speed. It was found that the lift is proportional to the reference area, whilst the weight is proportional to the volume. As a result the larger vehicles cannot sustain as much weight. This is compounded by the slower speed of very larger marine vehicles which further reduces the aerodynamic loading achievable.

Aerodynamic alleviation has been shown to improve the performance of a catamaran type planing vessel. In some cases the efficiency has been improved by over 50%. The effect of aerodynamic shaping of a catamaran hull structure appears to be beneficial to the performance at all speeds and sizes, and the eventual construction of a craft of greater load capacity than an aircraft with higher speed

than a standard sea-lift vessel appears attainable. In order to realize extremely heavy loads however, a hybrid vehicle may require unrealistic speeds, or design weights which are quite optimistic even for a state of the art vessel.

References

[1] Clark. D, Ellsworth. W, and Meyer. J. Quest for speed at sea. *Technical Digest*, 2004.

[2] Anderson. J. *Fundamentals of Aerodynamics.* Mc Graw Hill, ISBN 0-07-237335-0, 2001.

[3] http://www.se technology.com/wig/index.php, 2007.

[4] Hockberger. W. The quadrimaran. In *High speed high performance ships and craft symposium, American Society of Naval Engineers*, 2005.

[5] Lazauskas. L. Hydrodynamics of advanced high-speed sealift vessels. Master's thesis, University of Adelaide, 2005.

[6] Katz. J and Plotkin. A. *Low speed aerodynamics.* Cambridge aerospace series, 2001. ISBN 0 521 66219 2.

[7] Tani. I, Kogakusi, Taima. M, and Simidu. S. The effect of ground on the aerodynamic characteristics of a monoplane wing. Technical report, Tokyo Imperial University, 1937.

[8] Ward. T, Gooelzer. H, and Cook. P. Design and performance of the ram wing planing craft - kudu ii. Technical report, American Institute of Aeronautics and Astronautics, 1974.

[9] Savitsky. D. Hydrodynamic design of planing hulls. *Marine Technology*, 1(1):71–96, 1964.

[10] Fluent Europe Ltd-Sheffield business park-Europa link Sheffield-S9 1XU. Fluent 6.2 user's guide, 2008. Accessed through Cranfield University website.

[11] McKesson. C. Hull form and propulsor technology for high speed sealift. Technical report, Bremerton WA, February 1998. Conference workshop bringing together 200 people considered experts in their fields.

[12] Savitsky. D. On the subject of high-speed monohulls. In *Society of Naval Architects and Marine Engineers*, 2003.

[13] Savitsky. D and Brown. P. Procedures for hydrodynamic evaluation of planing hulls in smooth and rough water. *Marine technology*, 13(4):381–400, Oct 1976.

[14] Von Karman. T. The impact on seaplane floats during landing. Technical Report 321, NACA, October 1929.

[15] Wagner. H. Planing of watercraft (translation from work of 1933). Technical memorandum 1139, NACA, 1948.

[16] Payne. P. Recent developments in added-mass planing theory. In *Ocean Engineering*, volume 1, pages 257–309, 1994.

[17] Green. A. Note of sliding of a plate on the surface of a stream. In *Proceedings of the Cambridge Philosophical Society*, volume 1, pages 248–252, 1936.

[18] Pemberton. R, Turnock. S, Wright. A, and Blake. J. A comparison of computational methods for planing craft hydrodynamics. In *2nd international conference on high performance marine vehicles*, 2001.

[19] http://en.Wikipedia.org/wiki/catamaran, 2007.

[20] Doctors. L. On the great trimaran-catamaran debate. In *Proceedings of the fifth international conference on fast sea transportation, FAST*, 1999.

[21] Tuck. E and Lazauskas. L. Unconstrained ships of minimum total drag. In *www.cyberiad.net/hull.htm*. University of Adelaide, 1996.

[22] Tuck. E and Lazauskas. L. Optimum hull spacing of a family of multihulls. In *www.cyberiad.net/hull.htm*. University of Adelaide, 1998.

[23] Molland. A, Wilson. P, Turnock. S, Taunton. D, and Chandraprabha. S. The prediction of the characteristics of ship generated near-field wash waves. In *Proceedings of the Fast Sea Transport international conference FAST*, Southampton, September 2001. RINA.

[24] Gourlay. T, Duffy. J, and Forbes. A. The bore produced between the hulls of a high-speed catamaran in shallow water. *International Journal of Maritime Engineering*, 147(A3), 2005.

[25] http://www.marinetalk.com/articles-marine-companies/art/five-hulls-make-ships-faster-64639t.html, March 2006.

[26] http://www.swath.com/index.html, December 2007.

[27] Faltinsen. O. *Hydrodynamics of high-speed marine vehicles*. Cambridge university press, 2005.

[28] Piperni. P. A complete linearized theory for the design of two dimensional hydrofiols near a free surface. Technical report, University of Toronto, institute for aerospace studies, 1987.

[29] Lia. C and Troesch. A. A vortex lattice method for high-speed planing. *International journal for numerical methods in fluids*, 22:495–513, 1996.

[30] Barratt. M. The wave resistance of a hovercraft. *Journal of fluid mechanics*, 22:39–47, 1964.

[31] Doctors. L. The resistance components of a surface-effect ship. In *26th symposium on naval hydrodynamics*, 2006.

[32] Lavis. D and Spaulding. K. Surface effect ship (ses) developments worldwide. In *SNAME*. ASNE, 1991.

[33] Clements. R, Lewthwaite. J, Ivanov. P, Wilson. P, and Molland. A. The potential for the use of a novel craft, pacscat (partial air cushion supported catamaran), in inland european waterways. In *Proceedings of the Fast Sea Transport international conference FAST*, St. Petersburg, Russia, June 2005. RINA.

[34] Balow. F, Guglielmo. J, and Sivier. K. Design and evaluation of a midsize wing in ground effect transport. Technical report, AIAA, 1993.

[35] Carter. W. Effects of ground proximity on the aerodynamic characteristics of aspect ratio 1 airfoils with and without end plates. Technical report, NASA, 1961.

[36] Fink. M and Lastinger. J. Aerodynamic characteristics of low aspect ratio wings in close proximity to the ground. Technical report, NASA, 1961.

[37] Nangia. R. Aerodynamic and hydrodynamic aspects of high-speed water surface craft. In *Aeronautical journal*, pages 241–268, 1987.

[38] Kim. I, Elghobashi. S, and Sirignano. W. Three-dimensional flow over two spheres placed side by side. *Fluid Mechanics*, pages 465–488, 1993.

[39] Moore. N, Wilson. P, and Peters. A. An investigation into wing in ground effect airfoil geometry. *RTO SCI Symposium on "Challenges in Dynamics,*

Systems Identification, Control and Handling Qualities for Land, Air, Sea and Space Vehicles", (RTO-MP-095), 2002. Berlin, Germany.

[40] Raymond. A. Ground influence on aerofoils. Technical Report 67, NACA, Massachusetts Institute of Technology, December 1921.

[41] Hayashi. M and Endo. E. Measurement of flow fields around an aerofoil section with separation. *Transactions of the Japanese Society of Aerospace Sciences*, 21(52):69–75, 1978.

[42] Paulson. J and Kjelgaard. S. An experimental and theoretical investigation of thick wings at various sweep angles in and out of ground effect. Technical Report 2068, NASA, 1982.

[43] Zerihan. J and Zhang. X. A single element wing in ground effect; comparisons of experiments and computations. Technical report, 39th AIAA Aerospace Sciences Meeting and Exhibit, Reno, NV, January 2001.

[44] Chun. H and Chang. R. Turbulence flow simulation for wings in ground effect with two ground conditions: Fixed and moving ground. *International Journal of Maritime Engineering*, 145(A3):1–18, 2003.

[45] Ahmed. M, Takasaki. T, and Kohama. Y. Experiments on the aerodynamics of a cambered airfoil in ground effect. Technical report, 44th AIAA Aerospace Sciences Meeting and Exhibit, Reno, NV, January 2006.

[46] Tuck. E. A simple one-dimensional theory for air-supported vehicles over water. *Journal of ship research*, 28(4):290–292, 1984.

[47] Grundy. I. Airfoils moving in air close to a dynamic water surface. *Australian mathematical society*, B 27:327–345, 1986.

[48] Barber. T. A study of water surface deformation due to tip vortices of a wing-in-ground effect. *Journal of Ship Research*, 52(2):182–186, June 2007.

[49] Krause. F, Gallington. R, Rousseau. D, and Kidwell. G. The current level of power-augmented-ram wing technology. Technical report, AIAA, 1978.

[50] de Wolf. W. Aerodynamic investigation on a wing in ground effct. Technical report, Nationaal Lucht- en Ruimtevaartlaboratorium, 2002.

[51] Van Beek. C, Oskam. B, and Fantacci. G. Progress report on aerodynamic analysis of a surface piercing hydrofoil controlled wing in ground effct seabus configuration. Technical report, Nationaal Lucht- en Ruimtevaartlaboratorium, 1998.

[52] Allenstrom. B, Liljenberg. H, and Tudem. U. An airlifted catamaran - hydrodynamical aspects. *Royal Institution of Naval Architects*, 2001.

[53] Privalov. E and Kirillovikh. V. Transport amphibious platforms: a new type of high-speed craft. In *Workshop proceedings of Ekranoplams and very fast craft*, volume 1, pages 121–133. Institute of Marine Engineers, Sydney, 1996.

[54] Liang. Y, Cheng-Jie. Wu, and You-Nong. Xie. Investigation on aero-hydrodynamic characteristics of dynamic air cushion wing in ground effect craft (dacwig). In *HPMV china*, pages 53–61, 2001.

[55] Doctors. L. Analysis of the efficiency of an ekranocat: A very-high-speed catamaran with aerodynamic alleviation. *Royal Institution of Naval Architects*, 1997.

[56] Walker. G, Fougner. A, Younger. S, and Roberts. T. Aerodynamics of high speed multihull craft. In *Fourth international conference on FAST*, volume 1, pages 133–138, 1997.

[57] Matveev. K and Dubrovsky. V. Aerodynamic characteristics of a hybrid trimaran model. *Ocean Engineering*, 34(3-4):616–620, March 2007.

[58] Reif. T. A wind tunnel study of the aerodynamics of a tunnel boat hull with consideration of ground effect. In *High-speed surface craft*, pages 29–33, 1985.

[59] Michell. J. The wave resistance of a ship. *Philosophical magazine*, 1898.

[60] Thompson. N and Engineering sciences data unit. Performance in incompressible flow of plane walled diffusers with single-plane expansion 74015. In *ESDU*. 1974.

[61] Tuck. E and Lazauskas. L. Free-surface pressure distributions with minimum wave resistance. In *www.cyberiad.net/hull.htm*. University of Adelaide, 2001.

[62] Hess. J and Smith. A. Calculation of potential flow about arbitrary bodies. *Progress in aeronautical sciences*, 8, 1966.

[63] Newton. I. *Philosophiae Naturalis Principia Mathematica*. 1687.

[64] Kellog. O. *Foundations of potential theory*. The Murray printing company, 1929.

[65] Cosner. R. The importance of uncertainty estimation in computational fluid dynamics. *41st AIAA Aerospace Sciences Meeting and Exhibit*, 2003. The Boeing Company, St. Louise, MO.

[66] Drikakis. D and Geurts. B. *Turbulent Flow Computation*. Kluwer Academic Publishers, 2002.

[67] Spalart. P and Allmaras. S. A one-equation turbulence model for aerodynamic flows. Technical Report AIAA-92-0439, American Institute of Aeronautics and Astronautics, 1992.

[68] Launder. B and Spalding. D. Lectures in mathematical models of turbulence. *Academic Press, London*, 1972.

[69] Launder. B and Spalding. D. The numerical computation of turbulent flows. *Computer Methods in Applied Mechanics and Engineering*, 1974.

[70] Blevins. R. *Flow-Induced Vibration*. Krieger Publishing company, Malabar, Florida, 2001.

[71] Collu. M, Patel. M, and Trarieux. F. A mathematical model to analyze the static stability of hybrid (aero-hydrodynamically supported) vehicles. In *8th symposium on high speed marine vehicles*, 2008.

[72] Ikeda. Y, Yokomizo. K, Hamasaki. J, and Umeda. N. Simulation of running attitude and resistance of a high-speed craft using a database of hydrodynamic forces obtained by fully captive model experiments. In *FAST'93*, pages 583–594, 1993.

[73] Hoerner. S. *Fluid-dynamic drag: practical information on aerodynamic drag and hydrodynamic resistance*. John Wiley and Sons Inc, 1965.

[74] Mosaad. M, Gaafary. M, and Amin. I. Energy saving and dynamic stability of planing hull due to hydrodynamic control of trim angles. In *Maritime transportation and exploration of ocean and coastal resources*, pages 229–242, 2005.

[75] Trillo. R. High speed over water, ideas from the past, present and future. In *First international conference on FAST*, pages 17–34, 1991.

[76] Ritter. O and Templeman. M. High-speed sealift technology. Technical report, Naval Surface Warfare Centre, 1998.

Appendix A

Vector Diagrams

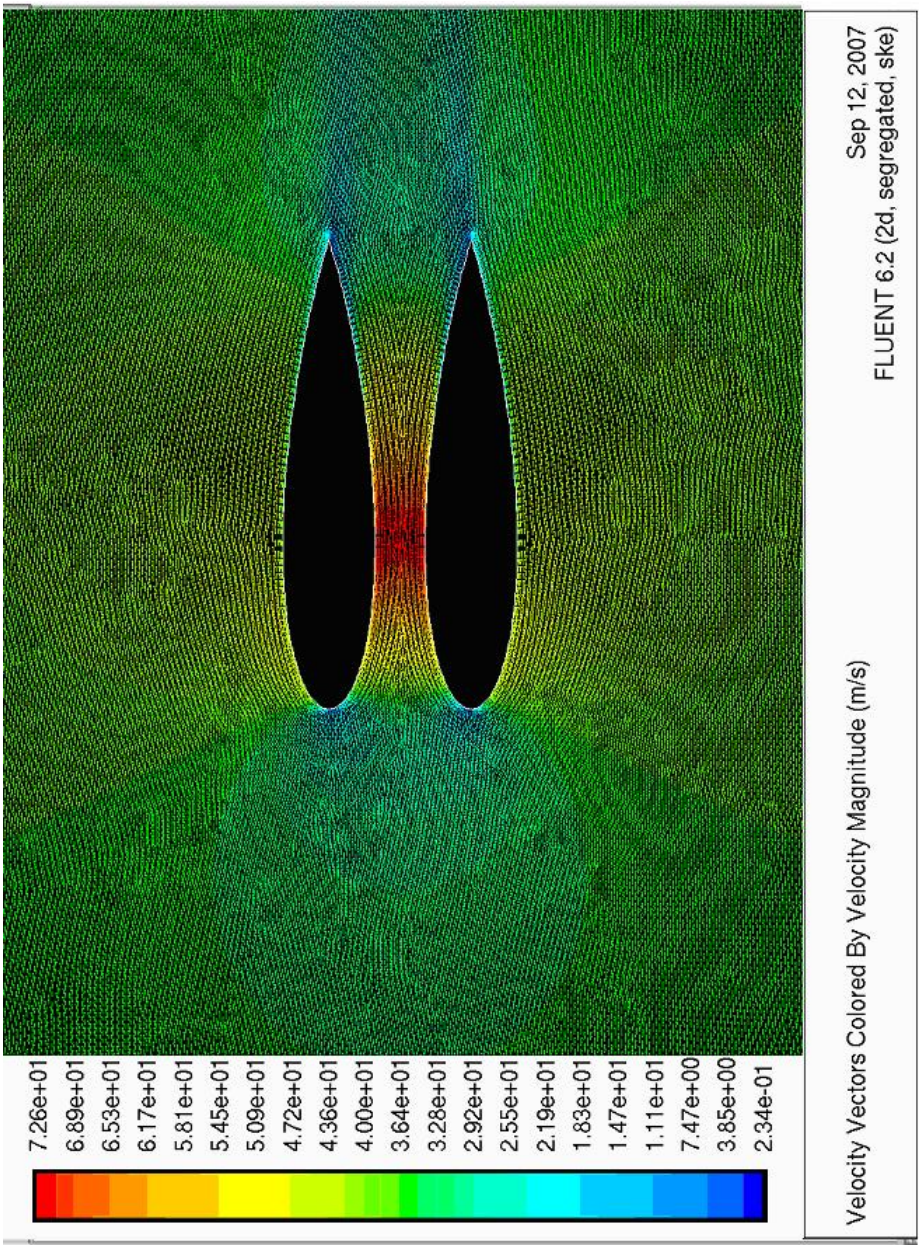

Figure A.1: Velocity vectors for the Hull shape at $B = 15$

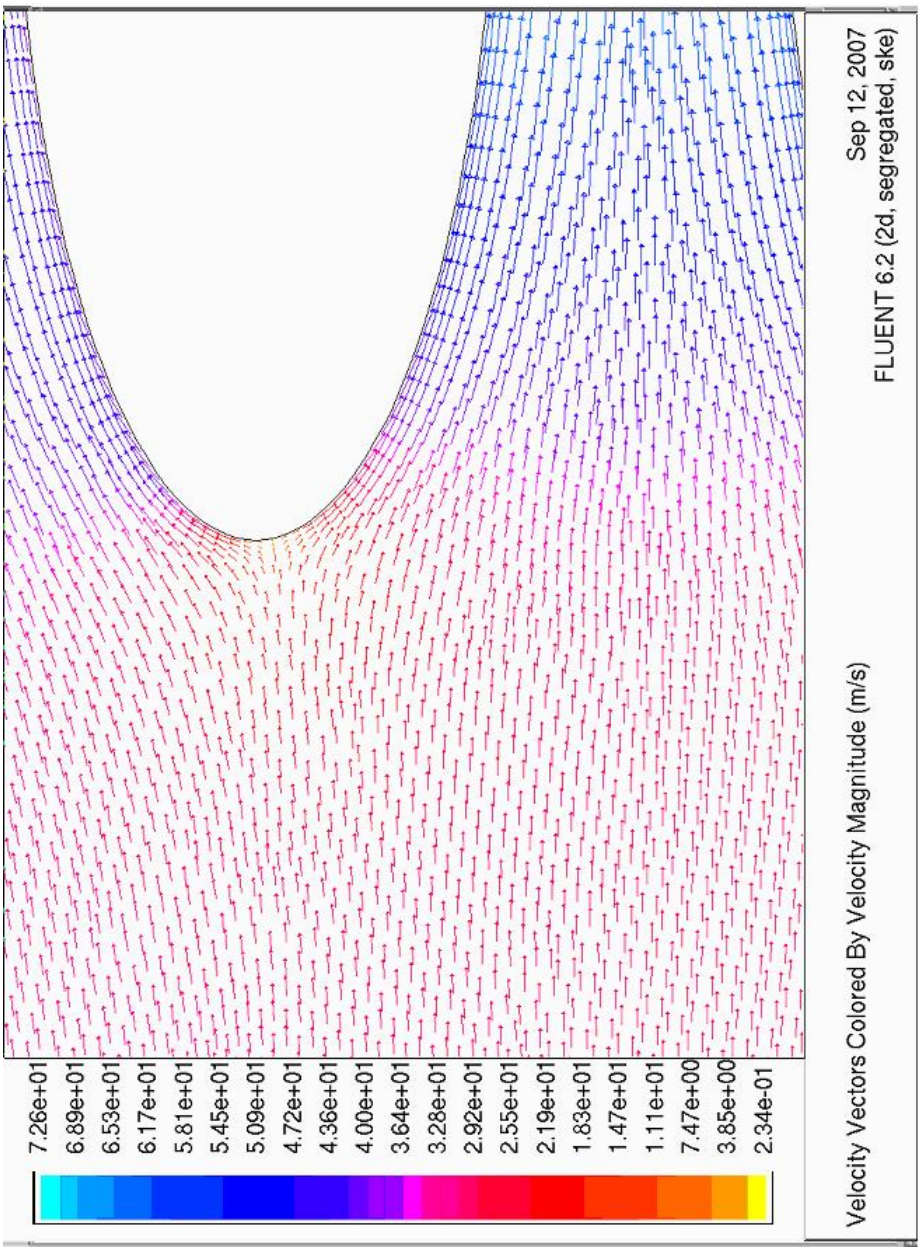

Figure A.2: Velocity vectors for the Hull shape at $B = 15$

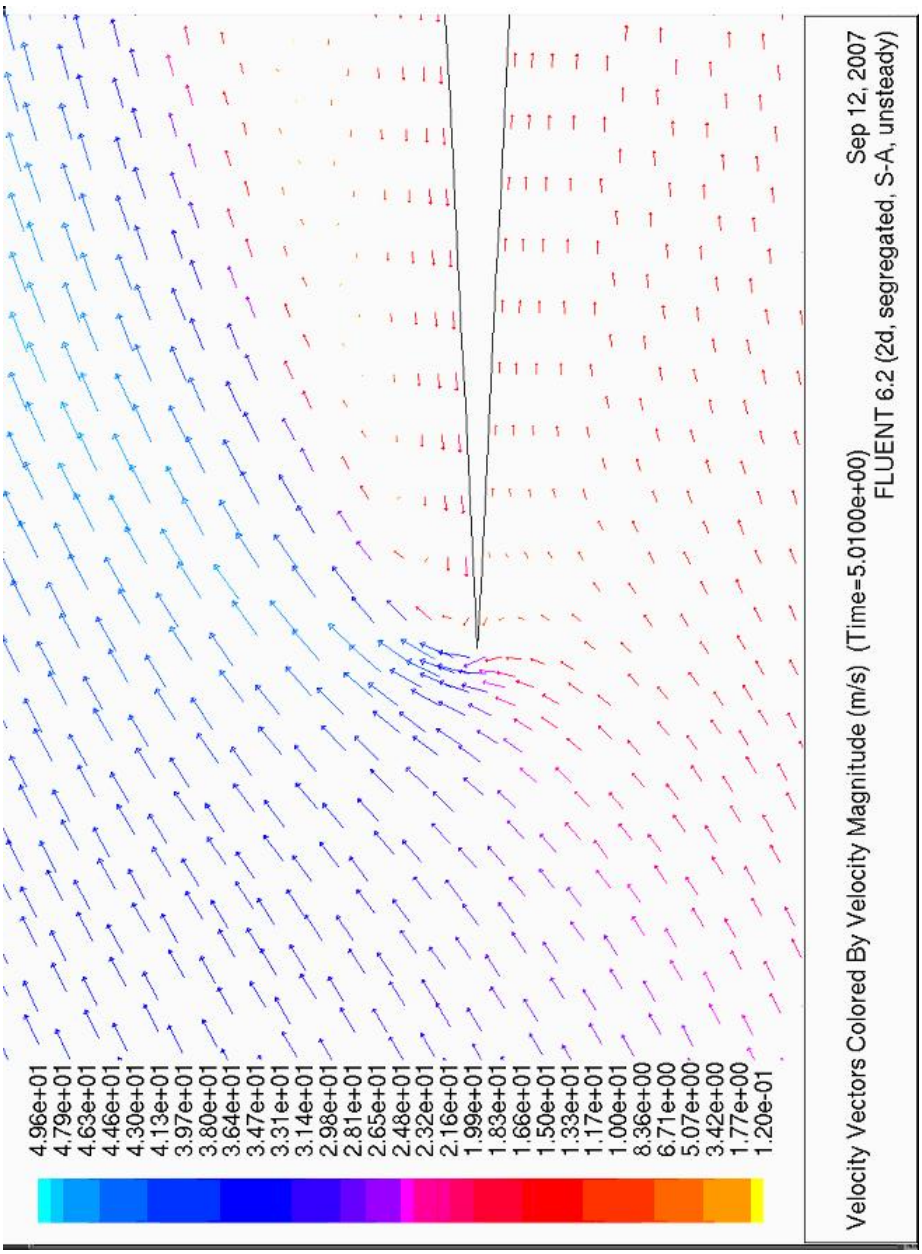

Figure A.3: Velocity vectors for the Quad 4x4 hull at $B = 24$

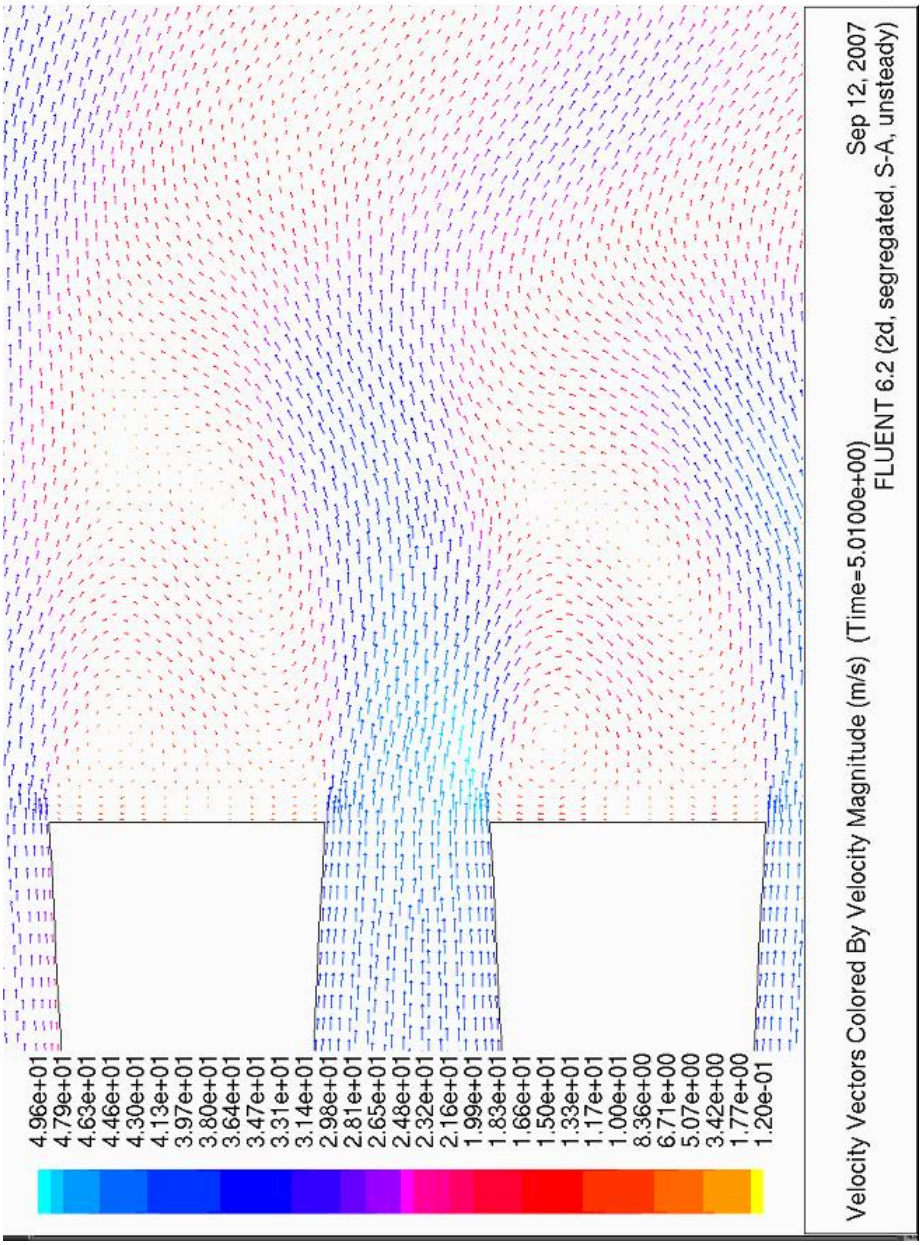

Figure A.4: Velocity vectors for the Quad 4x4 hull at $B = 24$

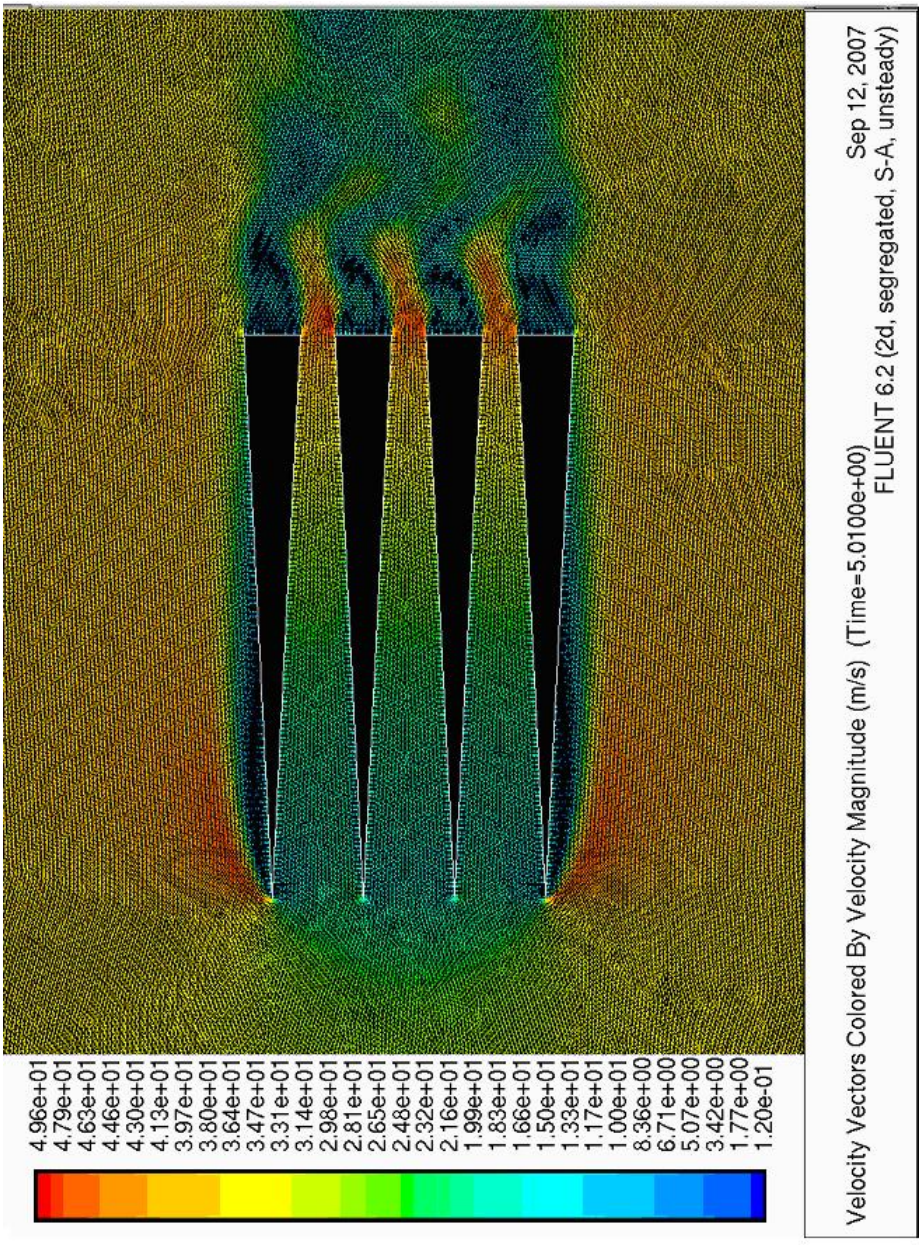

Figure A.5: Velocity vectors for the Quad 4x4 hull at $B = 24$

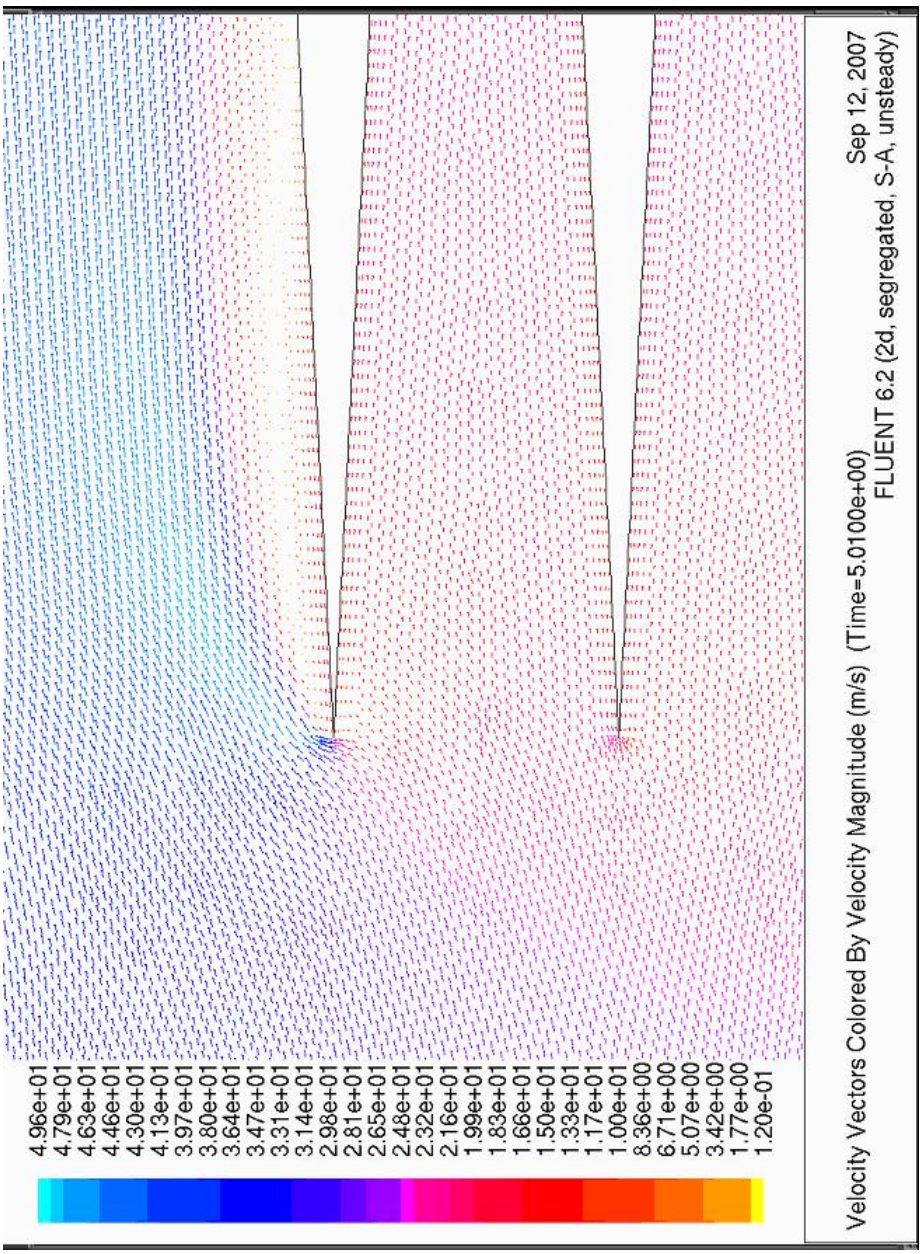

Figure A.6: Velocity vectors for the Quad 4x4 hull at $B = 24$